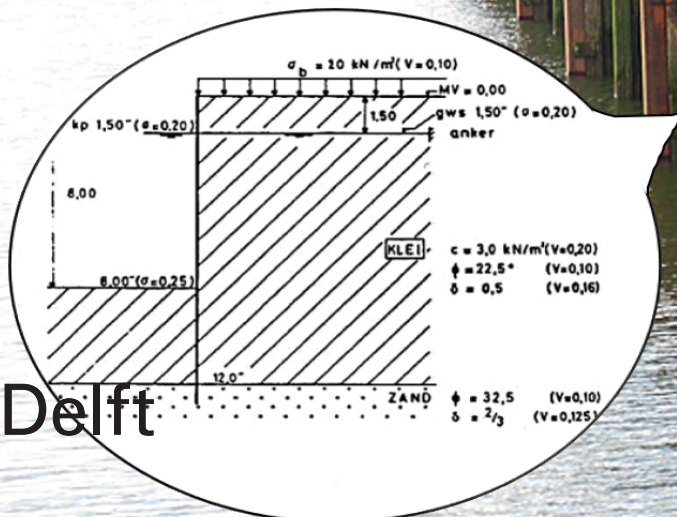
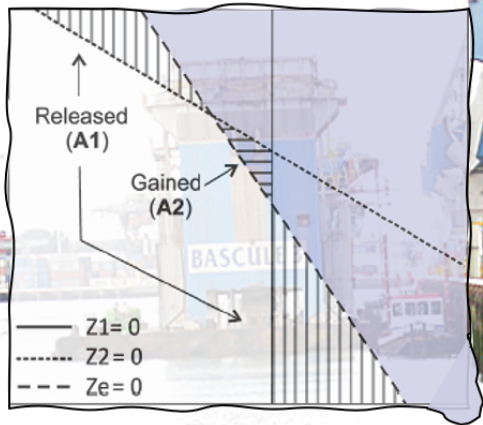


Reliability updating of existing quay walls based on the effects of past performance

Introduction of a novel mathematical application in the probabilistic assessment and evaluation of quay walls

Kamal Laghmouchi

MSc Thesis



Reliability updating of existing quay walls based on the effects of past performance

Introduction of a novel mathematical application in
the probabilistic
assessment and evaluation of quay walls

by

Kamal Laghmouchi

to obtain the degree of **Master of Science**

in Structural Engineering - Hydraulic Structures

at the Delft University of Technology,
to be defended publicly on 22 January 2021 at 11 am.

Student number: 4663969
Project duration: March 2, 2020 – January 22, 2021
Thesis committee: Dr. Ir. J.G. De Gijt, TU Delft, supervisor
Dr. Ir. A.A. Roubos, TU Delft
Dr. Ir. T. Schweckendiek, TU Delft
Dr. Ir. Y. Yang, TU Delft
Dr. Ir. O.M. Heeres, Arcadis
Prof. Ir. A.C.W.M. Vrouwenvelder, TNO & TU Delft

An electronic version of this thesis is available at <http://repository.tudelft.nl/>.

Preface

This research has been carried out as an MSc thesis within the Department of Civil Engineering and Geosciences at the Delft University of Technology. The main objective of this research was to study several effects of past performance on the semi-probabilistic design method for quay wall structures. Eventually, the outcomes should result in an evaluation on how past performance is considered in Level I design and evaluation method according to the Dutch National standards. Deltares has developed a probabilistic tool for the D-series, Python and FEM-software. This has been coupled with D-sheet Piling. Afterwards, MATLAB algorithms were developed and reliability updating analyses were performed. My thesis regards a subject which is very interesting from practical viewpoint.

First and foremost, I would like to thank everyone who in either way was involved with my MSc research. Special thanks go to Arcadis for providing me the amazing opportunity to perform this interesting research. I appreciate the cooperation and helpful experience from my colleague supervisor Otto Heeres. In addition, a special thanks goes to my tutors from TU Delft led by Jarit de Gijt. Their names are added on the title page. The time with Timo Schweckendiek, Alfred Roubos, Ton Vrouwenvelder and Yuguang Yang always resulted in interesting and fruitful discussions. Furthermore, I would also like to thank my other colleagues from Arcadis and Deltares, in particular Robbin Wesstein for supporting me during this course and Rob Brinkman for his consultation on the applied software. The last but not the least, I would love to thank my family and friends. They have always been supportive during my entire educational career and my personal life.

*Kamal Laghmouchi
Delft, January 2021*

Summary

In practice, many structures among which quay walls are designed according the Dutch national guidelines (CUR) [15] [17]. Dutch national practical guidelines (NPR), with guidelines for renovation, is still in development for the building industry. These guidelines follow the Dutch Norms (NEN) and Annexes [33] [35]. The guidelines propose procedures in which newly-built or existing quay walls are designed. This study investigates the effects of past performance on the semi-probabilistic level I method for the purpose of design and evaluation of quay walls. This research is performed with a case study considering a CUR class III quay wall from [72, p. 58]. The objective of this research is gathering insight into the different aspects of past performance, among which degradation and information about survived years, on the reliability level and corresponding influence factors.

Firstly, prior analyses including deterministic validation are performed. The output resulting from characteristic values X_d^* of the cross-section is validated by means of Blum and analyses with the subgrade reaction method. The computed deterministic output appears to be in accordance with the results from the reference study [71] [72]. Afterwards, prior probabilistic analyses were performed in which the reliability, weight factors and corresponding partial safety factors are reconsidered. Failure mechanism 'yielding of front wall' is a frequent phenomenon and is assessed in this research. Level II FORM is used for the calculation and level III Importance sampling for the validation. The cross-section is adjusted according the reference case and the results are reasonably in compliance with the results found by GeoDelft for CUR class III. The computed 50 year reliability index $\beta = 4.53$ corresponds well to the target reliability level $\beta_t = 4.5$.

Additionally, the situation in which random input variables are correlated and model uncertainty is included, is considered as well. These correlations and model uncertainty are determined based on previous researches among which [63]. The cohesion of clay, internal friction angles, wall friction angles and water levels are correlated. The model uncertainty factor is log-normally distributed and applies as multiplication factor on the maximum bending moment. Explicitly, the latter results in a significant influence on the limit state.

Effects given the reference period are considered as well. Large numbers of the dominant load variable q are simulated. The (extreme value) distribution converges to a Gumbel distribution with $\sigma_q = 0.61$. The stochastic distribution of the dominant load is transformed from and to different reference periods: $t_{ref} = 1, 5, 10, 25, 50, 100$ years. Eventually, for posterior analyses the 50 year reference case is translated to an annual situation in which the annual reliability index and sensitivity factors are derived. Including model uncertainty and cross correlated random variables, one finds $\beta_1 = 2.33$ as assumption for the posterior analyses.

The Equivalent Planes method (EPM) has already been applied in the field of flood defences for reliability updating. This method formulates an failure plane equivalent to two or more combined limit states. In this research, the method has been applied in the temporal context. This means that the Equivalent Planes method is considered in the derivation of the reliability given effect(s) of past performance. The annual reliability index and sensitivity factors are used in this reliability updating method. The auto-correlation represents the correlation of the concerned variable in time. Time-dependent variables including uniform load and water levels assume $\rho_{ijk} = 0$, other parameters initially assume $\rho_{ijk} = 1$. The annual reliability index and sensitivity values are iteratively applied in this method for combining limit states. The equivalent failure plane Z_e uses a simplified expression in the standard normal space consisting of $\beta_{F_i|S_{i-1}}$, u_{ik} and α_{ik} . Eventually a time-dependent reliability curve, as presented by the green line in figure 1, is found. Without model uncertainty, the blue curve is obtained. A higher initial annual reliability index results in a relatively smaller increase of the conditional reliability index. Hence, the effect of past performance decreases for higher initial β . Due to the reduced cross correlation $\rho(w_a, w_p)$ between water levels on both sides, the time-dependent reliability significantly increases.

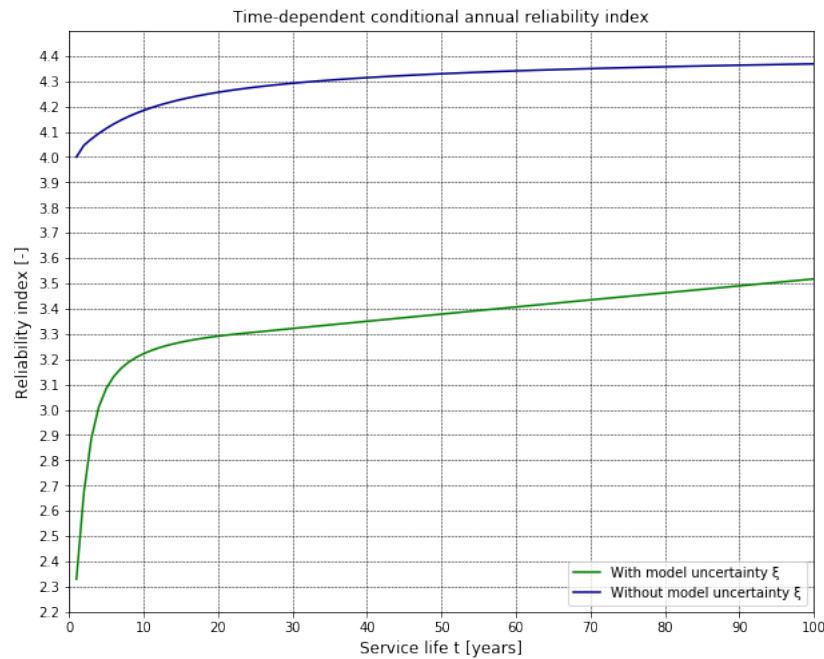


Figure 1: Time-dependent reliability index for the cases with and without model uncertainty. No model uncertainty results in a higher initial annual reliability index and consequently a smaller overall increase due to past performance.

At last, the time-related effects of quay walls are considered. These effects include:

- The irreducible time-dependent uncertainty related to the model uncertainty factor. Randomness or natural variation is included in the model uncertainty factor. This is performed by considering situations with a reduced auto-correlation $\rho_{ij\xi} = \{0.25, 0.50, 0.75\}$.
- The reducible time-dependent uncertainty of load variables including q , w_a and w_p . Knowledge uncertainties (epistemic uncertainties) are reducible in time, meaning auto-correlation approaching 1. The auto-correlations of the considered variables distributions are derived by using transformed random distributions.
- Degradation by corrosion of the stiffest elements in the steel front wall. Corrosion is studied by considering the effects of a log normally distributed wall thickness loss according to corrosion curve 3. This corrosion rate affects the primary element characteristics of the equivalent combined wall.

The correlation between the water levels on the active- and passive is reconsidered and changed from $\rho(w_a, w_p) = 0.75$ to 0.25. As follows, the below figures show the annual development of the annual reliability as a function of time t . Notice that the annual reliability index increases as the extent to which the uncertainty is epistemic increases. Further, the reliability converges less rapid to larger value(s) in case of $\rho_{ij\xi} \rightarrow 0$.

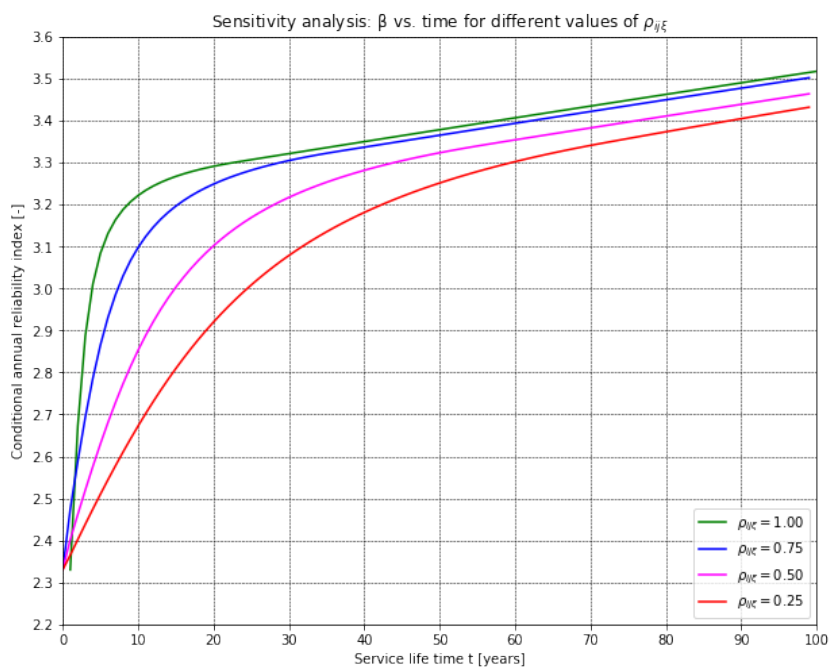


Figure 2: The effect of natural variation on the time-dependent conditional reliability index.

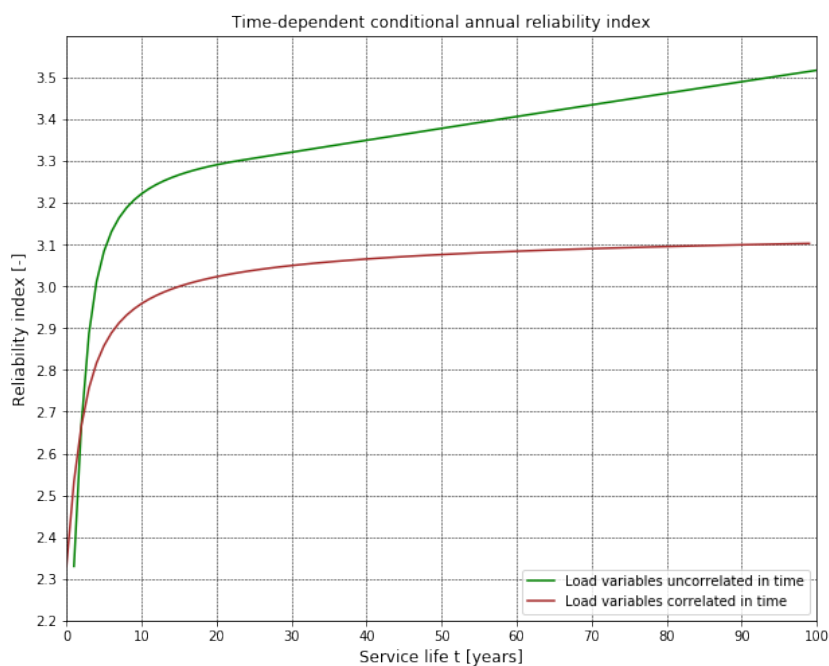


Figure 3: The effect of epistemic uncertainty on the time-dependent conditional reliability index.

In this research, corrosion is considered as an epistemic uncertainty. Two modelling approaches have been considered: an engineering approach, a second order approach. The engineering approach solely considers a reducing section modulus W , whereas the second order approach is additionally including the second moment of inertia I . Corrosion curve 3 results in both approaches to a flattening of the conditional reliability index as time progresses. In addition, the speed in which the influence of time-independent epistemic uncertainties decreases, is less in case of corrosion. Hence, the involvement of stochastic degradation $\Delta t \sim \text{LN}(\mu_{\Delta t}(t), 0.10\mu_{\Delta t}(t))$ negatively affects the extent to which the uncertainties are reducible.

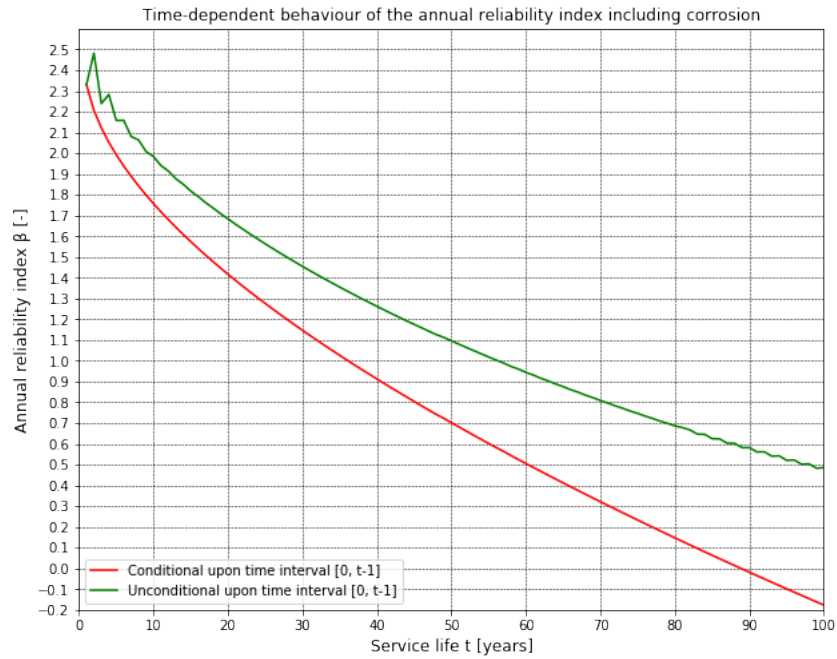


Figure 4: The time-dependent annual unconditional and conditional reliability index including the effects of corrosion.

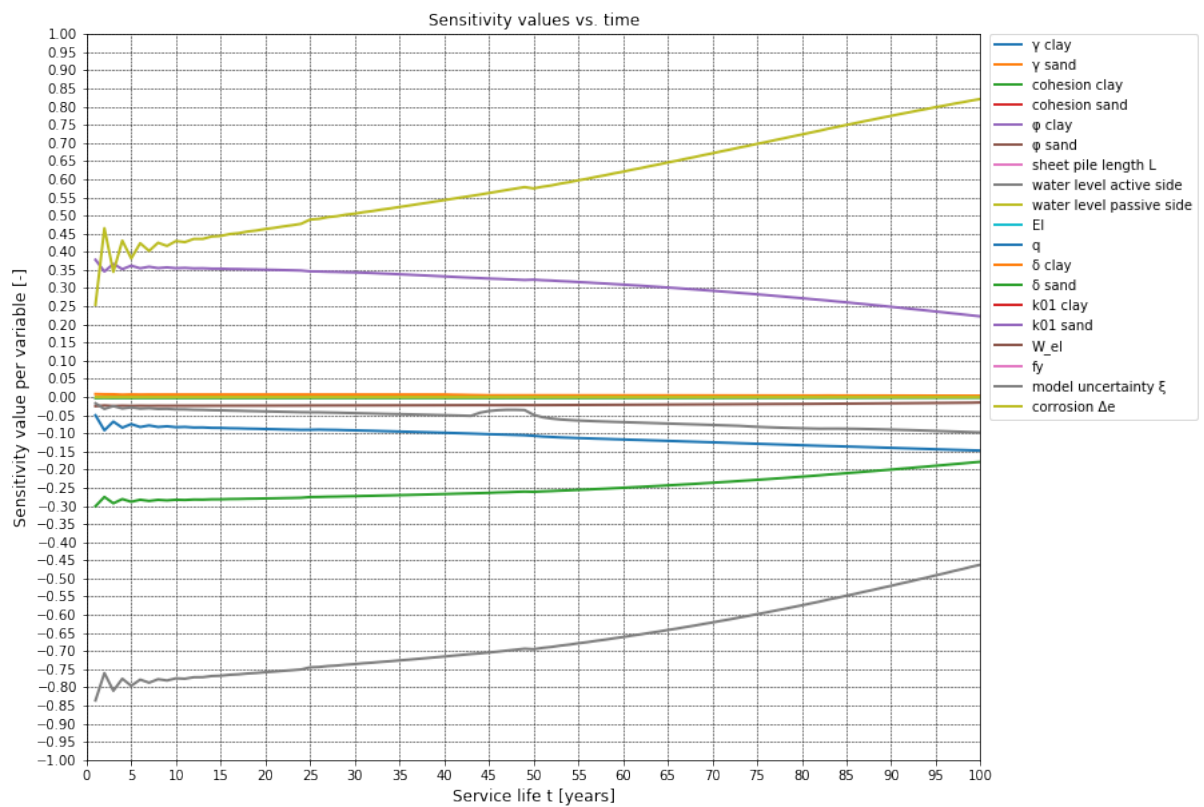


Figure 5: The effects of past performance including corrosion on the time-variant sensitivity values. These curves are derived with the engineering approach.

The updated reliability index is also calculated per reference period. This is performed with probabilistic calculation rules. The corresponding sensitivity values, given survival of previous years (see figure(s) 5), can be used in the semi-probabilistic level I method for derivation of the updated partial safety factors $\gamma_{x_{ik}}$. These factors can be applied in the derivation of the design values x_{ik}^* per random variable considering a service life time t . Hence, the reliability of a quay wall and the transformed sensitivity coefficients can be updated with the Equivalent Planes method. Incorporation of degradation and other time-related effects is seemingly possible. However, further research with finite element modelling is recommended for verification purposes.

List of Terms

Aleatory uncertainty	Uncertainty due to natural variation or randomness influencing the quantity of the concerning parameter
Annual reliability index	Reliability index per year
Auto-correlation	The statistical correspondence between a variable in one cross-section, with the same variable within an other cross-section in temporal or spatial context
Compaction	Process in which stress is applied to a soil causing a dense soil package as air is displaced from the pores between the soil particles
Conditional reliability index	The reliability that a component or system operates without failure at a moment, given that it already has survived the previous time interval up to that certain moment
Cross-correlation	The statistical correspondence between two variables within the same cross-section
Engineering approach	Approach in which effect(s) of corrosion are studied by solely applying a decreasing section modulus
Epistemic uncertainty	Uncertainty related to the extent of available knowledge which is present about the concerning parameter
Eurocode	European norms and guidelines prescribed for the construction industry
Liquefaction	Phenomenon in which water over pressure exists between loosely packed soil particles causing loss of bearing capacity
Past performance	Information on survived conditions in previous time units by which the reliability of a structure can be updated
Quay wall	An earth retaining structure at which floating vessels are docked and goods are transferred
Reference period	Period over which the reliability of the structure is considered

Reliability index

Quantitatively describes the reliability of a structure c.q. the certainty that the object fulfils its intended functions during a specific time under certain conditions

Second order approach

Approach in which effect(s) of corrosion are studied by imposing a decreasing section modulus and a decreasing second moment of inertia

List of Abbreviations

CC	Consequence Class
CoV	Coefficient of Variation ($CoV = \frac{\sigma}{\mu}$)
CUR	Civieltechnisch Centrum Uitvoering Research en Regelgeving (<i>En: Civil Engineering Centre Execution Research and regulations</i>)
EC	Eurocode
EN	European Norm
EPM	Equivalent Planes Method
ER	Economic Risk
EVD	Extreme Value Distribution
FEM	Finite Element Model
FORM	First Order Reliability Methods
FOSM	First Order Second Moment methods
GC	Geotechnical Class
HS	Hardening Soil model
HSS	Hardening Soil Small Strain model
IR	Individual Risk
IRPA	Individual Risk Per Annum
ISO	International Organisation for Standardisation
JCSS	Joint Committee on Structural Safety
LIRA	Localised Individual risk per annum
LN	Lognormal Distribution
LQI	Life Quality Index
LSF	Limit State Function
MC	Mohr-Coulomb
MUF	Model Uncertainty Factor
N	Normal Distribution
NaN	Not a Number
NEN	NEderlandse Norm (<i>En: Dutch Norm</i>)

NI	Numerical Integration
NPR	Nederlandse Praktische Richtlijnen (<i>En: Dutch Practical Guidelines</i>)
PTK	Probabilistic Toolkit
RC	Reliability Class
ROM	Recomendaciones de Obras Maritimas (<i>En: Maritime Works Recommendations</i>)
SERI	Societal and Environmental Repercussion Index
SLS	Serviceability Limit State
SORM	Second Order Reliability Method
SR	Societal Risk
SSC	Soft Soil Creep model
SWTP	Social Willingness To Pay
u-space	Independent Standard Normal Space
ULS	Ultimate Limit State
Z-function	Limit state function

List of Symbols

α	Sensitivity value	-
α_{ik}	Sensitivity value in year i for variable k	-
β_n	Reliability index given a reference period of n years	-
β_t	Target reliability index	-
Δe	Decrement of thickness	mm
Δt	Time step	years
δ_i	Wall friction angle	°
γ_i	Volumetric weight of considered soil layer	kN/m ³
γ_R	partial safety factor on the resistance	-
γ_S	partial safety factor on the load	-
γ_{x_n}	partial safety factor on a variable given a reference period of n years	-
γ_{soil_i}	Volumetric weight of considered soil layer	kN/m ³
μ	Mean value of a normal(ised) distribution	x
ϕ_i	Angle of internal friction	°
ρ	Pearson's correlation coefficient	-
ρ_{ijk}	Auto-correlation between a variable in year i and j	-
σ	Standard deviation of a normal(ised) distribution	x
ξ	Model uncertainty	-
a	Scale factor for a Gumbel distribution	x
C	costs	€
c	cohesion	kN/m ²
D	Diameter	mm
E	Young's modulus	Nmm ²
e	Thickness of element	mm
EI	Bending stiffness	kNm ²
f_y	Yield stress of steel	N/mm ²
h	Excavation depth	m
KA	Translation stiffness	kN/m ²
L	Sheet piling length	m
q	Uniformly distributed load	kN/m ²

s	Layer separation level	m
t	Time	years
u	Scaled mean value of a Gumbel distribution	x
u_{ik}	Design value in year i of variable k	-
A_{SP}	Cross-sectional area sheet pile	mm ²
d_i	Embedded depth	m
$F_{p,max}$	Maximum passive resistance	kN/m/m ¹
$F_{p,mob}$	Mobilised passive resistance	kN/m/m ¹
I	Second moment of area	mm ⁴
I_0	Initial second moment of area	mm ⁴
$I_{el,y}$	Elastic moment of inertia	mm ⁴
k_{01}	Subgrade reaction modulus	kN/m ²
K_i	Subgrade reaction modulus per layer i	kN/m ²
M_{max}	Maximum bending moment	kNm
t_n	Certain year in time	years
t_{ref}	Reference period	years
u_{max}	Maximum displacement	mm
V_{max}	Maximum shear force	kN
V_{x_i}	Coefficient of variation	-
W_0	Initial elastic section modulus	mm ³
w_a	Water level on the active side	GSL+m
$W_{el,y}$	Elastic section modulus	mm ³
w_p	Water level on the passive side	GSL+m
X_k	Characteristic value of a variable	x

Contents

Preface	iii
Summary	v
List of Terms	xi
List of Abbreviations	xiii
List of Symbols	xv
1 Introduction	1
1.1 Background	1
1.2 Problem definition	3
1.2.1 Problem analysis	3
1.2.2 Problem statement	4
1.3 Objective and research question	4
1.3.1 Project boundaries	5
1.3.2 Main research question	5
1.3.3 Sub-questions	5
1.4 Methodology	7
1.4.1 Introduction	7
1.4.2 Research methodology	7
1.4.3 Case study methodology	8
1.4.4 Case: single anchored sheet piling system	10
1.5 Thesis outline	13
2 Theoretical framework	15
2.1 Introduction	15
2.2 Short summary of literature review	15
2.3 Knowledge gaps in reliability updating of quay walls	16
3 Preliminary analyses	17
3.1 Introduction	17
3.2 Deterministic analyses: Blum and D-Sheet Piling	17
4 Prior analysis	21
4.1 Introduction	21
4.1.1 Approach CUR 166 by GeoDelft and C69	22
4.2 Influence of correlated variables	25
4.3 Influence of the model uncertainty	27
4.4 The influence of the reference period	29
4.5 Verification of the prior reliability analysis	34
5 Posterior analysis	41
5.1 Introduction	41
5.2 Starting points	41
5.3 Posterior analysis with Equivalent Planes method	42
5.4 Application of the Equivalent Planes method	46
6 Results from the case study	47
6.1 Introduction	47
6.2 Equivalent Planes method with two components	47
6.2.1 Method 1: EPM with Numerical Integration	49
6.2.2 Method 2: EPM with FORM analyses	49

6.3	Verification of the Equivalent Planes method	50
6.4	Equivalent Planes method for a multi-component system	51
6.4.1	Method	51
6.5	Results and differences	53
7	Time-dependent effects on the quay wall	59
7.1	Time-variant model uncertainty factor	59
7.2	Inclusion of time-variant loads	61
7.3	Degradation by corrosion	67
7.4	Method for updating partial safety factors	75
8	Conclusion, discussion and recommendations	79
8.1	Conclusion	79
8.2	Discussion	88
8.2.1	Incorporated model uncertainty	88
8.2.2	Significantly low calculated reliability index	88
8.2.3	Standardised normal space	88
8.2.4	Time-dependent reliability due to corrosion	89
8.2.5	Fully reducible uncertainty of corrosion	91
8.3	Recommendations	92
8.3.1	Follow-up research	93
	Bibliography	97
	Appendices	103
A	Methodology for the case study	105
B	Data gathering and analysis	107
C	Theoretical framework	109
C.1	Introduction	109
C.2	Quay walls	109
C.2.1	History of quay walls	109
C.2.2	Types of quay walls	114
C.2.3	Failure mechanisms	120
C.2.4	Quay walls in practice	122
C.3	Safety of structures	127
C.3.1	Introduction	127
C.3.2	Reliability differentiation of new structures	129
C.3.3	Reliability differentiation of existing structures	131
C.3.4	Reliability differentiation of new geotechnical structures	132
C.3.5	Reliability differentiation of existing geotechnical structures	133
C.4	Reliability calculus	135
C.4.1	Introduction	135
C.4.2	Level 0 method: Deterministic approach	135
C.4.3	Level IV methods: Risk-based approach	138
C.4.4	Level III methods: Full probabilistic approach.	141
C.4.5	Level II methods: Approximation of the design point	143
C.4.6	Level I methods: Semi-probabilistic approach	146
C.5	Previous approaches and thereby used applications	148
C.5.1	Previous studies on reliability updating	148
C.5.2	The concept of reliability updating	150
C.5.3	Uncertainties	151
C.5.4	Calculation models for quay wall design and assessment	152

D	Fault tree of a quay wall	157
E	Sampling methods	159
	E.1 Importance sampling	159
	E.2 Directional simulation.	160
F	Early analysis with Blum method	163
G	Early analysis with subgrade reaction method	169
H	Prior analyses	189
	H.1 Deformations and passive soil resistance.	189
	H.2 Yielding of the front wall	194
	H.2.1 Determination of sheet pile profile	195
I	Reliability index and sensitivity values found with a normally distributed yield stress f_y	197
	I.1 Approach CUR 166 by GeoDelft and C69.	199
J	A-priori reliability results: yielding of the front wall	201
	J.1 Example 3: Quay wall CUR class III.	201
	J.1.1 With equivalent sheet pile profile	204
	J.2 Example 2: building pit CUR class II	205
	J.2.1 With calibrated elastic section modulus	205
K	Verification of the level II analyses	207
	K.1 Verification of the results with Importance Sampling	207
L	Derivation of stochastic parameters for variable q	209
M	Hohenbichler-Rackwitz algorithm for reliability updating	213
	M.1 Two-component system	215
	M.2 Verification of a two-component system.	218
	M.2.1 Verification of the intermediate output	218
	M.2.2 Verification trough Bayesian updating with Deltares PTK	219
N	Results Hohenbichler-Rackwitz method combined with FORM	223
O	Effects of extreme loads	225
P	Derivation of the reduced W and EI	227
Q	Time-dependent effects on the quay wall	231
	Q.1 Refined or "second order" approach for including corrosion	231
	Q.2 Reliability index as a function of the reference period	233
R	Approach follow-up case study	235

1

Introduction

This thesis is a finalising assessment within a Master of Science program within the Civil Engineering department. The Master's thesis falls under the course code CIE5060-09, covers a relevant topic within the student his masters' specialisation and stands for 40 European Credits. The student will do a research on the subject that is found through an agreement between the student, TU Delft and Arcadis. Delft University of Technology facilitates the framework, graduation procedure and will assess the graduation work. A qualified subject within the track discipline of the Delft University of Technology and a knowledge gap in the company Arcadis are the main ingredients to the research problem. This research project developed over a time course of 10 months.

This chapter sets the outline for the research plan of the Master's thesis. Firstly, a summarised theoretical background of the subject is provided in section 1.1, subsequently the problem prior to this research is analysed and briefly stated. Afterwards, section 1.2 shortly describes the main problem of this research and additionally defines the problem statement. The purpose of this research is formulated in section 1.3. Section 1.3.1 uses the objective and project boundaries to define the scope of the graduation project. By stating the main research question and the underlying sub-questions one is able to list the points of interest for this project.

Following the research objective, the research plan presents the methodology on how this scientific thesis is executed in section 1.4. It is important that the applicable data that is used, fulfils certain requirements regarding quality and necessity with respect to the scope. Appendix B deals with the latter, potential resources for the literature research and the analyses are summarised in the subsequent subsection. An issue which is negligible is the way in which the obtained results are analysed and evaluated. The methodology deals with the case study approach as well. Section 1.4.3 describes the reference case(s) and the approach in steps and by means of flow charts. Section 1.5 finally summarises the treated aspects in this report.

1.1. Background

Rotterdam holds the largest seaport area of Europe and her leading position is largely due to its excellent accessibility from the sea, the river and at the intermodal connections by road and rail. The port of Rotterdam is directly and indirectly creating 385 thousand jobs at companies within the national borders of the Netherlands [52]. In 2019 the port of Rotterdam had a total throughput (including dry bulk, liquid bulk and containers) of 469,4 million metric tons. As a matter of fact, a study by the Erasmus University of Rotterdam ('Het Rotterdam-effect') [45] shows that the port of Rotterdam directly and indirectly realised an added value of 6.2% GDP to the Dutch economy in the year of 2017. The Gross Domestic Product, which is a commonly used value for indicating the economic health, is expected to have grown even further in 2030 [45].

Currently over a hundred thousand vessels, including seagoing and inland vessels, annually call at the port of Rotterdam [54]. Transshipment of goods has been estimated in 2018 at 149,1 million metric tonnes of containers and 289,5 million tonnes of dry- and wet bulk [52]. These quantities have been increasing with respect to their previous years. So the port of Rotterdam is of great importance for other economies as well. The significance of this Dutch port area to the Dutch and Northwest-European hinterland region is a key factor in the decision to reassess the current port infrastructure. The port infrastructure is losing its functionality over time due to for instance degradation. Degradation can be caused by steel corrosion due to environmental and climatic influences. The port infrastructure is subjected to loads exerted by water and harbour operations at land- and waterside while degradation is increasing over time. On top of that, in many cases a berthing place might become unavailable at the slightest deformations. The availability of the quay is relevant for the berthing capacity and therefore important for the port throughput as well. This throughput capacity is a significant factor for the port productivity serving the hinterland region [47]. Hence when looking at cross-sectional level, an important interface component between the wet infrastructure (port water area) and the dry infrastructure (the port terminal) is the quay wall. It is estimated that thousands of kilometres of quay walls are existing globally. The port of Rotterdam has in this a reasonable share with 77.3 km of quay walls [52].

Many quay walls in the harbours of Rotterdam, especially those that are built in the Western port area, were constructed after the Second World War. Especially parts in the Botlek, Europoort and Maasvlakte I were constructed during the late 60s and 70s, at the time of large port expansion programs. These programs were set up in order to keep pace with the demand for larger ships. Demand which was among other things due to the enormous expansion of containerisation in the mid-sixties and to the longer sailing distance as a result of political instability in the Middle East that had led to the closing of the Suez Canal by Egypt (the latter provoked the demand for larger oil- and gas tankers) [18]. In most cases, the quay walls in that time were constructed on the basis of a design lifetime of 50 years. Many of these structures are facing the end of their design life or are even older than 50 years. From experience it appears that a design life of 50 years is still very common nowadays due to financial reasons. The safety requirements in European guidelines for newly designed geotechnical structures are even more strengthened through the decades. On the other side, it appears that many quay walls have proven their functionality over the years without significant deformations¹. The focus of the Port of Rotterdam is increasingly shifting from constructing new quay walls towards the assessment and upgrade of existing ones.

Reliability levels of quay walls are generally determined in accordance with a design code such as Eurocode 0 (EN 1990) [61]. The reliability differentiation in this Eurocode is mainly focused on buildings and bridges where time-dependent variables, such as the state of the structural material influenced by fatigue, have a great influence. Each reliability class defines a set of partial factors to be used. A quay wall's time-dependent behaviour is different from that of closure dams, buildings or bridges. Structural elements of buildings and bridges undergo cyclic loads with small time periods and are more likely to fail as time develops (fig. 1.1C). Arch-gravity closure dams on the other hand, have teething problems in the first years and will therefore become prone to failures in that period. As time develops, the reliability of a closure dam will eventually remain constant (fig. 1.1A). It is expected that the behaviour of quay walls is somewhere in-between.

Aside from time-variant effects such as from compaction, liquefaction and consolidation, geotechnical structures are significantly dependent on time-invariant variables such as the effective soil parameters [50]. Moreover, there is the suspicion that the reliability of an existing quay wall develops over time as it already has proven its functionality under certain significant loads. The latter insight is not included in the currently used Dutch Norms (NEN-EN 9997, NEN 8707) for newly-built or existing geotechnical structures. The effect of past performance is not considered in the current Eurocode but may significantly influence the annual reliability indices of geotechnical structures. The upgraded annual reliability index is a means that could have the Port of Rotterdam delaying its annual expenses for the construction of new quay walls. These investments could go up to 10 to 12 million euros [50].

¹If the deformations are large enough in terms of units, the handling equipment will become unusable.

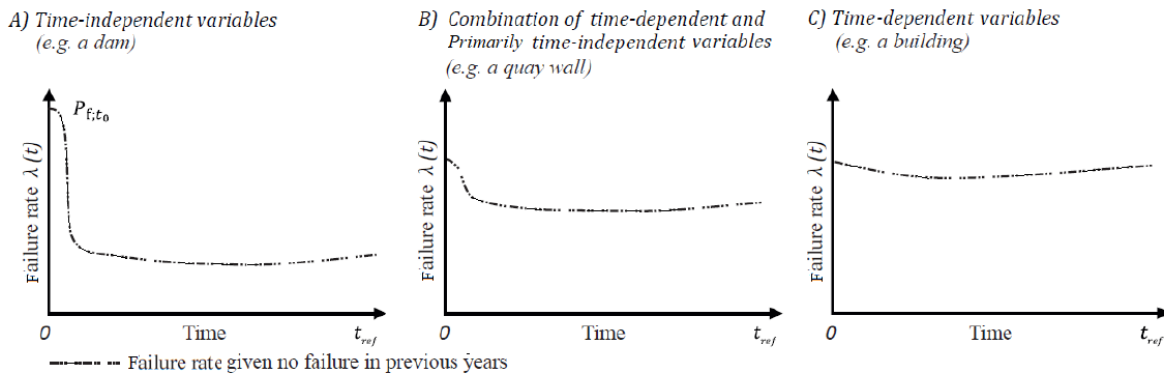


Figure 1.1: Conceptual bathtub curves for different civil engineering works [61].

The quantifiable effect of past performance on the reliability of existing quay walls is therefore worthwhile to consider. This chapter has dealt with the underlying information about the problem that needs to be assessed. Section 1.2 analyses the problem that has led to this research. This analysis will eventually narrow down to the problem statement that will be encountered in this research.

1.2. Problem definition

1.2.1. Problem analysis

Many quay walls approach the end of their intended design life and worldwide many harbour programs will be started for the assessment and renovation of these quay walls. It is relevant to properly assess the reliability of these structures in the time domain in order to make a sound decision about extending the structure's lifetime or executing proportional measures such as the construction of a new quay wall. From recent studies [61], [62], [63], it appears that the actual reliability of geotechnical structures such as quay walls can be determined on the basis of different aspects. Despite the degradation due to for instance corrosion, service life can be extended for many well-functioning quays. This is based on the fact that the time-independent uncertainty related to the effective soil parameters, which can be described with stochastic variables, positively influences this type of structure. Depending on the location, the effect of time-dependent uncertainties is smaller in the case of quay walls than in the case of multi-storey buildings and bridges.

Annual and lifetime reliability levels for quay walls should be determined in accordance with an international standard such as the ISO 2394:2015 and with a certain design code such as the Eurocode EN 1990:2011. These standards are concerned with structures at different stages of their lifetime: construction, in use, decommissioning [3]. The reliability classes in these international standards are mainly derived on the basis of consequences of failure and costs of safety measures. The consequences of failure can be expressed in loss of human life, social, environmental and economic repercussions [27]. The reliability classes that are defined in the current standards and codes are applied on new structures and on existing structures. The development of the reliability of a service-proven quay wall subject to corrosion-induced degradation over time has already been addressed in other literature [63]. The influence on the reliability and remaining service life of service-proven quay walls has been highlighted in literature as well. Accordingly, decisions on required proportional measures for quay walls is made on the basis of the conditional failure probability at a certain moment in time.

One should note that design life extending measures oftentimes require repair actions with relatively higher marginal safety costs than the construction of a new quay wall [75]. These costs are incremental costs per added quantity or unit. So in other words it is generally more expensive to achieve a certain target reliability level in case of an existing quay wall. Repair works at quay walls often require large time-consuming operations. These repair activities require an optimised planning for logistical opera-

tions within the harbours. It therefore becomes preferable in monetary terms to delay or minimise the expenditures on the quay walls.

On the other hand, current practical guidelines for geotechnical structures are not considering time-dependent strength. Papers written by Roubos [63] [62] illustrate the effect of degradation, economic optimisation and human safety requirements on the reliability of a quay wall. Reducing uncertainty in the evaluation of existing quay walls by analysing berthing records, has been studied in [65] and [6], the effect of test loading in [25]. The effect of past performance on the remaining service life of existing quay walls has not been studied thoroughly in previous papers while this aspect possibly improves the integrity of the structure. The translation of this effect in practice is important for the design codes NEN 9997-1 and NEN 8707. The practical guideline in the NPR that is backed by the NEN 9997-1 and NEN 8707 is lacking practical engineering methods that account for the effects of past performance. In fact, the quantified effect of (realistically) historical observations on the remaining service life of an existing quay wall is rather unknown. These historical observations may include (water) loads and/or displacements.

1.2.2. Problem statement

Many quay walls are facing the end of their intended design life. The replacement or repair of an existing quay wall is very costly as it comes to money and logistics. To make a sound decision between the construction of a new quay wall, the execution of proportional measures and the upgrade of an existing quay wall, the quay wall should be assessed and evaluated on whether it is in a technically sufficient state.

Current Dutch guidelines on geotechnical structures and quay walls provide information about the reliability classes and the use of safety factors in the design. However, many cases [64, p. 16 - 18] have shown that service-proven quay walls have not yet reached the end of their actual service life. By this fact, one supposes that the full capacity of such a quay wall is not exploited yet. Besides that, an analytical method for service-proven quay walls accounting for the quantifiable effect of past performance on the reliability level is still lacking. The Dutch (practical) guidelines presently used by engineers for geotechnical structures are lacking this method.

1.3. Objective and research question

This research aims at conducting analyses which derive insight into the structural reliability development of quay walls in time, where both the past performance and degradation have been taken into account. Taking into account the past performance of a structure yields knowledge about the development of the structural reliability in time. In anticipation of implementation in the NEN-EN 9997 and NEN 8707, the effect of past performance and degradation will eventually be used in the evaluation of a traditional design procedure. An example of such a design procedure can be found in the national practical guidelines for the assessment of quay walls such as the Dutch NPR. This research is intended to eventually provide added value in the approaches as investigated by the NEN commission. As is not earlier mentioned, the Dutch practical guideline will include the effect of past performance for the first time.

In short, the aim is to precisely predict the remaining service life of a quay wall by means of the updated annual failure probability and the standardised acceptable failure probability for commercial quay walls in the port of Rotterdam.

As part of the eventual objective, a selected representative case is studied. By means of a reliability updating method the effects of past performance for this representative case are studied. Therewith the design values can be calibrated to the effect of past performance. By means of the prediction of the residual life time one assesses whether the structure is technically stable. To obtain the objective as is defined in the previous paragraph a number of research questions have been identified. In addition, a

number of sub-questions are defined in order to construct an answer for the main research question.

1.3.1. Project boundaries

This graduation project is mainly focused on the quantifiable effect of past performance in the probabilistic analyses of an fictitious existing quay wall that was already studied by the CUR research commission C69 [71] [72]. Specifically speaking, a quay wall at a certain moment point in time is considered. Degradation by corrosion is thereby taken into account. This case study initially covers a fictitious quay wall with a simplified and more or less realistic geometry. The probabilistic analysis is performed by means of a Level II and Level I approach. These approaches are common engineering practice because they are less time-consuming than full probabilistic methods. Since significant information about the remaining service life is not yet available, the quay wall must be examined on an annual basis. For further application, it is necessary to have an applicable and effective method. The obtained information can be used for the evaluation of the effect of past performance on a reference period of 50 years. Section 1.4.3 treats the case study that is used.

In previous researches, the analyses were mainly concerned with combined walls supported by a relieving platform and anchorage [61]. This research will however mainly focus on the effect of past performance in a mathematical context. The effects of survived time intervals containing measured extreme loads or displacements and degradation by corrosion on the annual reliability level and the design value(s) are studied. The latter is performed for a given reference period. A major aspect is the way in which is dealt with variable uncertainties. By the use of a modelling software package (in this case D-Sheet Piling) coupled with a calculation toolkit (Probabilistic Toolkit) one is accommodated to perform calculations including these uncertainties.

Eventually, this updating method should be applicable for the assessment and evaluation of general cases in practice. A realistic case, addressing existing quay walls within the port of Rotterdam, is useful during a later stage of this Masters' research. The applicability of this method on a more complicated case is studied with such an extended case. In view of time, only normative failure mechanisms are considered in the extended case. Lastly, obtained results can be compared with the information from current design standards or guidelines.

1.3.2. Main research question

The main research question reads as follows:

"How can effects of past performance be taken into consideration in a semi-probabilistic assessment of existing quay walls, by means of a reliability updating method analogously to what is already applied in the field of flood defence systems?"

1.3.3. Sub-questions

The case study will be treated through investigation of certain research questions. The framework of output consists of answers to the following questions:

1. What is the optimal modelling approach for the selected reference case(s)?
2. How can Bayesian updating be applied for the selected reference case?
3. What are the impacts of adding information to the model regarding the reliability level of the existing quay wall?
4. How does the time-dependent behaviour of strength variables, due to degradation by corrosion during the previous years of service, impact the reliability analyses of the reference quay wall?
5. How do the transformed sensitivity factors of the model variables develop over time given the effects of past performance?
6. How is the information about the sensitivity factors reapplied in the semi-probabilistic analyses?

7. In what ways does the analyses output, realised by means of the effect of past performance, compare with the output that is realised by means of the original approach for the reference case(s)?

The aim of these sub-questions is to form a structure of premises to eventually answer the central question. Hence each individual sub-question is treated by the theoretical background and the subsequent case study and should contribute to the main research question.

1.4. Methodology

1.4.1. Introduction

Before the development of the theoretical framework for the Master's Thesis, one was confronted with different ways on how to encounter the problem as is stated in section 1.2. Before considering the problem statement in a practical case, one requires knowledge which is obtained by literature study. Such knowledge includes among other things the design framework of quay walls and background of the applicable design codes. The convenient reliability updating method is on the other hand a more practical approach in this Master's thesis and is thus handled through an adapted methodology which is outlined in section 1.4.3.

Each chapter in this thesis is based on a sub-question and uses added input and should result in an individual outcome which should be relevant for the subsequent part. The research methodology in section 1.4.2 describes the approach which is used in the literature research. The case study approach in section 1.4.3 describes the method used for analyses and evaluation of the calculation results. The case study is described in section 1.4.4.

1.4.2. Research methodology

The literature research can be subdivided into two main parts: a part that focuses on the theoretical background and the analytical part where the reliability updating aspects of a selected fictitious quay wall are discussed. Each part of the literature thesis follows an evident structure. Where the first part starts with general cases such as the history of quay walls, is the last part mainly concerned with a more specific application. Each chapter uses literature that has been studied thoroughly during the first weeks of the MSc research. Chapter 2 reviews on the theoretical framework and evaluates the previously performed studies for comparable cases.

This literature study is based on traditional desk research using papers and interviews within the company. This desk research will initially describe the theory about quay walls. This knowledge is mostly obtained from handbooks and university papers. Reliability calculus in general is an important aspect for this research and will be treated in more detail. Safety philosophy and standards that are used for various structures such as quay walls, are treated in this literature study as well. These sections will partly deal with structures in general and geotechnical structures. Much literature about the safety in Civil Engineering is available and will be applied in that part. The aspects related to design and (re)assessment of quay walls according to the standard gets significantly more focus as research develops. A part of the design approach goes about the design, assessment and monitoring in practice. The information for the latter subject is obtained from an interview that is conducted with an experienced professional (see section 1.4.2).

At last, the importance of reliability updating will be explained. Hence, it becomes important to distinguish between the reliability methods at hand, the quay wall design models and the implications that are involved. The end of this literature study will go briefly into the reliability updating methods for Civil Engineering structures. Regarding the latter, a short recap on the knowledge gaps within reliability updating for quay walls will be discussed. At this stage, it has been rather important to consult, recent research articles, guidelines, experienced professors and professionals. Previous studies on comparable subjects were resourceful at this stage of the literature study.

Field research

An usual way of collecting data on the second hand is through interviews and conversations with experienced professionals within the working field. A graduation at the company yields the opportunity. An automation design engineer, experienced in the coupling between programming and modelling tools and a project manager with a rich experience has been spoken to. By means of interviews one is anticipated with answers that yield information for the benefit of the case study.

1.4.3. Case study methodology

This section treats the case study approach. The applicability of the calculation methods for the case study is handled in this section as well. As measureability becomes a more significant aspect, an operationalisation plan will be provided at the end of this section.

Analytical approach in the case study

The probabilistic assessment in this case study follows a comparable approach as is used in [77]. For the probabilistic assessment, one reference case is initially considered. The reference case concerns a fictitious quay as is elaborated in the Deltares report [72]. Therewith, a set of calculation tools are applicable. Table 1.1 gives an overview of the packages that are used in this research. It is along the way important to use parameters that are applicable with the analysing tool.

Case	Modelling software package	Probabilistic tool
Reference case	D-sheet piling i.c.w. hand calculation in Python	Deltares probabilistic toolkit

Table 1.1: Applicable analytical tools for the case study

This case study considers a reference case that is used in the development of partial factors for the Eurocode. Example 3 from [72, p. 54] will be reconsidered and recalculated. The effects of past performance are studied with the same reference case. This reference case resembles some of the quays that are found in the port of Rotterdam but is not necessarily representative. A schematisation of the reference case cross-section is shown in figure 1.2.

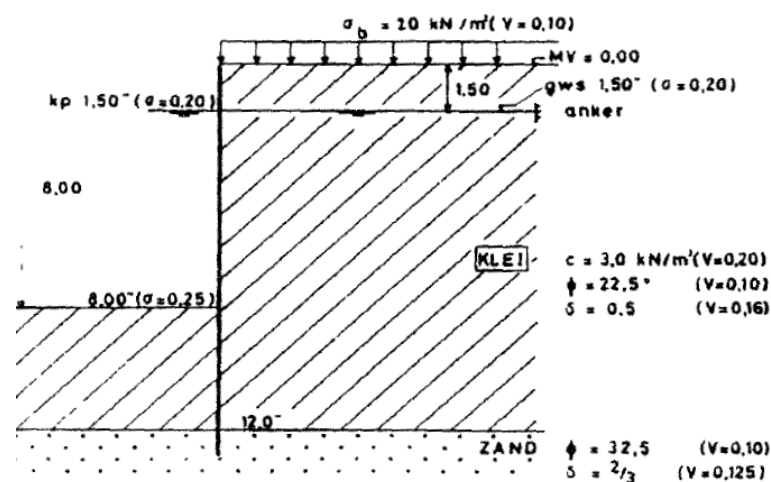


Figure 1.2: Reference case from the Deltares report for the development of the CUR 166 [72, p. 54].

Firstly, the initial quay wall cross-section, dimensions and characteristics are modelled in the program. A set of variables is listed which represent the model parameters. Initially, an (early) stability analysis is performed to verify the required type of sheet pile wall, anchorage system and other structural elements. This early analysis yields the normative failure mechanism(s), verifies the previously obtained results and whether the reference case is modelled correctly. Accordingly, the cross-section is adapted to meet the required stability.

After the model has been developed, the Deltares probabilistic toolkit will be coupled to the model. In addition, a part of the variables is modelled with stochastic properties. Hence, by means of the reference case one uses a set of variables as switches for the model. Not the soil-structure interaction but the structural behaviour of the quay wall itself is considered. For now, D-sheet piling is considered to be sufficiently accurate for modelling this schematic case. Besides, the Deltares probabilistic toolkit is

used to perform the probabilistic analyses. The method becomes more convenient as the probabilistic assessment and reliability updating of the quay wall is performed. The process of performing a reliability updating analysis is explained later on.

The application of D-Sheet Piling in combination with the Deltares Probabilistic Toolkit yields many opportunities. Some limitations although exist. Table 1.2 lists the possibilities and limitations regarding the applied software tools.

Possibilities	Limitations
Relatively less time- and effort consuming	Uncoupled soil springs, hence no arching.
	Limited analysis of soil-structure interaction
Simplified use	Relatively developing new software (beta-version(s))
Many available reliability methods	No interpretation of results for partial safety γ_{xn}
Can be coupled with Python and other executables	Requires conversion script(s) for FEM
	Memory exception errors(s) during large computations
	Less applicable for complex geometry

Table 1.2: Possibilities and limitations of the Deltares Probabilistic Toolkit running a D-Sheet Piling interface model.

Roughly, this method contains a prior analysis and a posterior analysis. Figure A.1 in appendix A presents flow charts of the case study approach. A few aspects are performed before the case study analyses are performed. A cross-sectional and environmental analysis is conducted in order to obtain the correct parameters for the model. Several steps are outlined in this approach:

1. Firstly, an early analysis of the quay wall is performed. The considered reference case is recalculated and the obtained results and model elements are verified according to the originally obtained results from Deltares report [71] [72].
2. Secondly, a normative failure mechanism is found through investigation of the model. This quay wall failure mechanism is translated into a limit state function.
3. Before the analysis a constitutive model is chosen. This model is used to generate the model's response as results from the loads, geometry and soil parameters.
4. A limit state function of the normative failure mechanism with a stochastic load parameter S is used in the prior analysis. The analyses are initially performed for a reference period of one year.
5. The computation output is validated and evaluated. Accordingly, an a-priori reliability for a reference period of one year is found.
6. Thereafter, an updated model is composed with appropriate random load variables and limit state function.
7. A posterior analysis is performed. The effects of past performance are taken into account. The latter is realised by means of an observation state function $h(X)$ and Bayesian updating. This observation function describes the information on survival(s).
8. New output is obtained and validated. Eventually, an a-posteriori annual reliability index is derived.

First Order Reliability Method (FORM) is adopted for the computation of the annual failure probability c.q. reliability index and the sensitivity factors. Afterwards, numerical integration (level III approach) is used in the posterior reliability updating analyses. Together with the distribution types and the covariance, it is possible to derive updated design values for strength and resistance. The latter can be performed by means of a semi-probabilistic Level I approach (see chapter C.4.6). Engineers use

design values to perform unity checks for e.g. stability. Furthermore, both prior and posterior analysis yield insight in the change of variables over time.

The remaining service life of an existing structure is oftentimes unknown on beforehand. Hence annual-based output from prior and posterior analyses are used for comparison and evaluation. Considering a reference period of 50 years, results are eventually compared and evaluated with the acceptable annual reliability index for existing quay walls at a certain moment in time t_n . Advantageously, annual failure probabilities are depending on the degree of dependence, easily translated for longer reference periods.

The validation of the achieved results happened in close communication with the company supervisor. Other supervisors might eminently be involved when they were familiar with the modelling toolkit. As follows, the evaluation of results happens in order to make sound decisions on (re-)calculations or adjustments in the parameter field. The progress is reported simultaneously with the adjustments that were made.

1.4.4. Case: single anchored sheet piling system

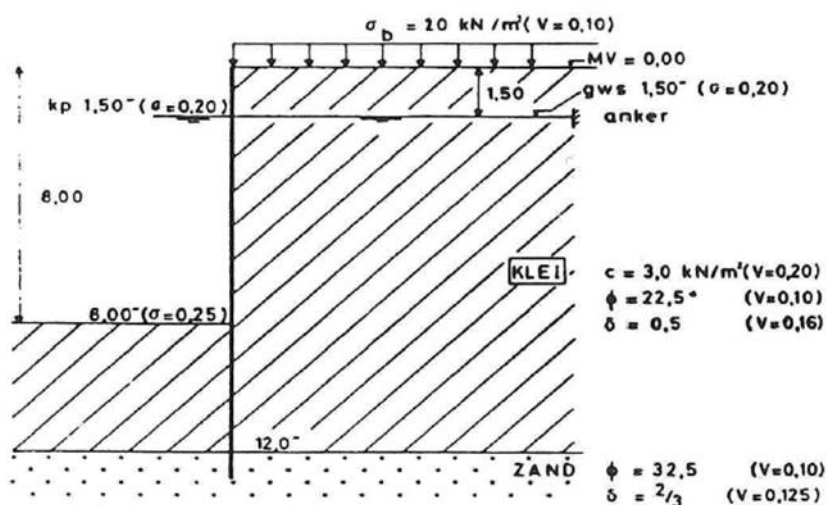
The reference case concerns a single anchored sheet piling system in typical soil conditions in older Rotterdam harbours. To simulate a representative Dutch quay cross-section, few aspects are strongly considered. Older harbours, which are predominantly located near the city centre, are typically built in soil layers such as clay or peat, on top of Pleistocene sand layers. Regarding the considered case, the top soil layers consist of clay, whereas the lower layers consist of sand. In addition, as in many cases within the Netherlands, this reference case has a high ground water table. The studied cross-section was analysed by GeoDelft (currently Deltares). Several cross-sections among which this quay wall cross-section for example 3 had been investigated. This was done at the beginning of the 1990s for the proposition of a level I probabilistic design code [72, p. 51]. The latter means a design procedure that was based on partial safety factors which were derived by conducting failure probability calculations. Furthermore, this research was commissioned by the 'Bouwdienst' of the Dutch Ministry of Infrastructure and Water Management (Rijkswaterstaat) [71].

In this former approach the (nowadays obsolete) 'DAMWAND' calculation program was used. This program used a spring model in which the sheet pile was considered as a beam supported by uncoupled springs. Within this program the soil reaction between the maximum passive and minimum active soil pressure was assumed to behave linearly. The latter is explained by figure C.32 in chapter C.5.4.

In the development of Dutch norms, a few cases were considered in the report by Deltares. This reference case is defined in [72, p. 54]. Figure 1.3 and 1.4 describe the cross-section that is used in the first analysis.

For the calculations of the quay wall section, a set of input parameters is used. Table 1.3 from [72, p. 58] summarises the values that are used for the deterministic analyses.

In this research the reconsidered case is modelled with D-Sheet Piling, which is to a small extent comparable to the obsolete program DAMWAND. The horizontal anchor in figure 1.3 is modelled as a spring support. At first, an infinite axial anchor stiffness is assumed. Within this program, $KA = 5 \cdot 10^9 \text{ kN/m}^1$ is realistically assumed for the translation stiffness. The rotation stiffness is conversely assumed to be zero for the same verification purposes. Stiffness values of the anchor(s) are chosen as such to realistically simulate the deformation behaviour of the elastically supported beam. The analyses are done simultaneously by applying the Blum method and the subgrade reaction method. The first-mentioned method is performed by hand and in Excel, while the latter method is performed with D-Sheet Piling. Importantly, these deterministic calculations use the adjusted design values X_{d^*} as is performed in [72]. Accordingly, results are validated with the output in the Deltares report (see [72, p. 55] onward).



Figuur 3.6 Kademuur

Figure 1.3: Example 3 from [72, p. 51] for the development of the CUR design procedure by GeoDelft.

Parameter	Symbol	Mean $\mu(i)$	Adjusted design point $X_{d^*}(i)$	Unit
Cohesion	c_1	3.0	1.89	kN/m ²
Angle of internal friction	ϕ_1	22.5	15.51	°
	ϕ_2	32.5	22.41	°
Angle of wall friction	δ_1	0.50	0.36	-
	δ_2	0.667	0.53	-
Surcharge load	q	20.0	23.28	kN/m ²
Retaining height rel. to ground surface level	h	-8.00	-8.51	m
Water level active side	w_a	-1.50	-1.17	m
Water level passive side	w_p	-1.50	-1.83	m
Layer separation	s	-12.00	-12.33	m
Specific weight	γ_1	18.0	18.0	kN/m ³
	γ_2	20.0	20.0	kN/m ³
Bending stiffness	EI	$5.0 \cdot 10^5$		kNm ²
Modulus of subgrade reaction	K_1	$1.0 \cdot 10^3$		kN/m ³
	K_2	$1.0 \cdot 10^4$		kN/m ³

Table 1.3: Input parameters according to [72].

The calculated results from [72] appeared to correspond to the recomputed deterministic results. The results of the deterministic Blum- and D-Sheet Piling computations can be found in appendices F-G.

1.5. Thesis outline

Chapter 1 covers the research background, the problem definition, objective and the research questions and serves as the research design of this Master's thesis. Secondly, chapter 2 presents the theoretical framework of the research subject. Elaboration on the theoretical background that is obtained from literature study, is provided in the appendices. By addressing topics such as the general structural safety philosophy, safety of geotechnical structures and the theory about quay walls in chapter 2, the reader gets familiar with the previous studies related to this subject. Also, pragmatic approach of design and maintenance of a quay wall and the reliability engineering methods are discussed. Finalising the first research part, a review on the previous studies, computation methods, uncertainties and the new engineering method of existing structures is given. Chapter 2.3 gives the reader a clear insight into the overview of the treated research subjects

The second part of the research is presented in chapter 3. This chapter covers the case description, starting points and boundary conditions for the deterministic and probabilistic analyses. These analyses are concerned with the described fictitious reference case. This is a simplified representative case at which the calculation steps are tested. The scope boundaries are focused on fictitious reference case.

The fictitious representative reference case is priority analysed. Here the effects of survived years are not yet considered. However, cross correlations and model uncertainty are included. This is done in chapter 3. From research but from practical viewpoint as well, the latter is performed to obtain realistic starting points for the reliability updating method. Afterwards, past performance including:

- Effect(s) of the reference period
- Effect(s) of survived years

are studied in chapter 6. The influence of time-related phenomena are subsequently discussed in chapter 7. These time-related phenomena include the effects of degradation. The time-related effects are studied in order to visualise a realistic time-dependent behaviour of the representative considered case. By then, the principles of reliability updating have already been explained in chapter 2.

Afterwards, posterior analyses with modelled uncertainties, new starting points, an updated method and boundary conditions are conducted. One finalising issue in this thesis is the translation of this reliability updating method into the engineering handbook. The last part of chapter 7 briefly focuses on the application of the results from chapter 7 in the semi-probabilistic method. Lastly, discussions on the results, conclusion and recommendation are addressed in chapter 8. In the recommendations, a brief preview of an extended follow-up research is provided in section 8.3.1.

2

Theoretical framework

2.1. Introduction

In the past, a substantial amount of theoretical background has been developed regarding the subject of this research. In appendix C, a literature review is presented. In here, it is attempted to draw a detailed theoretical foundation for the continuation of this research about reliability of quay walls. Different basic subjects were treated. In section 2, relevant aspects of the literature review are mentioned. Additionally important elements from previous researches are considered. For the purpose of the case study methodology, knowledge gaps in reliability updating of quay walls are summarised in section 2.3.

2.2. Short summary of literature review

Up until thirty years ago (1990s), quay walls were mostly designed in a deterministic way. Overall factors of 1.5 to 2.0 were chosen in accordance with partial safety factors for steel structures. For other materials, data obtained from experiments and practical experience from comparable projects were used to derive partial safety factors. As structures became larger and the consequences of failure were devastating, many projects were designed on acceptable failure risk (see Eastern Scheldt barrier in section C.2.4). Reliability engineering became more interesting and methods that were developed by for instance Hasofer & Lind (see section C.4.5) were applied in the development of international standards. The Eurocode series for example uses safety levels as consequence- or reliability classes. These safety levels and their corresponding reliability indices and partial factors are determined by means of reliability methods applied on reference projects. Accordingly, five reliability methods are arguably used: Risk-based approach (level IV), numerical approach (level III), by approximation (level II), semi-probabilistic approach (level I) and deterministic approach (level 0).

Focusing on the port of Rotterdam, different types of quay walls exist within the 43 kilometres long area. A significantly large part of existing quay walls is located in the Western areas such as Waalhaven, Eemhaven, Europoort (see section C.16). These quay walls are built between the 60s and 80s and at the end of the intended design life time. Most of the quay walls constructed in that period are anchored (combined) sheet piling systems. A part of them uses a combined anchor system with a relieving platform supported by piles. Evaluation of these older commercial quay walls is necessary in order to make an appropriate decision between replacement, repair or no actions. Current analytical methods use partial safety factors and additional margins in order to meet the required safety level as is outlined in section C.3. Part of these methods is explained in section C.5.1. Design calculations should satisfy the reliability levels as is explained before.

The safety philosophy for newly constructed Dutch quay walls is included in CUR 211 and the Dutch national standard for geotechnical structures NEN 9997-1 which is derived from Eurocode EN 1997.

Some norms such as NEN 8707 account for previous actions on geotechnical structures and are therefore used in the reassessment of existing quay walls. By the development of scientific knowledge and programming, different calculation methods and tools have been obtained. In correspondence with the NEN, Dutch practical guidelines (NPR) and design handbooks (CUR 211) are used for the calculation procedures. Currently, procedures on how to deal with quay wall loads of significant magnitude which are observed from historical records, proof loads or earthquakes are unfortunately not defined in the guidelines. The research methodology that is described in chapter 1.4.3 explains the approach that is used to investigate the quantifiable effect of taken into account the past performance. So the extensively described theory in this chapter, has contributed in the composition of the case methodology.

2.3. Knowledge gaps in reliability updating of quay walls

Previous studies among which [64], [25], enlightened important aspects regarding reliability-based assessments of existing quay walls. New insight in reliability updating was obtained through various analyses. Based on findings from the thesis by Roubos in 2019 [64, p. 172], topics for further research are mentioned:

- Current quay wall design methods accounting for past performance, are lacking.
- Many existing quay walls in the port of Rotterdam do not comply with modern code requirements for new structures.
- The current guidelines do not account for a decrease in epistemic uncertainty in strength parameters due to a successful service history or past performance.

This research, as has been described in chapter 1, studies the effects of survived years on the time-dependent reliability index and sensitivity values. In addition, this research is considered from a probabilistic viewpoint. By performing recalculations of the considered reference study, initial assumptions are established for the representative case, among which a reliability index given a reference period. By studying the effects of the reference period t_{ref} one is importantly able to translate the reliability to an annual basis. The following aspects relating to past performance are considered in subsequent order:

- The effect(s) of reference period t_{ref}
- The effect(s) of survived year(s)
- Time-related effects among which the effects by degradation

The reference case is initially reconsidered. The translation of a lifetime reliability index to an annual value results in a less time-consuming approach in the final calculation(s). Other aspects might be useful in the research and assessment of past performance. A few examples are mentioned. Fragility curves might be used to illustrate the reliability as a function of the governing load parameter. Proof loading can be useful in the assessment of the residual strength of the structure. Equivalent length L_{eq} is a phenomenon to cope with in the case of reliability updating considering longitudinal objects. However, fragility curves, equivalent length L_{eq} and proof loading are beyond scope boundaries. Therefore, these aspects are not considered in this research.

3

Preliminary analyses

3.1. Introduction

The initial part of the current study considers the deterministic analyses, also mentioned as early analysis in this research. The early analysis considers the reference case and validates its results as is found by the CUR Commission 63 in [71] and [72]. Chapter 1.4.4 already described the characteristics of the case study. Section 3.2 describes the method for the early analyses. This chapter mainly focuses on verification of the results found in the research report [71] [72]. These verification's are realised by means of the Blum method and spring model in D-Sheet Piling, see [71] [72]. The approach corresponds with the methodology as outlined in chapter 1.4.3.

3.2. Deterministic analyses: Blum and D-Sheet Piling

Firstly, a calculation with the method of Blum is performed to verify the ascribed sheet pile tip level(s). This method models the single anchored sheet piling system as a static determinate beam [49] [87] on which the normative forces are acting. Figure 3.1 illustrates a cross-section with the horizontal stresses. Water has an isotropic stress behaviour. The horizontal soil stresses are derived for the situation without the influence of wall friction δ . This wall friction can be different for each soil layer, and depends on whether the active or passive side is considered. Hence, in the case without the effect of δ , horizontal stress are obtained by multiplying the vertical stresses with the active and passive earth coefficients, which are determined by equations 3.1 and 3.2 respectively.

$$K_a = \frac{1 - \sin(\phi_i)}{1 + \sin(\phi_i)} \quad (3.1)$$

$$K_p = \frac{1 + \sin(\phi_i)}{1 - \sin(\phi_i)} \quad (3.2)$$

The vertical stresses and thereby horizontal stresses can be expressed in terms of the embedded depth d_0 . Through a moment equilibrium around the anchor point D the embedded depth d_0 can be determined. Figure 3.1 shows the cross-section including the stress diagram which is used for the determination of the embedded depth d_0 with the Blum method. Appendix F includes the Blum calculations.

The embedded depth d_0 is subsequently used in the horizontal force equilibrium to derive the anchor force F_A . Appendix F provides results that are obtained with the Blum method. The sheet pile

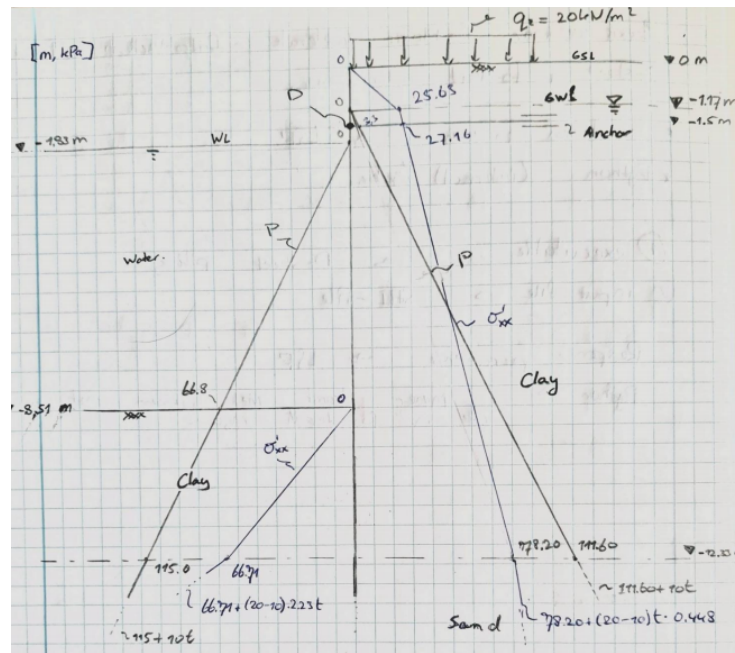


Figure 3.1: Cross-section of the case with the stress diagrams that is used for the determination of the embedded depth (see appendix F).

length calculated with the Blum method shows a small difference compared to the previous result. The penetration level D_1 , as is found in the report [72], equals 15.1 m BGS. On the other hand, the result by the Blum method equals 16.35 m. This means that the Blum method yields a more conservative result.

The calculation with the spring model in D-Sheet Piling yields a minimum bending moment of -729.6 kNm for a sheet piling length of 24.0 m. This clarifies the similar result for D_3 found in [72, p. 55], see table 3.1. Appendix G presents the results with the deterministic D-Sheet Piling computations.

Example	D_1 [NAP-m]	D_2 [NAP-m]	D_3 [NAP-m]
3	-15.1	-19.0	-24.0

Table 3.1: Penetration levels relative to ground surface level determined according to different calculation models

In the table above:

- D_1 : minimum required penetration level according to the Blum method
- D_2 : an intermediate penetration level
- D_3 : penetration level with a minimum field moment

The anchor force F_A is derived by horizontal force equilibrium in appendix F and can be used for the design of the anchor geometry. Given these results, one may confirm that the used model corresponds with the case as is presented in [71] [72, p. 58]. With the bending stiffness EI and the resulting maximum bending moment, one is able to determine the required sheet pile profile for a similar case.

By incorporating the anchor force F_A , a kink should be observed in the net shear force diagram (q [kN/m]). Subtracting the anchor force F_A from the shear force which is calculated at -1.5 m yields the maximum shear force V_{max} to be 308.91 kN. The maximum moment M_{max} is found after integration of the shear force diagram between $x = 0$ m and $x = 16.35$ m.

Output parameter	Value	Unit
Embedded depth d_0	7.81	m
Minimum penetration level L	16.35	m
Anchor force F_A	329.29	kN
Maximum shear force V_{max}	308.91	kN
Maximum bending moment M_{max}	1214.76	kNm
Maximum displacement u_{max}	n.a.	mm

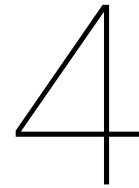
Table 3.2: Calculation results found with Blum method

For the deterministic D-Sheet Piling calculation of the sectional forces V_{max} , F_A and M_{max} a penetration level of -15.1 m is assumed. The characteristic values X_k from table 1.3 are used. The anchor is in the D-Sheet Piling assumed to be infinitely stiff in axial direction ($KA = 5 \cdot 10^9$ kN/m²).

Output parameter	Value	Unit
Embedded depth d_0	6.49	m
Minimum penetration level	GSL-15.10	m
Anchor force F_A	279.34	kN
Maximum shear force V_{max}	236.16	kN
Maximum bending moment M_{max}	697.79	kNm
Maximum displacement u_{max}	26.30	mm

Table 3.3: Calculation results found with subgrade reaction method

From table 3.2 and 3.3 it can be stated that results from both methods do differ, but are however still in line with the results obtained by GeoDelft [72, p. 59 - 62]. The large stiffnesses which were applied for both the anchor and sheet pile influence these differences. Besides, the differences between the results obtained with Blum and D-Sheet are caused by the numerical integration of the resulting stress diagram and V-diagram (which were part of the Blum analysis). Hence, differences are largely due the applied model input and the inaccuracies of a manual Excel calculation. Further results are provided in appendix F and G.



Prior analysis

4.1. Introduction

In the previous content, the reference case for the established CUR guidelines was studied. The deterministic analyses are performed with Blum and D-Sheet Piling. Both analyses are conducted with adjusted design values as illustrated in chapter 3. As a result, the obtained results correspond with the information the report by GeoDelft. This chapter introduces the application of reliability calculus in the considered reference case. In view of the latter, uncertainties and randomness are included in the definition of the calculation variables. Section H.1 initially illustrates the approach for the limit states regarding deformations and passive soil stress. Section H.2 will afterwards focus on the limit states regarding the strength of the steel front wall. In the latter approach, correspondence with the CUR guidelines is sought [71, p. 21].

For the reliability calculations, choices are made regarding the considered failure mechanisms. In practice, few failure mechanisms occur often. For the considered case, a non-finite element tool by the name of D-Sheet Piling is used. D-Sheet Piling considers a number of failure mechanisms among which yielding of the wall, anchor failure, Bisschop, Kranz stability. These failure mechanisms are as described in [19] as well. In [22] and [71] a few normative limit states are considered. Appendix D provides the fault tree and highlights the positions of the quay wall failure mechanisms that are considered in this case study.

- Loss of stability due to yielding of soil or loss of passive resistance (ULS)
- Loss of stability due to yielding of sheet pile wall (ULS)
- Excessive deformations due to incapability of the structural material or borehole (SLS)

Selection of the failure mechanisms is realised according to the design as described in [71]. The computations in the Deltares Probabilistic Toolkit are performed with the input parameters summarised in table 4.1. These parameters are obtained from the Deltares report [72] and use normally distributed random variables for the uncertainties. These uncertainties include among others: the cohesion, angle of internal friction, wall friction, loads and layer thicknesses. The specific weights, bending stiffness, moduli of subgrade reaction are characterised as deterministic variables. As follows, the cross-section corresponds with [72, p. 58]. The anchor stiffness is kept infinitely large with a $KA = 5 \cdot 10^9$ kN/m² [72, p. 51].

Parameter	Symbol	$\square(i)$	$\square(i)$	$\mathbf{X}_{kar}(i)$	$\mathbf{X}_d(i)$	$\mathbf{X}_{d^*}(i)$	Unit
Cohesion	c_1	3.0	0.60	2.02	1.89	1.89	kN/m ²
Angle of internal friction	ϕ_1	22.5	2.25	18.81	15.51	15.51	°
	ϕ_2	32.5	3.25	27.17	22.41	22.41	°
Angle of wall friction	δ_1	$0.50\phi_1$	0.16μ	0.36	0.44	0.36	-
	δ_2	$\frac{2}{3}\phi_2$	0.125μ	0.53	0.60	0.53	-
Surcharge load	q	20.0	2.0	23.28	22.16	23.28	kN/m ²
Retaining height rel. to ground surface level	h	-8.00	0.25	-8.41	-8.51	-8.51	m
Water level active side	w_a	-1.50	0.20	-1.17	-1.17	-1.17	m
Water level passive side	w_p	-1.50	0.20	-1.83	-1.83	-1.83	m
Layer separation	s	-12.00	0.20	-12.33	-12.33	-12.33	m
Specific weight	γ_1	18.0		18.0	18.0	18.0	kN/m ³
	γ_2	20.0		20.0	20.0	20.0	kN/m ³
Bending stiffness	EI	$5.0 \cdot 10^5$					kNm ²
Modulus of subgrade reaction	k_1	$1.0 \cdot 10^3$					kN/m ³
	k_2	$1.0 \cdot 10^4$					kN/m ³

Table 4.1: Input parameters [72, p. 53].

The reliability calculation is performed with response parameters including deformations and bending moments. These are obtained with the input parameters as defined in table 4.1. Appendix H describes the procedure in which necessary assumptions are derived. These assumptions include the required embedded depth of the sheet pile, overall safety factor on the bending moment. By means of considering: passive soil resistance and excessive deformations, one is able to obtain the required information. With the required information, the initial 50 year reliability, sensitivity factors and corresponding partial factors are derived. Naturally, the latter implicates the situation where eventually one limit state is considered. Section 4.1.1 describes the procedure in which the limit state is analysed. The probabilistic analyses do not take into account the variations in longitudinal direction of the sheet pile wall.

4.1.1. Approach CUR 166 by GeoDelft and C69

Three failure states are encountered with the spring model in D-Sheet Piling. The analyses are provided in sections H.1 and H.2 in the appendix. The third limit state is considered with yielding of the front wall. Evaluation of this failure mechanism is performed by means of load- and strength variables accounting for uncertainties (see table 1.3). The calculated reliability in sections H.1 and H.2 appears to be significantly high relative to the values described in [71] [72]. The necessary dimensions are derived from deterministic analyses. In the old CUR-approach, overall safety factors were commonly used. Characteristic values (5%- and 95%-fractile values) for the strength, load and geometry are used for the determination of the sheet pile length, moment capacity and maximum anchor force. The commonly applied overall safety factors in the Dutch engineering field were [71, p. 18, 28]:

1. Yielding of the soil $\gamma_{gr} \approx 1.5$
2. Moment capacity $\gamma_m \approx 1.1 \text{ to } 1.5$
3. Anchor capacity $\gamma_a = 1.5 \text{ to } 2.0$

Characteristic values for the parameters X_{ki} are used in the estimation of the required sheet pile profile. In addition, the yield stress of steel is, in accordance with [71], assumed as a deterministic variable. The ratio of the maximum- and mobilised passive soil resistance is equivalent to γ_{gr} . Given this latter fact, the length of the sheet pile can be varied until equation 4.1 holds:

$$\gamma_{gr} = \frac{F_{p,max}}{F_{p,mob}} \quad (4.1)$$

Eventually, the initial length L of the sheet pile is determined. At this stage it is confirmed that the penetration level is GSL-15.1 m (see 3.2). With the derived sheet pile length, the maximum bending moment M_{max} in the sheet pile is found with a deterministic calculation in D-Sheet Piling. The bending moment capacity, at which yielding at the outer fibre occurs, is additionally obtained through multiplication of the maximum bending moment capacity with the overall safety factor (see equation 4.2).

$$M_{yield} = M_{max} \cdot \gamma_m \quad (4.2)$$

At first the overall safety factor γ_m is set at 1.5. Afterwards, this calculated bending moment capacity is used for the determination of the elastic section modulus $W_{el,y}$. Initially, a value of $W_{el,y} = 4453.98 \cdot 10^3 \text{ mm}^3$ was found. This value yielded a high reliability value $\beta_{50} = 7.69$. This value is significantly different than the values $\beta_t = 4.5$ and $\beta_t = 4.3$ from the research report "Veiligheid van damwandconstructies" [71] and CUR166 [15] respectively.

$W_{el,y}$ is modified after using a deterministic steel yield stress with steel quality S235. The bending moment capacity is redetermined. A smaller value for the safety factor $\gamma_m = 1.2$ is applied. This value is used as a safety factor for sectional forces V and D [15, p. 46]. Accordingly, a $W_{el,y} = 3563.18 \cdot 10^3 \text{ mm}^3$ and a $\beta_{50} = 5.5$ are found. Hence, still a notably large value has been found. Eventually, the overall safety factor for the bending moment is set to $\gamma_m = 1.1$ (according to [71, p. 28]). An elastic section modulus $W_{el,y} = 3266.25 \cdot 10^3 \text{ mm}^3$ and consequently a reliability $\beta_{50} = 4.53$ is obtained. This value agrees with the prescribed value $\beta_t = 4.5$ from the research report [71] and marginally differs from the value which is found in the report $\beta_t = 4.2$. The broad view of the obtained sensitivity values agrees with the sensitivity values which were obtained in the research report "Veiligheid van damwandconstructies" [71]. In these outcomes, the internal friction angle of clay ϕ_1 has somewhat more influence on the limit state. This is at the expense of the cohesion of clay c_1 . However, the collective influence of the governing parameters are roughly the same (see table 4.2). The latter might be due to model differences between the computation software "DAMWAND" used at that time and the currently used D-Sheet Piling.

Other aspects, such as the absence of geometrical stochastic parameters, declare the differences between the α -values. The excavation depth $h \sim N(-8, 0.25)$ and the layer separation level $s \sim N(-12, 0.2)$ are not taken into account, since these parameters give convergence problems. No reliability index can be calculated with the involvement of s and h in the FORM-computations. Similar approach, as illustrated above, can be applied on a different example. This is shown in appendix I.1.

The continuation of this case study is concerned with example 3 representing a quay wall from CUR class III. Table 4.3 summarises the results of the FORM-analyses considering example 3 from [72]. Table 4.3 includes the safety factors derived with the level I reliability method C.4.6.

Given table 4.3, one observes minor differences between the partial safety factor(s) from CUR 166 and the safety factors that are derived with the calculated α -values (from table J.1 in appendix J) and equations 4.3 and 4.4. The factors in the last column of table 4.3 are prescribed for geotechnical A2-computations (GEO) [13] [17] with a spring supported beam or D-Sheet Piling. Descriptions are provided in the standard [33, p. 259]. The characteristic values X_k and design values x^* of the dominant stochastic parameters are used in the derivation of the partial factors γ_x . Equations 4.3 and 4.4 use

According to:	β_{50} [-]	
GeoDelft report	4.5	
CUR class III	4.3	
FORM given $\gamma_m = 1.1$	4.53	
	Calculated	Geodelft
Variable	α [-]	α [-]
Cohesion of clay: c_{clay}	0.189	0.41
Internal friction angle: ϕ_{clay}	0.825	0.69
Wall friction angle: δ_{clay}	0.147	0.17
Uniform load q	-0.252	-0.24

Table 4.2: Comparison between the obtained β_{50} - and α -values (with FORM) and the values found in the research report "Veiligheid van damwandconstructies" [71].

the target reliability index β_t (CUR class III uses 4.3) for the derivation of the partial safety factors in the third column.

Case	Computed β_{50}	Partial factor γ_x	β_t acc. to CUR211	Prescribed γ_x
Example 3: Quay wall (RC3/CURIII)	4.53	$\gamma_{\phi_{clay}} = \frac{18.81}{22.5(1-0.825-0.10-4.3)} \approx 1.30$ $\gamma_q = \frac{23.28}{20(1-0.252-0.10-4.3)} \approx 1.05$	4.3	$\gamma_{\phi'} = 1.20$ $\gamma_q = 1.00$

Table 4.3: Comparison of the reliability indices and the resulting partial factors for the dominant load and resistance parameters. Prescribed values are conform [17, ch. 6.4.4].

$$\gamma_S = \frac{S^*}{S_k} = \frac{\mu_S(1 - \alpha_x \beta_t V_x)}{\mu_S + k_S \sigma_S} \quad (4.3)$$

$$\gamma_R = \frac{R_k}{r^*} = \frac{\mu_R + k_R \sigma_R}{\mu_R(1 - \alpha_x \beta_t V_x)} \quad (4.4)$$

Afterwards, the situation is treated in which the section modulus is selected based on ArcelorMittal catalogue [8]. The sheet pile for the cross-section from example 3 is selected in accordance with the calculated moment of inertia I_y . The Young's Modulus of steel is well-known and is 210 GPa = 210·10⁶ kN/m².

$$I_y = \frac{EI}{E} \quad (4.5)$$

Example 3 has an $EI = 5.0 \cdot 10^5$ kNm². Eventually, the moment of inertia becomes $I_y = 238095.24 \cdot 10^4$ mm⁴/m¹. For the reference case (example 3), a comparable combined wall is selected. In this case a tube $\varnothing 1,016 \times 14.0$ mm in combination with 2xAZ25-800 with a $W_{sys} = 4770 \cdot 10^3$ mm³/m¹. FORM-computations are performed with the new sheet pile profile, table 4.4 presents the calculated and comparative results.

Case	Computed β_{50}	Partial factor γ_x	β_t acc. to CUR211	Prescribed γ_x
Example 3: Quay wall (RC3/CURIII)	8.37	$\gamma_{\phi_{clay}} \approx 1.32$ $\gamma_q \approx 1.07$	4.3	$\gamma_{\phi'} = 1.20$ $\gamma_q = 1.00$

Table 4.4: Secondary comparison between the reliability indices and the partial factors for the dominant load and resistance parameters. Here, a selected ArcelorMittal profile is applied. Prescribed values are conform [17, ch. 6.4.4.].

4.2. Influence of correlated variables

The previous calculations assumed uncorrelated parameters. In most cases however, probabilistic analyses require information about the correlations. These present the mutual dependency between two stochastic variables and are nominally measured with the correlation coefficient ρ [42, p. 54]. Let us assume the stochastic variables for the internal friction angle and the wall friction angle. Their correlation coefficient $\rho_{\phi\delta}$ is calculated with equation 4.6.

$$\rho_{\phi\delta} = \frac{COV(\phi, \delta)}{\sigma_{\phi}\sigma_{\delta}} \quad (4.6)$$

With the numerator representing the covariance between the two stochastic variables and the denominator the product of their standard deviations. By way of example, the correlation coefficient ρ describes the coherence of the scattered data points as is shown in figure 4.1 [24].

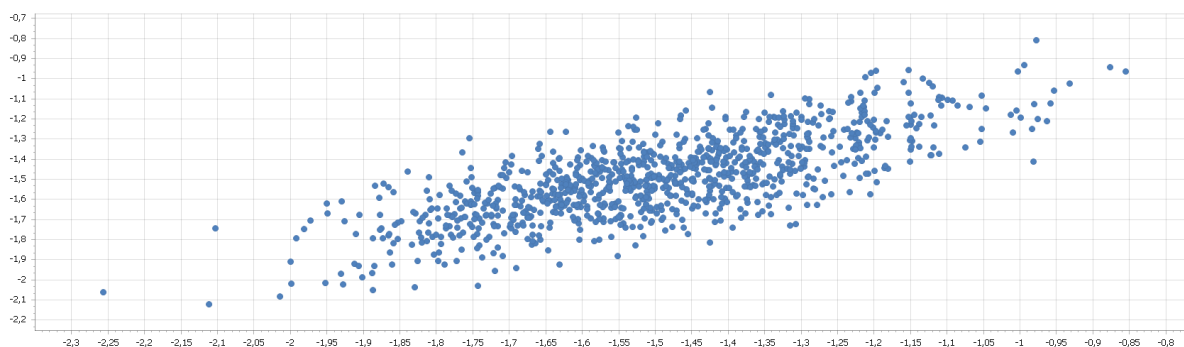


Figure 4.1: Scatter plot of positive correlation $\rho = 0.75$ between two stochastic variables.

The different correlation values mean the following:

- $\rho = 1$: positive linear dependence
 - $\rho = -1$: negative linear dependence
 - $\rho = 0$: no correlation and hence independence
- By definition it holds $-1 \leq \rho \leq 1$ [42]

The correlations summarised in table 4.5 are conform practical examples as mentioned in [64], [89] and based on large statistical analysis of large data sets of information. This information is for example obtained from various laboratory tests. This information is in the hands of the municipality of Rotterdam ('Gemeentewerken 2003').

These cross-correlations are determined, presuming the following information:

	Cohesion clay	ϕ clay	ϕ sand	Water level active side	Water level passive side	Uniform load q	δ clay	δ sand	
Cohesion clay	1	-0.65	0	0	0	0	-0.325	0	0
ϕ clay	-0.65	1	0	0	0	0	0.5	0	0
ϕ sand	0	0	1	0	0	0	0	0.66667	0
Water level active side	0	0	0	1	0.75 ¹	0	0	0	0
Water level passive side	0	0	0	0.75 ¹	1	0	0	0	0
Uniform load q	0	0	0	0	0	1	0	0	0
δ clay	-0.325	0.5	0	0	0	0	1	0	0
δ sand	0	0	0.66667	0	0	0	0	1	0

¹ This correlation coefficient is approximated on the basis of statistical analysis of the water head differences within the port of Rotterdam [64, p. 77].

Table 4.5: Correlations between the input variables.

1. The degree of correlation $\rho(w_a, w_p)$ depends on the permeability of the soil, retaining wall and the effectiveness of a drainage system [80, p. 48]. water head differences are assumed as non-dominant since the water level on both the passive and active side are non-dominant load variables (see table J.1). The value of $\rho(w_a, w_p) = 0.75$ is found in [64] and is only valid when the water level differences are non-dominant loads.
2. Given the Mohr-Coulomb shear failure criterion [82]: $\tau_f = c + \sigma' \tan(\phi)$, one finds a smaller value of the cohesion given a larger value of angle of internal friction. These two variables are negatively correlated to a certain extent [89] [64].
3. The wall friction angle is dependent on the magnitude of the angle of internal friction [49] [82] and in that way, to some extent correlated to the cohesion as well.

Example 3 from [72, p. 54] is recalculated with correlated variables according to table 4.5. Input variables from table 4.1 are applied. Consequently, different values are found for the reliability index, sensitivity values and design values. The results are listed in table J.2 in appendix J. Again, comparison is made between the target values, the prescribed partial safety factors and the calculated values. Table 4.6 presents an overview.

The results show that correlations between variables have resulted in an increased reliability index for example 3. As can be observed in table 4.5, the majority of the variables is mutually independent. For example 3 mainly resistance parameters such as ϕ_i , δ_i and c_1 are correlated to a significant extent. Given the latter, the stability of the structure is more likely to increase and hence resulting in a larger reliability index.

The load variables w_a and w_p are inter-correlated and almost positively linear dependent. As a result, various influence factors (slightly) altered. The influence of the water levels on both sides is negligible. In addition, the cohesion of clay became more correlated with the load parameter $\left(S = \frac{M_{max}}{W_{el,y}}\right)$ of the limit state function H.3. The latter can be seen in the change of sign of α_{c_1} (from positive to negative).

Case	Computed β_{50}	Partial factor γ_x	β_t acc. to CUR211	Prescribed γ_x
Example 3: Quay wall (RC3/CURIII)	4.97	$\gamma_{\phi_{clay}} \approx 1.23$ $\gamma_q \approx 1.036$	4.3	$\gamma_{\phi'} = 1.20$ $\gamma_q = 1.00$

Table 4.6: Summary of output taking into account the correlations between variables. Prescribed values are conform [17, ch. 6.4.4.].

For example 3 the same calculation is performed taking into account the selected sheet pile profile. Table 4.7 summarises the results.

Case	Computed β_{50}	Partial factor γ_x	β_t acc. to CUR211	Prescribed γ_x
Example 3: Quay wall (RC3/CURIII)	8.62	$\gamma_{\phi_{clay}} \approx 1.212$ $\gamma_q \approx 1.07$	4.3	$\gamma_{\phi'} = 1.20$ $\gamma_q = 1.00$

Table 4.7: Secondary summary of output taking into account the correlated variables and using an ArcelorMittal sheet pile profile. Prescribed values are conform [17, ch. 6.4.4.].

4.3. Influence of the model uncertainty

An other important aspect in the design of a earth-retaining structure is the model uncertainty. The model uncertainty can be included through adding a model factor and has proven to be inherent in limit state computations of quay walls [64] [67]. The model uncertainty factor accounts for the unforeseen effect(s) of a (structural) object in practice such as randomness in weather, loads and the development of the physical environment including soil behaviour. As a matter of fact, there is an uncertainty related to the behaviour of the design model compared with the cross-section in practice. The disagreement between the calculated model results and the observed data or experimental results is accounted for by a model uncertainty factor.

In this case study the model uncertainty factor ξ is added in the probabilistic computations with the Deltares Probabilistic Toolkit. This model uncertainty factor is added in the numerator as an additional multiplier on the output parameter M_{max} . This latter seems plausible, since in reality large uncertainty is involved in the magnitude of the maximum bending moment over a time period. Therefore equation H.3 becomes:

$$Z = fy - \frac{\xi M_{max}}{W_{el,y}} \quad (4.7)$$

For the state yielding, this model uncertainty factor is found to be lognormally distributed in previous researches [64]. Accordingly, the expected value $\mu_\xi = 1.0$ and the standard deviation $\sigma_\xi = 0.1$. In the Joint Probabilistic Model Code [55] a $V_\xi = 20\%$ is recommended for steel plate elements. However, the latter holds because measurements showed that models used are rather conservative than optimistic [64, p. 113]. Thus, it is anticipated that in the most certain case a model factor equal to one is applied. Given correlated variables and a reference period $t_{ref} = 50$ years, new reliability indices and partial factors are computed. Table 4.8 summarises the obtained results for the case with example 3 from [72]. Detailed results such as the influence factors are added in table J.3 in appendix J.

Case	Computed β_{50}	Partial factor γ_x	β_t acc. to CUR211	Prescribed γ_x
Example 3: Quay wall (RC3/CURIII)	2.83	$\gamma_{\phi_{clay}} \approx 1.00$ $\gamma_q \approx 1.08$	4.3	$\gamma_{\phi'} = 1.20$ $\gamma_q = 1.00$

Table 4.8: Summary of output taking into account correlations between variables and the model uncertainty factor $\xi \sim (1, 0.1)$. Prescribed values are conform [17, ch. 6.4.4.].

The model uncertainty is an additional load parameter in the limit state, see table J.3. Noteworthy to illustrate is the difference between the convergence diagrams from the FORM computations with and without the model uncertainty factor ξ . Figures 4.2 and 4.3 show the convergence charts for both cases respectively. The model uncertainty definitely has an influence on the iterations until convergence is reached. The number of iterations is larger in the case including the model uncertainty factor. Figures J.3 and J.4 in appendix J show the influence circle histograms for both cases. All the same, it appears that the model uncertainty is having a large influence on the failure state: yielding of the front wall.

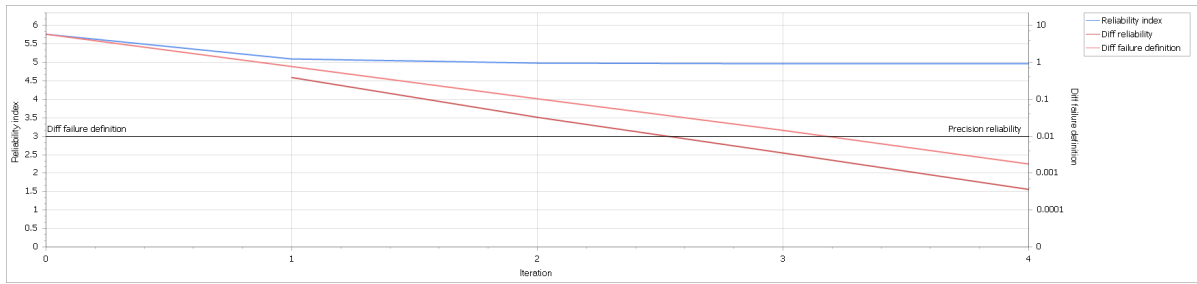


Figure 4.2: Convergence chart of the FORM analysis without model uncertainty, with on the horizontal axis: number of iterations, on the left vertical axis: 50 year reliability index and the right vertical axis: difference between subsequent standard normal design values.

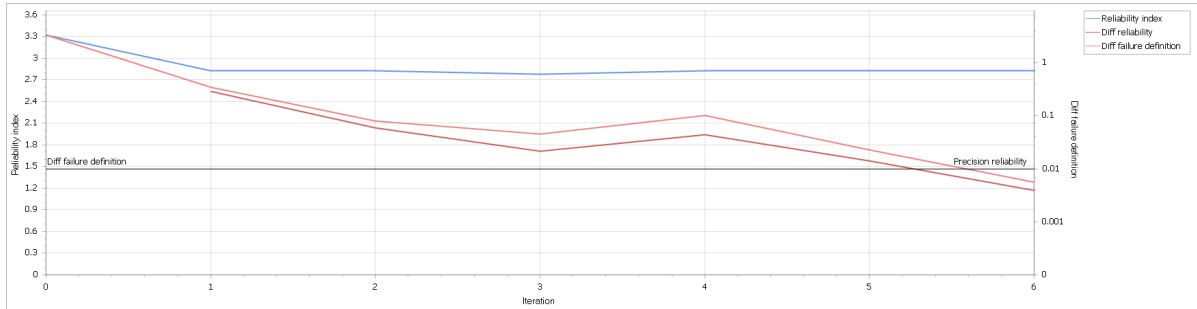


Figure 4.3: Convergence chart of the FORM analysis with model uncertainty.

At this stage, the computations are rerun for the model with the equivalent sheet pile profile. A combined wall, consisting of a tubular section and 2 x AU18-sections, was previously determined for example 3. Calculations, taking into account the correlations and model uncertainty, are performed for this model as well. Table 4.9 presents a summary of the results. As it appears, the partial safety factors γ_x have remarkably changed. The required safety factors have resulted in lower values than the prescribed values by NEN 9997-1. Appendix J contains table J.6 with further results.

Case	Computed β_{50}	Partial factor γ_x	β_t acc. to CUR211	Prescribed γ_x
Example 3: Quay wall (RC3/CURIII)	6	$\gamma_{\phi_{clay}} \approx 0.99$ $\gamma_q \approx 1.08$	4.3	$\gamma_{\phi'} = 1.20$ $\gamma_q = 1.00$

Table 4.9: Summary of output taking into account the correlations between variables and the model uncertainty factor $\xi \sim (1, 0.1)$. The results in this table are found with a selected sheet pile profile. Prescribed partial safety values are conform [17, ch. 6.4.4].

4.4. The influence of the reference period

In the previous considered cases the involved random variables were assumed as time-invariant. In order to perform an adequate analysis for the reliability over time, the influence of the reference period on the variance of the input variables must be examined. In this study the quay wall structure is considered for six reference periods t_{ref} :

$$t_{ref} = \{1, 5, 10, 25, 50, 100\} \text{ years} \quad (4.8)$$

Load parameters are oftentimes governed by aleatory uncertainty or random variability. The influence of the reference period on the failure probability, design points and sensitivity factors is mainly accompanied with the behaviour of time-variant load variables. At least time-variant on an engineering time scale. In many cases, extreme load(s) occur at an arbitrary moment in time. It is therefore conceivable that the probability of an extreme load (extremely low or high compared with the mean value) is lower during a short-term period. Furthermore, the mean quay load is oftentimes relatively smaller in more temporary sheet piling systems [72, p. 15]. As the considered reference period elongates, the probability of a larger mean value of the load variable μ_S increases. In practice it is oftentimes anticipated that this mean load value gets larger as the equipment size increases. This latter is a consequence of the increasing population(s) demand and due to increasing trading volume. The latter although might be affected by uncertain times as crises due to expected economic growth and consequently the enlarged capacity (e.g. scale of terrain equipment).

So it is expected that the mean value μ_S and standard deviation σ_S alter as the reference period increases. Time-related effects on the reliability are implicitly accounted for through adjustment of the governing load variable(s). One of the dominant load variables is the uniform load q . If model uncertainty is included in the probabilistic analyses, the influence of the load variable q will in the correlated case be equal to: $\alpha_q = -0.18$. The cohesion of the clay layer appears to have a large influence on the reliability value as well: $\alpha_{c_1} = -0.299$. The negative influence is caused by the negative cross-correlation with the dominant resistance parameter ϕ_1 (internal friction angle of clay). However, the uncertainty of cohesion is considered to be reducible since it is likely more feasible to acquire and include information which has a significant impact on the magnitude and uncertainty. Hence, uncertainties related to cohesion are epistemic and of time-independent nature and can be encountered through gathering and the interpretation of information. The model uncertainty factor ξ appears to have a significant impact as well. However, this model uncertainty is initially considered as time-invariant. At a later stage in this research, the effect of a time-variant model uncertainty is studied as well.

Therefore, only the load variable q is simulated for different reference periods. The considered reference periods are as earlier mentioned: 1, 5, 10, 25, 50 and 100 years. The normally distributed variable $q \sim N(20, 2)$ is assessed with FORM for $t_{ref} = 50$ years. A verification is performed with importance sampling using at most 600000 samples. Table K.1 and figure 4.7 in appendix K present the results of this verification. The characteristic load value q_k is determined by the 95%-fractile value since the variable is normally distributed for $t_{ref} = 50$ years. The characteristic value q_k is determined by equation 4.9:

$$q_k = \mu_q + k_q \sigma_q \quad (4.9)$$

where:

σ_q is a varying value and depending on the reference period (see table 4.11)

μ_q is an increasing value due to the likelihood of larger load actions in less temporary systems.

and $k_q = 1.645$ for normally distributed variables

A value of $q_k = 23.28 \text{ kN.m}^2$ is obtained. Same value is provided as input variable in table 1.3. The next step is to simulate longer or shorter time periods with the dominant time-variant variable q .

To simulate load distributions for different reference periods, a transformation method is required. A general applied statement for the transformation of a probability distribution function from a certain period T to a period nT is formulated by equation 4.10.

$$F_{nT}(x) = [F_T(x)]^n \quad (4.10)$$

Equation 4.10 can be applied in the reversed direction as well. Important to mention is that this statement assumes the load level to be independent and identically distributed in the successive intervals τ_i . The number of repetitions which occur during a reference period is determined as follows [42, p. 172] [42, p. 248]:

$$n_i = \frac{t_{ref}}{\tau_i} \quad (4.11)$$

So statement 4.10 solely applies for samples that are independent in different reference periods. Given the 50 year normal distribution $N(20, 2)$ for the permanent load q , one obtains the annual distribution by applying the transformation rule for the probability distribution function $F_T(x)$. Python is a programming tool which has been applied for the derivation of extreme value distribution. Initially, an extreme value distribution for the maxima considering $t_{ref} = 50$ years is simulated. This is realised by means of $n \cdot n$ samples with $n = 10,000$. The used parameters of the normal distribution are: $\mu_q = 20 \text{ kN/m}^2$ and $\sigma_q = 2 \text{ kN/m}^2$. The corresponding mean value and standard deviation of the 50-year maxima are $\mu_{max_q} = 27.7 \text{ kN/m}^2$ and $\sigma_{max_q} = 0.61 \text{ kN/m}^2$.

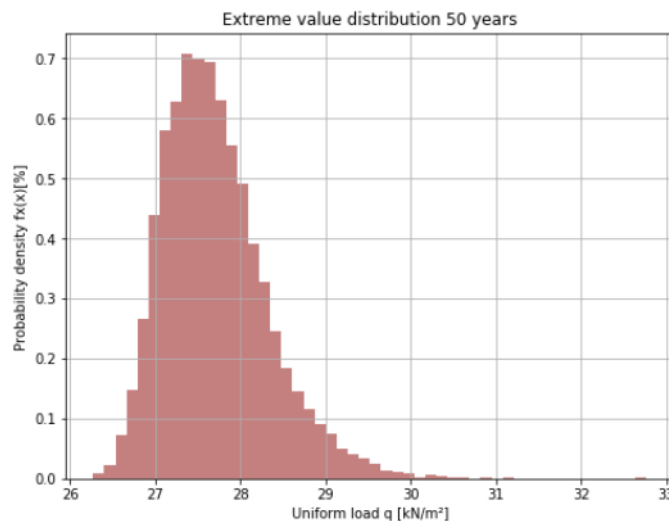


Figure 4.4: Probability density distribution of the 50 year maxima.

Figure 4.4 displays the probability density distribution of the maximum values for $t_{ref} = 50$ years. As can be observed, for large n the extreme value distribution $f_X(x)$ converges to a Type I extreme value distribution which is usually classified as a Gumbel distribution [42, p. 38]. Figure 4.5 exemplifies the transformation of an underlying normal distribution to an extreme value distribution for a varying quantity of interest (number of observations or samples) [48].

Accuracy is obtained by using a large sample n . The parameter of interest are the mode u and the shape factor a . Type I extreme value distribution has a range for x , $u \in (-\infty, \infty)$ and is valid for $a > 0$.

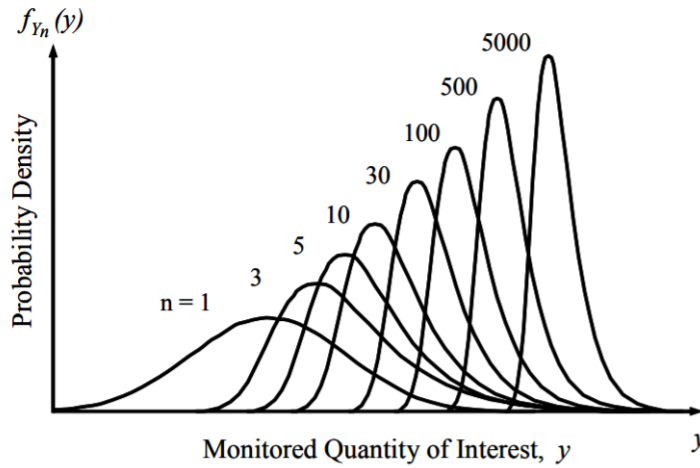


Figure 4.5: Transformation of an underlying normal probability density distribution to an extreme value distribution by number of samples [48, p. 133].

Both parameters are derived by standard equations 4.12 and 4.13 for Type I maxima (Gumbel) [42, p. 38].

$$\mu_x = u + \frac{\gamma}{a} \quad (4.12)$$

Here γ is the Euler-Mascheroni constant. This constant is approximately equal to 0.5772 [28].

$$\sigma_x = \frac{\pi}{a\sqrt{6}} \quad (4.13)$$

Consequently, the Gumbel distribution parameters can be determined: $u = 27.4$ and $a = 2.1$. These values are obtained by means of a large sample size n . If a larger n is used ($n > 10,000$) the values become more accurate. Given this information, the distribution parameters can be determined per reference period t_{ref} . This is performed according to the general rule stated by equation 4.10. Given a Gumbel probability distribution function and assuming that the maxima in different time intervals occur independently, one deduces the transformation equations as follows:

$$\begin{aligned} F_{nT}(x) &= [F_T(x)]^n \\ F_{nT}(x) &= [\exp[-e^{-a(x-u)}]]^n \\ F_{nT}(x) &= \exp[-ne^{-a(x-u)}] \\ F_{nT}(x) &= \exp[-e^{\ln(n)}e^{-a(x-u)}] \\ F_{nT}(x) &= \exp[-e^{\ln(n)-a(x-u)}] \\ F_{nT}(x) &= \exp\left[-e^{-a\left(\frac{\ln(n)}{a}+(x-u)\right)}\right] \\ F_{nT}(x) &= \exp\left[-e^{-a\left(x-u+\frac{\ln(n)}{a}\right)}\right] \\ F_{nT}(x) &= \exp[-e^{-a(x-u^*)}] \end{aligned}$$

As a result, for m intervals and given the initial reference period $t_{ref} = \tau$ the parameters of interest for different reference periods can be determined. Here, $t_{ref} = m \cdot \tau$ holds for the following equations:

$$u_{t_{ref}} = u_{\tau} + \frac{\ln(n)}{a} \quad (4.14)$$

$$\mu_{t_{ref}} = \mu_{\tau} + \frac{\ln(n)}{a} \quad (4.15)$$

$$\sigma_{t_{ref}} = \sigma_{\tau} = \frac{\pi}{\sqrt{6}a} \cong \frac{1.282}{a} \quad (4.16)$$

As appears, the shape factor a and standard deviation σ is equal for each reference period. Table 4.10 summarises the Gumbel distribution parameters of the uniform load for each considered reference period t_{ref} . The values are determined with Python and the algorithm is provided in appendix L. The effect of the reference period is investigated through varying the extreme load distributions for the dominant load variable q . FORM computations are accordingly performed for each t_{ref} .

Reference period t_{ref} [years]	Mean value μ_{max_q} [kN/m ²]	Standard deviation σ_{max_q} [kN/m ²]
1	25.8	0.61
5	26.6	0.61
10	26.9	0.61
25	27.4	0.61
50	27.7	0.61
100	28.0	0.61

Table 4.10: Parameters of the Gumbel-distributed load variable q for the purpose of the FORM computations per reference period.

So for modelling purposes, the surcharge load q is assumed to be governed by time-variant loads. It appears that for Type I maxima the standard deviations remain unchanged for subsequent considered reference periods. The mean value on the other hand shifts to larger values as t_{ref} increases. This is in line with other examples from [42, ch. 10.3.1] and [48]. Given correlated variables, model uncertainty and the derived distribution parameters as input, the reliability indices for varying t_{ref} are determined. The results for $\xi \sim \text{LN}(1, 0.1)$ are summarised in table 4.11. Further results including the sensitivity factors are added in appendix I.

Table 4.11 shows small differences over the subsequent considered reference periods. The reliability seems slightly decreasing as the reference period extends. All the same, given the correlations and model uncertainty one finds little influence of the altering extreme load distributions on the reliability index. The influence of the model uncertainty ξ is considerable as it appears in figures L.2 and L.3 in appendix L. The influence of the reference period is studied for the case without the lognormal model uncertainty and cross-correlations. Results are summarised in table 4.12.

The results from table 4.11 are plotted in a graph which is illustrated by figure 4.6.

Reference period t_{ref} [years]	Reliability index β_n [-]
1	2.36
5	2.29
10	2.26
25	2.22
50	2.19
100	2.16

Table 4.11: Reliability index for different reference periods t_{ref} , given correlated variables and a lognormal model uncertainty with CoV = 10%.

Reference period t_{ref} [years]	Reliability index β_n [-]
1	3.94
5	3.83
10	3.79
25	3.73
50	3.69
100	3.69

Table 4.12: Reliability index calculated with FORM for each reference period without correlated variables and neglecting model uncertainty.

Reference period t_{ref} [years]	Reliability index β_n [-]
1	4.31
5	4.2
10	4.15
25	4.09
50	4.04
100	3.99

Table 4.13: Reliability index calculated with FORM for each reference period with correlated variables and neglecting model uncertainty.

Table 4.11 and figure 4.6 portray a negative non-linear correlation between the reference period t_{ref} and the prior reliability index β_n . The course of the reliability index over t_{ref} is characterised by a 'hockey stick'-curve. Small changes are observed for shorter t_{ref} than for longer t_{ref} . The target reliability index (according to CUR166 and CUR211 [15] [17]) is 4.3 and is significantly higher than the computed values. Beside, the probability of extreme surcharge loads increases as the considered reference period expands. The uncertainty in the extreme value density distribution remains although unaltered. This is illustrated by an increasing σ_q . Additionally, the mean value μ_q increases as it is more likely that such loads occur during long reference periods t_{ref} .

The applicability of an extreme value distribution type is depending on the available information. An important condition is the fit of the distribution on the available data. Other relevant extreme value distributions are Type II (Frèchet) and Type III (Weibull). Both distributions have other characteristics regarding the mean value and standard deviation. The coefficient of variation remains constant for type II distributions. Therefore for a larger amount of drawings, both the mean value and standard deviation increase. On the other hand, type III maxima are characterised by a decreasing variance for larger number of distribution intervals m . Both type II and III have a lower respectively upper boundary equal to u , $x = 0$ [42].

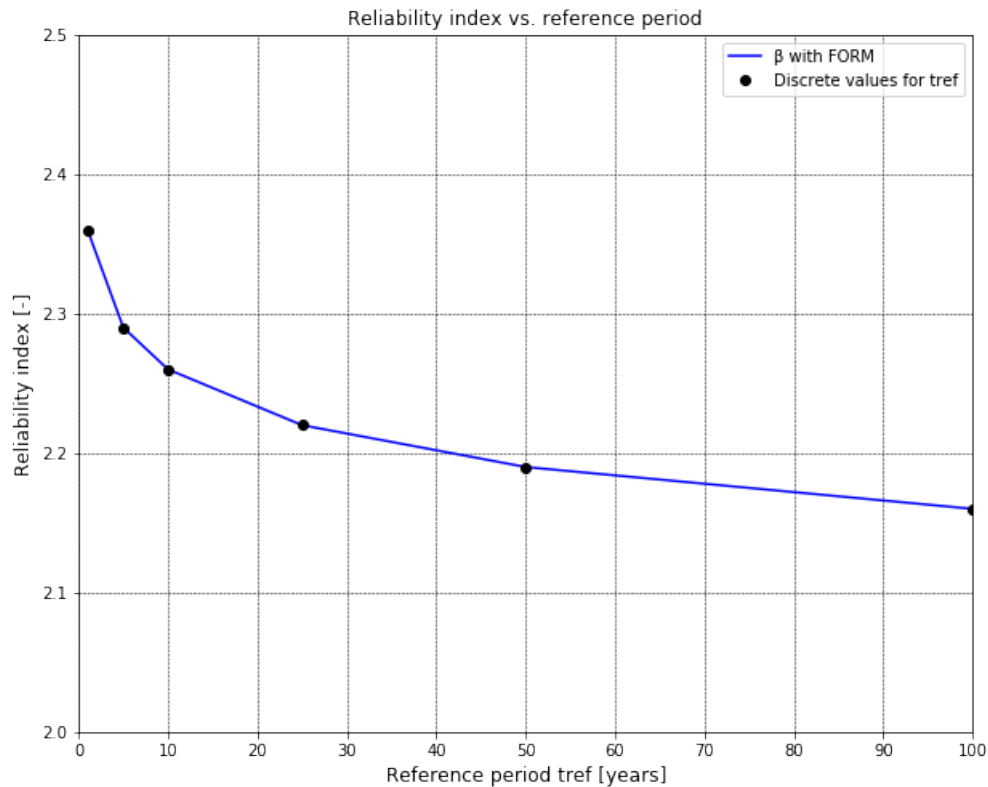


Figure 4.6: The a-priori reliability index β_n versus the reference period t_{ref} taking into account correlations, model uncertainty and without degradation of the structural material.

4.5. Verification of the prior reliability analysis

Part of the results is verified with level III reliability computations. Full probabilistic level III computations can be performed with numerical integration, crude Monte Carlo simulations, importance sampling and directional sampling. All methods are briefly explained in chapter C.4. Crude Monte Carlo simulations use a large number of samples, for accurate computations in many cases even above $N = 10,000$ samples. As a result, a significantly large computation time and disk space is required. An optimised alternative for the Crude Monte Carlo method is importance sampling in which the realisations are preferably performed in the zone around the edge between failure and non-failure. Crude Monte Carlo draws its realisations around the P_{50} values [24, p. 80]. This method uses a two-stage procedure in which random samples are drawn elsewhere to estimate the design point. Afterwards, a number of samples is generated around this "shifted" design point. The region where the realisations are drawn is determined by two factors:

- Variation factor f_{var} : the standardised normal value of the drawn realisation (u-value) is shifted from the mean value of the stochastic distributions through multiplication with a factor.
- Variation shift s_{var} : the standard normal value of the realisation is shifted through adding a value.

Each variable in one realisation is translated in the the standard normal space by equation 4.17. u_{var} represents the standard normalised variable per realisation while $u_{imp,var}$ is the shifted variable by importance sampling.

$$u_{imp,var} = f_{var} \cdot u_{var} + s_{var} \quad (4.17)$$

A convergence criterion is set in order to verify whether the obtained accuracy of the failure probability is sufficient. For that an acceptable relative error ϵ is determined with equation 4.18 [72, p. 222]:

$$\epsilon = \sqrt{\frac{W - P_f}{NP_f}} \quad (4.18)$$

For the computations with importance sampling the input in table 4.14 is used. The acceptable number of non-succeeded realisations is 10% of the minimum total number of realisations. In this case, it is prohibited that 100 realisations fail.

Minimum number of samples N_{min}	1000
Maximum number of samples N_{max}	600,000
Variation factor	1.5
Variation shift	6
Acceptable relative error ϵ	0.1

Table 4.14: Input for the reliability method: importance sampling.

The variation shift is only applied on the uniform load q . As a result, arbitrary realisations of the limit state function $g(\underline{X})$ are drawn around the edge between failure and non-failure. Appendix K shows results in combination with the convergence value and the number of runs. To compensate for the translation which is performed by equation 4.17, weight w_{VAR} is applied on each contributing variable per realisation [24, p. 80]. This weight per variable per realisation functions as a correction and is determined by equation 4.19.

$$w_{VAR} = \frac{f_{VAR} \cdot g(u_{imp,var})}{g(u_{var})} \quad (4.19)$$

where:

$g(\cdot)$ is the standard normal density function

This latter approach is equivalent to the application of an appropriate sampling function $f_s(\underline{s})$ (see appendix E.1). Importance sampling has realised simulations and the results are summarised in table K.1 of appendix K. By having a closer look, one notices insignificant differences ($\leq 0.3\beta$) between the output of the two reliability methods:

- Level II (FORM): 4.53
- Level III (importance sampling): 4.86

Attention should be provided to the large number of realisations in this sampling method. The minimum required number was 1000 samples. The importance sampling calculations yielding the above reliability used $N = 321,000$ samples. As a logical outcome, the results become significantly more accurate with respect to the First Order Reliability Methods. The obtained sensitivity factors are however largely different from the α 's found with FORM (see figure 4.7). FORM is relatively more efficient in the derivation of sensitivity factors. During each FORM-iteration the α 's are updated. Importance sampling is solely used for the verification of the reliability index.

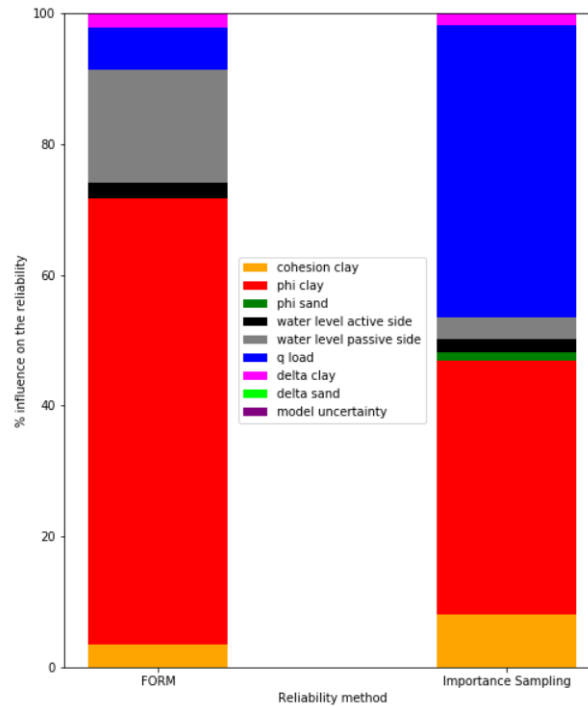


Figure 4.7: Bar diagrams illustrating the significantly large difference between influence coefficients obtained with importance sampling and with FORM for a reference period of 50 years.

For each applied reliability method, the behaviour of the basic random variables is different. Figures L.2-L.3 from appendix I visualise the relative influence of the random variables for different reference periods t_{ref} . These differences are analysed in chapter 6. These results are obtained with FORM-analyses for cases without and with model uncertainty and correlated variables respectively. As appeared in the previous paragraph, correlations between the stochastic input parameters results in a comparable decline of the reliability index β_n per reference period t_{ref} . Figure 4.6 illustrated a decline of the reliability for longer reference periods. Figure 4.8 shows again the plotted reliability index for different reference periods. This is done for cases with correlated and uncorrelated variables. The difference between the reliability indices decreases and becomes more constant as the considered reference period becomes longer (see figure 4.9). Nonetheless, the difference between the probabilities of failure is in either way marginal.

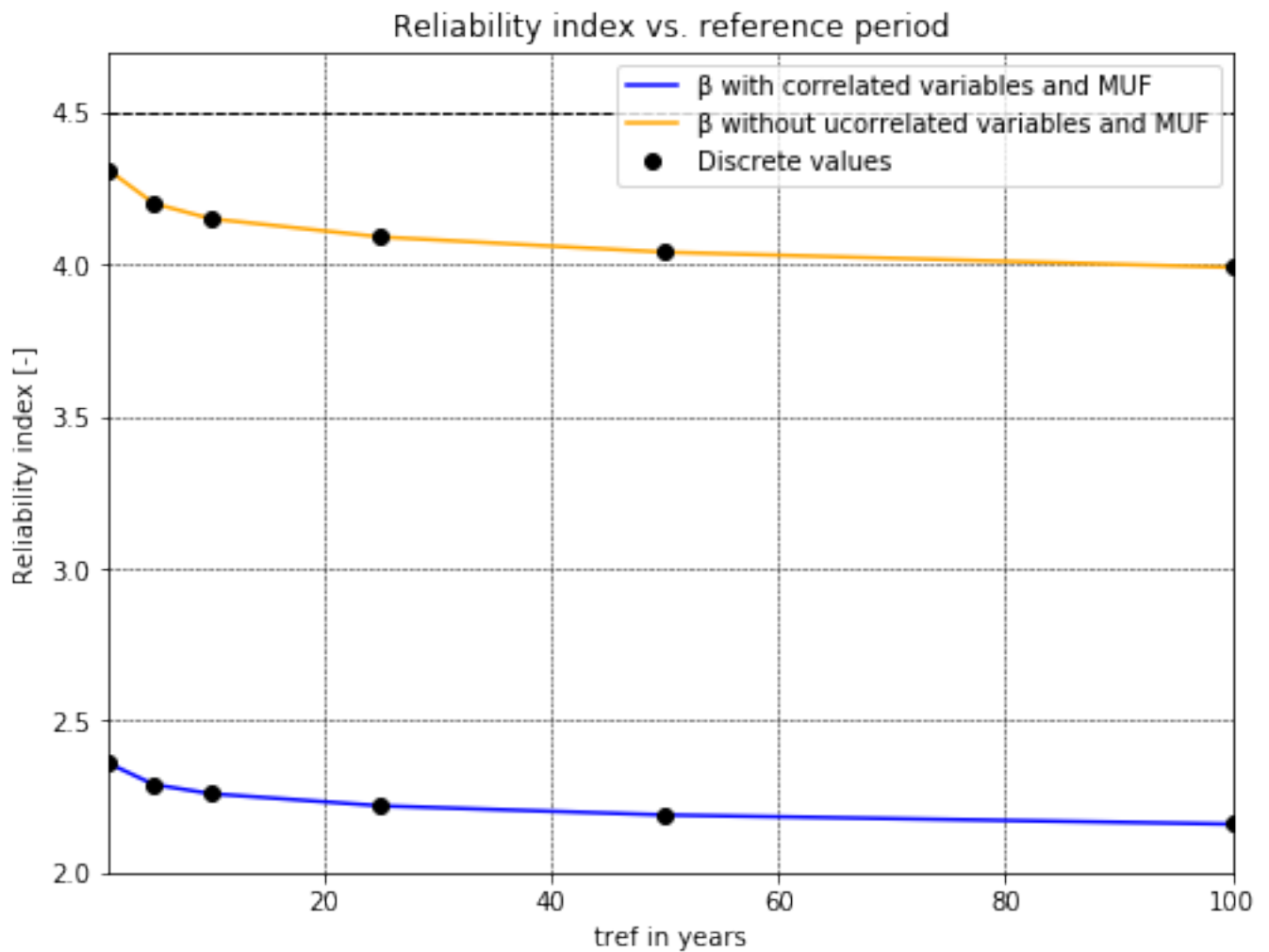


Figure 4.8: Reliability index given correlated and uncorrelated parameters plotted against the reference period.

The relative influence of the involved parameters is visualised by means of a bar diagram. Figure 4.10 visualises the relative influence for three cases:

1. Without correlations and without model uncertainty
2. With correlations and without model uncertainty
3. Including correlations and model uncertainty

The reference period of 50 years is here considered. One notices a decreasing relative importance of the internal friction angle in the case of cross-correlations and model uncertainty. The relative influence of the model uncertainty is extremely high at the expense of the other random variables. The uniform load q appears to have a relatively small influence on the end result for all cases.

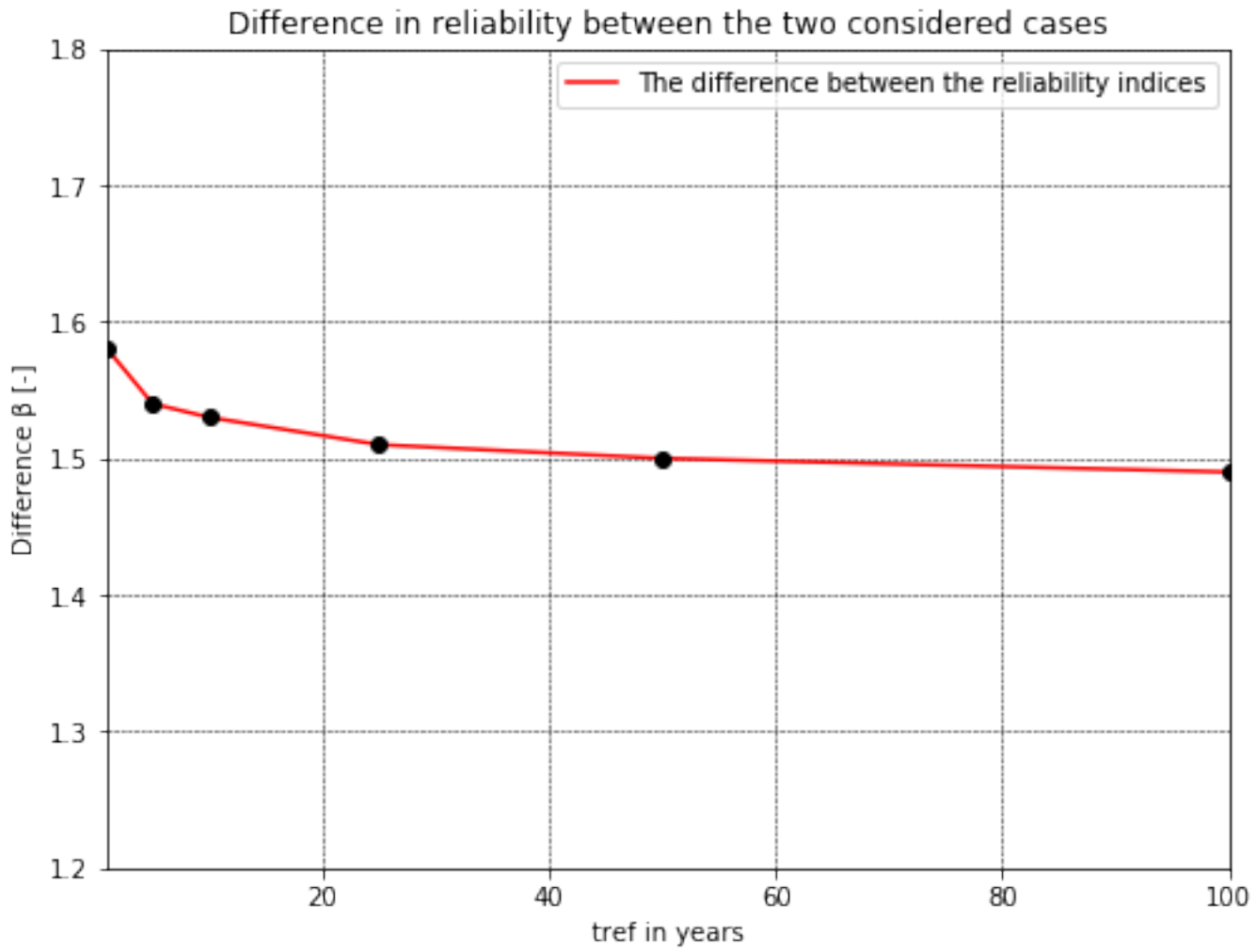
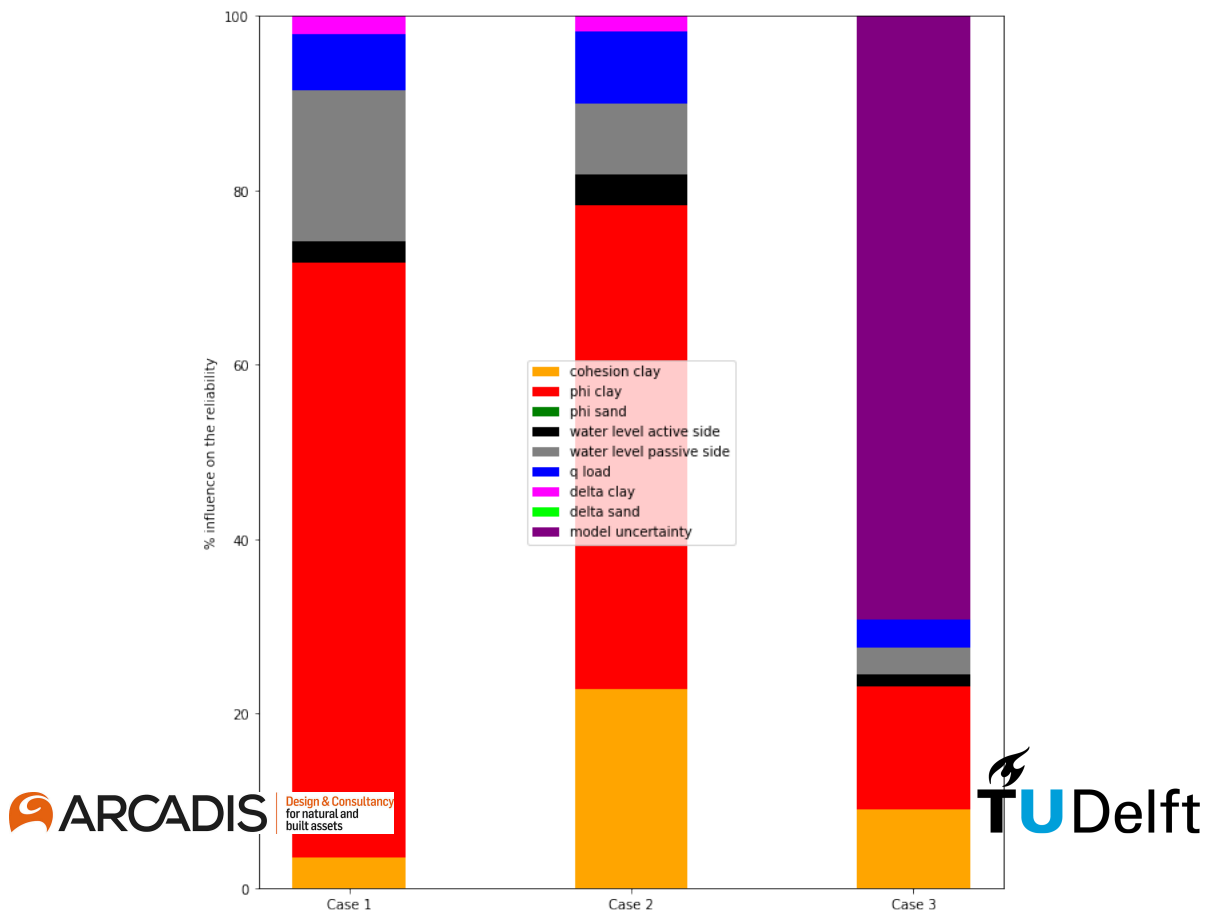


Figure 4.9: The difference between the reliability index given correlated variables and the reliability index given uncorrelated variables for different reference periods.



The influence of correlations between basic random variables on the considered limit state is initially analysed with FORM. Sampling methods appeared to yield marginal differences with respect to results obtained by FORM. At this point, the effect of the extensively time-consuming importance sampling computations is studied as well. The computation time for each reference period t_{ref} (1, 5, 10, 25, 50, 100 years) is significantly higher. Therefore it is chosen to perform computations for a $t_{ref} = 50$ years and for the before-mentioned cases (see figure 4.10). Appendix K shows the results of the computations. The results give an opinion about the correspondence between the level II and level III method given example 3 from the CUR research report [72].

A level III approach appears to create comparable results as the level II approach regarding prior reliability computations. Larger, but still marginal deviations are found upper tail of the graphs. These differences are explained through the lower probability of extreme loads. The uncertainties related to the dominant load variable q are in either case considerably small. Less differences are expected since the share of influence of the uniform load is less when considered a shorter reference period.

Further, large influence of the model uncertainty factor is observed for all cases. A sensitivity analysis is performed for $\xi \sim LN$. The random variables are cross-correlated. For a reference period of 50 years, several calculations with different distribution parameters of the model uncertainty factor are performed. Figure 4.11 visualises the 50 year reliability index as a function CoV of the model uncertainty factor. The applied model uncertainty has a mean value of 1.

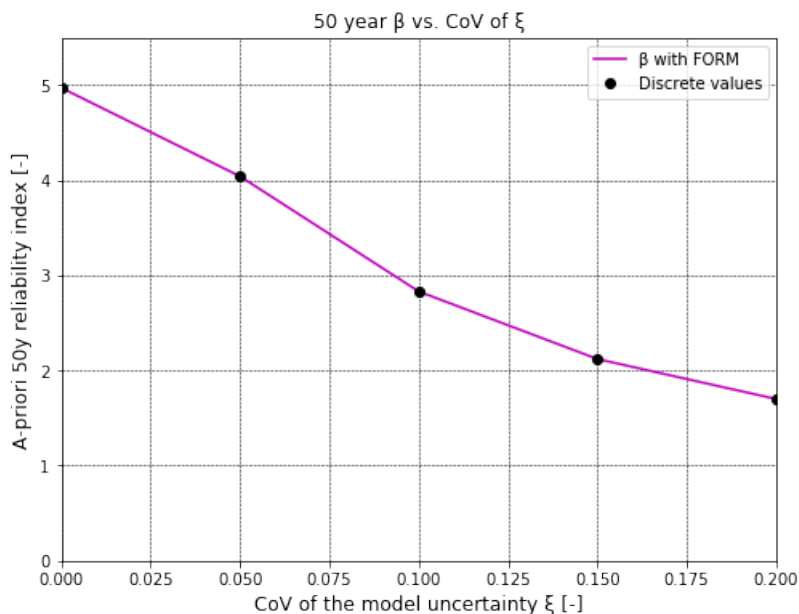


Figure 4.11: The 50 year a-priori reliability index as a function of the CoV of the model uncertainty ξ .

The subgrade reaction method c.q. spring model overestimates the maximum bending moment as has been the case in chapter 3.2. For a considerable part, overestimation is caused by not taking into account arching by the D-Sheet Model. Other causes might (indirectly) induce overestimation. Such calculation differences are observed in other research cases as well among which a research addressing laterally loaded tubular piles [5] Hence, a model uncertainty factor $V_{\xi} = 10\%$ seems a reasonable value. Accordingly, the rest of this research uses a model uncertainty factor $\xi \sim \text{LN}(1, 0.1)$ [64, p. 73].

However, influence of model uncertainty seems larger in this research compared with the GeoDelft research [71] [72]. Moreover, in the CUR research report no model uncertainty parameter has been applied at all. In [72], the uncertainty related to the anchor force and subgrade reaction modulus were studied through different deterministic calculations. Hence, the impact of adding such a stochastic model uncertainty on the reliability should be assessed. Chapter 6.5 concentrates on this matter. The continuation of this research is studies the effects of past performance with the derived annual reliability- and sensitivity values from table 4.6 in chapter 4.4.

5

Posterior analysis

5.1. Introduction

Different influential phenomena related to newly-built quay walls were investigated in the previous chapter. Three case-related failure mechanisms were therefore initially considered and the cross-section's initial reliability has been determined. As has been explained, mainly the overall aspects of a quay wall cross-section were considered. Correlations between variables and the effect of the structure's reference period are influential phenomena and were considered with both the level II and level III approach. Regarding the latter, results have shown differences in the failure probability, sensitivity- and design values. Accurate predictions of the quay wall's reliability requires more information about the cross-section.

Information about the past performance is necessary for predicting the residual life of the structure. Several aspects might be considered in studying the effects of past performance: structural degradation, modified reference period, effect(s) of test load(s), added information from measurements/investigations and survived years. This chapter deals with the effect(s) of past performance on the reliability of (existing) quay walls. Effect(s) of past performance is taken into account by appending data from survived previous years. At a later stage, information about structural degradation is included as well.

5.2. Starting points

Case 3 from [72, p. 54] is unaltered and regarded in the study on the effect(s) of past performance. Input variables and uncertainties from table 4.11 are used in the analyses of the cross-section. However, marginal comments can be added to the reference case. Initially, a reference period of one year is considered. A base case reference period can be used repeatedly in this posterior procedure, this is explained later on. Related to the quay wall cross-section as drawn in D-Sheet Piling, see figure 1.4, FORM computations are made. These computations are consequently validated through level III method.

Yielding of the steel front wall is considered as the governing failure mechanism. Hence, equation H.3 is viewed in this matter. Failure of the cross-section or exceeding of this ultimate limit state is reached when the steel stress in the front wall high the yield stress f_y . The maximum steel stress is determined by the maximum bending moment in the permanent immersion zone and the elastic section modulus of the front wall. The permanent immersion zone lies in the zone which is permanently under water. The maximum bending moment will act in this zone at the quay wall. The elastic section modulus is determined by the structure's dimensions. Chapter 4 goes into calibration of the sheet piling dimensions corresponding to the overall partial safety factors for moment capacity γ_m and passive soil resistance γ_g .

Firstly, the case is considered without degradation. The following limit state holds:

$$Z = fy - \frac{M_{max}}{W_{y,el}}$$

With a reference period $t_{ref} = 1$ year, FORM computations are realised and the following properties are used in this case:

- Relaxation factor $f_{rel} = 0.75$
- Maximum number of iterations of 50
- Gradient step size of 0.3

5.3. Posterior analysis with Equivalent Planes method

Prior reliability results of the reference case were obtained by calculations through the Probabilistic Toolkit which is coupled with D-Sheet Piling. Output without consideration of past performance was found. This approach is generally valid in a newly designed preliminary case. For existing quay walls, experiences from previous studies [64] [67] [77] [25] have resulted in different findings for the reliability and influence coefficients. In most cases, Bayesian updating is applied in the derivation of the posterior reliability. Recall that Bayesian updating for structural applications is applied by means of the following equation:

$$P_{f|S} = P(g(\underline{X}) \leq 0 | h(\underline{X}) > 0) = \frac{P(\{g(\underline{X}) \leq 0\} \cap \{h(\underline{X}) > 0\})}{P(h(\underline{X}) > 0)} \quad (5.1)$$

Where $h(\underline{X})$ is the limit state of the preceding situation or the "observed" situation. In many studies, such as [77] for levees, this method was applied by means of a Monte Carlo approach in which highly-reliable systems can be analysed. Monte Carlo based methods appeared to be suitable for obtaining accuracy in the case of large systems with highly-reliable components but are rather time consuming. [14] proposed a Monte Carlo based approach in which the tail of distributions is used to improve the efficiency of the computations. Additionally, several other methods are mentioned in [43, p. 54] for the derivation of the system reliability.

This research uses the Equivalent Planes method which is applicable with both level II- and level III methods. Equivalent Planes method as described in [43] clearly explains the derivation of the system's reliability with correlated components. Equivalent Planes method is sometimes also referred to as the Hohenbichler-Rackwitz method [57]. It was initially adopted for Dutch flood defence systems and developed to meet two requirements [43, p. 54]:

- Fast computations for large highly-reliable systems
- Computation of influence coefficients of the random variables of different components.

By application of the Equivalent Planes Method, an equivalent limit state function Z_e is derived from multiple components ($i = 1, \dots, n$) with limit state functions Z_1, \dots, Z_n . For example, a two-component series system with limit state functions Z_1 and Z_2 results in an equivalent limit state function Z_e .

$$P(Z_e < 0) = P(Z_1 < 0 \cup Z_2 < 0) = P_f \quad (5.2)$$

For multi-component systems and parallel systems, the latter approach is the same using $Z_i < 0$ and $Z_{i-1} < 0$. The failure probability of a system with two correlated components can be computed.

By iteratively applying this method, the reliability of a system with a larger amount of components can be computed. Since the analytical procedure is less time-consuming, this Equivalent Planes method appears to be very efficient. However, this method is an approximation and may cause errors in the results. Figure 5.1 illustrates the error which is initiated by the difference between the released and gained failure area (see A1 and A2). In view of the latter, this can be either an overestimate (fig. 5.1a) or an over- or underestimate (fig. 5.1b).

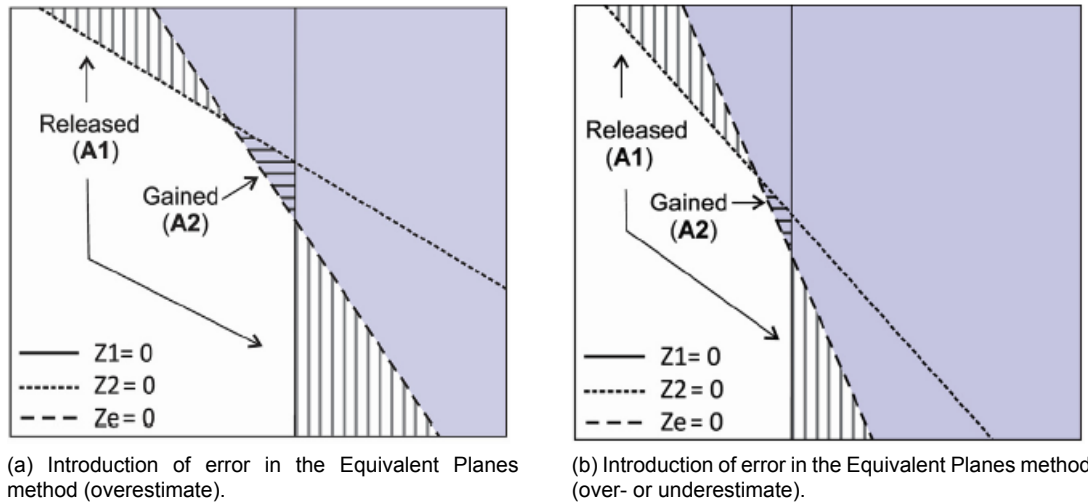


Figure 5.1: Situation after application of the Equivalent Planes method with the equivalent limit state function Z_e , the failure space, the released area A1 and gained area A2 [43].

In literature, this method is described for the computation of the failure probability of a system consisting of several spatial components. These components may be connected in parallel or in series [43] [21]. In this research, the components are selected as the same cross-section then considered at different of points in time. In this regard, the components (cross-section in year 1, 2, ..., n) are considered as components connected in a parallel system.

In this case study on past performance, the same cross-section in consideration of one failure mechanism is treated. Component 1 is the cross-section at the end of year 1, component 2 the same cross-section at the end of year 2 and so on. To apply the Equivalent Planes method, the failure probability of each individual component and the correlation between the components are required. To compute the correlation between failure in year i and subsequent year j , the auto-correlations between the random variables that are involved and the influence coefficients (or sensitivity factors) are required. Given n random variables, First Order Reliability methods (FORM) are used to obtain the influence coefficients $\alpha_i = \alpha_{i1}, \dots, \alpha_{ik}$ and the design values $u_i = u_{i1}, \dots, u_{in}$. The random variables are transformed from their actual distributions to standard normal distributions through FORM. All variables in this case study as normally distributed and can be standardised with equation 5.3. The design values are found afterwards.

$$u_i = \frac{x_i - \mu_{x_i}}{\sigma_{x_i}} \quad (5.3)$$

Equation 5.4 is applied to derive the correlation between the cross-section in year i and the cross-section in year j [43, p. 55].

$$\rho(Z_i, Z_j) = \sum_{k=1}^n \alpha_{ik} \cdot \alpha_{jk} \cdot \rho_{ijk} \quad (5.4)$$

Based on equation 5.4, one can state that the following information is necessary:

1. The auto-correlation ρ_{ijk} : the correlation between a variable u_{ik} in year i and the same variable u_{jk} in the subsequent year j .
2. Influence coefficients α_i and α_j : these coefficients describe how much each variable contributes to failure.

Auto-correlations can be found through measurements, field research and/or by expert opinion. On the other hand, influence coefficients are obtained by FORM calculations. The influence coefficients are normalised by application of FORM. As follows, the below-defined equation holds:

$$\sum_{k=1}^n \alpha_{ik}^2 = 1 \quad (5.5)$$

In anticipation of the Equivalent Planes method, FORM computations are performed to obtain the sensitivity coefficients and design values of the individual (annual) components. Secondly, component reliability can be found through linearised limit state functions Z_i and Z_j . A similar formulation for the limit state holds for both components. The linearised limit state function at the end of year i is for instance stated as follows:

$$Z_i = \beta_i - \alpha_{i1}u_{i1} - \alpha_{i2}u_{i2} - \dots - \alpha_{in}u_{in} \quad (5.6)$$

Once the individual random variables, the influence coefficients and correlation between the components $\rho(Z_i, Z_j)$ are determined, equation 5.6 can be simplified to equation 5.7 for year i and 5.8 for year j . The latter can be done since $Z_i - \beta_i$ is standard normalised.

$$Z_i = \beta_i - w_i \quad (5.7)$$

$$Z_j = \beta_j - w_j \quad (5.8)$$

Both w_i and w_j are standard normally distributed variables and are part of the simplified expressions. The reliability indexes of year i and j are both constants so statement 5.9 holds.

$$\rho(Z_i, Z_j) = \rho(w_i, w_j) \quad (5.9)$$

As it appears, correlation between the two components is the same as the correlation between the introduced variables. Hence w_j can be written in terms of w_i and an independent standard normally distributed variable w_j^* . This rewritten expression can thereafter be substituted for w_j in equation 5.8. The standard normal nature of w_j is preserved and w_i and w_j are even so correlated to an extent. In the following formulas and the corresponding paragraphs ρ_{ijk} is replaced by ρ .

$$Z_j = \beta_j - \left(\rho \cdot w_i + \sqrt{1 - \rho^2} \cdot w_j^* \right) \quad (5.10)$$

The Z-functions are simplified expressions and can be used for the formulation of the conditional probability $P(Z_j < 0 | Z_i < 0)$ in the subsequent year j . The condition $Z_i < 0$ is equivalent to β_i being smaller than w_i . In the standard normal u -space, that part of the w_i -distribution which is larger than the constant β_i is used to account for failure in year i . Equation 5.10 is transformed into equation 5.11 and implicitly takes into account the condition of $Z_i < 0$ (survival of year i).

$$Z'_j = \beta_j - \left(\rho \cdot w_i + \sqrt{1 - \rho^2} \cdot w_j^* \right) \quad (5.11)$$

Equation 5.11 is the Z-function which calculates the conditional failure probability. The condition describes failure the preceded year.

$$P(Z'_j < 0) = P(Z_e < 0) = P(Z_j < 0 | Z_i < 0) \quad (5.12)$$

By means of the law of total probability, as is described in appendix C.5.2 by equation C.42, the probability of failure given survival in the preceding year can be computed. Equation 5.13 computes the failure probability of the cross-section in year j . After rewriting formula 5.13, $P(Z_j < 0 | Z_i > 0)$ can be computed as yearly failure probabilities are known.

$$P(Z_j < 0) = P(Z_j < 0 | Z_i > 0)P(Z_i > 0) + P(Z_j < 0 | Z_i < 0)P(Z_i < 0) \quad (5.13)$$

An alternative expression for the conditional Z-function Z'_j is the equivalent failure plane Z_e . In the previous paragraphs, a two-component system was illustrated. Once a two-component system or two subsequent years are combined in an equivalent limit state function Z_e , it is possible to append a new component to the system. The analytical procedure works the same for $m > 2$ components, but the influence coefficients and design values of Z_e differ. As a result, the calculation of the correlation between the combined limit state function and the third component is rather difficult. The influence coefficients and design values have to be determined. When $u_{ik} = u_{jk}$, meaning that each variable in year i and j have auto-correlation equal to 1, the alphas can be obtained by partial differentiation of the combined beta with respect to the standard normal variable u_k ($\frac{\partial \beta_{ij}}{\partial u_k}$). This can be done by numerically estimating. u_k is for $\rho = 1$ equal to u_{ik} and u_{jk} . Equation 5.14 derives the influence coefficient of a variable by means of the obtained equivalent failure plane. The reliability is differentiated over the correlated- and uncorrelated standard normal space. In the case of $u_{ik} \neq u_{jk} \neq u_k$, the method for computing the individual influence coefficients will slightly differ.

$$\alpha_{ik} = \sqrt{\left(\frac{\partial \beta_i}{\partial u_{uc,ik}} \right)^2 + \left(\frac{\partial \beta_i}{\partial u_{c,ik}} \right)^2} \quad (5.14)$$

In each iteration step, the Equivalent Planes method or the Hohenbichler-Rackwitz method results a smaller number of variables in the equivalent limit state Z_e . Where equation 5.6 uses n variables, equation 5.11 is using two variables. Equation 5.12 is solvable with different probability methods such as numerical integration and FORM. Numerical integration is more efficient and even so accurate since the number of variables is small ($n = 2$). Numerical integration works well for a small number of variables because this probabilistic technique is computationally intensive. The number of integration steps increases exponentially with the number of variables. The analyses become significantly more difficult for cases with more than two variables [42, p. 120].

5.4. Application of the Equivalent Planes method

The algorithms for the computations with FORM, numerical integration method in the Equivalent Planes method or Hohenbichler-Rackwitz method were written in several MATLAB sheets. All of them were made available in an open-source library of Deltares [23]. MATLAB is a higher-level programming source for different mathematical problems. Various reliability methods are saved within this tool. The Hohenbichler scripts are adapted within for this case study. Appendix M provides a preview of the scripts for the computations. Within this scripts, the effect of past performance of the reference case cross-section is added. Intermediate results are provided as well and the results are evaluated in chapter 6.

Computations by means of the algorithm from Appendix M do not yet take degradation of structural elements into account. Chapter 7 treats the case in which degradation is involved.

6

Results from the case study

6.1. Introduction

Based on the approach as outlined in chapter 5.4, a significant amount of information is obtained. The results include amongst others the reliability indices and sensitivity factors. Depending on which reliability method (level II or III), design values are obtained as well. Equivalent Planes method uses two reliability methods: numerical integration (Level III) and FORM (Level II). Both approaches are shortly highlighted in this chapter. Consequently, results are illustrated and afterwards compared with the results obtained from a different computation tool. Section 6.3 describes a new reference case for the verification of the updated yearly β 's. This chapter is solely concerned with results without the effect(s) of degradation. The effects of degradation are studied in chapter 7.

6.2. Equivalent Planes method with two components

The Equivalent Planes method uses (an) equivalent failure plane(s) to derive the cross-sectional probabilities of multiple components. This latter method has been explained in chapter 5.3. A MATLAB algorithm for the computation of the (updated) reliability indices and transformed sensitivity factors is made available by Deltares. A preview is given in M.1. Information about the sensitivity factors, correlations, the reliability index, system (series or parallel) and reliability method are required input for the realisations. In this section a system consisting of two components will be treated. In this chapter derived sensitivity values are values in the transformed u -space.

Hohenbichler-Rackwitz computes the updated reliability of two individual failure components Z_1 and Z_2 combined. The MATLAB code provided by OpenEarthTools of Deltares was originally created for computing the updated reliability and influence coefficients considering the failure of both components: $P(\{Z_1 \leq 0\} \cap \{Z_2 \leq 0\})$ (parallel system) or $P(\{Z_1 \leq 0\} \cup \{Z_2 \leq 0\})$ (series system). In this research, survival of previous years is assumed to account for the effect(s) of past performance. So survival of year 1 is assumed. Accordingly, the failure statements are reformulated with eqs. 6.1 for parallel systems and 6.2 for series systems.

$$P(\{Z_1 > 0\} \cap \{Z_2 \leq 0\}) \quad (6.1)$$

$$P(\{Z_1 > 0\} \cup \{Z_2 \leq 0\}) \quad (6.2)$$

The mutual correlation between the individual components is required information for the computation of the combined probability. If the system is uncorrelated ($\rho_{ij} \rightarrow 0$), the smallest β_1 is used by the

series system. On the other hand, an uncorrelated parallel system uses the maximum β_1 . According to [21, p. 142], correlation implicates dependence between two variables but dependency does not necessarily implicate correlation. The numerical analyses start with the case of components being correlated. In this chapter, one is dealing with continuous distributions for the limit state variables with $dx \rightarrow 0$. Consequently, it does not matter which notation is used for inequality statements: $Z \leq 0$ or $Z < 0$.

$$P(Z_2 \leq 0 | Z_1 > 0) \quad (6.3)$$

By means of equation 6.3, the conditional annual reliability for both a series- and parallel system are computed. Probabilistic axioms are applied in each type of system. The parallel system uses Bayes' Theorem and the law of total probability (eq. 6.4) [21, p. 31]. By means of the cross-sectional probability, the union probability of a series system can be calculated. This is realised by eq. 6.5 [21, p. 18].

$$P(Z_2 \leq 0 \cap Z_1 > 0) = P(Z_2 \leq 0 | Z_1 > 0) \cdot P(Z_1 > 0) = P(Z_2 \leq 0) - P(Z_2 \leq 0 | Z_1 < 0) \cdot P(Z_1 < 0) \quad (6.4)$$

$$P(Z_2 \leq 0 \cup Z_1 > 0) = P(Z_2 \leq 0) + P(Z_1 > 0) - P(Z_2 \leq 0 \cap Z_1 > 0) \quad (6.5)$$

Both reliability methods use ρ_{ij} , which is the correlation between the considered limit state of the cross-section in year i and in year j . The correlation is determined by equation 5.4 using auto-correlations and influence coefficients. The auto-correlation of each variable describes the correlation in time and is in this research assumed as either uncorrelated or fully linearly correlated (0 or 1 resp.). Mainly load parameters and water levels are assumed to be uncorrelated or time-dependent due to their randomness: $\rho = 0$. Soil parameters such as the cohesion c_i and volumetric weight γ_i are assumed as fully linearly correlated. Figure 1.4 illustrates the cross-section which is considered with the Equivalent Planes method. Given similar input values from chapter 4.4 for $t_{ref} = 1$ year and the model uncertainty factor ξ being lognormal $\sim \text{LN}(1, 0.1)$, one obtains the results as presented in table 6.1. The distributed load variable q is in this case modelled with a Gumbel distribution with $\mu_q = 25.8 \text{ kN/m}^2$.

Reliability index [-]	Probability of failure [%]	Probability of non failure [%]		
2.36	0.922	99.1		
Variable	Alpha [-]	Influence factor [%]	Correlated alpha [-]	Physical value [x]
c_{clay}	-0.307	9.407	-0.306	3.4332
ϕ_{clay}	0.385	14.841	0.491	19.464
ϕ_{sand}	-0.0259	0.0671	-0.0259	32.698
w_a	0.114	1.306	0.114	-1.5537
w_p	0.176	3.094	0.202	-1.6032
q	-0.0513	0.263	-0.0511	25.767
δ_{clay}	$8.19 \cdot 10^{-3}$	$6.72 \cdot 10^{-3}$	0.253	9.1075
δ_{sand}	$-2.91 \cdot 10^{-3}$	$8.48 \cdot 10^{-4}$	-0.0194	21.869
ξ	-0.843	71.014	-0.841	1.2124

Table 6.1: Input values for computing the combined failure probability with the Equivalent Planes method.

An annual reliability index $\beta_1 = 2.33$ is found. An other important aspect which can be observed, is the relatively large influence of the model uncertainty factor $\alpha_\xi = -0.843$. In analytical form, uncertainty can explicitly be introduced as illustrated by equation 6.6. Since limit state variables are explicitly multiplied with ξ , large sensitivity to this factor is indeed expected.

$$Z = fy - \frac{\xi M_{max}}{W_{el,y}} \quad (6.6)$$

In the next sections, settings for the analyses with Numerical Integration and FORM are briefly explained.

6.2.1. Method 1: EPM with Numerical Integration

Numerical integration uses over 1000 grid points N for the computations. The grid centres are determined by using the mean values of the linearly spaced grid points. The integration between grid points (calculated surface area) and the derivation of the conditional failure probability follow subsequently. Numerical integration was in most combined reliability cases the default computation method as it is very accurate and straightforward [43, p. 55]. Eventually, the reliability indices for a series and parallel system are calculated following statements 6.4 and 6.5. The domain in the U -space over which numerical integration is performed spans $D_U = [-\beta_{t1} - 10, \beta_{t1}]$.

6.2.2. Method 2: EPM with FORM analyses

FORM on the other hand requires a more sophisticated approach. It uses a data structure including parameters such as the reliability index, correlation between components (see table 6.2). Secondly, method parameters such as the number of iteration steps, gradient step size, relaxation factor and the start values of the (u)-vector are determined. This method works sufficiently effective for larger number of variables. The method parameters as summarised in table 6.2 are applied in this case study. Method parameters are selected as such to quickly reach convergence.

Method parameter	Value	Unit
Max. number of iterations	50	[-]
Derivative sides	1	[-]
Start value for elements of the \underline{u} -vector	'u2', 'u3' = 0.5	[u]
Step size du for $\frac{dZ}{du}$	0.001	[u]
Convergence criterion ϵ	0.001	[-]
Relaxation factor f_{relax}	1	[-]
Max. allowed step size per iteration	∞	[u]

Table 6.2: Method parameters for the FORM analyses

In the case of a heavily non-linear limit state function, the number of iterations would be significantly large. In this case study, the maximum number of iterations is chosen as 50. du is selected as relatively small to effectively approximate the one-sided derivatives. f_{relax} should not have any significant effect on the calculation because the limit state is not non-linear. For that reason the relaxation factor is disregarded. Important to notice is the \underline{u} -vector containing the start values. The variables 'u2st' and 'u3st' are standard normally distributed and are derived from uniformly distributed variables. As a result, start values are selected as the mean of the $u_i \{0, 1\}$. The mean value $E[X] = \frac{1+0}{2} = 0.5$ is substituted as start value for 'u2' and 'u3'.

Results

The two-component system is calculated with both level II and level III method. Here the output from chapter 4.4 is considered. The correlated annual output ($t_{ref} = 1$ year) is applied in the computations of the combined reliability. An annual reliability $\beta_1 = 2.36$ and the sensitivity factors from column 2 of table 6.1 are used in the two-component analysis. The updated reliability index is calculated for a series and parallel system, results are listed in table 6.3.

	Reliability method	
	Level II: FORM	Level III: Numerical Integration
Series system	-2.36	-2.75
Parallel system	2.36	2.75

Table 6.3: The updated reliability index in the second year given a survived first year

The union probabilities of the series system in the first row of table 6.3 are calculated with the law of total probability (see equation 6.5): $P(\{Z_1 > 0\} \cup \{Z_2 < 0\})$. The latter probability describes an "OR"-gate in a fault tree, one of the events occur. Reliability indices that are obtained for a series system, have the same magnitude as reliability indices that are found for parallel systems. The values are however negative which means a considerably high probability of occurrence. The latter can be calculated. For β -values between 2 and 4, the following statement [42, p. 115] holds:

$$P_f = \Phi(-\beta) \approx 10^{-\beta} = 10^{-(-2.75)} \gg 100\%$$

Hence, failure or survival of one of the two components seems a plausible argument which results from this analysis.

6.3. Verification of the Equivalent Planes method

The previous section has dealt with the computation of the reliability for a two-component system. Computation of the combined reliability index is performed with the Hohenbichler-Rackwitz method. A preview of the algorithm is available and provided in appendix M.1. In this section, verification of this method is undertaken. The Hohenbichler-Rackwitz algorithm (see appendix M.1) forms the basis of the reliability updating method. Initially, the intermediate result(s) of the Hohenbichler-Rackwitz algorithm is verified. This is performed by validating the conditional annual reliability. A secondary verification follows in which Bayesian updating with the Deltares Probabilistic Toolkit is realised. All procedures are been described in appendix M.2. At a later stage, the algorithm should be iteratively applicable over an extended time period or service life time.

Results from the calculation with a two-component system appears to sufficiently correspond to results from Bayesian updating with Deltares Probabilistic Toolkit. The latter is proved in appendix M. Hence, the algorithm appears to be applicable for a two-component system. A multi-component system, consisting of three or more components, is considered in the next chapter.

6.4. Equivalent Planes method for a multi-component system

In this case study, the same cross-section as in chapter 3 is considered over an extended period. The reliability of the cross-section is examined over a varying time t . Hence, this method assumes the cross-section at different points in time as different components with each a limit state Z_i . Correlation between subsequent components i and j is denoted by ρ (short notation of ρ_{ij}). In this posterior analyses t_0 or $t = 0$ indicates the start of the use, whereas t_n is the notation of a certain year in time from t_0 . At most $t_{100} = 100$ years is approached. Hence, a multi-component system indicates the consideration of the reference case cross-section for several consecutive years from t_0 up and including t_n .

6.4.1. Method

The time-variant reliability curve is created by means of the Equivalent Planes method. This method was earlier explained in section 6.2 for the two-component system. Two probabilistic techniques have been explained: numerical integration (level III) and FORM (level II). The probabilistic techniques are applied in the same way but for a number of n iterations. In this research, a maximum time period t_n of 100 years is studied. This analysis assumes a parallel system, meaning that subsequent survivals must occur together.

The reliability indices and sensitivity values are updated for $t = 1, 2, \dots, 100$ years. The annual output ($t_{ref} = 1$ year) from table 6.1 is used in the Equivalent Planes method. To realise that, two zero matrices are created:

- For the β 's from t_0 to t_{100} a 100×1 matrix consisting of input entries
- For the α 's from t_0 to t_{100} a 100×18 matrix consisting input entries

The input entries are initially filled with NaN's (meaning Not a Number) or zeros. The first row of the matrices indicates the first year and it consists of the output considering $t_{ref} = 1$ year. The newly developed and adapted algorithm calls the Hohenbichler functions that computes the updated results the next year(s) in a nested loop. The Hohenbichler function computes numerically the sensitivity values and calls the nested function for the computation of the new (conditional) reliability indices. For each next year i , the correlation between year i and $i-1$ is updated.

A while loop is used for the number of the iterations denoting the number of years. Besides, this algorithm is used for the derivation of the conditional failure probability $P(F_i | S_1 \cap S_2 \cap \dots \cap S_{i-1})$ up till and including year i . This is the failure probability considering a reference period t_{ref} . A comparable approach with simulated load distributions is performed in chapter 4.4. In this case, failure of an object during the reference period is determined by failure in one of the subsequent years within that period from t_0 to t_{ref} . Hence one is dealing with a series system consisting of mutually exclusive events, since there is no positive correlation between these events [42, p. 198]. The latter implies that a certain event, for most cases, arbitrarily occurs. The failure events in the individual years are therefore mutually exclusive. Equation 6.7 is applied for the iterative calculation of the failure probability per t_{ref} .

$$P(F_i \cap S_1 \cap S_2 \cap \dots \cap S_{i-1}) = P(F_1) + P(F_2 | S_1) P(S_1) + \dots + P(F_i | S_1 \cap S_2 \cap \dots \cap S_{i-1}) P(S_1 \cap S_2 \cap \dots \cap S_{i-1}) \quad (6.7)$$

With the Equivalent Planes method, the reliability indices are determined for various reference periods. This is synchronously performed with the reliability updating calculation. Figure 6.1 shows the failure probability P_f as a function of t_{ref} , whereas figure 6.2a is showing the reliability index β_n for

various reference periods t_{ref} . For comparison reasons, figure 4.6 from chapter 4.4 is added next to graph obtained with the Equivalent Planes method: figure 6.2a.

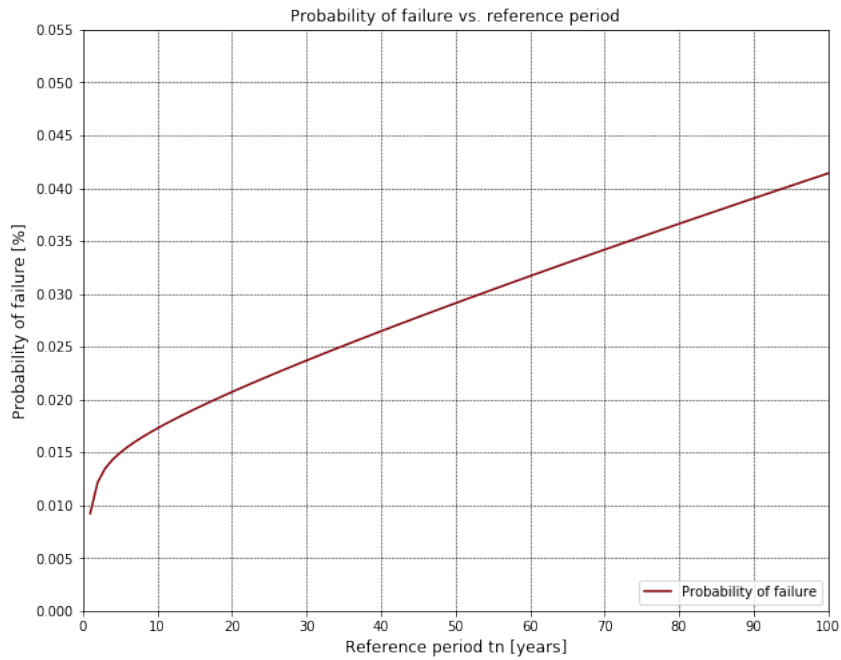
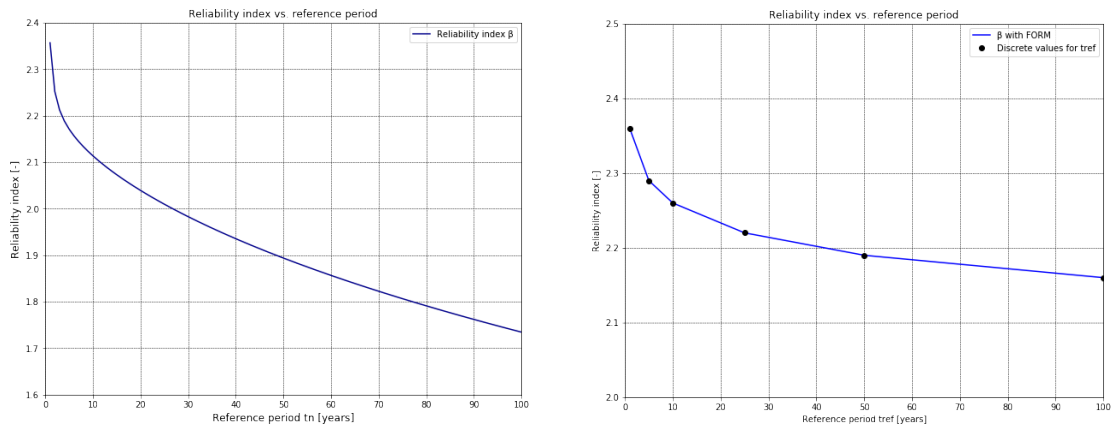


Figure 6.1: The probability of failure during a certain reference period t_{ref} based on the mutual exclusivity and equation 6.7.



(a) Derived with equation 6.7 given the conditional failure probabilities calculated with EPM. The series system describes the failure in a reference period as the sum of failure events in each year within that period.

(b) Based on the dominant load variable q transformed to different time intervals (see chapter 4.4)

Figure 6.2: The reliability index β_n as a function of the reference period t_{ref} based on two approaches.

6.5. Results and differences

Numerical integration or FORM is iteratively applied in the computation of the updated reliability $\beta_{F_t|S_{t-1}}$ as a function of the service life t in years. The output which is obtained by the level II and III methods results in a time-dependent reliability curve. Figures 6.3 (and N.1 in appendix N) illustrate the time-dependent reliability curve for numerical integration and FORM respectively. In the case of numerical integration, figure 6.3 initially shows a sharp increase of the conditional annual reliability in the first years. Afterwards, stagnation of the increase occurs. Eventually, β_n becomes almost constant. The Equivalent Planes method in combination with FORM shows an increase as well. However, this increase appears to be linear for all years which seems not reasonable from practical reasons. The differences might be due to numerical instabilities in the FORM analyses within the standard normal u -space. The derivation of a local design point instead of the real design point might cause this issue since this regularly happens with FORM. Hence, the FORM approach is not (yet) precisely predicting the time-dependent reliability curve (see appendix N). For this reason, the algorithm requires adjustments in order to become compatible for the combined application with FORM.

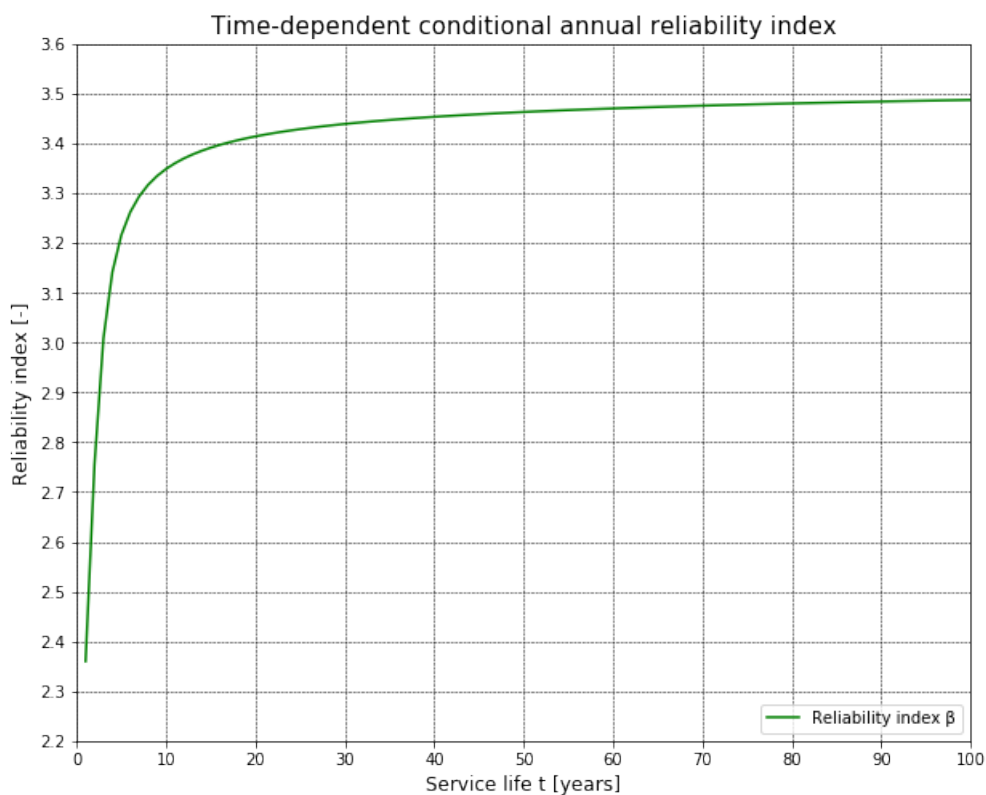


Figure 6.3: Time-dependent reliability curve of example 3 from [72] derived with numerical integration, given correlated variables and model uncertainty.

In addition, sensitivity values for varying t are derived for all input parameters. These values are calculated for the years t during service life. Considering a maximum service life t_{100} and an annually updated auto-correlation ρ_{ij} of the cross-section, one obtains time-dependent sensitivity values as presented by figures 6.4 (and N.2 in appendix N). The input parameters are listed in the plot legend. Again, the differences between the probabilistic techniques are observed. The differences between numerical integration and FORM are mainly caused by the numerical approach in the derivation of the updated sensitivity values α_k . The numerical approach uses the difference of the consecutively determined reliability indices divided by the stated perturbation value (ϵ). FORM results in different reliability compared to numerical integration.

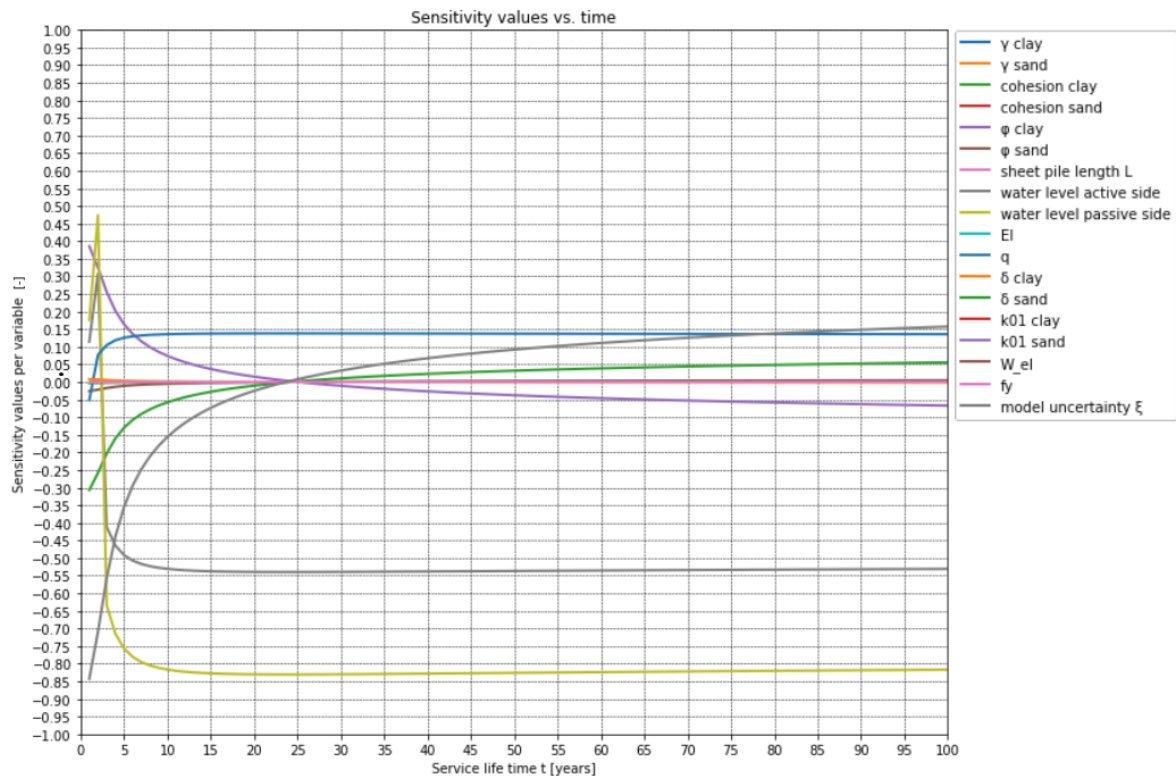


Figure 6.4: Time-dependent sensitivity values that are numerically calculated by means of the information found about the reliability which is obtained with numerical integration.

In both cases, the differences between the curves are remarkable. Numerical integration yields smooth curves concerning the time-dependent behaviour of the sensitivity values. The time dependent sensitivity values found with EPM in combination with FORM are shown in appendix N. These curves show an illogical development of the relative influence. For several variables, a peculiar kink is observed around $t = 25$ years. The fluctuations of the influence of both water levels for example, seem not reasonable. Numerical instabilities likely appear to be the case in these peculiar results. Besides, the time-invariant behaviour of some of the highly influencing variables (ϕ_1 , c_1 and ξ) opposes the time-dependent behaviour which was earlier observed with numerical integration and by other researches [64]. Therefore, the method of numerical integration is applied in the next part of the research.

The sensitivity values of both water levels are characterised with a kink at $t = 2$ years. This is due to an initial adjustment during the numerical calculation of the α -values. The open water level or the water level on the passive side appears to eventually affect the reliability of the cross-section, which seems peculiar. The water level on the passive side normally should result in a (distributed) stabilising force on the retaining wall. The positive and high degree of correlation between the water levels ($\rho(w_a, w_p) = 0.75$) results in a positive influence from both the active as the passive side. Hence, this correlation is reconsidered. There is always a correlation between the water levels to some extent according to [4]. For the reanalysis, the correlation is assumed to be lower but unequal to 0: $\rho(w_a, w_p) = 0.25$. Other cross-correlations remain unchanged. These assumption should result in a negative influence from the ground water level and a positive influence from the open water level. Table 6.4 shows the annual output given an adjusted cross-correlation between the water level(s). This information is used for the recalculation of the time-dependent reliability and sensitivity values.

Different from calculations that were performed for figures 6.3 - N.2, the same signs as for the first year sensitivity values are applied. As a result, figure 6.5 is created. The relative influence of the active water level becomes negligibly small compared with for instance the passive water level. The influence of the

Reliability index [-]	Probability of failure [%]	Probability of non failure [%]	Return period [years]	
2.33	0.99	99	101	
Variable	Alpha [-]	Influence factor [%]	Correlated alpha [-]	Physical value [x]
c_{clay}	-0.301	9.041	-0.300	3.42
ϕ_{clay}	0.378	14.326	0.482	19.555
ϕ_{sand}	-0.0254	0.0645	-0.0254	32.692
w_a	-0.0175	0.0308	-0.0179	-1.4917
w_p	0.254	6.461	0.242	-1.6069
q	-0.0505	0.255	-0.0503	25.765
δ_{clay}	$8.13 \cdot 10^{-3}$	$6.62 \cdot 10^{-3}$	0.248	9.1706
δ_{sand}	$-2.87 \cdot 10^{-3}$	$8.24 \cdot 10^{-4}$	-0.0191	21.863
ξ	-0.836	69.815	-0.833	1.2077

Table 6.4: Stochastic output for $t_{ref} = 1$ year given correlated variables and model uncertainty,

uniform load q and especially the passive water level w_p increases significantly, whereas the relative influence of for instance the model uncertainty ξ continuously decreases. Hence, a pattern is observed between the time-varying sensitivity values and the extent to which the uncertainties of the variable is reducible.

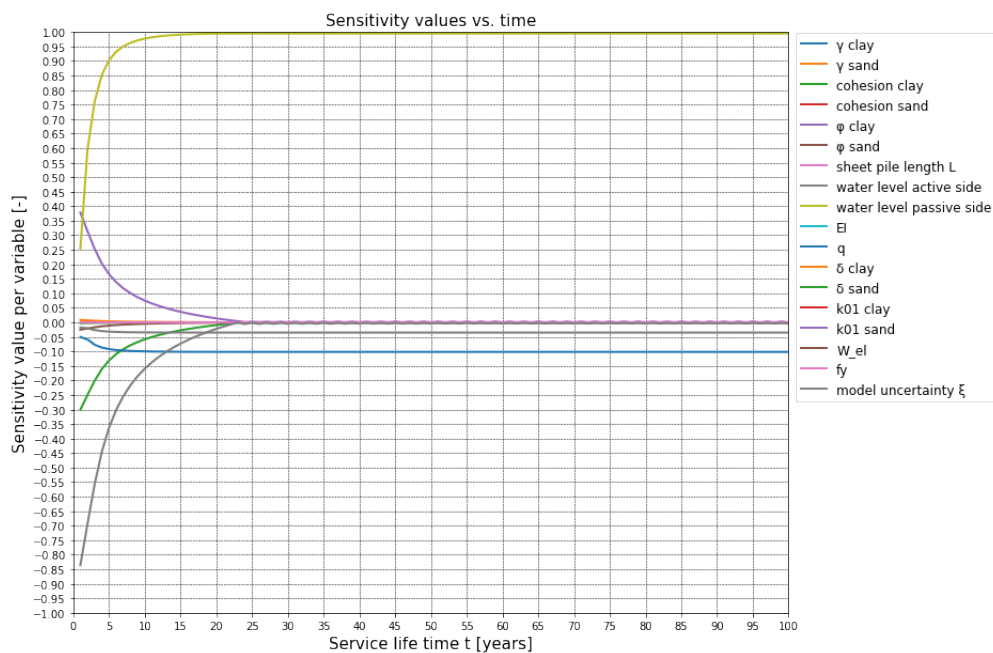


Figure 6.5: Time-dependent sensitivity values that are numerically calculated by means of the iteratively found reliability indices. Here, numerical integration is applied.

The sensitivity values per input variable are initially positioned in the same sequence as the auto-correlation per concerned input variable. No changes are observed despite applied mutations in the sequence of the auto-correlation and initial sensitivity value of each input variable. The time-dependent curves of the auto-correlation of the cross-section and the sensitivity values remain unchanged. Figure 6.6 shows the time-dependent curve of the correlation between the cross-section in year i and year $i + 1$.

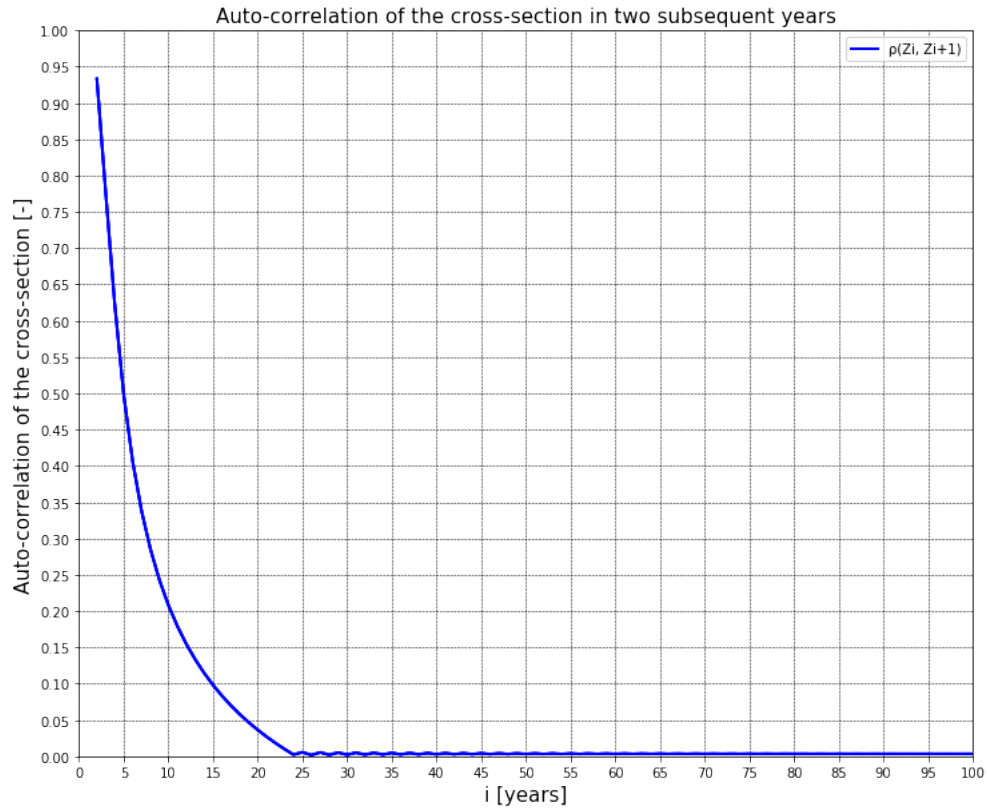


Figure 6.6: Time-dependent auto-correlation of the cross-section in year i and subsequent year $i + 1$.

The start value of β_1 is the computed annual reliability index in the case including cross-correlated variables and model uncertainty but without degradation. Initially, a relatively low annual reliability index $\beta_1 = 2.33$ was used in the EPM algorithm. The same reference case without degradation, correlations and model uncertainty is reconsidered in the Equivalent Planes method. Firstly, a start reliability index is redetermined given $t_{ref} = 1$ year: $\beta = 4$. The corresponding start sensitivity values are found as well:

$$\underline{\alpha} = [0, 0, 0.175, 0, 0.875, -0.0164, 0, -0.0482, 0.419, 0, -0.0850, 0.136, -0.00258, 0, 0, 0, 0] \quad (6.8)$$

Note that the model uncertainty factor ξ is now excluded. The 1×17 -matrix is input for the EPM-algorithm. As a result, a time-dependent reliability curve is obtained. Figure 6.7 shows the time-dependent reliability curve, whereas figure 6.8 is illustrating the behaviour of the auto-correlation between cross-sections versus time t .

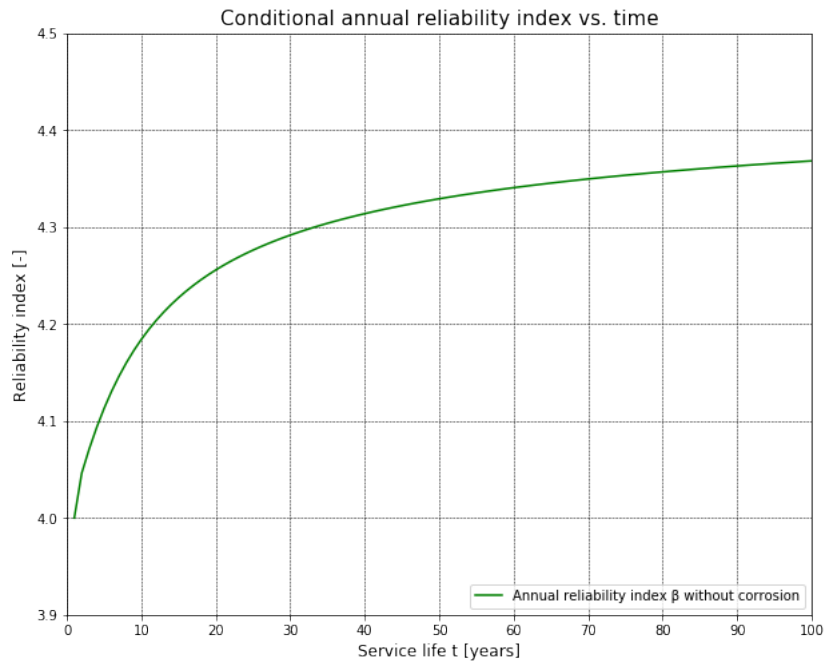


Figure 6.7: Time-dependent conditional reliability curve given a larger start value of the annual reliability index.

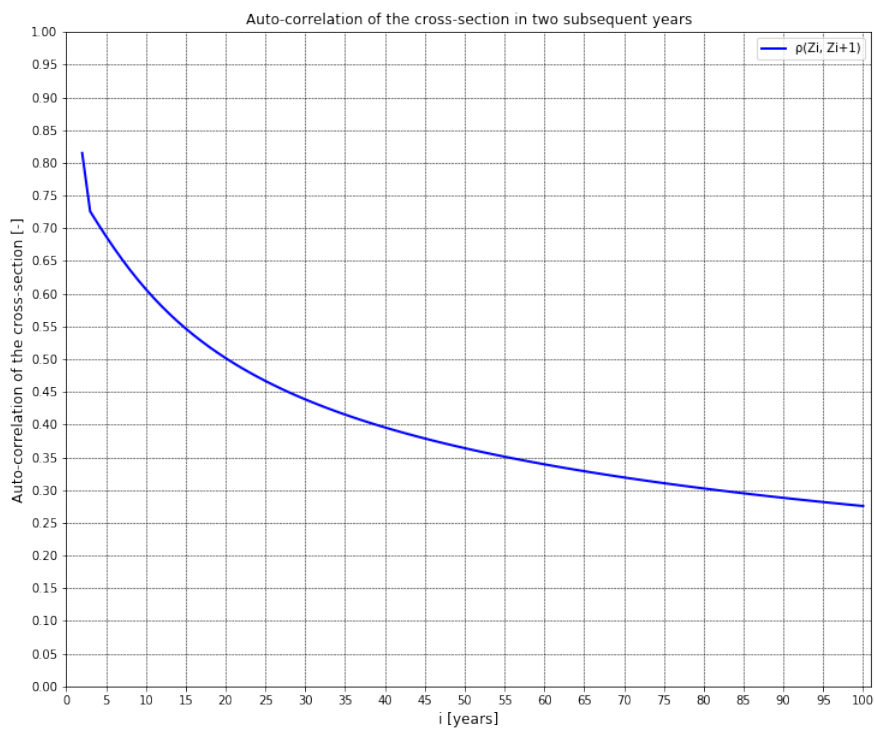


Figure 6.8: Time-dependent auto-correlation between the cross-section in year i and $i + 1$.

So in case of a significantly higher initial β_1 , a relatively much smaller increase of the reliability is found. In terms of probabilities, the decrease of P_f in the case of without cross correlations, degradation and model uncertainty factor is equal to:

$$\Delta P_f \approx 10^{-4.37} - 10^{-4} = -5.73 \cdot 10^{-5}$$

The above value is relatively much smaller than the failure probability decrease which is obtained with the input from table 6.4 ($\beta_1 = 2.33$) in chapter 6.5:

$$\Delta P_f \approx 10^{-3.61} - 10^{-2.33} = -0.004431$$

The effects of past performance appear to be considerably less in the case of a higher initial reliability indices due to the absence of an epistemic model uncertainty and cross-correlated variables. Furthermore, the correlation of the cross-section with time appears to behave differently as time progresses. The decrease of the auto-correlation is relatively smaller in the case without model uncertainty which is an epistemic uncertainty. Hence, the correlation of the cross-section in time is largely dependent on the amount of epistemic uncertainty.

Time-dependent effects on the quay wall

In the previous analyses, time-related effects such as effect(s) of a decreasing strength have been disregarded. Nevertheless, this latter aspect has a significant impact on the time-dependent reliability of the reference case cross-section. Besides degradation, other effects such as the change of model uncertainty or the loads over time have not been studied yet. Yet, all these aspects should have a significant influence in the course of the (conditional) reliability index over time, as is explained in chapter 1.

7.1. Time-variant model uncertainty factor

The model uncertainty factor takes uncertainty relating to the correspondence between the model and reality into account. Chapter 6 treated the reference case in which the auto-correlation $\rho_{ij} = 1$. As explained earlier, ρ_{ij} is the correlation in time of the model uncertainty factor ξ . $\rho_{ij} = 1$ physically means that the uncertainties are fully reducible as time progresses. Hence by doing more research one is able to reduce these epistemic (knowledge) uncertainties, as was explained in chapter C.5.3.

Figure 6.4 shows a decrease in the relative influence of the model uncertainty. This sensitivity value is influenced by the uncertainty i.e. variance of the considered variable ξ . ξ has a lognormal distribution with mean value $\mu_\xi = 1$ and standard deviation $\sigma_\xi = 0.1$. This decrease indicates a reduction of the knowledge uncertainty.

The first case considered full dependence between the model uncertainty in two individual years. The same cross-section is now studied with a model uncertainty which is partly influenced by randomness or aleatory uncertainties. The upcoming case supposes a $\rho_{ij\xi} = 0.75$. Hence, the auto-correlation $\rho_{ij\xi}$ assumes no fully linear dependence between the variables in two individual years. This physically means that the largeness of the model uncertainty cannot be fully be derived with a value in a different year. Statement 7.1 presents the row vector of the auto-correlation in time. The sensitivity values of year 1 remain unchanged as presented by α -matrix 6.8 in section 6.5.

$$\begin{aligned} \underline{\rho}_{ij} = & [\rho_{ij\gamma_1} \rho_{ij\gamma_2} \rho_{ijc_1} \rho_{ijc_2} \rho_{ij\phi_1} \rho_{ij\phi_2} \rho_{ijL} \rho_{ijw_a} \dots \\ & \rho_{ijw_p} \rho_{ijEI} \rho_{ijq} \rho_{ij\delta_1} \rho_{ij\delta_2} \rho_{ijk_{01,clay}} \rho_{ijk_{01,sand}} \rho_{ijW_{el}} \rho_{ijf_y} \rho_{ij\xi}] \\ = & [1, 1, 1, 1, 1, 1, 1, 0, 0, 1, 0, 1, 1, 1, 1, 1, 1, 0.75] \quad (7.1) \end{aligned}$$

As a result, the time-dependent reliability curve as presented in blue in figure 7.1 is obtained. The same procedure is performed for $\rho_{ij\xi} = 0.25$ and 0.50. Both lines are plotted in figure 7.1 as well.

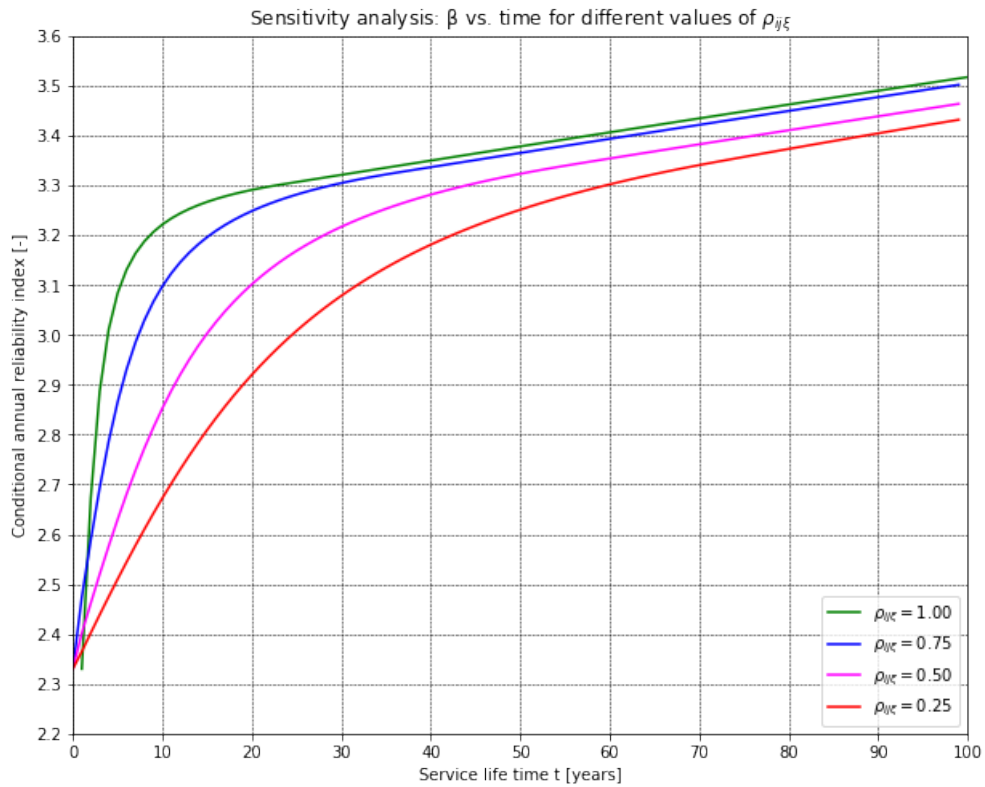


Figure 7.1: Sensitivity analysis of the reliability index on the condition that previous years are survived. The time-dependent conditional reliability index is calculated for 100 years in the case without degradation and for different auto-correlations $\rho_{ij\xi}$

The sensitivity analysis for figure 7.1 results in a gradient which is different for each case. For larger $\rho_{ij\xi}$, the conditional annual reliability index appears to increase more quickly in the first years. Additionally, the absolute gradient of the curve becomes smaller when $\rho_{ij\xi}$ approaches 1 in comparison with $\rho_{ij\xi}$ approaching 0. This phenomenon is explained by the change of the governing model uncertainty parameter. Figure 7.2 illustrates several curves resulting from a sensitivity analysis with the time-variant sensitivity value of the model uncertainty factor ξ .

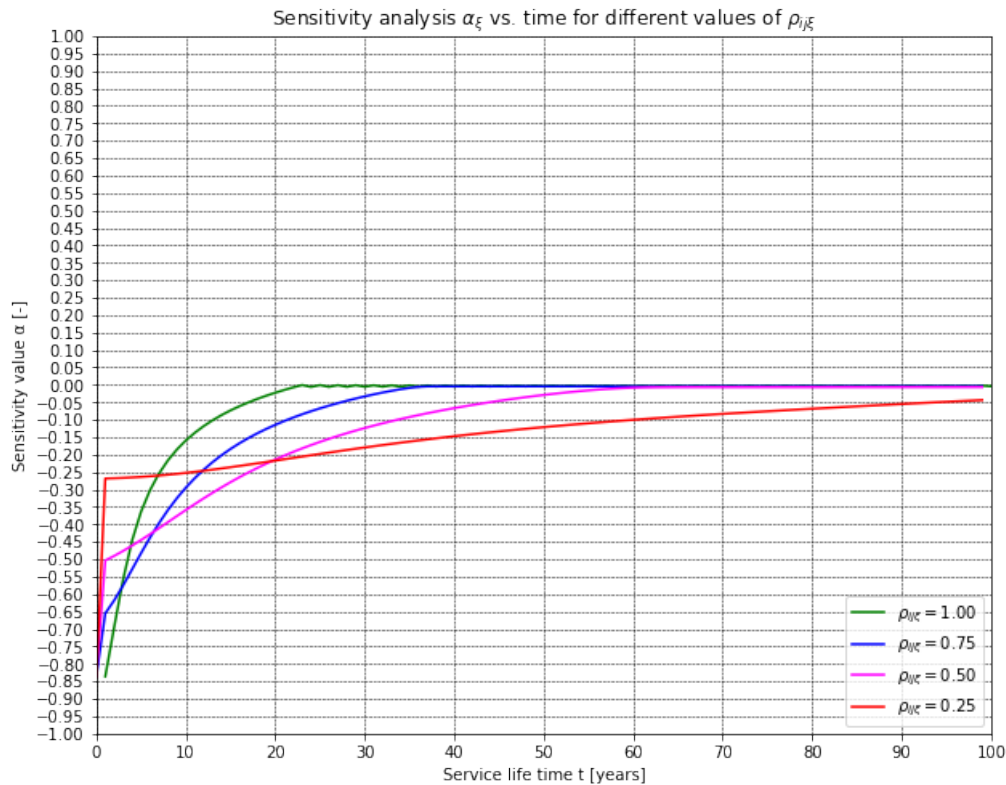


Figure 7.2: Sensitivity analysis for the time-dependent α_ξ considering no degradation and given the auto-correlation $\rho_{ij\xi}$

For smaller values of $\rho_{ij\xi}$, the absolute value of α_{xi} converges relatively slow to zero. The numerical approximation of α_{ik} results in a kink in some of the curves. This is observed for $\rho_{ij\xi} < 0$ at $t = 2$ years. This kink is likely the result of a setting problem in the numerical routine for deriving the updated α_{ik} . This kink becomes less visible for larger values of the correlation in time $\rho_{ij\xi}$. So a value $\rho_{ij\xi}$ between 0 and 1 indicates that the considered variable and its uncertainty are influenced by both epistemic and aleatory uncertainty. A smaller $\rho_{ij\xi}$ implies that the considered variable is increasingly influenced by random events. Hence, the influence of the model uncertainty (pertaining to the correspondence between the model and the reality) decreases insignificantly smaller in the case of larger irreducible uncertainty ($\rho_{ij\xi} \rightarrow 0$). The latter has an effect on the reliability over time which is affected by the magnitude of the lognormally distributed model uncertainty. As the aleatory uncertainty increases, the convergence of the model uncertainty to 0 and of the reliability index to its maximum value decelerate (see fig. 7.1 and 7.2). Eventually, for all values of $\rho_{ij\xi}$ the lines converge to zero.

7.2. Inclusion of time-variant loads

Previously in chapter 4.4 the reliability indices as a function of the reference period t_{ref} were determined. The dominant load parameter q was modelled with extreme value distributions for different numbers of independent time intervals m . This method was performed for $t_{ref} = 1, 5, 10, 25, 50$ and 100 years. Initially, the load variables w_a , w_p and q were assumed to have an auto-correlation $\rho_{ijk} = 0$. The latter means that these variables are time-dependent and fully governed by aleatory or irreducible uncertainties. In the case of $\rho_{ijk} = 0$, no correlation exists between the maxima of the variables in different years. In this section, the correlations of the load parameters (w_a , w_p and q) with time t are studied.

To realise that, a similar method as described in chapter 4.4 applies for the random variables w_a and w_p . Appendix L presents the algorithm which was used in chapter 4.4 for the derivation of the uniform

load distribution parameters given t_{ref} , see equation 4.8. For the derivation of the correlation between each load variable and time t , 10 reference periods are considered as interpolation points (see eq. 7.2). A for most earth-retaining structures' unfavourable situation is considered in which the difference between the water levels on both size is increasing as t_{ref} extends. The type I maxima (Gumbel) for the uniform load distribution q remains applicable for this analysis.

$$t_{ref} = \{10, 20, 30, 40, 50, 60, 70, 80, 90, 100\} \quad (7.2)$$

The 50 year minimum- and maximum value distribution of the water level(s) are simulated by means of $n \cdot n = 10,000 \times 10,000$ samples from the normally distributed water level(s) $w_a, w_p \sim N(-1.5, 0.20)$. Similarly, the 50 year maximum value distribution of the uniform load $q \sim N(20, 2)$ is modelled. Afterwards, several parameters can be determined among which the location parameter u_i with $i = 10, 20, \dots, 100$. The procedure for deriving the distribution parameters given the reference period is provided in an algorithm by figure O.1 in appendix O.

As a result, type I minima- and maxima distributions are found for w_p and w_a respectively. These distributions are presented by figures 7.3-7.4.

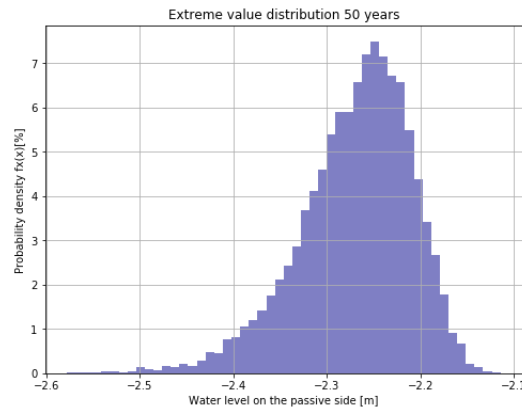


Figure 7.3: The minimum value distribution of w_p results in a type I minima presenting the water level relative to the ground surface level (G.S.L.).

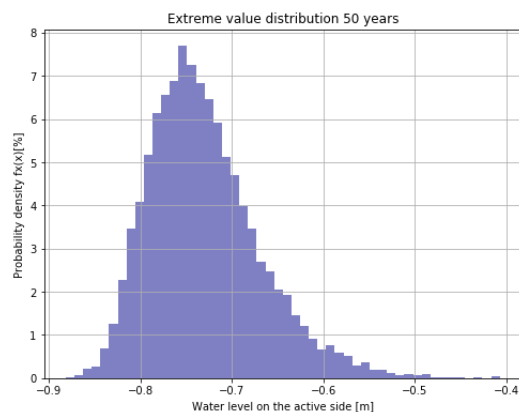


Figure 7.4: The maximum value distribution of w_a results in a type I maxima presenting the water level relative to G.S.L.

Table 7.1 lists the extreme value distribution parameters for the considered reference periods from eq. 7.2. These parameters are derived using Gumbel transformations, assuming independent loading

intervals m.

t_{ref} in years	μ_{w_a} in m+GSL	σ_{w_a} in m+GSL	μ_{w_p} in m+GSL	σ_{w_p} in m+GSL	μ_q in kN/m ²	σ_q in kN/m ²
10	-0.752	0.061	-2.194	0.060	26.937	0.610
20	-0.720	0.061	-2.227	0.060	27.267	0.610
30	-0.700	0.061	-2.246	0.060	27.460	0.610
40	-0.687	0.061	-2.259	0.060	27.560	0.610
50	-0.676	0.061	-2.270	0.060	27.703	0.610
60	-0.667	0.061	-2.279	0.060	27.790	0.610
70	-0.660	0.061	-2.286	0.060	27.863	0.610
80	-0.654	0.061	-2.292	0.060	27.927	0.610
90	-0.648	0.061	-2.298	0.060	27.983	0.610
100	-0.643	0.061	-2.303	0.060	28.032	0.610

Table 7.1: Distribution parameters of the type I maxima per reference period.

Consequently, the auto-correlation of each load variable is derived. This is performed by means of mathematical rules presented by equations 7.3-7.4. Table 7.2 provides the information which is used for these calculations. The auto-correlation, or in other words correlation in time ρ_{ijk} , can be found in the last row of table 7.2.

$$\rho_{XY} = \frac{cov(X, Y)}{\sigma_X \sigma_Y} \quad (7.3)$$

$$cov(X, Y) = E [(X - E [X]) (Y - E [Y])] \quad (7.4)$$

Variable	t_{ref} in years	X-E[X]	μ_{w_a} in m+GSL	Y1-E[Y1]	μ_{w_p} in m+GSL	Y2-E[Y2]	μ_q in kN/m ²	Y3-E[Y3]	COV(X, Y1)	COV(X, Y2)	COV(X, Y3)
	10	-45	-0.752	-0.072	-2.194	0.071	26.937	-0.715	3.229	-3.202	32.184
	20	-35	-0.720	-0.039	-2.227	0.039	27.267	-0.385	1.359	-1.348	13.482
	30	-25	-0.700	-0.020	-2.246	0.019	27.460	-0.192	0.489	-0.485	4.805
	40	-15	-0.687	-0.006	-2.259	0.006	27.560	-0.092	0.088	-0.088	1.383
	50	-5	-0.676	0.005	-2.270	-0.005	27.703	0.051	-0.024	0.023	-0.254
	60	5	-0.667	0.013	-2.279	-0.013	27.790	0.138	0.067	-0.066	0.689
	70	15	-0.660	0.021	-2.286	-0.021	27.863	0.211	0.310	-0.308	3.162
	80	25	-0.654	0.027	-2.292	-0.027	27.927	0.275	0.676	-0.670	6.870
	90	35	-0.648	0.033	-2.298	-0.032	27.983	0.331	1.142	-1.132	11.578
	100	45	-0.643	0.038	-2.303	-0.037	28.032	0.380	1.693	-1.679	17.091
Mean value:	55		-0.681		-2.265		27.652		0.903	-0.896	9.099
Standard deviation:		28.7228		0.033		0.033		0.332			
ρ_{w_a}	ρ_{w_p}	ρ_q									
0.9517	-0.9517	0.9549									

Table 7.2: Information which is used for the derivation of the auto-correlation ρ_{ijk} of each type I distributed load variable (w_a , w_p and q) between the considered reference periods according eq. 7.2.

In each case a Pearson coefficient $|\rho_{ijk}| = 0.95$ (with $k = w_a, w_p$ and q) is found. For longer reference periods the expected values of the type I distributed load variables appear to almost linearly increase for w_a and q ($\rho = 0.95$) and linearly decrease for w_p ($\rho = -0.95$). Hence, the simulated distributions for the considered reference periods result in an auto-correlation unequal to 0. The reliability updating method with Hohenbichler is reexamined with new auto-correlation values for the load parameters. The model uncertainty ξ is assumed to be time-independent:

$$\begin{aligned} \underline{\rho}_{ij} &= [\rho_{ij\gamma_1} \rho_{ij\gamma_2} \rho_{ijc_1} \rho_{ijc_2} \rho_{ij\phi_1} \rho_{ij\phi_2} \rho_{ijL} \rho_{ijw_a} \dots \\ &\dots \rho_{ijw_p} \rho_{ijEI} \rho_{ijq} \rho_{ij\delta_1} \rho_{ij\delta_2} \rho_{ijk_{01,clay}} \rho_{ijk_{01,sand}} \rho_{ijW_{el}} \rho_{ijf_y} \rho_{ij\xi}] \\ &= [1, 1, 1, 1, 1, 1, 1, 0.95, -0.95, 1, 0.95, 1, 1, 1, 1, 1, 1, 1] \end{aligned}$$

As a result, the correlation of the cross-section in time $\rho(Z_i, Z_{i-1})$ becomes 0.9389. This value is marginally smaller than the value which was initially found: $\rho(Z_i, Z_{i-1}) = 0.9534$. The Equivalent Planes method is repeated for the new auto-correlations between subsequent years $i - 1$ and i . For comparison, the new time-dependent reliability curves are plotted with a dark brown colour in the same figure as the lines from chapter 6.5. The sensitivity values of each variable are separately plotted in figure 7.6.

Figure 7.7 shows the reliability index as a function of the reference period t_{ref} . In this figure two situations are considered, load variables (w_a , w_p and q) not correlated in time and load variables correlated in time.

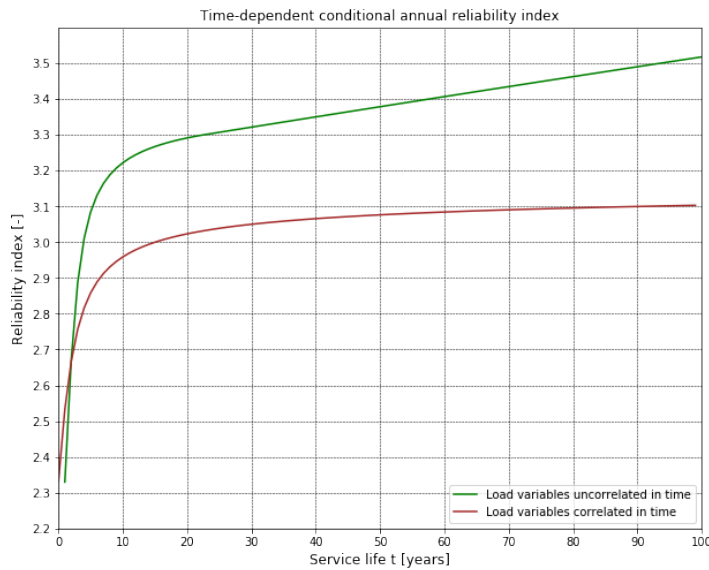


Figure 7.5: Conditional annual reliability index as a function of time for two cases: variables w_a , w_p and q being correlated with time $\rho_{ijk} \neq 0$ (red) and the same variables uncorrelated with time $\rho_{ijk} = 0$ (green).

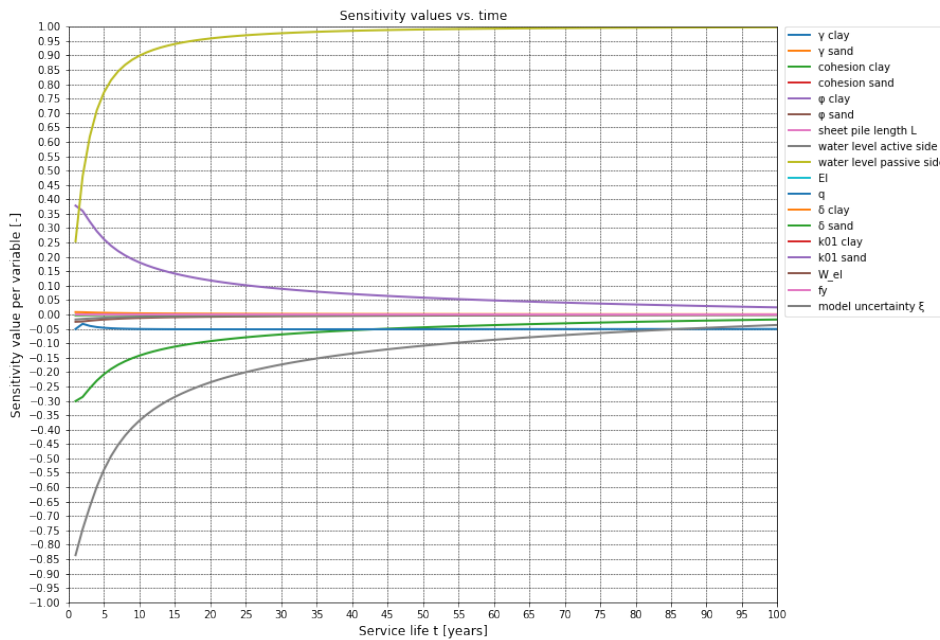


Figure 7.6: Time-dependent sensitivity values as a result of passive water level ($\rho_{ijw_p} = -0.95$), active water level ($\rho_{ijw_a} = 0.95$) and uniform load ($\rho_{ijq} = 0.95$) being correlated with time t .

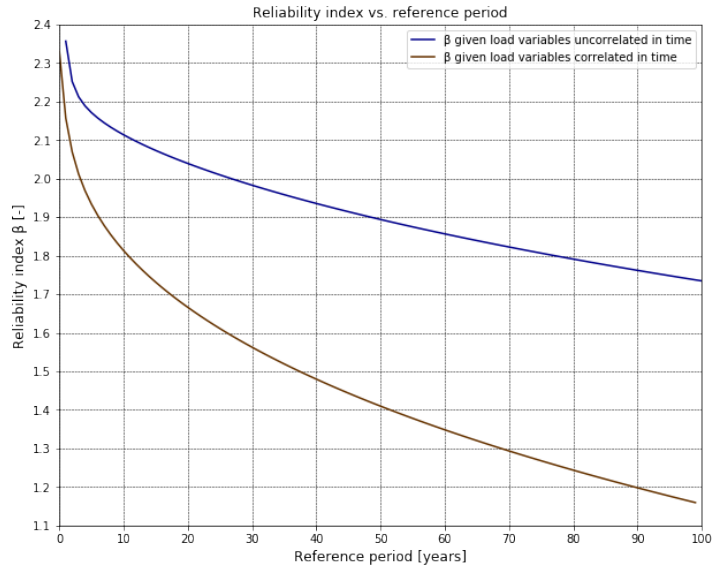


Figure 7.7: The reliability index β_n as a function of the reference period t_{ref} for two cases: load variables not auto-correlated $\rho_{ijk} = 0$ (blue), load variables auto-correlated $\rho_{ijk} \neq 0$ (brown).

A few points are noticeable. The time-dependent reliability index slowly ascends to larger values in the case of $\rho_{w_a} = \rho_q = 0.95$ and $\rho_{w_p} = -0.95$. The reliability as a function of the reference period t_{ref} quickly decreases. This is in accordance with the smaller annual reliability indices and the fact that the difference between the water level increases over time t . As a matter of fact, the sensitivity values are almost unchanged. The influence of the passive water level becomes considerably present as time passes by, which is in accordance with the previous figures. The influence of the water level on the active side converges from a small year 1 value eventually to zero. The influence of uniform load q is present, increases but is not dominant. Hence, these phenomena seem arguable. The reason for that is the fact that the uncertainties related to these variables are predominantly epistemic since $\rho_{w_a}, \rho_q \rightarrow 1$.

7.3. Degradation by corrosion

Many objects including quay walls are in practice confronted with the effects from surrounding environment, climate and extreme actions. A considerable part has already been discussed in the previous sections. Sections 7.2 and 7.1 treated the effects of a changing model uncertainty or extreme loads over time. In fact, the load variable was considered as time-dependent $S(t)$. This section addresses the effects of the strength as a result from degradation on the time-dependent reliability. Degradation is in this research caused by corrosion of the retaining wall. Hence, in this case the load is constant whereas the resistance is a function of time $R(t)$. In view of the research boundaries (dynamic) loading or fatigue are not taken into account.

Recall the limit state function formulated by equation 4.7 from chapter 4.3. This equation addresses yielding of the front wall and is a function of the deterministic yield stress f_y , maximum bending moment M_{max} and the elastic section modulus of the retaining wall around its relatively weaker y-axis $W_{el,y}$. Model uncertainty is introduced through the variable ξ . The bending moment M is directly linear proportional with the elastic bending stiffness EI of the beam according to Euler-Bernoulli. The front wall is in this case considered as the beam. Equation 7.5 describes the case conform [88].

$$M = -EI_y \frac{d^2u}{dz^2} = EI_y \cdot \kappa \quad (7.5)$$

where:

$\frac{d^2u}{dz^2}$ is the second derivative of the front wall deflection with respect to the z-coordinate of the sheet pile wall.

κ is the curvature of the sheet pile wall or the slope of an elastic stress-strain diagram [88].

EI_y is the bending stiffness around the y-axis of the sheet pile wall per system width.

Hence, the proportionality between the bending moment and the bending stiffness is an important fact. The bending stiffness EI is a product of the Young's modulus E and the moment of inertia I . The analyses in which corrosion is included, is performed within the range where the largest bending moment occurs. The permanent immersion zone is annotated by region D in figure 7.8. This region of the retaining wall is critical for the derivation of the time-dependent reliability.

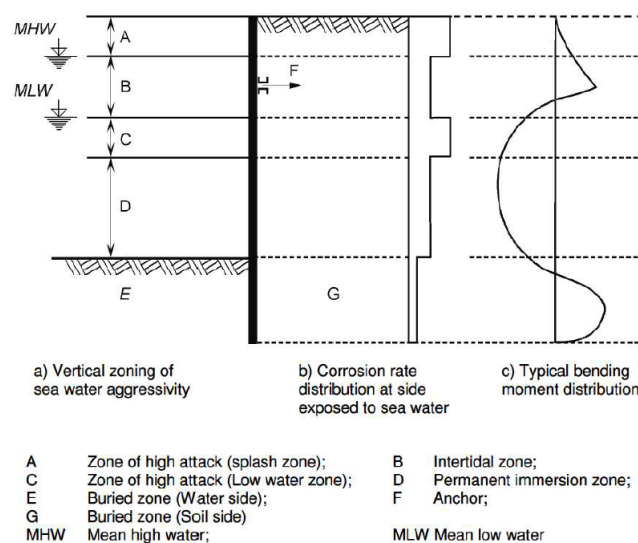


Figure 7.8: Corrosion rate distribution and zones of severity around a marine structure according to EC 3, EN1993 for steel structures [51, ch. 4]

Based on deterministic analyses from chapter 3.2, one finds a maximum bending moment M_{max} within the permanent immersion zone. Figure 7.9 presents the moment diagram of the considered CUR class III cross-section.

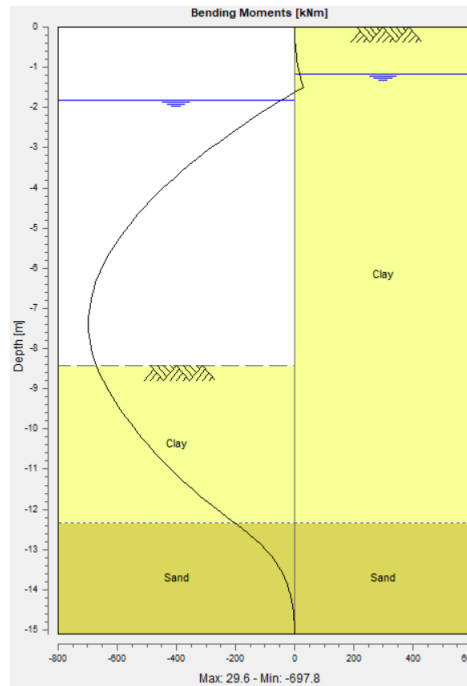


Figure 7.9: The moment diagram which is obtained by deterministic analyses in chapter 3.2.

Corrosion ultimately affects the steel sheet pile profile parameters [63] [67]. The interaction between the soil and the sheet pile is performed by means of the subgrade-reaction model (see chapter C.5.4). Hence, the mechanical behaviour of the quay wall is influenced by the reduction of the section modulus and inertia, as the bending stiffness EI which is determined by inertia. Hence a decrease in bending stiffness should result in a different moment distribution along the quay wall height [59]. Table 7.3 lists the characteristics of the quay wall which are used in the CUR research report by GeoDelft [72]. The derivation of these parameters was illustrated in chapter 4.1.1. Notice that the initial parameters $I_{el,y}$ and $W_{el,y}$ are from this point onward mentioned as $I_{el,y;0}$ and $W_{el,y;0}$.

Parameter	Value	Unit/m
$EI_{el,y;0}$	500000	kNm^2
E	$210 \cdot 10^6$	kN/m^2
$W_{el,y;0}$	$3266.25 \cdot 10^3$	mm^3
$I_{el,y;0}$	$238095.24 \cdot 10^4$	mm^4

Table 7.3: Initial geometric sheet pile characteristics.

As was found in [9], these characteristics are comparable with the characteristics of a an combined Arcelor profile. Chapter 4 described the combined wall profile consisting of primary tubular elements $\varnothing 1,016 - 14 \text{ mm}$ and 2 intermediate secondary elements AU18 ($I_{el,y} = 238,559 \cdot 10^4 \text{ mm}^4/\text{m}$ and $W_{el,y} = 4,696 \cdot 10^3 \text{ mm}^3$). For this case study, an initial wall thickness $e_0 = 14 \text{ mm}$ is assumed. $W_{el,y}$, $I_{el,y}$ and e_0 are all deterministic variables.

Table 4-1 and 4-2 in EC3 NEN-EN 1993 part 5: Piling [51] recommend values for the loss of thick-

ness due to corrosion in mm. These values are prescribed for several circumstances on both the land- and sea side of (sheet) piles. However, the linearly increasing loss of thickness (as prescribed in EC3) appears to be significantly unrealistic compared with the corrosion curves proposed by Jongbloed. These curves are constructed on the basis of measurements over an extended time period. Figure 7.10 shows the curve based on the by EC3 recommended values, relate to the corrosion curves 1 - 9 by Jongbloed (see figure C.28 from chapter 2.2). The black solid line in figure 7.10 represents the corrosion rate as recommended by EC3. The Jongbloed's curves in figure 7.10 represent the equivalent mean value over a period of 50 years. This equivalent mean value equals the sum of the mean uniform corrosion and pitting corrosion with an accuracy of 1 mm during this 50 years exposure period [63, p. 3].

Required design working life	5 years	25 years	50 years	75 years	100 years
Undisturbed natural soils (sand, silt, clay, schist, ...)	0.00	0.30	0.60	0.90	1.20
Sea water in temperate climate in the zone of permanent immersion or in the intertidal zone	0.25	0.90	1.75	2.60	3.50

¹ The values for 5 and 25 years are based on data sets consisting many measurements. The other values are extrapolated [51, p. 31].

² Corrosion rates in compacted fills are lower than for non-compacted fills. The recommended figures in this table should be divided by two for compacted fills [51, p. 31].

Table 7.4: Recommended value for thickness losses [mm] due to corrosion for piles and sheet piles in soils (with or without groundwater), fresh water or in sea water.

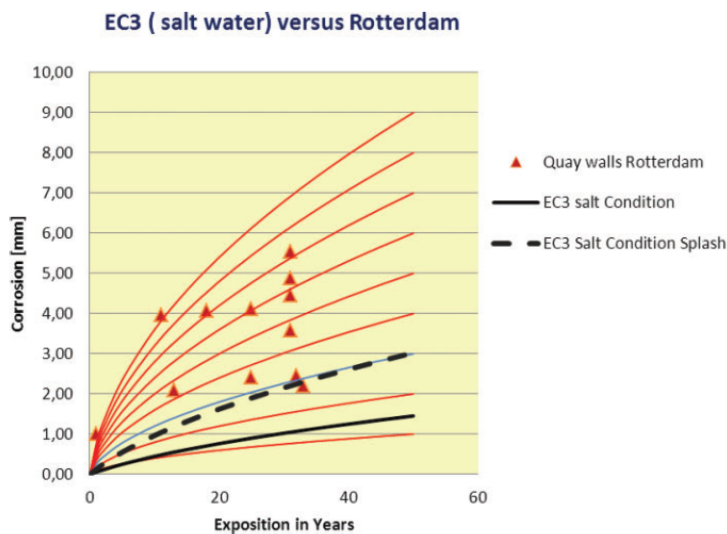


Figure 7.10: The by NEN-EN 1993 recommended loss of thickness due to corrosion (black solid line) and Jongbloed's corrosion curves versus the exposure period in years [17, p. 394].

For the reference case a situation with a compacted, non-aggressive soil is assumed. Furthermore, the cross-section is bordered by salt water in temperate climate conditions. Due to compaction and a high groundwater table, relatively low oxygen is present in the soil (which mainly consists of clay). The latter makes it assumable that recommended corrosion rates at the land side are negligible compared with the recommended values for the sea side. Lower corrosion curves are representative for a quay wall located in Dutch climate conditions. In this case study, equivalent mean corrosion values accord-

ing to curve 3 are assumed. For the considered situation in the permanent immersion zone, curve 3 is reasonably consistent with the prescribed thickness losses in table 7.4. The mean corrosion rate following curve 3 is described by equation 7.6.

$$\Delta e (a_{scale}, y_{scale}, n) = \frac{-2a_{scale}y_{scale} + \sqrt{(2a_{scale}y_{scale})^2 + 4a_{scale}n}}{2a_{scale}} \quad (7.6)$$

where:

n is a variable number in [years]

$a_{scale} = 4.630$ is a dimensionless scale parameter of corrosion curve 3 [-]

$y_{scale} = 0.300$ is a dimensionless scale parameter of corrosion curve 3 [-]

Δe is the corrosion after n years [mm]

The corrosion scale parameters a_{scale} and y_{scale} are deterministic and found by fitting through a large amount of scattered data. The above expression includes both uniform and pitting corrosion with a tolerance of 1 mm. Figure 7.11 illustrates corrosion curve 3 over a service life of 100 years.

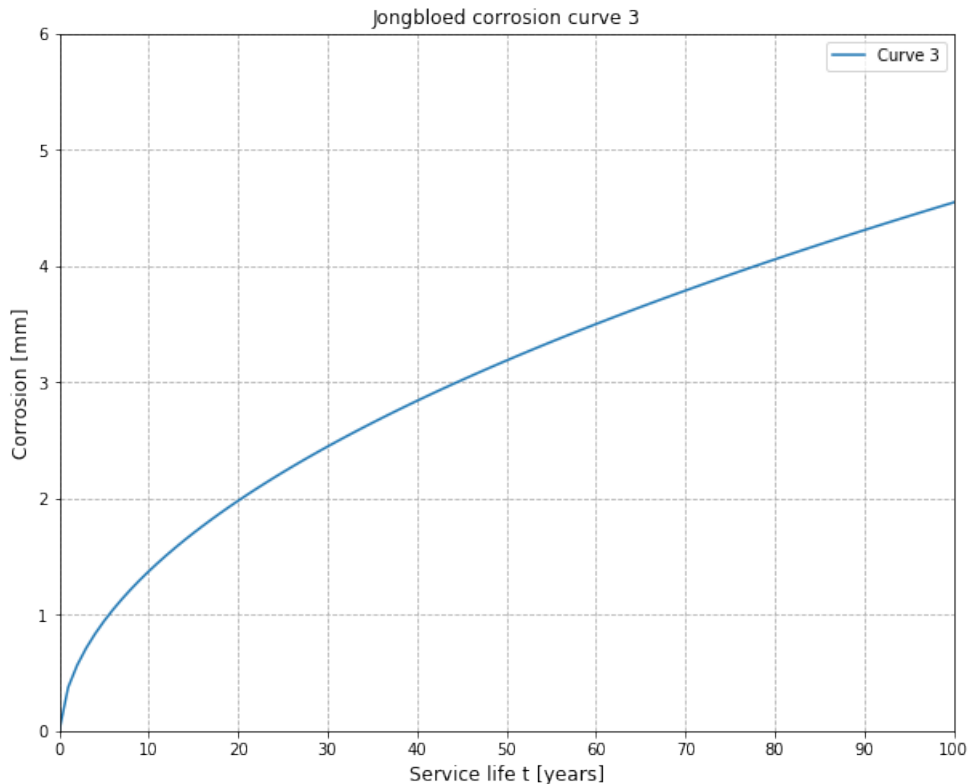


Figure 7.11: Corrosion curve 3 give a service life of 100 years.

The equivalent mean value of the corrosion rate influences the geometric cross-sectional properties I and W . An equivalent combined wall profile ($\varnothing 1016-14$ 2xAU18) (similar bending stiffness EI) is used for studying the effects of corrosion. As explained in chapter C.2.2, forces are mainly transferred via the primary elements. Corrosion solely affects the tubular profile at the water side. As a result, the outer wall thickness at the water side is decreasing. In addition, the position of the central axis changes. The result is a reduced section modulus at the water side: $W_{e,y;waterside}$. The corroded inertia I and

section modulus W of the tubular pile are determined according to equations P.1 - P.15 in appendix R. In this chapter two methods are distinguished for the derivation of the time-dependent reliability curve as a result of corrosion:

- The engineering method in which solely the section modulus is repeatedly influenced by corrosion.
- A "second order" method in which both the section modulus and inertia are affected by corrosion.

Appendix P shows the equations through which the new sectional parameters are derived. The first method does not consider equation P.15. Hence, the engineering method solely includes the effects on section modulus $W_{el,y}$. A second order approach with a time-variant EI is additionally considered. The bending stiffness is assumed to vary along the total height of the sheet pile wall.

Several literature sources [39] [67] describe a lognormally distributed corrosion rate for different corrosion zones. [63] proposed a truncated normal distribution with a variable mean for all Jongbloed's corrosion curves, each curve is truncated by its adjacent curves. In this research, the equivalent mean corrosion rate is described by equation 7.6. The profile characteristics W_0 and I_0 change according to the equations above. Predominantly the primary quay wall elements are affected by corrosion, since these elements mainly comprise base metal in contrast with the secondary intermediate sheet piles [63]. As emphasised in [63, ch. 4.3.3], many measurements in the port of Rotterdam appear to result in coefficients of variation CoV mostly in the range between 0.1 and 0.5. In this research a situation with a lower CoV = 10% of the corrosion variable Δe is assumed. Since recommended values for thickness losses due to corrosion are mainly determined by measurements, epistemic uncertainty appears to be governing. Hence, in this research an auto-correlation of $\rho_{ij\Delta e} = 1.0$ is assumed.

The section modulus W_{corr} and inertia I_{corr} are determined for subsequent $t = 1, 2, \dots, 100$ years. This is performed by means of a composite model (D-Sheet Piling run through a Python script) within the Deltares Probabilistic Toolkit. A lognormal distributed corrosion curve is applied: $\Delta e \sim \text{LN}(\Delta e(a_{scale}, y_{scale}, n), 0.1\mu)$. Similar values are selected for the input variables as in the previous case. The calculation is performed with multiple rounds. Each round computes the maximum bending moment in the sheet pile wall given a reduced cross-section. As a result, the annual reliability index as a function of time $\beta(t)$ given varying $W_{el,y}$ and constant EI is calculated. This is repeatedly performed with a FORM routine. The red line in figure 7.12 presents the development of the annual reliability index due to corrosion curve 3. The green line represents the annual reliability index conditional upon survival of previous years [0, t-1].

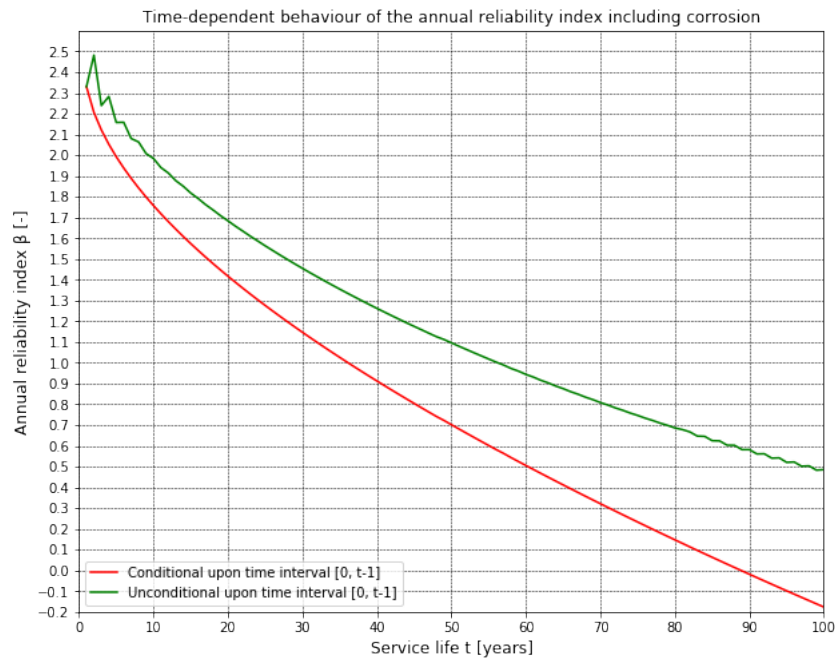


Figure 7.12: Development of the annual reliability index including corrosion and unconditional upon time interval $[0, t-1]$ (red), including corrosion and conditional upon survival in the time interval $[0, t-1]$ (green).

In figure 7.12, the effect(s) of survived years can be observed by the upward shift of the tail. The above time-variant curves are derived with the engineering approach. Flutter is observed in the upper and lower tail. This flutter is caused by the numerical routine in the derivation of the updated reliability index $\beta_{F_i|S_{i-1}}$ with the Equivalent Planes method. The algorithm uses yearly reliability indices (shown by the red curve in figure 7.12) in the calculation of the reliability given survived years.

The sensitivity values are calculated in advance with FORM. The corrosion rate described by Jongbloed curve 3 is assumed as a fully epistemic uncertainty ($\rho_{ij\Delta e}$) and log normal variable. Figure 7.13 shows the sensitivity values in individual years given degradation. The lines are derived with the engineering approach.

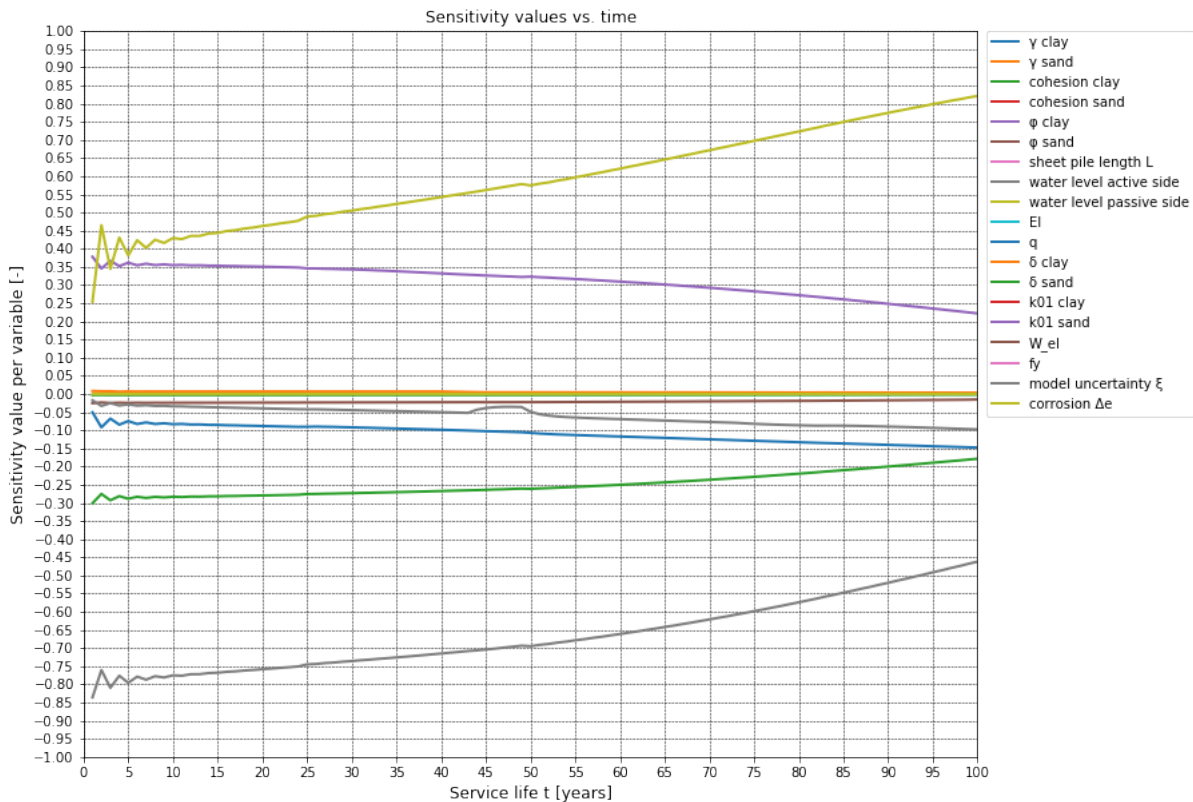


Figure 7.13: Time-dependent sensitivity values given degradation and survived years, derived with the engineering approach.

The time-dependent reliability index given survived years and degradation, derived with the engineering approach (see figure 7.12), follows a descending trend. In the first few years, a marginal upsurge of the conditional annual reliability index is observed. This is due to the application of the Hohenbichler function given information about marginally lower annual reliability (see figure 7.12 and survived years). Afterwards the curve gradient sharply declines. Eventually, the gradient of the descending curve becomes smaller. The corresponding sensitivity values undergo no significant changes at all. Epistemic uncertainties (including ϕ_2 and c_1) slowly converge to smaller values. Aleatory uncertainty among which the water levels w_a and w_p gradually diverge. These converging and diverging processes accelerate when t approaches 100 years. The results incorporating degradation, show a considerably different behaviour relative to the results found in chapter 6. In the engineering approach, the effects of degradation appear to cancel out for a significant part effects of survived years.

Figure Q.1 in appendix Q.1 presents the time-dependent annual reliability derived with the "second order" approach. Notice that solely the permanent immersion zone is considered. Hence, the reduction of bending stiffness results in a favourable effect on M_{max} in this considered zone. The effect(s) of past performance become visible in the early years. The upper part of the green line, representing the conditional annual reliability index given corrosion and survived years, lies above the red line. The red line represents the time-dependent unconditional annual reliability indices as a result of Jongbloed corrosion curve number 3. The conditional annual reliability index increases as time progresses. Eventually, the time-dependent behaviour flattens and marginally decreases. Hence, in this specific considered case of the refined approach, the influence of corrosion is relatively small compared to information about survived years.

The time-dependent sensitivity values, resulting from the refined approach, show flutter in many years. Figure Q.2 in appendix Q.1 shows different behaviour of the sensitivity values. In contract to the engineering approach and the case without corrosion, the epistemic uncertainties do not necessarily converge (abruptly or gradually). On the other hand, the aleatory uncertainties do not necessarily

diverge as time progresses. Hence, the view has changed a lot. The numerical routine for the derivation of β 's and α 's results in numerical instabilities as well. From $t \approx 63$ years onward, no limit state value(s) are obtained.

The reliability index β_n as a function of the reference period t_{ref} also shows a sharp decline in the first years (see figure Q.3 in appendix Q.2). This decline is considerably more for the case with corrosion compared with the case without corrosion. Hence, the corroded profile as considered with the refined approach for the specific case, results in a significant decrease of the reliability index β_n as the reference period extends.

Figure Q.3 in appendix Q.2 is derived with the "second order" approach and presents reliability indices for each reference period given $t \in (0, 100]$. Figure Q.4 in appendix Q.2 also presents the reliability indices per reference period. These values are found with the engineering approach. Normally, both approaches yield recommended reliability indices for the derivation of partial safety factors. However, both approaches result in a significantly lower target reliability value per reference period in comparison with the recommended values in [15] and [12]. From a practical point of view, the latter seems not representative for all quay walls. Nevertheless, the development of the reliability as a function of the reference period is clarified through figures Q.3-Q.4 in appendix Q.

7.4. Method for updating partial safety factors

This research treats the effects of past performance on the sensitivity factors. The research describes the method for deriving the updated partial safety factors. The values for the partial safety factors are although not computed in this research, solely the application of the obtained sensitivity values and reliability indices in the (semi-probabilistic) level I method is shown.

Partial safety factors are applicable in the physical X_i -space derived by formulas 7.7 and 7.8 (see chapter C.37). The NEN-EN 1990 and many other European or national standards prescribe partial safety factors according the reliability level [12] [15].

$$\gamma_S = \frac{s^*}{S_k} \quad (7.7)$$

Here:

s^* is the design value of the considered load variable.

S_k is the characteristic value of the considered load variable.

γ_S is the load factor.

$$\gamma_R = \frac{R_k}{r^*} \quad (7.8)$$

Here:

r^* is the design value of the considered resistance variable.

R_k is the characteristic value of the considered resistance variable.

γ_R is the safety factor on the resistance.

The time-dependent sensitivity values are derived in the standard normal space. This is performed by means of a numerical approach. The reliability index equals the shortest distance from the origin to the plane $g(\underline{U}) = 0$ in the U_1, U_2 -space. Formula 5.14 calculates the influence coefficient. In this research 5.14 is applied with a numerical algorithm. A gradient step size (or perturbation value) $du = 0.01$ is used. Figure 7.14 visualises the meaning of the sensitivity value. The point that is crossed on the line $g(\underline{U}) = 0$, is the design point \underline{u}^* . The design value changes each year a calculation is performed. Equation 7.9 shows how a design value is computed with the sensitivity value α_{ik} of the considered variable and the reliability index β_i in a certain year.

$$u_i^* = -\alpha_{ik}\beta \quad (7.9)$$

In case of independent non-normally distributed random variables, the reliability function in the physical space is not normally distributed either. Level II (FORM) approximation methods becomes applicable if the non-normally distributed variables are transformed to normally distributed variables [42, p. 132]. In this research corrosion Δe , model uncertainty ξ are independent log normally distributed variables. Uniform load q is an independent Gumbel distributed variable. The distribution variables are normalised by means of equation 7.10.

$$x_i^* = F_{x_i}^{-1} [\Phi (u_i^*)] = F_{x_i}^{-1} [\Phi (-\alpha_{ik}\beta)] \quad (7.10)$$

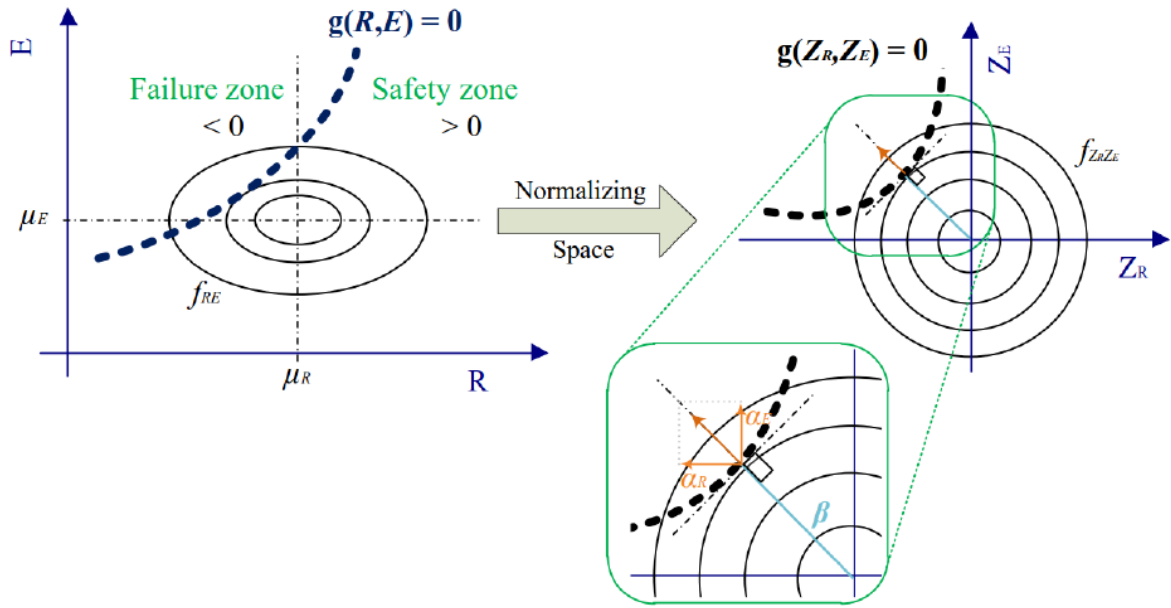


Figure 7.14: The transformation of the joint probability density function and failure plane from the physical space to the normal space including a visualisation of the influence coefficient.

Here, α_{ik} is the updated sensitivity coefficient of the concerning variable and β the corresponding reliability index. Respectively, for log normal- and Gumbel distributed variables equation 7.11 and 7.12 hold.

$$x_i^* = \frac{\mu_{x_i}}{\sqrt{1 + V_{x_i}^2}} \exp\left(-\alpha_i \beta \sqrt{\ln(1 + V_{x_i}^2)}\right) \quad (7.11)$$

In cases where $V_{x_i} < 0$

$$x_i^* = u - \frac{1}{\alpha} \ln[-\ln(\Phi(-\alpha_i \beta))] \quad (7.12)$$

The above expressions derive the design value of the considered variables. Eventually, the partial safety factors are determined for each subsequent year by equations 7.7 and 7.8. In many cases, the characteristic value(s) x_k (S_k and R_k) is predetermined and constant. In this research, the characteristic value of a random variable is determined based on the stochastic distribution. The characteristic value of a normal distribution is determined by equation 7.13 and remains unchanged over time t in years.

$$x_k = \mu_x \pm 1.645\sigma_x \quad (7.13)$$

The characteristic value of a log normal distribution is determined with eq. 7.14¹.

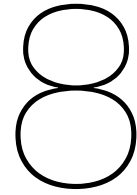
$$x_k = \mu_x \exp(\pm 1.645V_{x_i}) \quad (7.14)$$

¹This expression is valid for cases in which the CoV < 0.2 [42, p. 233]

The Gumbel distributed uniform load q uses a characteristic value which equals the value with an exceedance probability of 2% during a reference period of 1 year [42, p. 249]. With the latter knowledge equation 7.15 is found.

$$Q_k = \mu_1 + 2.593\sigma_1 \quad (7.15)$$

In all expressions above, a characteristic load value is calculated with a plus sign whereas the resistance value is determined with a minus sign. As follows, the partial safety factors can be iteratively determined by application of equations 7.7 and 7.8 in the Equivalent Planes method. The sensitivity coefficient determines whether the concerning variable works favourable- or unfavourable in the considered limit state.



Conclusion, discussion and recommendations

This final chapter treats the conclusion, discussion and recommendations. The results in the previous chapter lead to research answers. The research outcomes result in a discussion which is treated in section 8.2. Eventually, recommendations for further research are provided in section 8.3.

8.1. Conclusion

This research has drawn several conclusions considering the effects of past performance on the semi-probabilistic method for the design and/or evaluation of (existing) quay walls. In this chapter the main conclusions and consequently the recommendations are treated. The main aspects are treated in accordance with the research questions.

The case study is treated through investigation of several research questions. Answers on these research questions follow from findings from the case study. The main objective of this research is:

"Studying the effect(s) of past performance on the semi-probabilistic Level I method for the design and evaluation of (existing) quay walls."

The solution to this main object is composed from the answers of the different research sub-questions. The research treats a case study representing of a CUR class III sheet pile cross-section. The reference case was described in chapter 3 according to [71]. The aim of these sub-questions is to form a structure of premises to eventually answer the central question:

"How can effects of past performance be taken into consideration in a semi-probabilistic assessment of existing quay walls, by means of a reliability updating method analogously to what is already applied in the field of flood defence systems?"

Hence each individual sub-question is treated by the theoretical background and the subsequent case study and should contribute to the main research question.

What is the optimal modelling approach for the selected reference case(s)?

In this research the Equivalent Planes method has been considered. Currently, this is considered as the most optimal approach for the selected reference case, since it already is successively applied in the field of flood defence systems [43]. The optimal modelling approach with the Equivalent Planes method needs to be validated. The required steps for the EPM-method, with results from FORM-analyses realised by probabilistic software coupled with a spring model, is although thoroughly described in this research. In addition, updating reliability with the obtained prior results by means of Equivalent Planes method appears to be effective. However, higher accuracy of the prior results comprising the input reliability indices and sensitivity factors should be pursued. The latter can be achieved by performing level III analyses in the Deltares PTK coupled with D-Sheet Piling. It is expected that it also can work by using FEM software coupled with a probabilistic interface but this was not investigated.

Using FEM-results with the Equivalent Planes method requires assessment on the efficiency of the required steps that need to be taken. Hence, it should be investigated for what design purposes the approach with for instance PLAXIS is necessary. This is performed by means of a new research or case study. Table 8.1 summarises the computation time for each part of the analyses. The prior analyses require little time for the FORM analyses, but significantly larger amount for level III verification. In addition, much efficient time is required for the analyses including degradation.

Type of calculation(s)	Value	Time unit(s)
<i>Prior analyses</i>		
<i>FORM</i>		
Basic case	1 to 5	min
Including correlations	1 to 5	min
Model uncertainty factor	1 to 5	min
Incl. degradation (100 rounds)	2 to 3 ¹	h
<i>Importance Sampling</i>		
Basic case	2 to 3	h
<i>Posterior analyses</i>		
<i>EPM without degradation</i>		
FORM	1 to 5	mins
Numerical Integration	1 to 5	min
<i>EPM with degradation</i>		
FORM	1 to 5	min
Numerical Integration	1 to 5	min

¹ The effective time means the time without interruptions due to memory exception errors in D-Sheet Piling. Some calculation(s) take a total time of multiple days (2 to 3 days).

Table 8.1: Effective time¹ per calculation(s).

A procedure in which FEM is used with reliability updated, is schematised in chapter 8.3.1. The required computation time(s) per type of calculation needs to be studied in the case of application with FEM.

How can Bayesian updating be applied in the case study?

Bayesian updating or reliability updating can be applied by means of an iterative application of the Hohenbichler-Rackwitz method. In some literature this repeatable method is named as Equivalent Planes method. The cases study has proven that this method works sufficiently effective in the derivation of conditional annual reliability indices and sensitivity factors.

The output from the probabilistic calculations with the spring model consists of yearly reliability results, sensitivity factors and is input for the Equivalent Planes algorithm in MATLAB. This method derives an equivalent failure plane in the standard normal space representing the failure state of/in two or more components/failure states. Numerical integration appears to be sufficiently accurate in the case where two unknown variables emerge in the equivalent limit state function. Each failure plane represents the limit state of the cross-section in a specific year given survival of the previous year(s). The obtained results are successively applied in a new iteration of the Hohenbichler function. As a result newly updated conditional annual reliability, sensitivity values and auto-correlations are obtained. The Bayesian updating method is studied with the failure mechanism: yielding of the front wall. For comparison reasons and because of its relative practical importance this mechanism has been considered.

What are the impacts of adding information to the model regarding the reliability level of the existing quay wall?

As was explained in chapter C.5.3, two main types of uncertainties exist in this area of knowledge:

- Epistemic uncertainties (time-independent uncertainties)
- Aleatory uncertainties (time-dependent uncertainties)

Reliability updating considers both types of uncertainties. Adding information to the model of the reference case most likely results in a reduction of the uncertainty. Time-independent uncertainty is mostly related to the amount of knowledge about the involved parameters among which geotechnical parameters such as ϕ_{sand} and c_{clay} . These parameters are called reducible uncertainties. More information can be obtained by field- or lab research.

Reduction of the epistemic uncertainty leads to narrowing of the probability density distribution of the time-independent random variables. As a consequence, the influence of the time-independent variables decrease. For this specific reference case without degradation, the net result of the reduction is an gradual increase of the conditional annual reliability of the quay wall. The following effect is a reduction on the auto-correlation between cross-section considered in year i and year $i + 1$. Eventually, the annual reliability index ascend less quickly to larger values. Moreover the influence of the reduced epistemic variable converges slower to significantly small absolute values.

How do the sensitivity factors of the model variables develop over time given the effects of past performance?

The behaviour of the sensitivity factors over time is illustrated with several figures (see figure 6.4, N.2, 6.5 in chapters 6 and 7 resp.). The relative influence of a random variable on the failure mechanism is embodied by the annual sensitivity. In the case without degradation, two noticeable kinds of behaviour are observed:

- The relative influence of time-independent variables converges to very small absolute values as time progresses. The extent to which such a variable is correlated in time (measured by ρ_{ijk}) influences the speed of convergence. The lower the auto-correlation ρ_{ijk} , the slower the relative influence of the concerning epistemic variable converges.

- The relative influence of time-dependent variables, which are more governed by natural variations, diverges as time progresses. These variables have a negative influence on the correlation of the cross-section in time. In other words, the more aleatory variables the lower the auto-correlation of the cross-sections in year i and $i + 1$ $\rho(Z_i, Z_{i+1})$, the slower the increase of the annual reliability index.

In the case with degradation, different types of behaviour are found. Firstly, two approaches have been considered:

- The engineering approach in which solely the section modulus $W_{el,y}$ is affected by corrosion.
- A refined or "second order" approach in which a change of I_0 due to corrosion is considered as well.

The engineering approach results in time-dependent reliability curves as is represented by the green line in figure 8.1. The graph firstly adjusts itself in this numerical iteration procedure. Thereafter, the reliability index given degradation and survival of previous years, sharply decreases and flattens gradually as time progresses. As a consequence, the time-dependent sensitivity values marginally change. As time t progress to many years, epistemic uncertainties slowly converge to smaller values whereas aleatory variables slowly diverge.

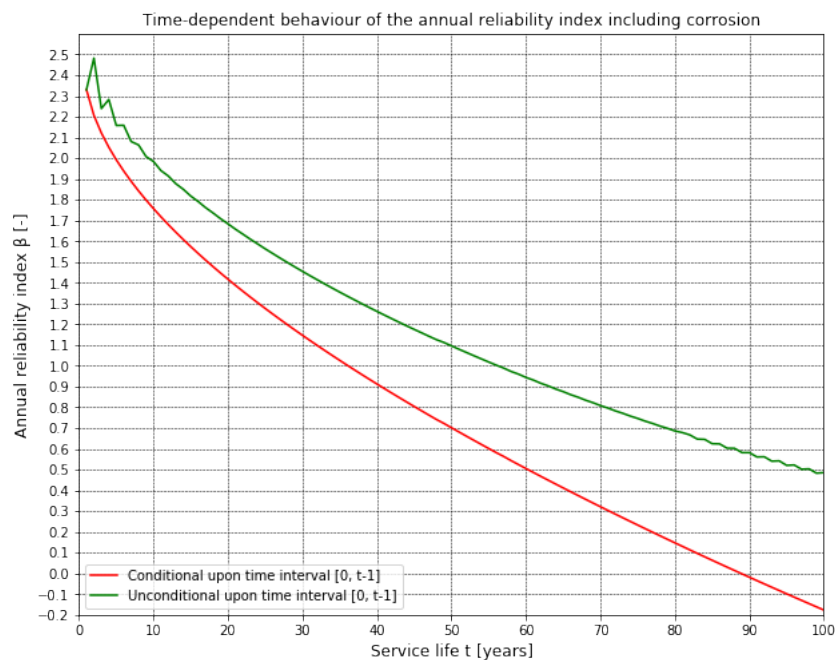


Figure 8.1: Development of the annual reliability index including corrosion and unconditional upon time interval $[0, t-1]$ (red), including corrosion and conditional upon survival in the time interval $[0, t-1]$ (green).

The refined approach results in a decreasing bending stiffness along the total height of the retaining wall. As a result, a significantly different time-dependent conditional annual reliability curve is obtained. This is shown by the green curve in figure Q.1 in appendix Q. The results that are obtained with this approach depend on the geometry, geotechnical stratification and structural stiffness compared to soil stiffness. Therefore, it is difficult whether this approach always result in a more realistic and less conservative result. Nevertheless, in the results from the considered approach, the latter appears to be the case. The engineering approach is generally applicable, so this approach is further considered.

How does the time-dependent behaviour of strength variables, due to degradation by corrosion during the previous years of service, impact the reliability analyses of the reference quay wall?

Some resistance variables among which the deterministic steel yield stress f_y and $W_{el,y}$ are explicitly stated in equation 8.1. Other strength variables such as the internal friction angle of clay ϕ_1 , wall friction angle of clay δ_1 and the passive water level w_p are implicitly characterised as strength variables by a positive sensitivity coefficients α_{ik} . These variables were initially found as strength variables due to their positive influence in the prior computations

$$Z = f_y - \frac{\xi M_{max}}{W_{el,y}} \tag{8.1}$$

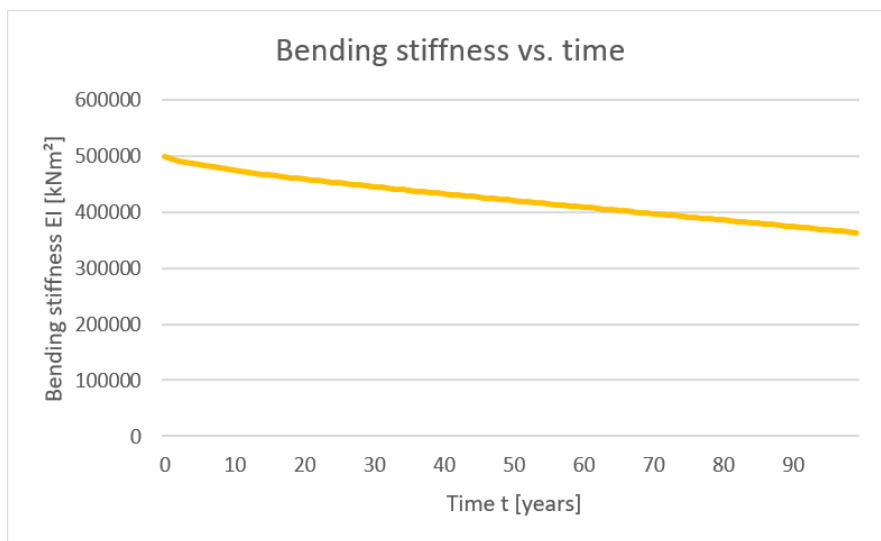


Figure 8.2: Bending stiffness EI as a function of time due to corrosion curve 3.

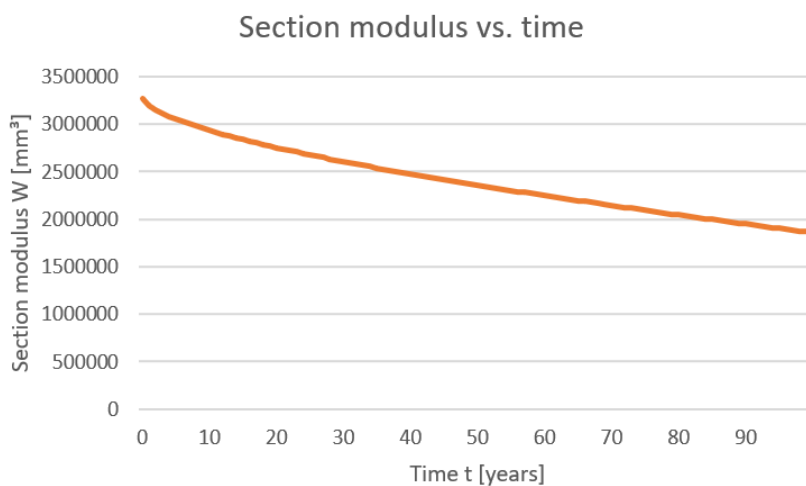


Figure 8.3: Section modulus $W_{el,y}$ as a function of time due to corrosion curve 3.

The time-dependent behaviour of the strength variables $r_i(t)$ can be observed through the varying sensitivity values α_{r_i} . EI and $W_{el,y}$ are deterministic resistance variables and change according the

corrosion curve 3 as is illustrated in figures 8.2 and 8.3. The deterministic yield stress f_y remains constant. Considering limit state by equation 8.1, one finds a smaller maximum bending moment M_{max} due to a decreasing EI. In addition, a reduced section modulus results in a larger bending stress. The time-dependent reliability is decreasing for all years using the engineering approach. The bending stiffness decreases relatively quicker compared to the section modulus. As a consequence, with the second order approach the reliability is initially positively influenced by a reduced bending stiffness due to corrosion. After many years, the reliability decreases as a consequence of the reduced section modulus. It appears that the reduction of bending stiffness has a larger impact than the reduced section modulus. Additionally, the effect(s) of survived years seems to be relatively smaller compared to the reduction of strength variables.

The time-dependent behaviour of other strength variables, including epistemic- and aleatory uncertainties, is observed in figure(s) 8.4 (engineering approach) and Q.2 ("second order" approach) in appendix Q. For the engineering approach, no significant changes are found for the (positive) sensitivity values. The "second order" or refined approach results in relatively bigger modifications of the sensitivity coefficients. As a result, the design value $u_{ik}^* = -\alpha_{ik}\beta$, after transformation x_{ik}^* and the partial safety factors γ_{xi} change. It appears that a more realistic view regarding corrosion is obtained by the more refined approach. However, it becomes questionable whether this approach can be generalised. The increment in β is considerably high (in figure Q.1) and merely one corrosion zone is studied.

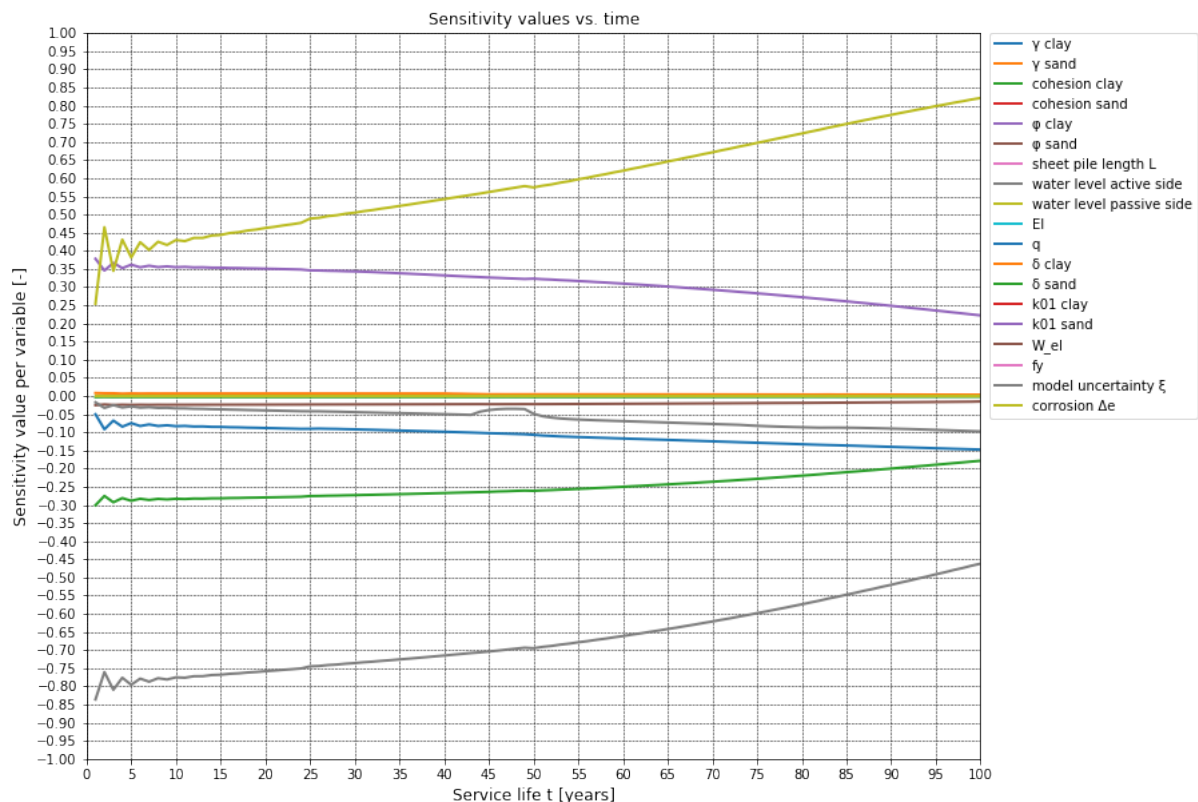


Figure 8.4: The time-variant sensitivity values derived with the engineering approach, given past performance including randomly distributed corrosion.

How is the information about the sensitivity factors reapplied in the semi-probabilistic analyses?

Semi-probabilistic level I analyses are commonly used in the derivation of partial factors γ_{x_i} for strength- and resistance variables. For that, equation C.39 is used. The obtained information about the time-variant sensitivity values is not directly applied in semi-probabilistic level I analyses, since these values are obtained in the correlated and uncorrelated u -space (see equation below).

$$\alpha_{ik} = \sqrt{\frac{\partial \beta_i}{\partial u_{uc,ik}} + \frac{\partial \beta_i}{\partial u_{c,ik}}}$$

Moreover, the derived values may represent the sensitivity values of a local design point. The standard normal design point u^* , which is found with equation 7.9, can be transformed to the physical X -space. By means of level I approach, as outlined in chapter 7, the partial safety factors for load(s) γ_S and strength γ_R is determined.

In what ways does the analyses output, realised by means of the effect of past performance, compare with the output that is realised by means of the original approach for the reference case(s)?

The differences between the outcomes are observed in several ways. The prior analyses output already showed marginal differences due to software limitations and the unavailable information in the reference report. The model uncertainty factor $\xi \sim \text{LN}(1, 0.1)$ as a multiplication factor arrogated a large influence on the failure mechanism: yielding of the front wall. Initially, this influence ($\alpha_\xi = 0.836$) is considerably larger compared with what was found in [71]. In addition, figure 4.11 showed how the coefficient of variation CoV significantly affects the reliability index.

The posterior analyses output among which the updated reliability indices and sensitivity factors differ substantially from the recommended target values conform the Eurocode [17][12]. As time progresses, the epistemic uncertainties converge to zero, whereas the aleatory uncertainties diverge. Model uncertainty factor results in a significantly low annual reliability index $\beta = 2.33$. The latter input results in a relatively larger increase of reliability due to survived years. Effects of past performance are relatively less visible in case of larger reliability indices. Figure 6.2(a) shows the reliability index as a function of the reference period (without degradation). These reliability values are used in the level I approach as explained in chapter 7.4. The proportions between 1-year and 50-year reliability indices obtained with the Equivalent Planes method, are almost equal to the ratios found with the CUR166/211 which are conform NEN-EN 1990, see table 8.2.

	$t_{ref} = 1 \text{ year}$	$t_{ref} = 50 \text{ years}$	$t_{ref,1}/t_{ref,50}$
Equivalent Planes method	2.33	1.9	1.226
CUR 211 RC3 cf. NEN-EN 1990 [12] [17]	5.2	4.3	1.209

Table 8.2: Comparison between the two approaches

Additionally, the effects of past performance are found in the time-dependent behaviour of the sensitivity values in figures 6.5 and Q.2. Extended service life periods result in changing $\alpha_{F_i|S_{i-1}}$. The influence values decrease for each additional year t in case of reducible time-independent uncertainties.

The knowledge about the changing influence coefficients must result in considerably different partial factors given the prior analyses values of table 8.4 and effects of past performance.

	Equivalent Planes method
Variable	$\alpha_{F_i S_{i-1}}$ [-]
Cohesion of clay: c_{clay}	Converging to 0
Internal friction angle: ϕ_{clay}	Converging to 0
Wall friction angle: δ_{clay}	Converging to 0
Uniform load q	Diverging to -0.10

Table 8.3: Annual sensitivity values [-] given the effects of past performance and extension of service life time in years.

According to:	β [-]	
GeoDelft report	4.5	
CUR class III	4.3	
FORM given $\gamma_m = 1.1$	4.53	
	Calculated	Geodelft
Variable	α [-]	α [-]
Cohesion of clay: c_{clay}	0.189	0.41
Internal friction angle: ϕ_{clay}	0.825	0.69
Wall friction angle: δ_{clay}	0.147	0.17
Uniform load q	-0.252	-0.24

Table 8.4: Comparison between the β - and α -values calculated with form and the values found in the research report "Veiligheid van damwandconstructies" [71].

The previously answered research questions lead to sufficient information in order to answer the main research question. Still considerable research is needed to obtain about the derived reliability- and sensitivity values in this research. The main research question reads as follows:

"How can past performance be taken into consideration in a semi-probabilistic assessment of existing quay walls, by means of a reliability updating method analogously to what is already applied in the field of flood defence systems?"

As a final point, the main research question is answered. The application and effects of past performance have been studied for a significantly large part. In this research, past performance is considered through several aspects:

- By changing the reference period t_{ref}
- By taking survived years t into account
- By taking degradation by e.g. corrosion into account

The reliability index and corresponding influence coefficients are derived for a certain reference period t_{ref} and can be translated for different reference periods. In this research, the information is translated on an annual basis. Consequently, the annual values are used in the Equivalent Planes method. This is an effective method for updating reliability indices and sensitivity values based on past performance. On beforehand, the required information is calculated with probabilistic software coupled with a modelled cross-section. The case study, which is considered with the spring model, appears to yield sufficient information about the applicability of the Equivalent Planes method.

The derived time-dependent annual (conditional and unconditional) reliability indices, time-variant sensitivity values and reliability indices as function of t_{ref} appear to provide much knowledge on the

development of the residual strength and partial factors over time. The residual strength is noticeable from the updated time-dependent annual reliability index. In addition, the updated sensitivity values are useful indicators for the effect of past performance on the magnitude of the partial safety factors γ_{x_i} . The reliability indices as a function of t_{ref} (see among others fig. 6.2a) can be applied in the Level I method for the derivation of γ_{x_i} . The transformation rules which were illustrated at the end of chapter 7 in and the level I method, as is explained in chapter C.37, are resourceful for the iterative procedure of deriving the partial safety factors γ_{x_i} . Naturally, the latter including the effects of past performance.

8.2. Discussion

During this research, several simplifications and assumptions have been made. These aspects have influence on the results and the subsequent interpretations. In this section the main assumptions, simplifications and findings are discussed.

8.2.1. Incorporated model uncertainty

The response parameters, based on the stochastic input variables, are in the case study studied with the introduction of model uncertainty. This model uncertainty represents the correspondence between the considered CUR class III D-Sheet Piling model and the reality. The research does not engage with large data sets consisting calculated bending moments for the derivation of this factor. In fact, the distribution of the model uncertainty ξ is determined conform [55], [64].

Model uncertainty has a significant influence on the start values of the (conditional) annual reliability index as was found with FORM analyses in chapter 4.3. The 50 year reliability index including model uncertainty is considerably lower than the outcome which is found in the reference case report [71] [72]. However, the reports [71] [72] did not include a model uncertainty factor in the computations. Hence, the application of model uncertainty factor in the coupled subgrade reaction analysis should be reassessed, if necessary for varying situations and evaluated. Considerations in which the standard deviation of the model uncertainty σ_ξ is varied provides useful insight into the development of the time-dependent reliability and sensitivity values, given the Equivalent Planes method. Figure 4.11 yields insight in the effect of model uncertainty on the reliability calculations with the spring model. Figure 7.1 for instance clearly visualises the time-dependent behaviour by means of sensitivity analyses of the auto-correlation regarding the model uncertainty.

8.2.2. Significantly low calculated reliability index

The applied model uncertainty factor results in a significantly high failure probability or low values of the (annual) reliability index for the cross-section. It is uncertain whether these obtained reliability indices (including effects of degradation and survived years) are representative for all retaining walls. Especially when these calculated values are compared with the recommended target reliability values according [15] [17] and [12]. Seeing this, the calculated values incorporating model uncertainty are not acceptable for practical reasons (see for instance figure 4.11). Hence, The conditional annual reliability indices and updated sensitivity values should be considered with caution. Despite the unrealistically low values, the overall procedure of applying the Equivalent Planes method has been clarified. Further recommendations are provided in section 8.3.

8.2.3. Standardised normal space

The Equivalent Planes method considers and (re)formulates the failure plane(s) Z_i in the standard normal u -space. Equation 5.6 uses the (updated) reliability index, standard normal design values ($u_{ik} \sim N(0, 1)$) and transformed influence coefficients α_{ik} of the subsequently derived (equivalent) failure plane. An influence factor α_{ik} describes the relative influence of a certain variable x_{ik} on the considered limit state in the transformed u -space. The influence coefficients are derived by taking the derivative of the equivalent failure plane for $Z_i = 0$ in terms of the correlated and uncorrelated design points in the U_1, U_2 -plane. Numerical algorithms are used for this latter approach. Hence, the calculated influence coefficients are for a significant part dependent on the assumed perturbation value or gradient step size du . In this research $du = 0.01$ is assumed, which appears a reasonably accurate value considering the expected development of epistemic and aleatory uncertainties.

$$u_i = \frac{x_i - \mu_{x_i}}{\sigma_{x_i}} \quad (8.2)$$

The sensitivity values are found with the normalised Euclidean distance of the vector representing the derivative of Z_i in the correlated- and uncorrelated standard normalised u -space. Equation 8.2 transforms the design variables \underline{x}^* and \underline{u}^* from and to one each other. In case of normally distributed variables an equivalent relation exists between the sensitivity values in the different spaces according to method 1. Equation 8.3 formulates the sensitivity values conform [42].

$$\alpha_i = \frac{\frac{\partial Z}{\partial u_i^*}}{\left| \frac{\partial Z}{\partial \underline{u}^*} \right|} = \frac{\sigma_{x_i} \frac{\partial Z}{\partial x_i^*}}{\left| \frac{\partial Z}{\partial \underline{x}^*} \right|} \quad (8.3)$$

Accordingly, the influence coefficients of the normally distributed variables can be interpreted for the physical space as well. It is in either case necessary to verify whether $\sum \alpha_{ik}^2 = 1$ holds. In this research however, certain random variables among which $\xi \sim \text{LN}(1, 0.1)$, $q \sim \text{G}(25.8, 0.61)$ and $\Delta e \sim \text{LN}(0.2532, 0.025)$ do not engage with this approach. Hence, the design values for these variables become significantly different compared to normalised variables. Equation 8.4 derives the design value, whereas equations 7.13-7.15 from chapter 7 derive characteristic values according the distribution type.

$$x_i^* = F_{x_i}^{-1} [\Phi(u_i^*)] = F_{x_i}^{-1} [\Phi(-\alpha_{ik}\beta)] \quad (8.4)$$

The partial factors are not derived in this research. The method in which these safety factors are derived is obvious. Given 7.7 and 7.8, the γ_{x_i} values are iteratively (for each year) derived in the cases with and without degradation. The design point moves in the u -space, as the equivalent failure plane Z_e adapts itself. The corresponding sensitivity coefficients α_{ik} and design values u_{ik}^* change accordingly.

8.2.4. Time-dependent reliability due to corrosion

In this research, solely the Jongbloed corrosion curve number 3 has been considered. In realistic situations, several corrosion models need to be considered in order to provide a specific explanation of the corrosion-induced behaviour. Extended knowledge on the corrosion-induced reliability development is significantly more meaningful when comparing figures resulting from different corrosion rates. In addition, corrosion depends on the location at the quay wall which is considered (see figure C.30 in chapter 7). In this research, one corrosion zone has been considered: permanent immersion zone. This is the zone where the largest bending moment occurs.

The engineering approach follows a stress-based approach in which solely the elastic section modulus $W_{el,y}(t)$ is varied according to the corrosion curve number 3. This approach is commonly applied in engineering. In reality the bending stiffness, which influences the deformations and thereby the bending moment, is affected by corrosion as well. The refined approach, here referred to as "second order approach", takes the reducing bending stiffness into account and illustrates a largely different development of the time-dependent reliability, sensitivity values and corresponding partial safety factors. The bathtub curve, illustrating the conditional failure rate of civil engineering objects in [42], provides a general view on the degradation-induced reliability development. However, the curves in figure 8.6 considerably deviate. The obtained conditional annual reliability values are significantly larger on the long term. Therefore, the "second order" approach in combination with a log normally distributed corrosion variable becomes questionable.

The second order approach requires to be applied carefully. The bending moment depends for a significant part on the applied calculation model. In this research, a spring model has been used. In addition, the cross-sectional geometry and corresponding soil-structure stiffness relationships influence the bending moment distribution. The soil behaviour (subgrade reaction, saturation degree, arching e.g.) is of considerable influence as well. Hence, interpretation of the maximum bending moment directly from D-Sheet Piling by means of one considered corrosion curve 3 is reasonably biased. In a

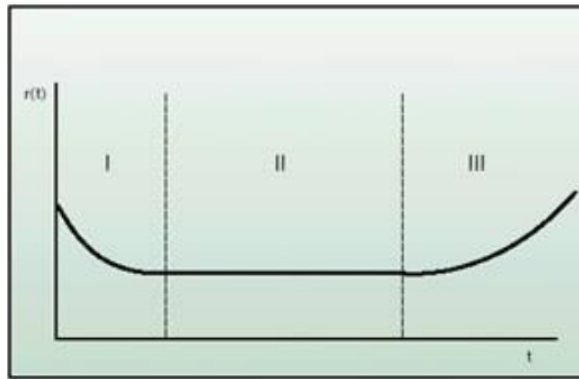


Figure 8.5: Bathtub curve illustrating the conditional failure rate $r(t)$ versus time t in years [42, p.177].

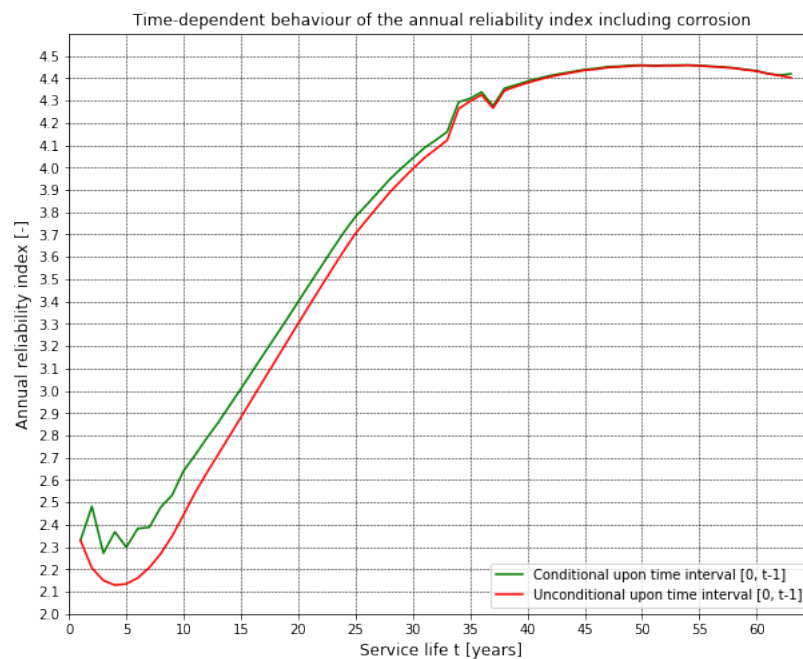


Figure 8.6: The time-independent development of the annual reliability index including corrosion and unconditional upon time interval $[0, t-1]$ (red line), including corrosion and conditional upon time interval $[0, t-1]$ (green line). The time-dependent annual reliability index is calculated for 100 years with the "second order" approach.

relatively more accurate approach (e.g. with FEM-models), the simulation of the force effect(s) becomes more appropriate and realistic. As a consequence, the reliability curve possibly converges to more realistic outcomes. Results obtained with the "second order" or "refined" method, can therefore not be generalised.

Solely the permanent immersion zone has been considered in this case study. In the posterior analyse, the bending stiffness is reduced along the total height of the retaining wall. This likely results in an increase of the absolute bending moment elsewhere. Accordingly, the maximum bending moment might be different. Hence, the reduction of bending stiffness most likely has a less favourable effect at a different location along the height of the quay wall. This latter effect is although not considered yet.

Due to the decrease of bending stiffness EI , the sheet pile deformations increase. The latter has for the considered case a reducing effect on the maximum bending moment. On the other hand, the decreasing section modulus W has an amplifying effect on the bending stress σ_y . This result can although not be generalised. Due to the reducing M_{max} in the studied permanent immersion zone the cross-section might be not critical anymore. Hence, the reliability values depend on how the safety of the cross-section is assessed. Therefore, the outcome as presented by figure 8.6 requires to be treated carefully.

8.2.5. Fully reducible uncertainty of corrosion

This study is unable to encompass different situations of corrosion. Uncertainty related to corrosion of the steel front wall determined by natural variation or randomness is for instance not studied yet. Corrosion has solely been studied an epistemic uncertainty ($\rho_{ij\Delta e} = 1.0$). The latter implies a stationary corrosion process and having an uncertainty largely based on available of data consisting measurements. Certain assumptions neglect natural variations such as climate change, intermediate application of cathodic protection which seems unreasonable in practice.

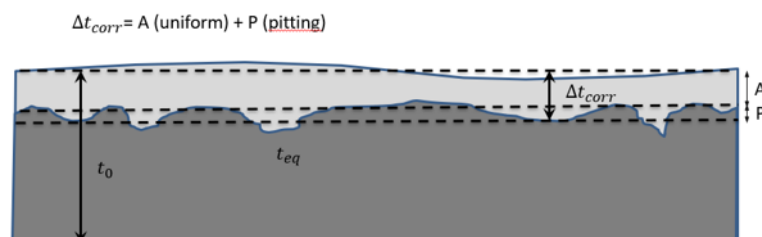


Figure 8.7: Schematisation of the equivalent wall thickness and corrosion.

In addition, neither corrosion following different Jongbloed's curves [63] nor larger coefficients of variation are studied. For a more substantiated interpretation of the consequences based on results, the following aspects have to be considered:

- The Equivalent Planes method using different speeds of corrosion. For instance by examining other Jongbloed's curves as well.
- Application of a truncated normal distribution as is assumed in [66].
- Natural variation in the uncertainty of corrosion by assuming situations in which $\rho_{ij\Delta e} < 1$.
- Random decrease of tubular wall thickness is not considered. This however applies in realistic situations.
- The coefficient of variation on uniform and pitting corrosion varies between 0.1 and 0.5. Solely 10% is treated in this research, less favourable situations in which 50% is assumed, leads to relatively more substantiation.

8.3. Recommendations

Continuation of this research is of significant importance. As a matter of fact, further research must obtain sufficient insight into the method for deriving partial factors on the basis of the updated actual reliability of a quay wall cross-section. Based on findings in this report, several directions are proposed:

- In the first place, a second case study is necessary to validate the outcomes of the spring model analyses. Heterogeneity of the soil and the 'length-effect' (for background information see appendix C.5) are not treated while conducting this research. The limitations of the spring model, which are described in chapter 1.4.3, result in encouragement to the application of a FEM-model in a further research. In addition, the ratios of soil-structure stiffness's differ significantly from a practical situation. It is most likely that limitations of the applied method caused differences in the reliability indices and sensitivity factors relative to the information found in the reference study [71] [72]. Therefore, use of the Finite Element Method should be contributory in the verification and (partly) validation of the Equivalent Planes method, which has been applied in combination with the spring model. A procedure for deriving updated reliability and sensitivity values in combination with FEM, is elaborated in section 8.3.1. The application of a model uncertainty factor (in this research referred to as ξ) originates from the field of flood defences. A prescribed model uncertainty variable according to the Joint Probabilistic Model Code [55] is used. In a follow-up research, it should be studied what impact is caused by the factor ξ when a FEM-model is used.
- In a realistic reference case, measurement data is most likely available. The included model uncertainty factor (from JCSS [55]), which in this case study resulted in low start values for β , can in further research be determined on the basis of the correspondence between the model calculation results and the measurement data from practice. Hence, investigation of a realistic reference case is of added value for the model uncertainty.
- Further it is meaningful to validate the prior analyses output with cross-correlated variables and subsequently the model uncertainty through level III analyses. Level III Importance Sampling is found to be considerably more efficient than Crude Monte Carlo simulations. With the latter, the input for the reliability updating method (Equivalent Planes method) can be validated prior to the reliability updating analyses.
- The refined or "second order" approach resulted in optimistic reliability values. However, the obtained values should be treated carefully as the bending moments are solely (re)calculated in the permanent immersion zone and could be different in another zone. For a more meaningful result, one must consider the development of the deformations and bending moment along the whole retaining height.
- Further research should also be concerned with the impact of randomness on the corrosion of the front wall. This research treated corrosion as a reducible epistemic uncertainty, meaning $\rho_{ij\Delta e} = 1$. Random variations in the corrosion behaviour and increasing uncertainty has not been treated yet. Besides, solely corrosion curve 3 was studied. Consideration of other Jongbloed's curves should provide useful insights as well.
- Besides, the iterative application of the updated sensitivity value(s) and reliability indices in the level I methods should be studied thoroughly. A procedure in which α_{ik} and β is applied for safety factors, was described at the end of chapter 7.3. The visualisation of the partial safety factors of the involved variables should yield a clear insight into the development of the involved random variables over time. Furthermore, it should additionally be verified whether the transformed α -values are representative for the partial safety in the physical X -space. The latter can possibly be checked for other reference cases as well.
- Python is an emergent open source programming software and is vastly educated to engineering students and to young professionals. Possibly for compatibility reasons, the application of python considering the effects of past performance should be studied.

In any case, the perspectives of the method which is treated in this research are promising. The application of the reliability updating method works sufficiently well. Additional verification analyses

and detailed investigation of several normative failure mechanisms are key to relatively more comprehensive findings. Section 8.3.1 substantiates the progressive insights and a possible procedure for a follow-up case study. The prospects and possible approach are based on findings from this research.

8.3.1. Follow-up research

The reference case that is considered in this research, is a basic CUR class III cross-section as described by example 3 in [72]. The spring model in D-sheet Piling is used for the analyses of this reference case. The procedure has been laid out in chapters 3-6. For the case which is treated with the subgrade reaction method, several limitations and possibilities emerged. In order to examine the general applicability of the Equivalent Planes method, it is logic to also consider an extended follow-up case. Secondly, a second case is preferably more realistic and thus complex-shaped than the case that was treated in this Thesis. In view of the current possibilities, such case and its results are not thoroughly analysed in this research. This chapter provides the reader insight into the possibilities and limitations of the EPM-method combined with the subgrade reaction method and thereafter in combination with progressive and more sophisticated analysing tools. At first, section 8.3.1 treats the (progressive) insights found within the research. In addition, newly obtained knowledge and experience is treated in the consideration of an extended follow-up case study in section 8.3.1.

Progressive insights

The simplified case is considered with the Deltares Probabilistic Toolkit. During the research, the software had some technical issues. All earlier calculations without degradation were performed with a beta-version v2.0.3. The calculations with degradation were performed with an upgraded version v2.1.0. In spite of the version still being in development, many options (among which reliability calculations, model running, sensitivity analysis) are included. The coupling between Deltares Probabilistic Toolkit and D-Sheet Piling works sufficiently well, most information can be translated from and to the executable file in D-Sheet Piling. However, despite the use of a powerful calculation computer (provided by Arcadis), heavy computations with level III methods (Crude Monte Carlo or Importance Sampling) frequently resulted in an increased effort and memory exception errors. In view of this, not all outcomes were recalculated with level III Importance Sampling.

As explained in appendix H.1, stochastic input variables among which the layer separation level $s \sim N(-12, 0.2)$ and excavation depth $h \sim N(-8, 0.25)$ caused instabilities in reliability analyses and were therefore disregarded. D-sheet Piling was in some cases unable to translate stochastic information, especially geometric parameters such as cross-sectional dimensions. The with subgrade reaction modelled quay wall cross-section follows an obvious analysis procedure. Figure R.1 in appendix R sketches a circuit diagram of the applied reliability updating procedure.

Remarkable effects on the reliability index and corresponding sensitivity factors have already been found with the spring model. A second spring model case would plausibly not lead to significantly deviating expectations. In the case of a preliminary design, D-sheet Piling is sufficient. Due to contemporary developments of finite element methods, reliability of quay walls including the effects of past performance should be investigated with FEM as well.

Second case study

More refined results could possibly be obtained by performing analyses with FEM software [5]. A thereby promising tool is PLAXIS. A short explanation about the spring model and finite element method is already provided in chapter C.5.4. Table 8.5 provides a short overview of the distinctions between the spring model (e.g. D-sheet Piling) and finite element method (e.g. PLAXIS).

Aspect	Spring model	Finite element model
Geometry	Simplified quay wall	Complex-shaped quay wall
Modelling	Elasto-plastic beam continuously supported by uncoupled elasto-plastic springs	Cross-section constituted from triangular- and rectangular grid elements
Soil-structure interaction	Linear stress-strain No soil arching	Non-linear stress-strain Soil arching
Equilibrium	Uncoupled and discrete springs	Nodal elements
Applicability	Two-dimensional problems	Two- and three-dimensional problems
Suitability	Simple cross-sections, preliminary or draft design	Complex-shaped structures or final design

Table 8.5: Characteristic differences between the spring- and finite element model.

It becomes obvious that PLAXIS can be relatively more valuable in subsequent case study analysis. Besides, recent options have been developed and implemented within the software. It is possible to realistically take into account the soil pressures on an inclined combi-wall and model foundation piles by using embedded beam rows [66]. Hence, the new case should be studied with PLAXIS. The Deltares Probabilistic Toolkit can be coupled with PLAXIS by means of a conversion algorithm in a Python-script. The input parameters are interpreted as stochastic or deterministic parameters. As follows, the information is translated through a script into the PLAXIS executable. The reliability method is selected in the Deltares PTK and the calculations are controlled through Python.

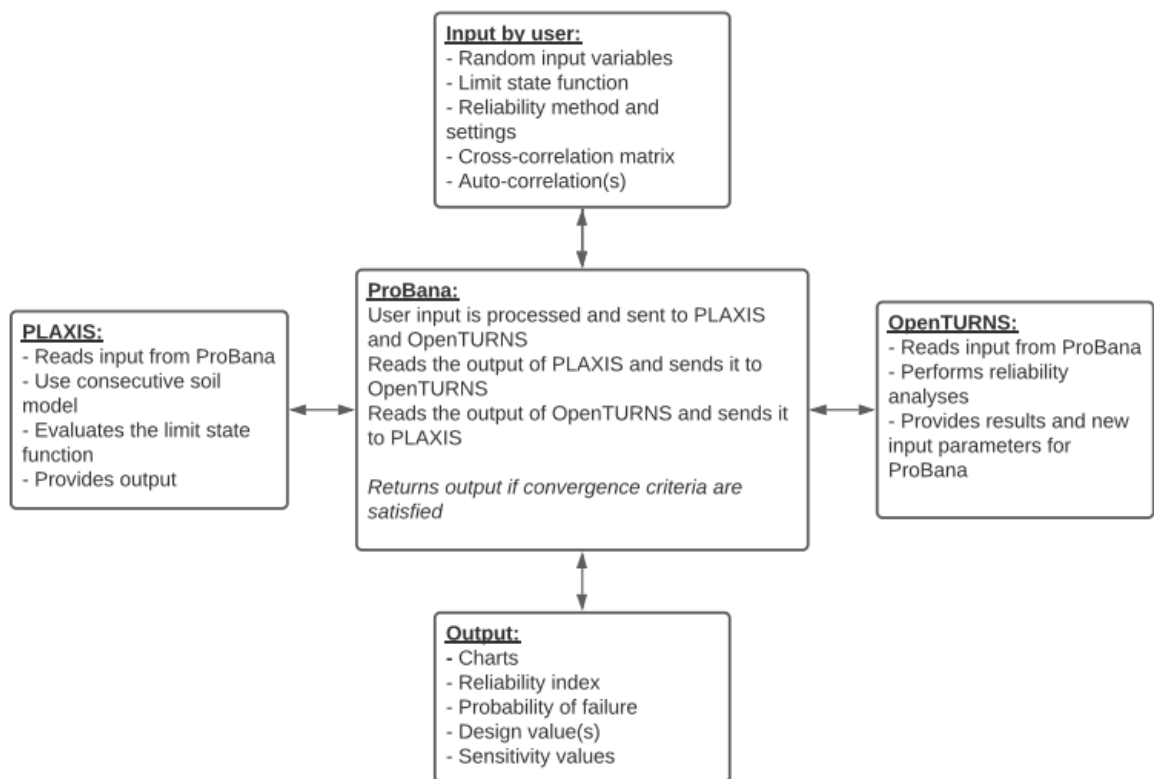


Figure 8.8: The coupling between the FEM-model and uncertainty library by the reliability interface [4] [66].

A different option for the probabilistic analyses could be the reliability interface ProBana (abbreviation for Probabilistic Analysis [80]). This application uses an open source library named OpenTURNS to perform probabilistic analyses on a geotechnical structure. This geotechnical structure is modelled by an FEM-model in PLAXIS and is coupled with the uncertainty treatment library OpenTURNS [4]. The PLAXIS FEM-model, OpenTURNS library and the user of the tools are connected through this

ProBana interface. Within OpenTURNs several reliability methods (e.g. FORM, Crude Monte Carlo, Directional Sampling) and distributions (e.g. normal, lognormal, Gumbel) are applicable. Figure 8.8 illustrates a diagram with the modelling possibilities. The required steps for a second case study are highlighted by a diagram in figure R.2 in appendix R.

Bibliography

- [1] ISO/TC 98/SC 2. Bases for design of structures - Assessment of existing structures. Standard, International Organisation for Standardisation, Geneva, Switzerland, August 2010.
- [2] ISO/TC 98/SC 2. General principles on reliability for structures. Standard, International Organization for Standardization, Geneva, Switzerland, August 2015.
- [3] ISO/TC 98. Preview; iso 2394:2015(en) general principles on reliability for structures. <https://www.iso.org/obp/ui/#iso:std:iso:2394:ed-4:v1:en>, 2015. Online; accessed 16 March 2020.
- [4] R.B.J. Brinkgreve A. Laera. Site response analysis and liquefaction evaluation. Technical report, PLAXIS B.V. and Delft University of Technology, 2015.
- [5] D.J. Peters A. Roubos, D.J. Jaspers Focks. Innovation flexible dolphins by full scale field test laterally loaded tubular piles. In *Proceedings of the 9th PIANC-COPEDEC 2016 Conference*, October 2016.
- [6] L. Groenewegen & D.J. Peters A.A. Roubos. Berthing velocity of large seagoing vessels in the port of rotterdam. *Marine Structures*, 51:202 – 219, 2017.
- [7] A. K. Another and H. A. M. S. ter Tisha. Detection of earth rotation with a diamagnetically levitating gyroscope. *Physica B: Condensed Matter*, 294–295:736–739, 2001. doi: 10.1016/S0921-4526(00)00753-5.
- [8] ArcelorMittal. Az sheet piles. url:<https://sheetpiling.arcelormittal.com/products-services/production-range/az-sections/>, January 2020. Online; accessed on 01 June 2020.
- [9] ArcelorMittal. Tubes and combined walls. url:https://projects.arcelormittal.com/foundationolutions/support/calculation_tool/tubes_and_combined_walls_calculation/language/EN, January 2020. Online; accessed on 01 June 2020.
- [10] IISc Bangalore. 5. levels of reliability methods. https://nptel.ac.in/content/storage2/courses/105108128/pdf/Mod5/Basics_M5.pdf, 2016. Online; accessed on 3 April 2020.
- [11] Infram B.V. Bewezen sterkte markermeerdijken: geotechnische stabiliteit en kostenschattning voor stabiliteitsverbetering van voormalige zuiderzeedijken. Technical report, Rijkswaterstaat, Dienst Weg- en Waterbouwkunde, 2000.
- [12] CEN. Eurocode 0: Basis of Structural Design. European standard, European Committee for Standardization, Brussels, Belgium, November 2002.
- [13] CEN. Eurocode 7: Geotechnical design - Part 1: General rules. European standard, European Committee for Standardisation, Brussels, Belgium, November 2004.
- [14] S. K. Chakrabarti, editor. *Handbook of Offshore Engineering*, chapter 5.8.2.1 FORM/SORM. Elsevier, 2005.
- [15] CUR commissie C 126. CUR 166 Damwandconstructies, 6^e herziene druk deel 1. Dutch guidelines, CUR Bouw&Infra, Gouda, Netherlands, August 2012.
- [16] CUR commissie C 126. CUR 166 Damwandconstructies, 6^e herziene druk deel 2. Dutch guidelines, CUR Bouw&Infra, Gouda, Netherlands, August 2012.
- [17] CUR commissie C 126. CUR 211, handbook of quay walls. Dutch guidelines, CUR Bouw&Infra, Gouda, Netherlands, August 2013.

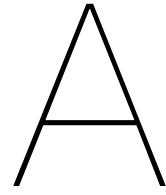
- [18] J.G. de Gijt. Developments in the port of rotterdam in relation to the history of quay wall construction in the world. In *Seeh fur Containerschiffe zukunftiger Generationen*, February 2008.
- [19] J.G. de Gijt. *A History of Quay Walls: Techniques, types, costs and future*. PhD thesis, Delft University of Technology, 2010.
- [20] de Volkskrant. Dijkdoorbraak in wilnis. <https://www.volkskrant.nl/nieuws-achtergrond/dijkdoorbraak-in-wilnis~bdb01263/>, August 2003. Online; accessed on 12 April 2020.
- [21] F.M. Dekking, C. Kraaikamp, H.P. Lopuhaä, and L.E. Meester. *A Modern Introduction to Probability and Statistics*. Springer, 2005.
- [22] *D-Sheet Piling User Manual*. Deltares, 2016.
- [23] Deltares. Openearth. url:<https://publicwiki.deltares.nl/display/OET/OpenEarth>, July 2016. Online; accessed on 15 July 2020.
- [24] *Probabilistic Toolkit Manual*. Deltares, 2019.
- [25] N. den Adel. Load testing of a quay wall: Evaluating the use of load testing by an application of bayesian updating. Master's thesis, Delft University of Technology, 2018.
- [26] Q. De Rochemont & H. Desprez. *Cours de travaux maritimes. 2ème partie*. École Nationale des pont et Chaussées, 1897.
- [27] D. Diamantidis. A critical view on environmental and human risk acceptance criteria. *International Journal of Environmental Science and Development*, 8(1), 2017.
- [28] Eric. W. Weisstein. Euler-Mascheroni Constant. <https://mathworld.wolfram.com/Euler-MascheroniConstant.html>, 2020. Online; accessed 1 July 2020.
- [29] European Committee for Standardization. ISO standards. <https://eurocodes.jrc.ec.europa.eu/showpage.php?id=145>, 2020. Online; accessed 2 April 2020.
- [30] The International Federation for Structural Concrete. *Textbook on behaviour, design and performance*, volume 5. FIB, 2nd edition, 2012. ISBN 978-2-88394-102-1.
- [31] Committee for Waterfront Structures. *Recommendations of the Committee for Waterfront Structures Harbours and Waterways EAU 1996*. Ernst & Sohn, January 2000.
- [32] A. K. Geim and H. A. M. S. ter Tisha. Detection of earth rotation with a diamagnetically levitating gyroscope. *Physica B: Condensed Matter*, 294–295:736–739, 2001. doi: 10.1016/S0921-4526(00)00753-5.
- [33] Normcommissie 351006 'Geotechniek'. NEN 9997-1: Geotechnical design of structures. Technical report, Koninklijk Nederlands Normalisatie Instituut, Delft, Netherlands, November 2017.
- [34] Normcommissie 351006 'Geotechniek'. NEN 8707: Assessment of an existing sturture in case of reconstruction and disapproval. Technical report, Koninklijk Nederlands Normalisatie Instituut, Delft, Netherlands, September 2018.
- [35] Normcommissie 351006 'Geotechniek'. NEN 8707: Assessment of an existing sturture in case of reconstruction and disapproval - Geotechnical constructions. Technical report, Koninklijk Nederlands Normalisatie Instituut, Delft, Netherlands, September 2018.
- [36] W. Brent Hall and M. Tsai. Load testing, structural reliability and test evaluation. *Structural Safety*, 6:285 – 302, 1989.
- [37] B. Hofland. Bed, bank and shore protection assignment. url:<https://brightspace.tudelft.nl/d21/le/content/125707/viewContent/1196074/View>, December 2018. Online; accessed on 14 April 2020.

- [38] D. Diamantidis & M. Holický. Reliability differentiation in the eurocodes. In *SEMC International Conference*, September 2010.
- [39] C. Houyoux. Design method for steel structures in marine environment including the corrosion behaviour. Technical report, European Commission, 2007.
- [40] C.W. Huang, A. El Hami, and B. Radi. Overview of structural reliability analysis methods — part ii : Sampling methods. *ISTE Ltd.*, 17, February 2017.
- [41] MEA Marine Engineering Societies Inc. What are cofferdams? <http://meacorporation.com/category/cofferdams/>, 2020. Online; accessed on 09-04-2020.
- [42] S.N. Jonkman, R.D.J.M. Steenbergen, O. Morales-Napolés, A.C.W.M. Vrouwenvelder, J.K. Vrijling, M.H.G. Baas, M.A. van der Lugt, and A. Kusters. *Probabilistic Design: Risk and Reliability Analysis in Civil Engineering*. Delft University of Technology, November 2017.
- [43] F. Diermanse K. Roscoe and T. Vrouwenvelder. System reliability with correlated components: Accuracy of the equivalent planes method. *Structural Safety*, 57:53–64, October 2016.
- [44] T. Schweckendiek & W. Kanning. Handreiking faalkansanalyse en faalkans updating groene versie - macrostabiliteit binnenwaarts. Technical report, Deltares, 2017.
- [45] B Kuipers. "het rotterdam effect". Technical report, Erasmus UPT, Erasmus Universiteit Rotterdam, November 2018.
- [46] A.J. Lansen. Port city interaction. <url:https://brightspace.tudelft.nl/d21/le/content/193370/viewContent/1550873/View>, September 2019. Online; accessed on 13 April 2020.
- [47] H. Ligteringen. *Ports and Terminals*, chapter Quay length and number of STS cranes, page 197. Delft Academic Press, 2017.
- [48] T. Messervey. *Integration of Structural Health Monitoring into the Design, Assessment and Management of Civil Infrastructures*. PhD thesis, University of Pavia, February 2009.
- [49] M.Z. Voorendt & W.F. Molenaar. *Manual Hydraulic Structures 2019*. Delft University of Technology, February 2019.
- [50] Moliijn, Cosette. 'Oude kademuren hebben al bewezen dat ze werken'. <https://www.nrc.nl/nieuws/2020/02/21/oude-kademuren-hebben-al-bewezen-dat-ze-werken-a3991272>, 2020. Online; accessed 6 March 2020.
- [51] NEN norm commission 251 001. Eurocode 3: Design of steel structures - Part 5: Piling. Dutch norm, Dutch Normalisation Institute, Delft, Netherlands, February 2008.
- [52] Port of Rotterdam NV. Feiten en cijfers over de haven van rotterdam. <https://www.portofrotterdam.com/sites/default/files/feiten-en-cijfers-haven-rotterdam.pdf>, 2019. Online; accessed 10 March 2020.
- [53] Port of Rotterdam NV. Over het havenbedrijf. <https://www.portofrotterdam.com/nl/havenbedrijf/over-het-havenbedrijf>, 2020. Online; accessed 31 March 2020.
- [54] Port of Rotterdam NV. Feiten en cijfers: schepen. <https://www.portofrotterdam.com/nl/onze-haven/feiten-en-cijfers/feiten-en-cijfers-over-de-haven/schepen>, 2020. Online; accessed 9 March 2020.
- [55] Joint Committee on Structural Safety. *Probabilistic model code*, chapter Part I. JCSS, 2001.
- [56] Joint Committee on Structural Safety. *Probabilistic model code*, resistance models: Static properties of structural steel. Technical report, JCSS, 2001.
- [57] Joint Committee on Structural Safety. Veiligheid nederland in kaart: de methode van vnk2 nader verklaard. Technical report, Projectbureau VNK2, March 2011.

- [58] OpenEarth. Openearth: Getting started. <https://publicwiki.deltares.nl/display/OET/OpenEarth>, 2020. Online; accessed 1 July 2020.
- [59] P. Osório, C. Odenbreit, and S. van Baars. Failure probability of marine steel sheet pile structures with special consideration of the corrosion impact. In *Oceans IEEE - Spain*, 2011.
- [60] P. Quist. Container terminals. url:<https://brightspace.tudelft.nl/d21/le/content/193370/viewContent/1545166/View>, September 2019. Online; accessed on 13 April 2020.
- [61] A. Roubos, R.J.D.M. Steenbergen, T. Schweckendiek, and S.N. Jonkman. Risk-based target reliability indices for quay walls. *Elsevier Structural Safety*, 75:89 – 109, 2018.
- [62] A. Roubos, D. Allaix, K. Fischer, R.J.D.M. Steenbergen, and S.N. Jonkman. Target reliability indices for existing quay walls derived on the basis of economic optimisation and human safety requirements. *Structure and Infrastructure Engineering*, 16(4):613 – 625, 2019.
- [63] A. Roubos, D. Allaix, T. Schweckendiek, R.J.D.M. Steenbergen, and S.N. Jonkman. Time-dependent reliability analysis of service-proven quay walls subject to corrosion-induced degradation. *Structure and Infrastructure Engineering*, 2019.
- [64] A.A. Roubos. *Enhancing reliability-based assessments of quay walls*. PhD thesis, Delft University of Technology, 2019.
- [65] A.A. Roubos, D.J. Peters, L. Groenewegen, and R.D.J.M. Steenbergen. Partial safety factors for berthing velocity and loads on marine structures. *Marine Structures*, 58:73 – 91, 2018.
- [66] A.A. Roubos, T. Schweckendiek, R. Brinkgreve, R.D.J.M. Steenbergen, and S.N. Jonkman. Finite element-based reliability assessment of quay walls. *Georisk: Assessment and Management of Risk for Engineered Systems and Geohazards*, pages 1 – 17, 2019.
- [67] T. Schweckendiek, W.M.G. Courage, and P.H.A.J.M. van Gelder. Reliability of sheet pile walls and the influence of corrosion: Structural reliability analysis with finite elements. In *Risk, reliability and societal safety - Proceedings of the European Safety and Reliability Conference 2007*, 2017.
- [68] T. Schweckendiek, M. van der Krogt, B. Rijnveld, and A.M. Teixeira. Handreiking faalkansanalyse macrostabiliteit. Technical report, Deltares, 2017.
- [69] S.N. Jonkman and R.D.J.M. Steenbergen and O. Morales-Napolés and A.C.W.M. Vrouwenvelder and J.K. Vrijling. *Probabilistic Design: Risk and Reliability Analysis in Civil Engineering*, chapter 7.1 Probability of failure and life span. Delft University of Technology, November 2017.
- [70] S.N. Jonkman and R.D.J.M. Steenbergen and O. Morales-Napolés and A.C.W.M. Vrouwenvelder and J.K. Vrijling. *Probabilistic Design: Risk and Reliability Analysis in Civil Engineering*, chapter 3.6 Probabilistic design: the relationship between safety standards and engineering design. Delft University of Technology, November 2017.
- [71] E.O.F. Calle & S.E.J. Spierenburg. Onderzoeksrapportage deel I: veiligheid van damwandconstructies. Research report, CUR onderzoekscommissie C69, Delft, Netherlands, July 1991.
- [72] E.O.F. Calle & S.E.J. Spierenburg. Onderzoeksrapportage deel II: veiligheid van damwandconstructies. Research report, CUR onderzoekscommissie C69, Delft, Netherlands, August 1991.
- [73] M.H. Faber & M.G. Stewart. Risk assessment for civil engineering facilities: critical overview and discussion. *Reliability Engineering and System Safety*, 80:173 – 184, January 2003.
- [74] H. Straub. *Die Geschichte der Bauingenieurkunst*. Birkhauser Verlag, 1975.
- [75] M. Sykora and M. Holický. Target reliability levels for the assessment of existing structures. *Proc.ICASP11*, 8:1048 – 1056, 2011.
- [76] M. Sýkora, D. Diamantidis, M. Holický, and K. Jung. Target reliability for existing structures considering economic and societal aspects. *Structure and Infrastructure Engineering*, 13-1:1 – 14, 2017.

- [77] W. Kanning T. Schweckendiek. Reliability updating for slope stability of dikes. Technical report, Deltares, 2017.
- [78] Cambridge University. Definition of: Safety. <https://dictionary.cambridge.org/dictionary/english/safety>, 2020. Online; accessed 26 March 2020.
- [79] J.M. van der Sanden, H. Kwint, and N. ter Heide. Parametrisch modelleren binnen de waterbouw. *Vakblad Civiele Techniek*, 2020:24 – 25, March 2020.
- [80] T. van der Wel. Reliability based assessment of quay walls. Master's thesis, Delft University of Technology, 2018.
- [81] M. van Koningsveld and P. Taneja. Port functions and organisation. url:<https://brightspace.tudelft.nl/d21/1e/content/193370/viewContent/1538872/View>, September 2019. Online; accessed on 13 April 2020.
- [82] A. Verruijt. *Soil Mechanics*. Delft University of Technology, 2001.
- [83] G. Verwolf. Actuele sterkte van dijken. Technical report, Expertisenetwerk Waterveiligheid, 2009.
- [84] M. Holický & J.V. Retief & D. Diamantidis & C. Viljoen. On standardisation of the reliability basis of structural design. In *12th International Conference on Applications of Statistics and Probability in Civil Engineering*, July 2015.
- [85] R.D.J.M. Steenbergen & A.C.W.M. Vrouwenvelder. Safety philosophy for existing structures and partial factors for traffic loads on bridges. *HERON*, 55:123 – 140, 2010.
- [86] R.D.J.M. Steenbergen & M. Sýkora & D. Diamantidis & M. Holický & A.C.W.M. Vrouwenvelder. Target reliability levels for assessment of existing structures based on economic optimisation and human safety criteria. *Structural Concrete*, 16:323–332, September 2015.
- [87] R. Wesstein. Relationship between construction costs and reliability of quay walls. Master's thesis, Delft University of Technology, 2019.
- [88] E.A. Witmer. Elementary bernoulli-euler beam theory. Technical report, MIT, 1991 - 1992.
- [89] H.J. Wolters. Reliability of quay walls. Master's thesis, Delft University of Technology, 2012.

Appendices



Methodology for the case study

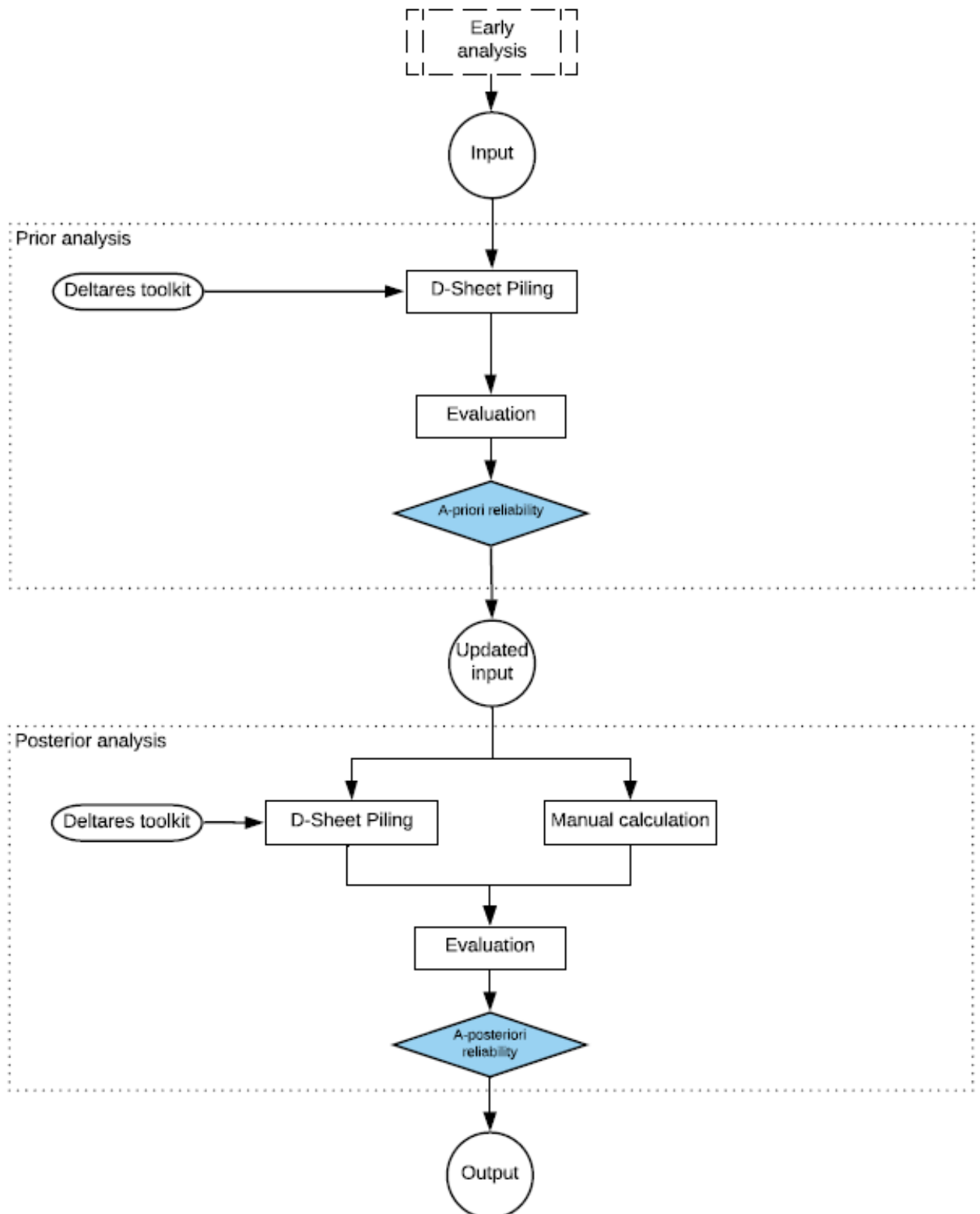


Figure A.1: Simple case approach

B

Data gathering and analysis

In order to validate the gathered data and conduct sufficient analyses, one uses a set of requirements and boundary conditions to analyse the data and the tools to be used. A scientific way The tools are in this case modelling software packages and the calculation tools, see section 1.4.2. There are some categories in which the data and analysing tools are being assessed:

- The source(s) of the data
 - Author(s)
 - Time
 - Area
- Applicability

To elaborate further on this categorisation one should bear a few things in mind. The source(s) of the data is among other things about the author, commission or institution that composed this source. It is important to consider the time and the area in which it has been used. An old design manual for masonry quay walls in the Amsterdam Canals from the 19th century might not be recognised as a justified source since this manual is concerned with an area with different soil conditions, tidal elevations and a potentially different logistical productivity than in the case study within Rotterdam. The applicability deals with the means such as the reliability updating method and reference quay wall that are used for the case study and the (probabilistic) analyses. In this category it has to be checked whether the tools are user-friendly or do not consume the time and effort from the essence of this research.

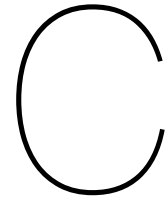
Requirements and boundary conditions

In order to obtain an efficient research, a few requirements and boundary conditions are stated. Table B.1 presents the requirements and boundary conditions of the obtained data and the calculation tools.

Nr.	Requirement (R)
1.	The used design code has to be more recent than the latest Eurocode or it should be a basis document of an earlier design guidelines.
2.	The literature should be scientifically substantiated or based on experiences in the professional field.
3.	Acquired numbers from calculations should be corresponding to the outcomes resulting from approaches as is prescribed by the theory.
4.	When in doubt one has to inform and consult the daily supervisor or an other member of the commission.
5.	The tools that are used should be permitted and authorised by the graduation company Arcadis.
6.	Fundamental information which is obtained from news articles has to be underpinned by a recognised scholar.
Nr.	Boundary condition (BC)
1.	Understanding the basic utilisation of the toolkit should be achievable within 1 month.
2.	The computation time of the toolkit should be less than 1 day.
3.	Acquired data such as results from computations should be completed within the first 8 months of the MSc research.

Table B.1: Requirements and boundary conditions for the data and the tools.

These requirements and boundary conditions should act as a support in the back while conducting the literature study and the case study. Differently speaking, these composition of statements can be used as a checklist as the research develops.



Theoretical framework

C.1. Introduction

A composition of aspects related to quay walls has been studied prior to the development of chapter 2 and appendix C. The theoretical background in this chapter initially focuses on the safety of structures in general. Newly-built and existing structures are separately approached. In this way the regulations and norms for the safety philosophy of general civil engineering structures is treated. Section C.2 contains a brief study on quay walls describing the history, types of quay walls and the failure mechanisms. Eventually, the last part of this section lists the significant practical aspects related to quay walls in which the functional requirements and the process of monitoring the conditions is treated. This latter section is concerned with the pragmatic approach as is done for real projects. Following on that, the safety standards and guidelines related to existing geotechnical structures will emphatically be discussed. After that, insight in the different reliability methods is provided. These methods encompass the approaches that are used for civil engineering structures. In the end, a short recap on the previous studies, the concept of reliability updating methods and their purposes will be provided. Accordingly, the importance of these methods and further the recommendations are explained.

C.2. Quay walls

As one already is aware of, civil engineering structures can be subdivided into several categories: Concrete/Steel Structures, Hydraulic Structures, Geo-Engineered Structures, Pavement Engineering. A particular structure which falls in different categories is the quay wall. Quay walls are constructive elements for a reliably rapid transshipment and belong to harbour structures and constitute the interface between the hydraulic environment, the subsoil and the ground level infrastructure. Quay walls have experienced many developments throughout the centuries. The developments are firstly discussed in section C.2.1. Quay walls themselves can be constructed in different types. These different types are distinguished in categories and explained in section C.2.2. Further descriptions on their characteristics are provided as well. Section C.2.4 deals with the developments regarding the industrial quay walls in the port of Rotterdam, the functional aspects and practical asset management of quay walls. Examples are provided where necessary.

C.2.1. History of quay walls

Seagoing trade has been taking place for a number of millennia. History teaches that certainly since 6000 BC, seagoing expeditions are taking place. River and delta regions such as the Nile, Tigris, Euphrates, Indus and Yellow Rivers allowed for expeditions in the first era of water transport. In the following time period spanning up to even the end of the first millennium (1000 AD), different peoples among which Indians, Chinese and Arabs have been dominating the transport of goods throughout

Eurasia and other parts of the world. Phoenicians and in a later stage Greeks and Romans established a trading network throughout the Mediterranean Sea and even reaching Western Europe [18].

Expeditions and voyages where the transport of people and goods were involved, are part of the earliest history of globalisation. The Northern part of Europe (see figure C.1), including Norwegian, German, Swedish, Dutch and Belgian territories committed trade during during the Hanze-era, which lasted 5 centuries between 900 - 1400 AD. Their monopoly existed in the trade between Western Europe and the countries around the Baltic Sea. The Dutch traded with the Southern regions of Europe during that time. Not long after this and the first Chinese expedition to Africa by Cheng Ho, the Portuguese, Spanish and Dutch started their expeditions to for them distinct areas on the planet. Several countries in Europe started advancing their capabilities after the overland journey of Marco Polo around 1296 AD. The Medieval Ages marked the ascent of foreign journeys, where large port cities as Amsterdam, Antwerp and Bruges emerged [19]. The role of the Netherlands in global trade got emphatically present during the VOC-era between 1600 - 1800, especially in the trade of Asian goods. The English eventually took a significant share of that monopoly in Asian trade.

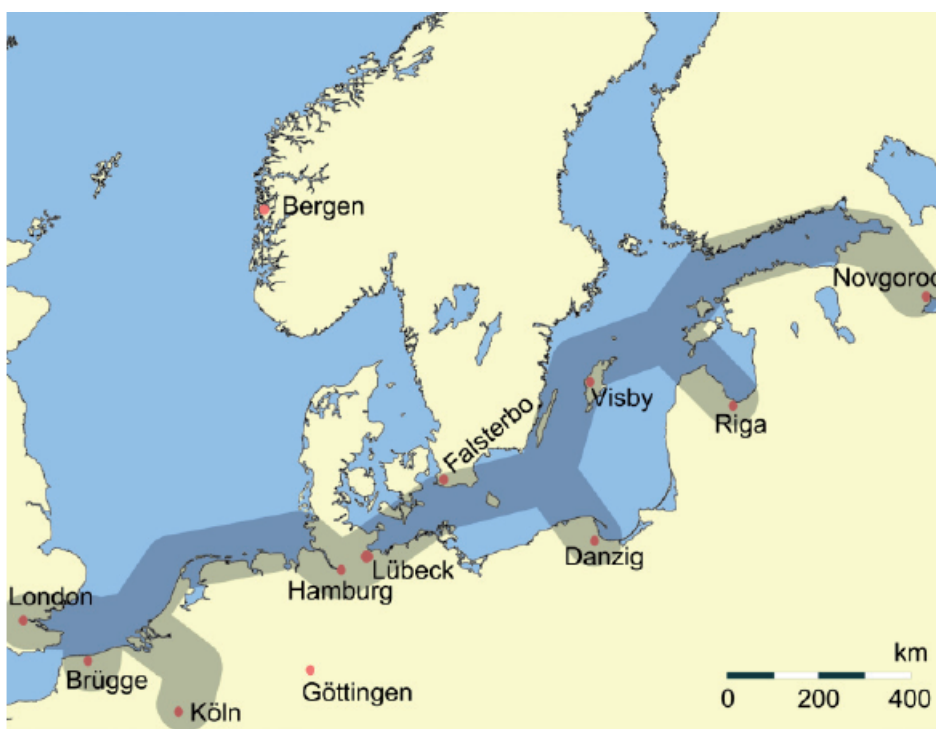


Figure C.1: Seagoing trade by the Hanze League with a water connection between the Western Europe and the Baltic Region [19, p. 24]

Indeed, the industrial revolution around 1750 AD contributed in the rapid changes of the world trade and the globalisation. The developments of quay walls developed gradually over time, but was exceptionally influenced by industrialisation. The history of quay wall is in all probability initiated by the quay walls that emerged in Lothal India in 2400 BC. Romans were the first people in Europe that constructed quay walls, often in combination with flood defences (harbour dams). These quay walls were often wooden sheet piles or gravity structures such as caissons, with retaining height of approximately 3 to 4 meters. Pozzolanic earth-cement mixtures were used in the development of Roman building works but for quay walls as well [19].

As appears in [19, Ch. 3 - 9], different developments have influenced the design and construction of quay walls throughout the centuries and eventually the port layout of today. Among these developments, the most significant will be discussed in this section.

General port development

Ports developed, with the increasing number of cargoes and sea trading, from ancient ports to the ports of today. Up to 1600 the Middle East, Iberian countries, the Chinese and Hanseatic league had the lead in sea trade and port(s) development. Only after 1700 America began to take part. Also, development stages from mid 19th century, up to the 21th century influenced the potential for advances in shipping, constructing and manufacturing [19, p. 33]. One example is the change of the port in spatial scale. The port developed from a closer port-city connection with risers in trade of general cargo to a secluded, client-aware port network with different commodities.

Development of ships

Up to the end of 18th century sailing and rudder-driven ships were used as seagoing vessels. The ancient, medieval and early modern-time vessels were smaller-built and constructed with wood. The industrial revolution initiated the gradual shifting towards propulsion by steam engines. The change of materials such as steel instead of wood and the propulsion by steam engines, propellers and later on diesel engines led to an increase in vessel size (length, beam, draught), vessel speed and cargo handling capacity (see figure C.4). Average vessel speed increased over 5000 years from 3 to 50 km/h. Furthermore, the changes in ship layout resulted in the possibility of dry-, liquid bulk and later container cargo instead of only carrying general cargo.

Development of cargo handling equipment

Prior to and around 1800, vessels commonly had a volume of around 200 tonnes. Ports often had some small quays, jetties and ships were even grounded in order for the crew to manually load and discharge the ship. On a timescale, treadmills, mechanically driven gantry cranes, hydro powered cranes and eventually electric cranes all passed the revue. The increasing scale of transshipment was largely due to the increasing vessel size and port throughput [19, p. 60]. The containerisation and the expansion of the beam increased the lifting capacity as the outreach increased. As a consequence, the loads on the terrain and the quay wall got even bigger.

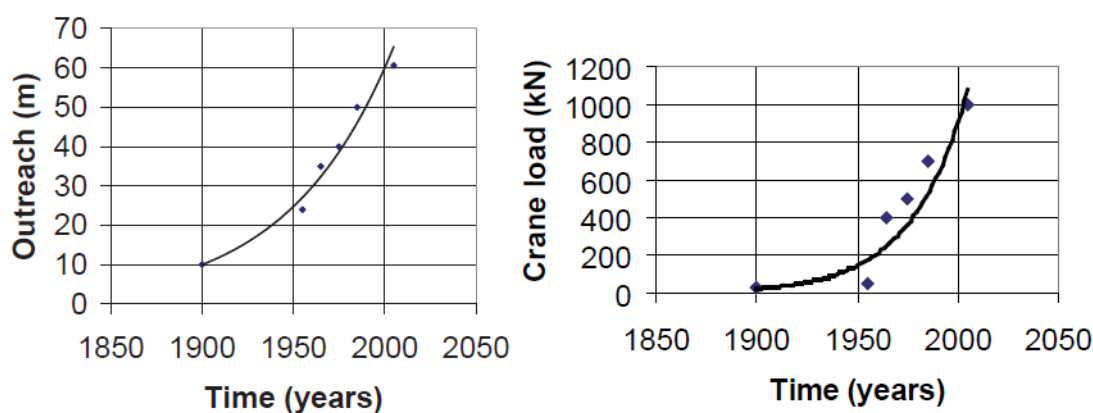


Figure C.2: Development of the outreach and crane load capacity versus time [19, p. 62]

Materials used in port construction

Nature stone and wood have always been present as construction materials for quay walls. Limited retaining heights were achieved due to the inability of stone and wood to resist high tensile forces. With the development of cast iron and cement in the early modern times the retaining height had increased. By the introduction to steel and reinforced concrete around 1900, it became possible to sustain large bending moments. These materials became globally available. The improvements of steel and concrete (prestressed concrete, high strength) made optimisations of the characteristics related to strength, workability and durability possible.

Development of construction techniques

In ancient times, quay wall construction was often manually executed. Shallow foundations were pre-

ferred over deep foundations by pile driving. Pile driving although was possible. Shorter piles were mechanically driven in the subsoil by hammering workers (before Roman times <1000 BC) or later on by small equipment. The decision between shallow and pile foundations was made on the basis of trial and error and the experience with soil layer characteristics. Pile driving and foundation construction became more sophisticated as the equipment increased in size throughout the centuries. Knowledge about dry, wet and combined construction methods became available with the experience on dewatering installations and pontoons. Because of the latter, more robust structures such as caissons could be constructed. The large impact of the industrial revolution was visible in the heavy equipment and the different forms of power. The diversity of equipment improved the working conditions and it permitted the construction of more extensive quay walls.

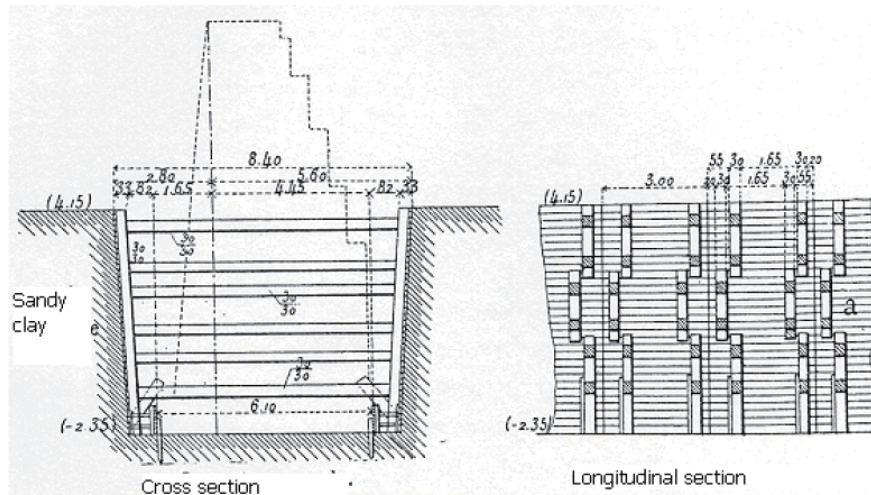


Figure C.3: Cross-section and plan view showing a strutted excavation under dry conditions for the construction of a gravity structure (concrete wall with no reinforcement) around 1890 [26].

Development design aspects for quay wall

Several methods and design tools came at our disposal as time developed in the past. Scientific knowledge in a set of disciplines became necessary for the design. Theories in Structural Mechanics is up to now present due to contributions from da Vinci, Newton, Poisson, Hooke and Coulomb between the 16th and 18th century. Major contributions to the development of the theoretical framework for fluid mechanics were delivered by Navier, Stokes, Bernoulli, Chézy and Izbash. Knowledge about Soil Mechanics became available and widely applied due to contributions from Rankine, Coulomb and in 20th century by Terzaghi. Based on the developed theory, together with experimental learning, experience-based learning (e.g. with materials such as concrete, steel, wood/timber) and the improvements in computing power, it became possible to design complex quay wall structures [19, p. 127]. Currently, new design methods are still being developed.

Beside the above-mentioned developments, environment factors are also not to be left out. These factors contain loads, tidal variations and soil conditions. Most factors were influenced by the previously mentioned developments. Such developments are for instance the emergence of larger cranes. The latter provoked a higher crane load. The occurring climate change is another development which has an impact on tidal variations.

Experience, which is likely the most important aspect as with all things in human life, is the experience on dealing with the mechanical behaviour of materials and structures. In earlier times, quay wall construction was based on trial and error. Nowadays, quay walls are designed to resist forces, moment and loads. Rare soil conditions might impose restrictions. However based on predictions and experiences from comparable structures, one has become able to minimise errors and component failures.

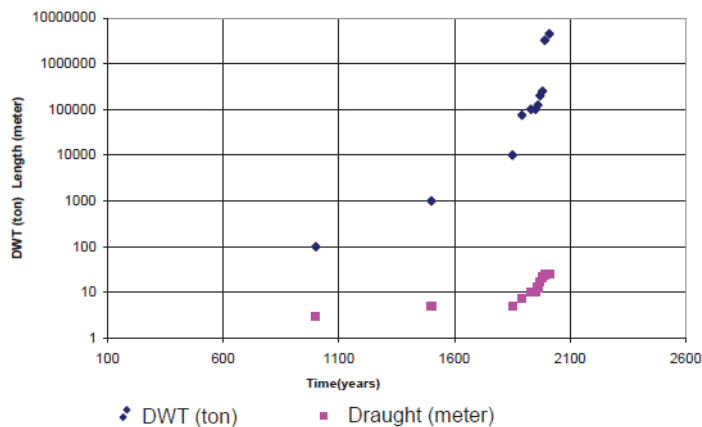


Figure C.4: Density distribution of the vessel size over time, expressed in the DWT (dead weight tonnage) and the draught [19, p. 51].

Shapes and types of quay walls remain almost unaltered in the last 4000 years. The total structural size although increased at least with a factor 10 [19, Ch. 13]. All the developments which are previously mentioned, led to improvements in the design and construction of quay walls. Nowadays, many design recommendations are standardised and many design guidelines are developed. Especially the design knowledge that is based on theories derived by scientists, experimental work, practice-based learning (see figure C.5), the industrial revolution between 1750 and 1900, have improved the tools for the design and construction of large quay wall structures [17, Ch. 1] [19, Ch. 12]. By these improvements, quay walls were able to meet the demand caused by the increasing ship sizes, global trade and industrialisation. All in all, quay walls have improved from the beginning of (Dutch) industrial revolution (1850) up to now in different ways [19, p. 6]:

- The material use has been reduced with 20 to 40%
- The speed of construction is accelerated with a factor 40 to 60
- Retaining height has increased from 5 up to 30 meters
- Obviously, the construction techniques such as pile driving, the logistics and concrete technology are far more developed.

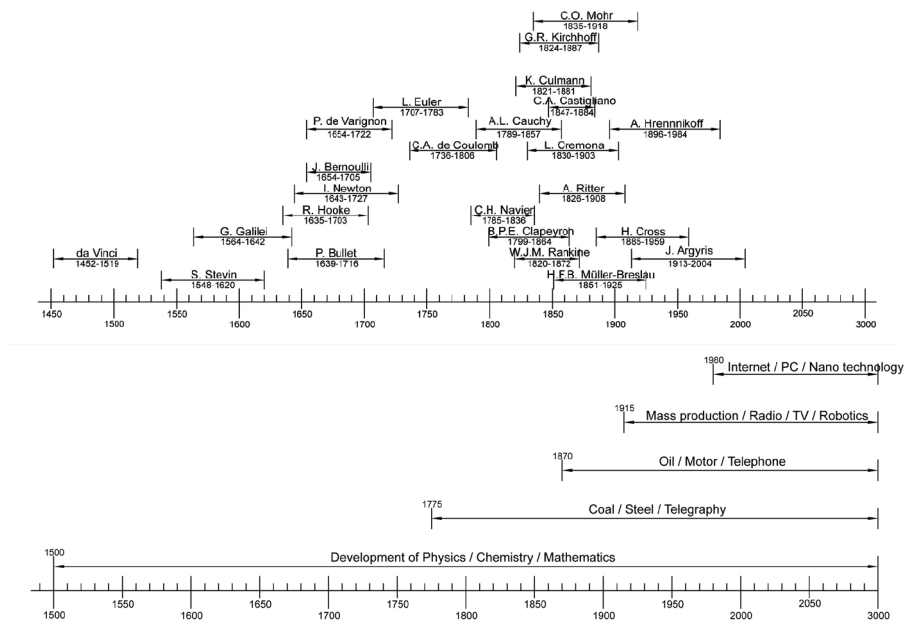


Figure C.5: Selection of people and technologies that contributed to the development and understanding of quay walls [74] [19, p. 127].

C.2.2. Types of quay walls

In various countries many different construction methods have arisen over the years. These construction methods consequently lead to different types of quay walls structures. A large number of quay wall structures have been built around the world. It has therefore become necessary to classify the quay walls in order to create an understanding in the mechanical behaviour and to perform comparisons. There are four categories in which quay wall types can be subdivided [17, Ch. 3]. The categories contain quay wall types which can be made from different materials: Steel, concrete, bricks, stone, wood.

- Gravity walls
- Sheet pile walls
- Structures with relieving platforms
- Open berth quays

An open berth quay is a different type of structure because the interface of water and soil is not bordered by a vertical wall but by a slope. This last category will not be described in this research. Important fact is that the choice of quay wall depends on the composition of the subsoil, forecasts of freight and shipping requirements. Not to mention the local conditions such as the water levels, tidal influences, soil characteristics and local climate conditions that have to be dealt with. Accordingly, a quay wall should be designed in a way that its costs are outstripped by its future benefits. Simultaneously, the quay wall should be capable of executing its functions. A quay wall must [17, Ch. 3]:

- Provide sufficient draught for the biggest forecasted vessel to berth
- Retain soil for the area behind the quay wall
- Possibly serve as a water retaining wall for the area behind the quay wall during periods of high water
- Provide bearing capacity

At the same time, quay walls should be able to resist the loads as is schematised in figure C.6.

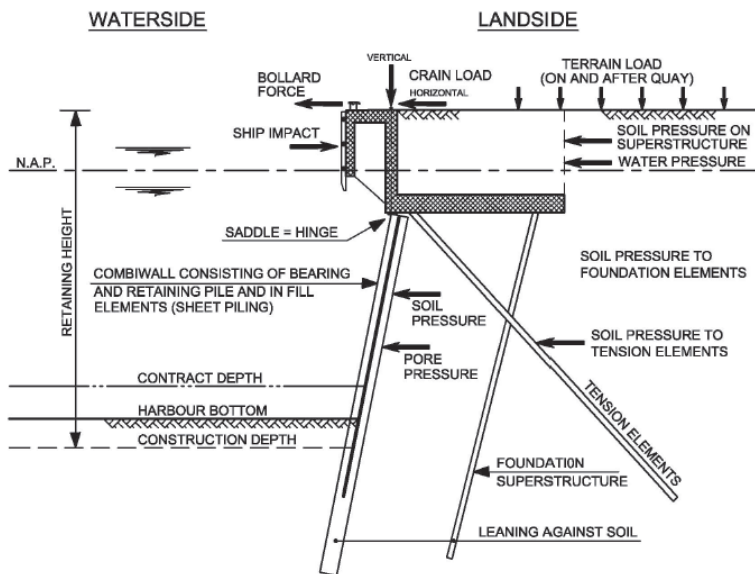


Figure C.6: Design features and active loads regarding a quay wall structure during its service [19, p. 126].

In the following sections, the main quay wall categories are discussed. Next to that, typical examples belonging to these categories are described.

Gravity walls

The first type of quay wall to be described is the gravity wall. Gravity walls obtain their retaining function by their self-weight. Sometimes gravity walls are accompanied with a soil layer on top, this extra weight has its impact on the retaining height as well. The bearing stratum beneath the gravity structure is of great importance since it is subjected to the vertical weight from the wall and of any additional soil on top. At the same time, the structure withstands the horizontal load to a large extent by friction between the wall bottom surface and the bearing layer. The characteristics of this underneath layer should therefore be favourable. The self-weight is enormous. The self-weight and the shearing capacity are able to provide sufficient resilience against tilt which is caused by driving moments.

Gravity walls often consist of prefabricated elements which lie directly on natural foundations. Opting for gravity walls is mainly due to the characteristics of the subsoil and the consideration between the costs of materials and labour [17, p. 48]. Prefabricated elements are often more attractive in the case of large quantities about which the one-off costs for the form work, placement and transport are depreciated. Gravity walls are mainly suitable for subsoil consisting of solid rock or stiff sand, or when the subsoil has sufficient bearing. Sheet piles are in the last case less favourable. Hence, gravity walls can be further subdivided based on their properties.

Block wall

Block walls are a simple variant consisting of prefabricated elements made of concrete or stone. The elements are piled on top of each other. A block wall is generally placed from the water side on a foundation layer of crushed rocks or coarse grains such as gravel. A reinforced concrete capping beam is often constructed on top of the prefabricated elements. Boulders and fender works are constructed on this capping beam which is besides casted in situ. Block elements, often made from nature stone, were already used in ancient times by Romans or in India [19, p. 149].

The large vertical and horizontal joints in block walls are very advantageous, since water can be released to reduce over pressure. In order to prevent soil behind the structure from being transported, a filter structure of crushed rocks or soil grinds with sufficiently large particle sizes is constructed. Figure C.7 shows the principle of a block wall.

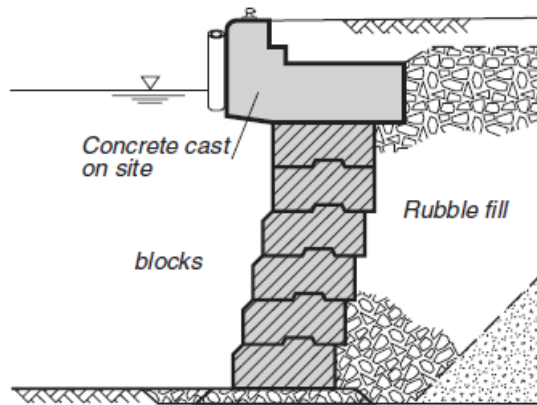


Figure C.7: Typical block wall

L-wall

Different from block walls is the L-wall consisting of just one element in vertical direction. A L-wall consists of prefabricated concrete elements in a L-shape. A L-wall additionally owes his stability, unlike in the case of a block wall, to the weight of the soil that rests on the heel. The prefabricated elements are made on the waterborne equipment on site or, in case of large elements, in a dewatered building pit elsewhere. These elements are placed by heavy lifting equipment and partly embedded in a foundation layer consisting of crushed rocks or coarse gravel. L-walls are financially interesting for long quays, because the direct costs for a building pit, transport and construction are high. L-shaped walls are suitable in the case when the foundation is not sufficiently solid for block walls. The stability of L-walls against tilting is ensured by the additional vertical weight of the soil resting on the beam. The interfaces between the individual elements must be carefully observed to prevent soil from washing out. One can achieve the latter by securely monitoring the joints.

Caisson wall

As is not mentioned, the caisson quay and its construction technique was already invented by the Romans. This method was however reinvented in 1886 and applied in the construction of the Brooklyn Bridge foundation. Sadly 30 workers lost their life by caisson diseases. This kind of disease happens when workers find themselves in an area with much lower pressure after working under a high pressure [19, p. 149]. Nevertheless, caisson walls are hollow, cellular concrete units that are built in a construction dock. These large units can be prefabricated in a dry building dock elsewhere and floated to the construction site. Afterwards, the caisson wall is placed on a robust soil layer to avoid settlements when the caisson is filled. Weak layers have to be removed in advance. A caisson is filled with ballast material in order to create resilience against horizontal loads. Considering the material use, a caisson is financially attractive. However, the construction is labour intensive and is preferably used for projects with a repetitive character. Furthermore, the project site requires accessibility for the floated caissons.

Cellular wall

Cellular walls are cylindrical steel profiles filled with soil. These elements stand on the bed level of the water or are extended a little below the bed level. These cellular walls are considered as gravity walls since the elements are not largely embedded in the soil. Oftentimes, these elements are firstly placed and then filled with soil or ballast material. Cylindrical elements can directly be joined together or by an intermediate element like a steel web. Important positive aspects are the relatively low amount of required materials and the relatively higher steel capacity against tensile stresses. The corrosive behaviour of the structure should however be checked, especially in aggressive environments [17, p. 51].

Reinforced earth wall

Reinforced earth walls consist of vertical panels, a capping beam and tension elements. The vertical panels are usually prefabricated concrete elements that are sealed and piled up on each other. The vertical panels are supported by horizontal tension elements that are penetrated in the soil just behind

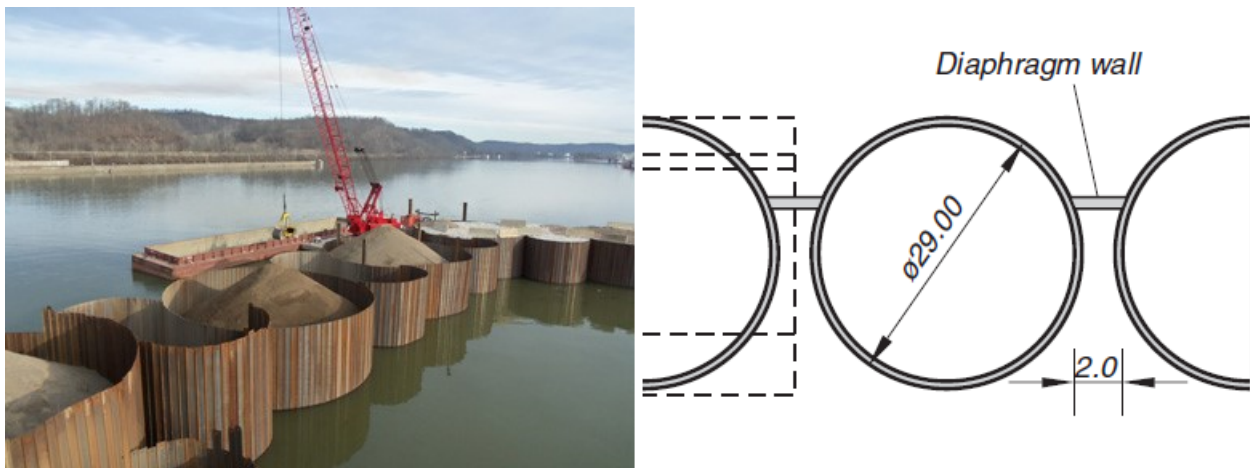


Figure C.8: Cellular walls applied at the construction of a cofferdam [41] and a top view of a cellular quay wall in Zeebrugge [17, p. 64].

the wall. These tension elements often are steel rods, steel sheets or polymer reinforced fibres such as geotextiles. The stress is transferred from the tension elements to the soil through shear between the soil layer and the elements' surfaces. In this case, stress is for instance caused by horizontal loads. Reinforced earth is constructed through alternately back filling of soil and fastening of the tension elements [17, p. 51].

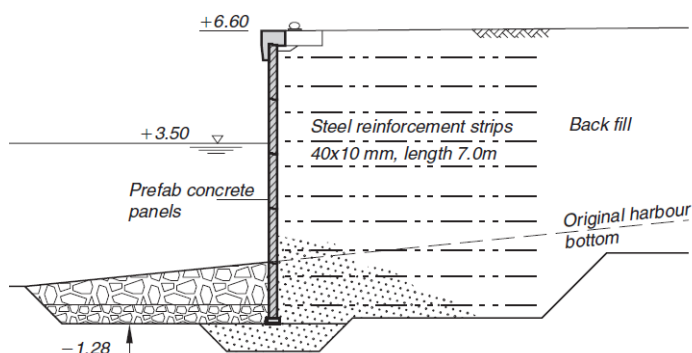


Figure C.9: A reinforced earth wall in Swansea [17, p. 67]

Sheet pile walls

This category discusses the different types of sheet piling systems. Structural piles had already been invented a long time ago during the Roman period (200 BC). During that time wooden piles were used. Nowadays, piles are available in different shapes and materials. Wood, steel and concrete are frequently used for sheet piling systems. Sheet pile walls are characterised by a larger embedded depth, this depth indicates the depth difference between the pile tip and the level of the water bed. By means of this embedded depth, one is able to counteract the destabilising soil stress by a passive soil stress. This destabilising soil stress is also called the active soil stress that is initiated by the soil behind the sheet pile wall [19, p. 148].

The main focus of this research lies of the concepts of the frequently-used systems in the port of Rotterdam. A more extensive consideration of sheet piling systems is provided in the literature. The different types of sheet piling systems being treated here are:

- Single sheet piling
- Combined sheet piling

- Diaphragm walls
- Fixed cofferdams

Diaphragm walls are reinforced concrete walls that are made in situ. These walls are often approximately 0.5 to 2.0 meters thick and consist of panels with a width varying between 2.50 and 7.0 m. Firstly, cross-beams are placed in order to navigate the hydraulic grab. To construct a diaphragm wall, one must simultaneously dig a narrow deep trench and inject bentonite slurry in the soil. The latter is to prevent the subsoil from collapsing into the narrow trench. After the reinforcement cages are placed, one can pour the concrete and discharge the supporting fluid (bentonite slurry) at the same time. A cofferdam wall consists of two sheet pile walls which are often connected by one or more anchors. The space between the sheet pile walls is filled with soil. This soil is part of the retaining structure, acting as an entity and deriving its resistance from the shear resistance and the weight of the soil [17, p. 56].

Two frequently used sheet piling systems are elaborately treated here, the single sheet pile wall and the combined sheet pile wall. Both systems can be combined with anchorages or a relieving platform. The latter is however treated in section C.2.2.

Single sheet pile wall: Sheet pile structures are used in subsoil with a poor bearing capacity and where the walls are easily penetrable. These systems can reach large retaining heights and the elements are connected by interlocking, welding, punching. In the case of quay walls, the top sides are connected by a concrete capping beam where the fenders and bollards are constructed. A sheet pile wall is mainly subjected to horizontal loads initiated by the soil and surcharge loads caused by ground level structures or operations. Other loads are influencing the structure as well, see figure C.6. Loads acting on the sheet piles can be transferred to the subsoil through fixation or anchorage. Single sheet piles can be made of wood, these wooden piles reach limited retaining heights. Mostly, sheet piles are prefabricated as steel U, H, Z or flat sections. Each cross-section has a different moment of resistance and are installed by means of vibrating, driving or pressing (vibration-free). Two types sheet piling systems can be further distinguished.

- **Freestanding sheet pile walls:** Freestanding sheet pile walls derive their stability and retaining function through fixation of the subsoil. The sheet pile wall transfers the soil pressure as a continuously elastically supported to the subsoil. As a matter of fact, the freestanding quay wall is installed with a larger embedded depth. This embedded depth creates a larger mobilising passive soil pressure (see figure C.10).

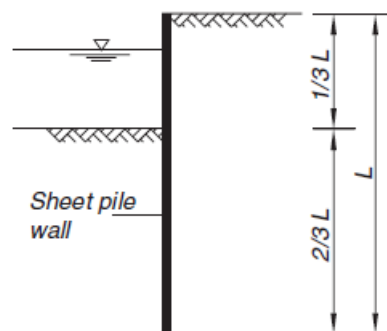


Figure C.10: Single sheet piling system without anchorage [17, p. 53].

- **Anchored sheet pile walls:** An anchoring system is usually necessary in the case of high retaining heights or extreme loads at ground level. To facilitate the prevention of excessive deformation of the upper side, anchorage by means of anchors or tension piles are provided. Anchors are fixed at the sheet pile and can be placed horizontally (e.g. bar anchors, pile trestles, screw anchors) or inclined (grout anchors or screw injection anchors), in the latter case a vertical force component is additionally acting on the sheet pile wall. For tension piles, closed concrete piles, H-piles, MV-piles can be used. All anchorage systems derive their tensile force from shaft friction.

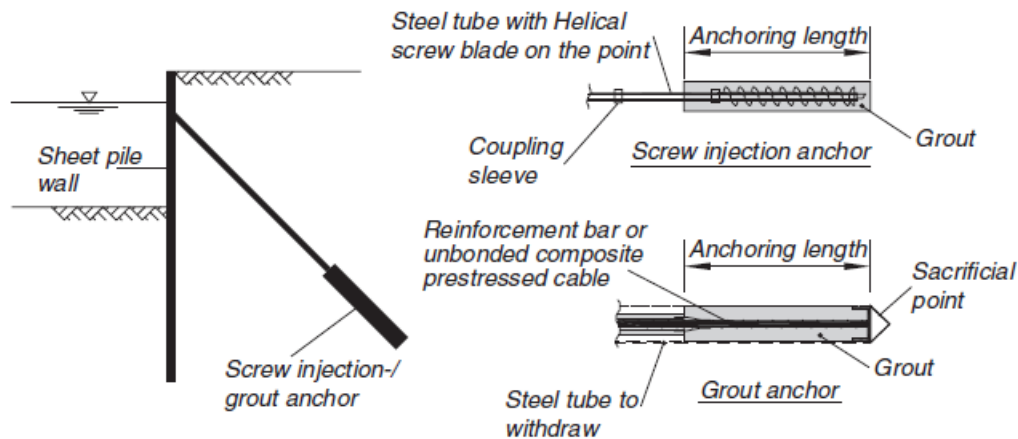


Figure C.11: Anchored sheet pile wall with an inclined anchor body.

An other frequently used concept is the **combined sheet piling system**. This system consists of heavy primary elements which are deeply embedded into the soil. These elements can be tubular piles or steel sections that are welded to each other (H-sections, U-sections) and overcome the soil pressure. Consequently, the forces are transferred from the primary elements to the subsoil or the anchorages. The secondary elements can be shorter and are welded between the primary elements. These elements have a sealing function. Combined walls are often economically attractive, frequently-applied high strength tubular piles are relatively easily installed in the subsoil.

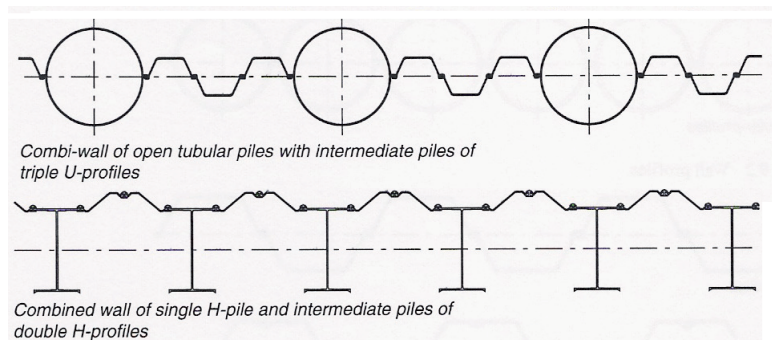


Figure C.12: Two types of modern combined wall systems [19, p. 152].

Sheet piles with relieving platforms

Besides horizontal-, inclined anchors and piles, relieving platforms are used to reduce the horizontal load on the front wall. Many times, especially at quay walls with high retaining heights and heavy quay loads in the port of Rotterdam, relieving platforms are applied. This method is usually applied when high demands related to allowable deformations, such as for crane tracks, are present. Relieving platforms are considered as the horizontal connection between the front wall, which is often a bearing (combined) sheet pile wall or a diaphragm wall and the pile trestle. The pile trestle is a foundation element consisting of a row with bearing piles and a row with tension piles. The pile trestle is used to take up excessive horizontal loads on the quay wall and heavy vertical loads from the superstructure.

Figure C.13 shows a quay wall structure with a high relieving platform. Two construction methods for relieving platforms can be described: High relieving platform and low relieving platform. The decision between the two has often to do with the required retaining height and the local soil conditions. Additional pile rows can be installed if the bearing capacity of the relieving platform is reduced.

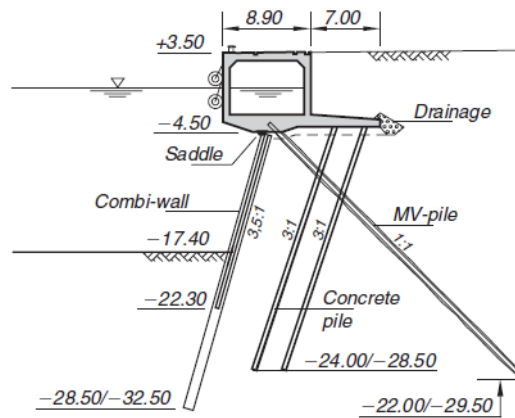


Figure C.13: Quay wall cross-section of the Delta 2 container terminal in Rotterdam, principle of a low relieving platform [17, p. 74].

C.2.3. Failure mechanisms

In order to obtain insight in the points of attention during the design and construction of a quay wall, one must consider which aspects do contribute the most to the failure of a system. The failure mechanisms which are related to quay walls can be distinguished into three main modes of failure [67, Ch. 4]. These failure modes are related to retaining walls in general and focusing on the limit state at which the bearing capacity of the structure is lost:

- Z_1 : Failure of the retaining wall (front wall c.q. gravity wall, sheet pile wall)
- Z_2 : Failure of the support (anchors, tension piles, relieving platform)
- Z_3 : Failure of the soil

Geotechnical failures and structural failures occur in all three failure modes. First aspect is mainly dealing with the consequences related to the instability within the soil, while the structural aspect is dealing with the incapability of the construction materials. As a result, the failure mechanisms can be allocated to a failure mode as is listed above. Of course does the failure mechanism depend on what type of quay wall is constructed.

Failure mechanisms of retaining walls according to [15], [16], [67], [61]:

1. Yielding of the sheet piling system
2. Crushing of the concrete
3. Failure of the anchor grout
4. Piping failure
5. Active failure
6. Passive failure
7. Macro-instability or overall instability
8. Kranz-instability ("failure of anchor system" in figure C.14)
9. Shear failure of the soil around the support (e.g. anchor pull-out)
10. Yielding of the support

Item 1 and 10 happen when the maximum steel stress in the retaining wall or support, which is caused by the soil pressure, exceeds the yield stress of the material f_y . Equations C.1 and C.2 show how the maximum steel stress is calculated for the retaining wall and support respectively.

$$\sigma_{SP} = \max\left\{\frac{M(z)}{W_{el}(z)} + \frac{F_N(z)}{A(z)}\right\} \quad (\text{C.1})$$

$$\sigma_A = \frac{F_A(z)}{A_A(z)} \tag{C.2}$$

In the case of a retaining wall where the water level at each side of the wall is different, a flow gradient may occur when permeable layers are present. If the soil downstream is not completely homogeneous and when the hydraulic gradient has developed, heave occurs. In an advanced stage, soil has locally been eroded as such that more water is attracted. This can lead to further erosion and eventually a 'pipe' is created. This phenomenon is called piping and can lead to failure of a structure [82, p. 71] (item 4).

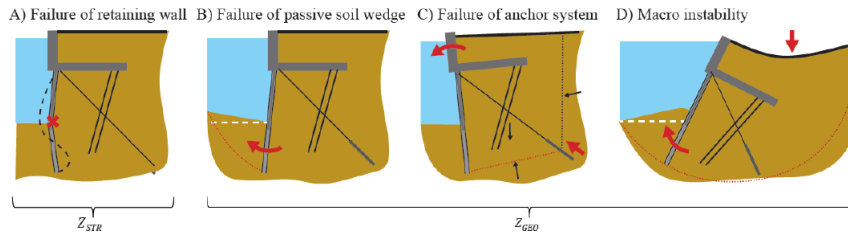


Figure C.14: Impression of some of the structural and geotechnical failure mechanisms [61, Ch. 1.3.2.].

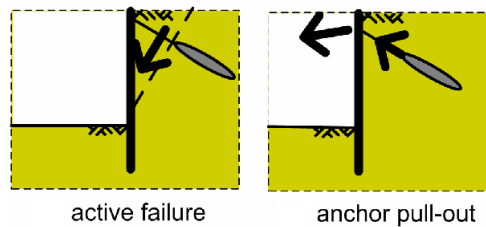


Figure C.15: Impression of some of the geotechnical failure mechanisms [67, Ch. 4.4]

The defined failure mechanisms can be classified in categories as is described above. Depending on site investigations, computing models, structural and geotechnical analyses, one is able to ascribe failure components to a certain quay wall structure. The accompanied failure probabilities can be stated in a fault tree as is shown in figure D.1 in appendix D.

C.2.4. Quay walls in practice

Many quay wall structures are designed and constructed according to theoretic knowledge which is obtained from fundamental scientific theories by among others the famous Archimedes, Terzaghi and many experiments. Many experiments such as triaxial tests with soil samples or falling head tests with less permeable soil samples describe the behaviour for different types of soils [82]. However, the uncertainties due to staggered outcomes may lead to uncertainty in particular situations considering specific built objects. Many historical examples of failure such as the dike breach at Wilnis in 2003 [20] or quay wall collapses in urban areas (Amsterdam, Utrecht e.g.) show the great uncertainty within structures related to soil and groundwater. Port of Rotterdam is dealing with these uncertainties as well. This section describes the role of the port of Rotterdam in the design, construction and management of quay walls. Frequently raised questions are on how the quay walls are designed and reassessed throughout the years and how conditions of quay walls are recorded and used. Both aspects are briefly treated in this section.

The port of Rotterdam

Port of Rotterdam is a public limited company of which its shareholders are the municipality of Rotterdam (approx. 70%) and the Dutch State (approx. 30%) [53]. This company manages the largest European seaport at the New Waterway and Rhine connection. The management of the Port of Rotterdam is although mainly concerned with the port infrastructure as in a landlord port administration model. Different companies and users of the port have the ownership of the superstructure (terminal equipment) and stevedoring labour [81, Sl. 46]. Nowadays, Port of Rotterdam facilitates 77.3 km of quay walls for several companies within three major commodities: Petrochemical-, bulk- and container industries [52].

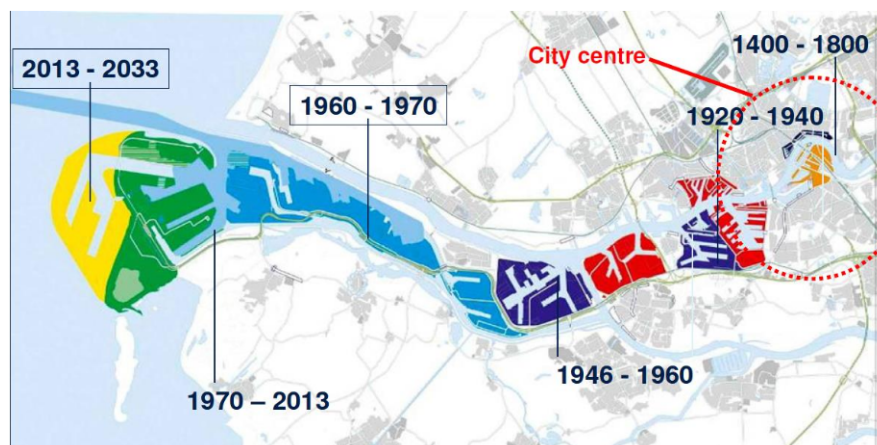


Figure C.16: Port development stages over the decades [46].

The Rotte was in the 14th century a small fishing village at the river the Rotte. This initial village owes its origin to the dam that was built near the river mouth. This dam was initially built in 1250 AD to create fresh water polders in the region. Notably however, it created potential for fisheries and human settlement. Consequently, trade and shipping were developing in that region. In 1340 AD, Rotterdam was granted city rights and it slowly grew further over the centuries. The small fishing village at the bend of the Rotte river grew, despite the war with Spain in the 16th century, to a significant port in the Netherlands. Initially the port was situated at the Northern side of the river, but it slowly expanded southward and subsequently westward. The developments in the age of Industrial Revolution gave rise to the construction of new harbours and the population expansion [18]. Between the 1960s and 2004, Rotterdam was the largest port of the world. Nowadays, Rotterdam has become number 11 by trading volume [81].

The total throughput in 2019 including dry bulk, liquid bulk and containers, had been estimated to be 469,4 million metric tons. Intermodal connections with the railroad and vehicle road and the great

accessibility from the sea and rivers were success factors in the directly and indirectly realised added value of 6.2% GDP to the Dutch economy in 2017. This value is expected to have grown further in 2030. Mainly the Dutch and Northwest-European region (including Germany) take advantage of the ever developing port of Rotterdam [45]. Rotterdam is a hub port where transshipment takes place, approximately 25% of the throughput is transferred from deep-sea vessels to smaller vessels (feeders) or vice-versa [60]. The transshipment in 2018 has been estimated to be 149,1 million metric tonnes of containers and 289,5 million tonnes of dry- and wet bulk [52].

The port of Rotterdam is situated at the delta of the Rhine and Meuse. Both rivers and their dynamics have had an influence on the current situation of the soil conditions. The soil in the area near the city of Rotterdam consists of soft peat and clay layers of up to 18 meters thick, whereas the Botlek and Maasvlakte I area in the West are characterised by a more sandy soil profile. These changes in soil conditions are due to human activities such as soil reclamation.

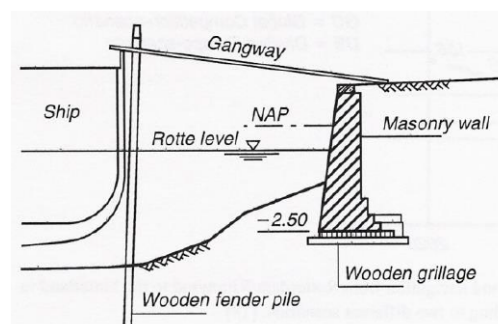


Figure C.17: The first quay wall in Rotterdam Leuvehaven in 1604 [18].

The modernisation and growth of vessels, cargo handling techniques and development in scientific knowledge has led to changes in the design and construction of quay walls within the harbours of Rotterdam. Figure C.17 shows the cross-section of the first quay wall in Rotterdam. During that time, construction of a masonry quay wall on a wooden floor was feasible in practice. This quay wall was situated near the city centre, constructed on soft soil and prone to settlements. With the developments of prefabricated materials and deep foundations it has become possible to reach solid soil layers. Currently, many types of quay walls exist in the port of Rotterdam. The construction of ore quay walls for relatively high retaining heights, became more dominant between the 1960s and 1990s. These quay walls are characterised by a steel combined wall, relieving concrete platform, prefabricated (reinforced) concrete tension and bearing piles as is schematised in figure C.18 [18].

The pragmatic approach in the design and management of quay walls

Since the World War II, a significant number of quay walls has been designed and constructed (see figure C.16). Yet, improvements are continuously made in order to comply with increasing ship dimensions and changing nautical conditions. The functional use did not significantly change in time when regarding quay walls of 40 to 50 years ago. Nowadays, quay wall structures are renewed once in every five years due to changes types of loads. A significantly large amount of quay walls in the port of Rotterdam are (combined) sheet piling systems with anchors or a combined anchor system. The latter is a system where e.g. inclined and horizontal anchors are together used. Relieving platforms founded on bearing piles and tension piles are abundantly present as well. Before the establishment of international design codes in the nineties a limited amount of construction projects were executed on the basis of detailed probabilistic analyses. The design of the Eastern Scheldt barrier is an example from the past where the acceptable risk of flooding of Zeeland was used for the derivation of the probabilities of failure [42, Ch. 1]. The probabilities of failure were related to failure of structural components or non-closure of the gate. Other projects at the end of the seventies, where probabilistic analyses and mutual dependency were applied, are the Delta works and the Haringvliet barrier. Previously was mentioned that fault trees are suitable in these cases.

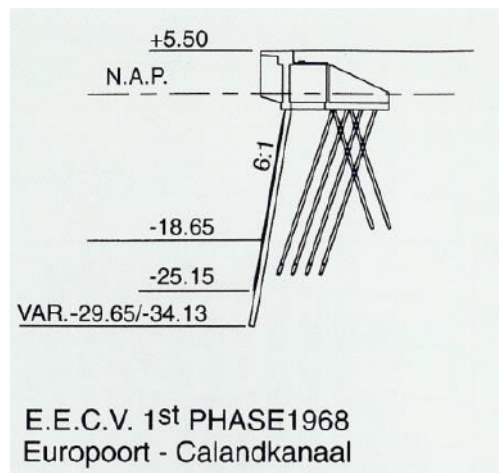


Figure C.18: An example of a typical quay wall in Rotterdam which is built between 1960 and 1990.

In the past, a safety factor of 1.5 to 2.0 was commonly used for steel structures. The monitoring procedure and decision to execute measures was by evaluating safety factors. To get that realised, three safety levels were often distinguished and this differentiation was in accordance with the state of the quay wall at that considered point in time. The safety levels and the corresponding measures are listed below.

1. $\gamma = 1.35 - 1.5$: This is the below range which is acceptable given an initial safety factor $\gamma = 1.5$. A quay wall with this safety factor satisfies the safety requirement.
2. $\gamma = 1.2 - 1.35$: Measures are required if the safety factor takes this value on the of moment of assessment. Application of cathodic protection on the sheet pile wall is a measure.
3. $\gamma < 1.2$: Below this threshold value the structure does not longer meet the standard. Cathodic protected steel strips are applied on the sheet pile wall.

These methods were not derived based on a scientific theory but purely experience-based. These overall safety factors were in accordance with the initial state of the quay wall ($\gamma = 1.5$). Given the initial value, overall safety factors were derived after degradation had taken place. By taking into account the decrease of the front wall thickness t , it was possible to derive the new safety factor. To clarify this, consider a tubular sheet pile with wall thickness: $e = 15$ mm. If the wall thickness decreases due to corrosion to $e_{corr} = 12$ mm, then the pragmatic overall safety factor $\gamma = 1.5$ decreases proportionally to 1.2. Similar to the deterministic level 0 approach, as explained in section C.4.2, the new load variable s_d got tested against the strength variable r_d . Current regulations regarding design life time do differ not much from the regulations that were used in the seventies, where at most partial factors were used. Recommendations from the EAU and TGB provided partial safety factors for infrastructures and concrete respectively until international standards were developed. The German committee EAU founded in 1950, gives recommendations about every five years on port related structures whereas the TGB gives recommendations on utility structures.

Since the 1990s, reliability engineering and safety levels became widely applied by the introduction of international standards such as the Eurocode 0 - 7. These codes are updated every few years. Current national design guidelines and recommendations are deduced from the Eurocodes that were developed in the nineties. Frameworks of recommendations on load factors, reliability classes, combination values and calculation methods had become widely applied after the introduction of these Eurocodes.

Nowadays, design and reassessment of quay walls are based on the CUR-publications 166 I/II, 211, NEN-EN 9997-1 and NEN 8707 [17]. Many boundary conditions and requirements regarding the quay wall are formulated. However in practice, the following requirements are mainly considered according to interviewed professionals:

- Strength of the quay wall: The quay wall should have sufficient bearing capacity and must not yield, regardless of any degradation.
- Soil density of the quay: Failure mechanisms in the soil are hard to observe at ground level. Oftentimes, the pavement and foundation layer cover the soil beneath. Detection of failure is only possible in case of functional failure given a passing vehicle.
- Load capacity anchor system: In some cases, such when the yield stress is exceeded, the anchorage is the failing element.

In theory, several failure mechanisms as listed in section C.2.3 can be observed. Oftentimes different sliding failure mechanisms are observed in practice. According to experienced professionals, sliding planes within the boundary region between different soil layers are frequently observed. Different finite element methods can be used in the analysis for the design and reassessment of quay walls. However, PLAXIS is according to many professionals a complete and detailed tool in comparison with M-Sheet or D-Sheet Piling and is therefore mostly used.

Monitoring of quay walls

In the port of Rotterdam quay walls are examined once in every few years. Oftentimes, quay walls are inspected and analysed with sample tests and divers' measurements. The obtained data is statistically edited and through this data, corrosion behaviour over time can be mapped and extrapolated. This procedure holds for front walls. Here, wall thicknesses from different points in time are compared with one another and arranged in order.

Many quay walls in the port of Rotterdam are built between 1950 and 1980. Most of these structures are reconsidered for obsolescence. The monitoring of quay walls is distinguished by different types of investigations [17, p. 91 - 92]:

- Meteorological investigations
- Morphological investigations
- Nautical investigations
- Seismological investigations
- Geo technical and geohydrological investigations
- Environmental investigations
- Hydraulic investigations (water levels, waves and currents)
- Topographic surveys
- Bathymetric/hydro graphic surveys
- Investigations into ice loads

Topographic surveys for instance, are carried out by the Port of Rotterdam through coordinates in the national system of triangle measurements (*Dutch: Rijksdriehoekskoördinaten*). The concrete capping beam of quay walls are accommodated with bolts that are placed in the longitudinal direction with intermediate distances of 25 to 50 meters. Additionally, these bolts are monitored by means of xyz-measurements once in every five years and deformations are recorded. In order to carry out an efficient approach where design parameters and boundary conditions are taken into account, an investigation plan is often set up. This plan contains [17, p. 91]:

- The objective of the investigation
- Method(s) of investigation(s)/survey(s)
- Phasing of investigation and motivations
- The desired result
- Justification for the type of survey or investigation

- Costs

Port of Rotterdam N.V. uses a landlord model for the port management and arranges lease contracts of 20 to 25 years with clients. The latter is according to an conducted interview with a project manager. The public infrastructure (quay walls, harbour basins) is managed by the port company, so monitoring surveys and investigations are under close supervision of Port of Rotterdam. In many practical cases, the monitoring of quay walls is accompanied with limiting factors:

- As-built drawings from the past are oftentimes not available anymore
- Design drawings are not available anymore
- No correspondence between the situation in practice and the original design drawings and as-built drawings
- Design calculations from the past with the Blum-method are often not available anymore
- A different safety philosophy was used in the past
 - Safety levels and failure probabilities were not widely applied
 - Therefore no associated partial factors for load combinations
 - Different overall safety factors

Luckily, many developments have taken place in the past ten years. Asset management and the rise of Build Information Modelling (BIM) nowadays puts the management of documentation first. Positive signals of the future exist as well. Parametric modelling of hydraulic structures such as quay walls becomes significantly more applied in the design and consultancy [79]. The increasing expertise in programming languages and Finite Element tools stimulates the efficient approach in design, monitoring and upgrading of quay wall structures.

C.3. Safety of structures

C.3.1. Introduction

Considering an end product or a system, one always has to verify whether the case or object is sufficiently safe. As long as humans are alive, the set of measures concerning safety has always been an issue of itself. Safety is a concept that comes up in different areas. The society of nowadays, production industry, aviation industry, the infrastructure and building industry all have something to do with safety. The definition of safety according to [78] reads as follows:

"Safety is a state in which or a place where someone is safe and not in danger nor at risk"

This thesis is concerned with safety concerning large-scale infrastructure and later on with quay walls specifically. The safety philosophy as is familiar within the civil engineering sector is according to the Eurocodes that were developed in the 90s. Next sections further address the recorded definitions and classification as is done in the codes. Safety of a structure is known as the situation at which the structure and its inhabitants are not at danger nor at any significant risk of danger. Hence most end products are characterised by a level of risk. Risk is by this a key concept regarding the safety of a structure. Risk is according to [73] defined as:

Risk is the probability of occurrence of an undesired event multiplied with the consequences.

Once the risk sources of an engineering system are defined and analysed in respect to their chronological and causal components, logic trees such as:

- Fault trees
- Event trees
- Cause/consequence charts

can for instance be formulated for the quantitative analysis of the total risk as well for the risk distribution of different components [73, p.175].

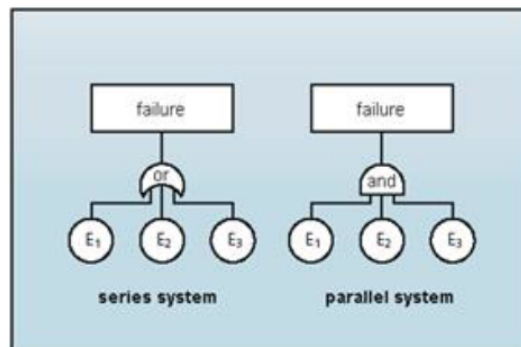


Figure C.19: Fault trees for a series system and a parallel system [42, p.218]

The overall risk or the risk of an individual component can be evaluated on the basis of risk-acceptance criteria from different safety regulations. Risk and its accompanying acceptance criteria are introduced as benchmarks for the safety of a structure:

- Individual risk (IR)
 - Individual risk per annum (IRPA): Annual probability that an individual or hypothetical group member will die due to exposure to hazardous events.
 - Localised risk per annum (LIRA): Annual probability that an unprotected, permanently present individual will die due to an accident at a hazardous site.

- Societal risk (SR): This is the risk of an accident with multiple fatalities.
- Social and Environmental Repercussion Index (SERI): Representing the loss of human lives, social disruption, environmental, historical damages and damages to historical and cultural heritage. This index is derived on the basis of the guidance which is set up by the Spanish standard for harbour and maritime structures (ROM) [61, p.97].
- Economic risk

Economic risk defines the capitalised risk, so the costs in different segments related to economic, societal and environmental damage due to exposure to hazardous events. On the other hand, this concept describes the costs of safety measures in saving an additional life or the restoration of an originally safe situation. One example is the social willingness to pay (SWTP), this is the amount of money that should be invested in saving one additional life. Required information for the SWTP is provided by the Life Quality Index acceptance criterion (LQI), which is derived on the basis of an acceptable target reliability index and cost minimisation if the capitalised societal risk is taken into consideration [61, p.97].

Risk-acceptance criteria are introduced in terms of target and acceptable (conditional) failure probabilities. The obtained failure probability is then related to the reliability index through [38]:

$$P_f = \Phi(-\beta) \approx 10^{-\beta} \quad (\text{C.3})$$

$\Phi(-\beta)$ denotes the probability distribution function of a standardised normal distribution [38] with $-\beta$ as the argument for z :

$$\Phi(z) = \int_{-\infty}^z \frac{1}{\sqrt{2 * \pi}} e^{-\frac{z^2}{2}} \quad (\text{C.4})$$

Where the reliability index β is obtained by dividing the mean value (μ_z) and standard deviation (σ_z) of the limit state function. Section C.4 will dive further into this theory. The acceptable failure probability $P_{f:acc}$ is determined by the maximum failure probability of a system given the consequences. Different risk segments related to a system such as the individual risk (IR), societal risk (SR) and economic risk (ER) are considered. A hard value follows from the acceptability of consequences in each risk category. These values are used in deriving an acceptable failure probability per segment. The minimum acceptable failure probability is determined by comparing the consequences from each risk segment: IR, SR, ER. The dominant risk criterion is determined by an FN-diagram. For the lowest probability of exceedance a high number of fatalities can be found.

Each failure mechanism of a structure is evaluated on the system's acceptable failure probability over the different system elements [42, p.99]. Derived target reliability indices or accepted failure probabilities that result from the acceptable risk criteria is further depending on the reference period t_{ref} on which it is applied [70]. Given independent events in subsequent time periods, the failure probability for a reference period t_{ref} can be determined according to equation C.5 [76].

$$P_{f:t_{ref}} = 1 - (1 - P_{f:t_1})^{n_{ref}} \approx P_{f:t_1} \cdot n_{ref} \quad (\text{C.5})$$

Where:

- $P_{f:t_{ref}}$ Probability of failure in the interval given time-independence $[0, t_{ref})$ [-]
 $P_{f:t_1}$ Probability of failure in the interval $[0, t_1)$ [-]
 n_{ref} Number of years in reference period t_{ref} $[0, t_{ref})$ [-]

t_1 Reference period of one year [years]

Many structures are however partly time-dependent, think of structural elements that deteriorate in time. Formula C.5 is therefore only applicable for few cases. In short, this probabilistic approach is the common premise in the currently used guidelines. Based on this approach, load and resistance factors are derived. An unity check is then performed to check the stability or functionality of a structure given the load and resistance parameter. Including a load or a resistance factor which is calibrated through the reliability index, one is accounting for the safety margin in the calculation of a structure. This is all explained more in detail in section C.4.

C.3.2. Reliability differentiation of new structures

International organisations such as the Joint Committee of Structural Safety (JCSS) and the International Organisation for Standardisation (ISO) support the reliability-based approach for the design and assessment of structures. Reliability differentiation and the associated target reliability indices of civil engineering structures is provided in a large set of foreign standards. These reliability indices are in most cases derived by, calibrating the indices as obtained in the new method against previous design methods [61, p.91]. These methods are further explained later on. For civil engineering structures, the target reliability level is often classified in certain safety classes such as reliability, consequence or occupancy classes. Depending on in which sub-area the reliability differentiation is used, one recognises insignificant differences between target reliability indices at each column of table C.1. Sub-areas are in this case recognised as buildings, bridges, concrete, geotechnical, hydraulic. Table C.1 presents an overview of the annual target reliability indices and table C.2 presents the lifetime target reliability indices as provided in literature. These target reliability indices are derived for the ultimate limit state (ULS) and applied on newly built structures [61].

Codes & Standards	Application	Consequence classes				
		A Low	B Some	C Considerable	D High	E Very high
ISO 2394 (2015) ¹	All	Class 1	Class 2 4.2	Class 3 4.4	Class 4 4.7	Class 5
JCSS (2001) ¹	All		Minor 4.2	Moderate 4.4	Large 4.7	
Structural concrete (2012) ¹	Concrete	Small 3.5	Some 4.1		Moderate 4.7	Great 5.1
EN 1990 (2002) Eurocode 0	All		RC1 4.2		RC2 4.7	RC3 5.2
Rackwitz (2000) ¹	Bridges	Insignificant 3.7		Normal 4.3	Large 4.7	

Table C.1: Annual target reliability indices for the ultimate limit state (ULS)

All codes and standards that are shown in C.1 and C.2, use their own reliability differentiation. However, when the assessment criteria and associated target indices are subsequently ordered according to ISO 2394:2015, one finds the reliability differentiation of the different standards to be fairly uniform and consistent. ISO 2394 determined a framework consisting of five consequence classes including assessment criteria (A, B, C, D and E). Many standards among which Structural Concrete [30] and Japanese standards on harbour and port facilities implement the basic principles of ISO 2394 [61, p.91]. General principles are the assessment criteria regarding human safety (people at risk, fatalities) and

Codes & Standards	Application	Consequence classes				
		A Low	B Some	C Considerable	D High	E Very high
ISO 2394 (1998) ¹	All	Class 1	Class 2 4.2	Class 3 4.4	Class 4 4.7	Class 5
ISO 23822 (2010) ¹	All	Small 2.3	Some 3.1		Moderate 3.8	Great 4.3
EN 1990 (2002)	All		RC1 3.3		RC2 3.8	RC3 4.3
SANS 10160 (2010) South African National Standard	All	RC1 2.5	RC2 3.0	RC3 3.5		RC4 4.0
ASCE (2010) ²	All	I ^a 2.5	II ^a , III ^a & I ^b 3.0/3.25/3.0	IV ^a , II ^b & I ^c 3.5/3.5/3.5	III ^b 3.75	IV ^b , II ^c , III ^c & IV ^c 4.0/4.0/4.25/4.5

¹ Target reliability indices derived by assuming relatively low relative costs of safety measures (optimistic approach). Note that for existing quay walls, the relative costs of safety measures can be higher.

² Development and scatter of the consequences: not sudden and not widespread (a), sudden or widespread (b), sudden and widespread (c) [61].

Table C.2: Lifetime target reliability indices for the ultimate limit state (ULS)

economic consequences (damage costs) and are converted in operational design procedures as used in the Eurocode EN 1990. Procedures for the treatment of actions, combinations of actions and material independent provisions are emphasised in this operational design standard [84]. This reliability-based approach was mainly developed for buildings and bridges initially. However, this procedure can be adopted for different types of civil engineering works [61].

Table B1 - Definition of consequences classes

Consequences Class	Description	Examples of buildings and civil engineering works
CC3	High consequence for loss of human life, or economic, social or environmental consequences very great	Grandstands, public buildings where consequences of failure are high (e.g. a concert hall)
CC2	Medium consequence for loss of human life, economic, social or environmental consequences considerable	Residential and office buildings, public buildings where consequences of failure are medium (e.g. an office building)
CC1	Low consequence for loss of human life, and economic, social or environmental consequences small or negligible	Agricultural buildings where people do not normally enter (e.g. storage buildings), greenhouses

Figure C.20: Reliability differentiation as performed in the EN 1990 on the basis of ISO 2394

Fundamental requirements regarding a structure in a design situation¹ use so-called limit states. Briefly speaking, a limit state is a condition beyond which the structure or a part of it does no longer fulfil its performance requirements [42, p.240]. Several issues can be stated as performance requirements: The maximum deformed state, vibrations leading to discomfort or damages with a negative effect on the durability are amongst these requirements. In engineering, one recognises two types of limit states:

- Serviceability limit state (SLS): Referring to the state beyond which one or more requirements with respect to the functionality is not fulfilled anymore.

¹The variation of load actions, environmental influences and structural properties during a structure's design life [42, p.239].

- Ultimate limit state (ULS): Referring to the state at which the ultimate bearing capacity of the structure is defined, beyond which the structure or part of it fails.

In its most simplified form, a limit state function is described by a strength variable and a load variable. This approach is adopted from the probabilistic design code of JCSS [55]. Further explanation about this probabilistic approach in the assessment of structures is provided in section C.4.

C.3.3. Reliability differentiation of existing structures

Section C.3.2 has addressed the reliability-based approach for the design and assessment of newly-constructed works in general. For large parts in the first world, especially in the port area of Rotterdam, space is lacking. Existing structures therefore become relatively more important. A large part of the infrastructure and buildings the design life has been reached, will be reached in the near future or is already exceeded. For existing structures, a slightly different approach is adopted for the differentiation and derivation of target reliability levels. The reliability assessment differs that from a newly-designed structure in a number of ways [86]:

- An increase in safety level is often more expensive for an existing structure than for a new structure.
- The remaining working life for existing structures is mostly shorter than the intended design working life for new structures.
- Information that is obtained from monitoring, structural inspection(s) and conditional tests are relevant for the assessment of existing structures.

Whereas the target reliability levels as recommended in EN 1990 (basis of structural design) are defined for newly-built structures and where ISO 2394 gives recommendations on general principles for structural reliability, the ISO 13822 provides options for defining target reliability levels for existing structures. ISO 13822 provides general requirements and procedures for the assessment of different civil engineering works such as buildings, bridges, industrial structures. Moreover, these requirements are based on the international standard ISO 2394 [1]. Mostly, such assessments are done under the following circumstances [1, p.1]:

- Anticipated change in use of the structure;
- extension of design working life;
- reliability check as required by authorities, shareholders or owners;
- structural deterioration due to time-dependent actions such as corrosion or fatigue;
- structural damage by accidental actions.

It is beforehand necessary to acquire an overview in the specification of the objectives, scenarios, inspections, properties and further recommendations of the structure to be assessed. In addition to that, this international standard ISO 13822:2010 serves as a basis for preparing European and national standards and guidelines. These standards and codes are in accordance with the current engineering practice and economic conditions within the borders. The Dutch NEN-EN 8700 is such a national standard and provides recommendations on target reliability levels for the remaining working life and cases of reconstruction and condemnation. Both cost optimisation and human safety are taken into account in the determination of the target reliability levels.

Where:

wn = wint not dominant

wd = wind dominant

Consequence class	Minimum reference period	β_n new		β_r repair		β_u unfit for use	
		wn	wd	wn	wd	wn	wd
1A	1 year	3.3	2.3	2.8	1.8	1.8	0.8
1B	15 years	3.3	2.3	2.8	1.8	1.8	1.1*
2	15 years	3.8	2.8	3.3	2.5*	2.5*	2.5*
3	15 years	4.3	3.3	3.8	3.3*	3.3*	3.3*

Table C.3: Required target reliability indices for the minimum reference period.

(*) = in this case the minimum limit for human safety is decisive

Because of economical reasons it is not recommended to specify these target reliability levels for all existing structures to be the same as new structures [86]. From the latter point of view, the required safety level for an existing structure is often relatively lower than for a new structure on the condition that the human safety limits is not exceeded. From the same study it appeared that the conditional failure probability exceeds the level for human safety in case of a design working life of less than 15 years. Hence the Dutch standard implies a minimum design life of 15 years for CC2 and CC3 instead of the raising of partial factors [85, p. 130]. Table C.3 provides the target reliability indices considering economics and human safety [85, p. 134]. The subscript "n" denotes new structures while subscripts "r" and "u" in the same order denote existing structure in the cases of repair and unfitness for use. In short, cost optimisation and the consequence of failures are important factors in the determination of target reliability indices as is performed in ISO 13822:2010 and NEN-EN 8700.

Sections C.3.2 and C.3.3 have dealt with the standardisation and differentiation of general civil engineering structures. Illustrated standards and codes were mainly developed for a wide range of applications and the examples from the papers were mainly addressing buildings or bridges. There are although standards which are mainly developed for geotechnical structures. For this reason, the next sections will encounter the safety according to geotechnical standards. Firstly the newly-built geotechnical structures will be treated and after that the existing geotechnical structures.

C.3.4. Reliability differentiation of new geotechnical structures

Nearly thirty years of closely cooperation exists between the International Organisation for Standardisation (ISO) and the European Committee for Standardisation (CEN). The Vienna Agreement, also called as the Agreement on Technical Cooperation between the CEN and ISO, was formally approved in 1991 [29]. ISO standards are in this agreement prioritised but the requirements for the development of standards on the European level are recognised as well. This might be caused by the state of the European Market or construction industry. Nevertheless, ISO has set a number of standards which are related to the EN Eurocodes for geotechnical design [29]:

The last two rows of table C.4 provides globally recognised ISO standards that are normalised for the European Market. On an European level, the standardisation for geotechnical design is written in Eurocode 7 EN 1997 which consists of two parts. Part 1 is concerned with the general rules for geotechnical design and part 2 is concerned with the use of field investigations and laboratory testing. The second part is in accordance with EN ISO 14688 - 14689. In the Netherlands, national guidelines such as the NEN-EN 9997-1 for geotechnical design, comprise the full text of the Eurocode including a national annex. This national annex contains information on parameters that are left open in the Eurocode. Such parameters are related to civil engineering works in the considered country and include:

ISO Standards related to the Eurocodes for geotechnical design	
ISO 2394	General principles on reliability for structures
ISO 3898	Basis for design of structures - Notations - General symbols
European normalised ISO Standards related to geotechnical design	
EN ISO 14688	Geotechnical investigation and testing - Qualification and description of soil
EN ISO 14689	Geotechnical investigation and testing - Description of rock

Table C.4: Standards developed by the independent, non-governmental global standardisation organisation ISO

Country specific geographic and climatic data, values, symbols and classes. Alternatives for this kind of information is given in Eurocodes [13].

EN 1997 and NEN-EN 9997-1 are both implemented in the Dutch guideline for sheet piles (CUR 166) and the Dutch guideline for quay walls (CUR 211). In fact, the reliability differentiation with lifetime reliability values, as is done for general structures (according to EN 1990), has been applied unaltered in the CUR 211 as well [61]. The CUR 166 is developed for the design of sheet pile walls, often without a relieving platform or (tension) piles, and uses different lifetime target reliability indices. Table C.5 presents the reliability classes (RC) conform EN 1990 and the withdrawn NEN 6700.

Literature	Application	Consequence classes				
		Low	Some	Considerable	High	Very high
EN 1990 (2010)	All		RC1 3.3		RC2 3.8	RC3 4.3
Withdrawn NEN 6700 (2005)	All		Class 1 3.2	Class 2 3.4	Class 3 3.6	
CUR 166 (2012)	Sheet piles	Class I 2.5		Class II 3.4		Class II 4.2
CUR 211 (2013)	Quay walls		RC1 3.3		RC2 3.8	RC3 4.3

Table C.5: Overview of lifetime target reliability indices in standards for the ultimate limit state (ULS)

As can be seen from table C.5, sheet piles use a different bottom safety level than quay walls. Class I holds for simple constructions with limited consequences after failure and RC1 for quay walls is more or less comparable with class II of sheet piles. Given that observation, one can argue that CUR 211 follows the Eurocode 0 EN 1990 whereas the CUR 166 implements both the old NEN 6700 and the EN 1990 [15, p. 18]. Obviously small differences between the values can be observed, these small differences are although negligible after the derivation of target failure probabilities has taken place. Beside the mentioned consequence classes (CC), geotechnical categories (GC-classes 1 to 3) are used in NEN-EN 9997-1 as well. The extent of the soil investigation to be carried out is dealing with the project complexity as is stated in GC1, GC2 and GC3.

C.3.5. Reliability differentiation of existing geotechnical structures

Previously, standards and design guidelines regarding new geotechnical structures have been discussed. However, this research is mainly concerned with the reliability of existing quay walls. Yet are standards regarding existing structures dependent on the reliability differentiation as is done for new structures. Quay walls in particular use reliability classes RC1, RC2 and RC3 in accordance with the

NEN-EN 1990. The derivation of the accompanying reliability levels happens with the defined failure of the main functions. Main functions thereby are [17, p. 221]:

- Earth retaining
- Load bearing when the quay wall is in use
- Resistance against current-induced scour by ships, tide or canal discharge

In either way a design life of 50 years is considered. In addition to that, new quay walls are classified by the degree of economic consequences and risk of danger to human [61]. Reliability indices of existing quay walls and other existing geotechnical structures are derived in a different way. The Dutch standard NEN 8707 is part of the NEN 8700-serie and sets the regulations concerning the assessment of the structural safety of existing geotechnical structures [35]. This consolidated version of the standard is concerned with shallow foundations, pile foundations, retaining structures, anchorage, dams and other (under)ground works. In addition, the standard provides procedures for the assessment and evaluation of geotechnical works within the Dutch built environment.

In accordance with the NEN 8700, partial factors γ_{geo} and surcharges δa are derived according the reliability levels for structures that are subject to non-dominant wind load(s). Table C.6 presents the reliability differentiation for soil-retaining structures (e.g. quay walls) in accordance with the NEN 8700 [34].

Parameter	γ and Δ for characteristic value X_k												Design value
	Repair												
	Safety class after 'Bouwbesluit 2003'						Safety class before 'Bouwbesluit 2003'						
	RC1		RC2		RC3		RC1		RC2		RC3		
	$\beta = 2.8$		$\beta = 3.3$		$\beta = 3.8$		$\beta = 2.8$		$\beta = 3.1$		$\beta = 3.6$		
	γ_{geo}	Δa	γ_{geo}	Δa	γ_{geo}	Δa	γ_{geo}	Δa	γ_{geo}	Δa	γ_{geo}	Δa	
Retaining height (h) in m	1.8	0.24	2.15	0.29	2.40	0.33	1.8	0.24	2.0	0.27	2.25	0.31	$\max\{\mu + \gamma_{geo} \cdot \sigma; \mu + \Delta\}$

Table C.6: Partial and additional factors for in soil embedded walls according to NEN 8707 [35, p. 44]

'Bouwbesluit 2003' is a report of prescriptions composed for newly built structures. These prescriptions contain environmental permits that influenced soil-retaining walls such as quay walls. So this 'Bouwbesluit 2003' has to be taken into account in the reassessment and the reliability evaluation of existing quay walls. The target reliability values are in accordance with the target reliability values as presented in table C.3 in section C.3.3. As is previously mentioned, the target reliability indices are derived on the basis of economic optimisation of the total building costs and the product of damage costs and probability of failure [85, p. 131], given that the human safety is guaranteed (below risk-acceptance limits). Reliability differentiation for commercial quay walls, on the basis of life quality criterion, societal and individual risk acceptance criterion appeared to be slightly lower than in the case of economic optimisation [62]. An other study [63] has proven different outcomes for the reliability indices when corrosion-induced degradation has been taken into account. As a result, the determined target reliability indices in the NEN 8707 might be questioned on whether these are sufficiently calibrated through financial criteria or live environmental actions.

Section C.3 has addressed aspects related to safety in the area of Civil Engineering. These safety levels are derived through reliability calculations. Section C.4 treats the different methods that are used in the reliability differentiation.

C.4. Reliability calculus

C.4.1. Introduction

In theory, the safety of a structure can be described with two stochastic parameters: the resistance R^2 of the system and on the other side load S of the system. The reliability is then derived with equation C.7 which is called the limit state function. Hence, a non-failure of the system is achieved if the resistance is larger than the solicitation, so if condition C.6 is met:

$$R > S \quad (\text{C.6})$$

$$Z = R - S \quad (\text{C.7})$$

The limit state function is used to determine the failure probability and thus the reliability index, see equation C.8.

Here the failure domain is defined as the situation where the load variable exceeds the strength variable. In other words, if the limit state function Z is below 0 than the structure does not longer fulfil its fundamental requirements. In that case the domain of the failed structure can be defined as:

$$P_f = P[Z < 0] \quad (\text{C.8})$$

The stochastic quantities R and S can for instance be the [42, p. 105]:

R	S
Bending moment resistance	Maximum existing bending moment
Permissible deflection of a member	Maximum deflection in the member
Flow capacity of a channel	Discharge of the channel
Soil cohesion and shear strength	Soil stresses due to external loading

Table C.7: Examples of the stochastic parameters R and S

As can be observed in the table above, stochastic parameters might be used for cases in the serviceability limit state (permissible deflections) as well as for ultimate limit state (max bending moment resistance). The following sections deal with the different reliability methods for the evaluation of the reliability of structures. The deterministic level 0 approach is firstly explained, in follow-up to that, reliability methods I to IV are described.

C.4.2. Level 0 method: Deterministic approach

In the case of a deterministic approach the parameters are not assumed as stochastic. This approach is traditionally used for civil engineering problems. By substituting design variables, r_d for the resistance and s_d for the load, one obtains a statement in which two single values are compared. These values are derived by using a data set of discrete characteristic values for determining the representative value. That is to say, for instance the minimum resistance value and the maximum load value from that data set.

²The variables R and S originate from the French words *résistance* and *solicitation*. Other terms, such as strength or capacity for R and solicitation or action for S are regularly used as well.

$$R_{nom} \geq \gamma_d S_{nom} \quad (C.9)$$

According to equation C.9 the basic variable accounts for nominal values [42, p. 113], which represent values from a data series with a minimal variance. The design value of the load variable can be obtained by multiplying the design variable with an empirically global safety factor. This factor can be found by the use of empirical data which obtained through measurements. Measurements of wind speed data can for instance be modelled with a Weibull distribution given the return period in years. This distribution goes along in combination with scattered data that lies between a confidence interval. In that case, a global safety factor can be determined by the division of the maximum perceived value (red dot) and the analytical value (blue dot), see figure C.21. The measured maximum value is a discrete value.

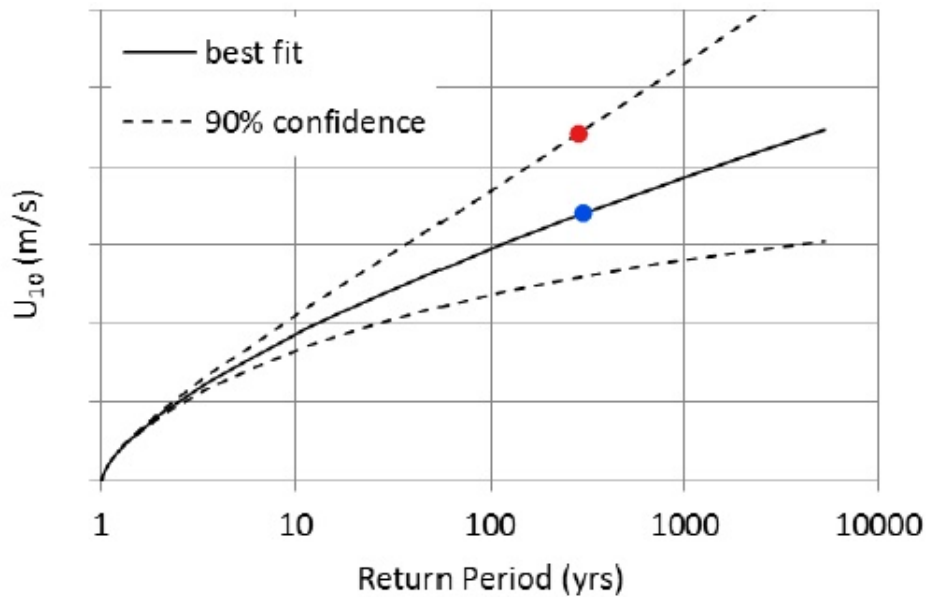


Figure C.21: Example of a cumulative Weibull distribution with scale factor $l = 4.5$ and shape factor $k = 1.5$ [37].

Additionally, the same approach can be used for the resistance or strength. This resistance can be modelled as a parameter which depends on:

- Model uncertainties: m
- Measured material properties (e.g. compressive strength): f
- Measured dimensions or quantities: d

In each case, an unfavourable value is used. That is to say, for the model uncertainty m one uses the largest division between the test result r_{exp} and the corresponding model result that is obtained with a (fitted) curve (e.g. by an analytical theorem) [42, p. 106].

$$r_d = m \cdot f \cdot d \quad (C.10)$$

Where:

$$m = \frac{r_{exp}}{r_{mod}} \quad (C.11)$$

Notice that m is a value smaller than one, since one uses the most unfavourable value from the experiment data set. So briefly speaking, deterministic values of the dimensions, quantities or properties are discrete values without any incorporated uncertainties. The neglected involvement of uncertainties is therefore an important argument for not frequently using this method anymore.

C.4.3. Level IV methods: Risk-based approach

The first group of methods that is discussed, is the risk-based level IV approach. These methods are appropriate for structures with major economic importance and that are extremely profound such as nuclear power plants, highway bridges, transmission towers and centres. In this approach, the economic consequences or consequences of failure are taken into account. Uncertainty, costs and benefits of construction, repair, maintenance and decommissioning are thereby appropriately taken into account [10].

Since this concept is already discussed in [86] [62], it will not be extensively explained in this research. Main idea of this approach is to determine an acceptable failure probability on the basis of cost optimisation provided that human safety is sufficiently guaranteed and the risks are minimised. According to [2], the target level may be selected solely on the basis of economic optimised outcomes whenever human fatalities are not involved. Individual or societal risk criteria and the Life Quality Index approach can be used to assess the risk exposures and the corresponding failure probabilities.

The target reliability optimum obtained by cost minimisation is in accordance with [76] and is determined by minimising the total cost function C.12. This total cost function is considered over the equivalent length L_{eq} , the length along a quay wall for which failure events are independent:

$$\min\{C_{Total}(\beta) = C_{Investments}(\beta) + C_{CapitalisedRisk}(\beta)\} \quad (C.12)$$

in which:

$$C_{Investments}(\beta, x) = C_0 + C_m(x)\beta \quad (C.13)$$

with,

C_0 = initial construction costs independent of the reliability index [€]

and

$$C_{CapitalisedRisk}(\beta) = C_f P_{f;0}(\beta) + C_f \cdot \sum_{n=1}^{n_{ref}} \frac{\Delta P_{f;t_n}(\beta)}{(1+r)^n} \quad \text{for } n \in (1, n_{ref}) \quad (C.14)$$

Here the parameters describe:

C_f = the summation of direct and indirect economic consequences of failure [€]

$P_{f;0}$ = the time-independent probability of failure [-]

$\Delta P_{f;t_n}$ = the time-dependent probability of failure over a certain time interval [-]

$\frac{1}{(1+r)^n}$ = the discount factor over a certain time interval t_n [-]

The marginal construction cost per meter $C_m(x)$ depends on the reliability index β and the changes in structural dimensions. The latter happens in the case of longitudinal structures such as quay walls or tunnels [62, ch. 3.4]. Here it is assumed that the structure is subdivided into equivalent sections. Hence, the marginal costs are derived for an equivalent section (with length L_{eq} with independent failure events [62]):

$$C_m(x) = L_{eq} \frac{\Delta C(x)}{\Delta \beta(x)} \quad (\text{C.15})$$

Where:

x = vector representing changes in structural properties in the longitudinal direction

L_{eq} = equivalent length along a structure for which failure events are independent [m]

ΔC = change in costs of safety measures [€/m]

$\Delta \beta$ = change in reliability index [-]

$\frac{\Delta C}{\Delta \beta}$ represents the safety investments per metre [€/m]

The total cost function in euros consists of the investment in safety measures $C_{Investments}$ and the present value of future risks $C_{CapitalisedRisk}$. This function of total costs can be minimised (see eq. C.12) and differentiated over the decision parameter which is the reliability index β . Thereafter, the optimal reliability (see figure C.22) index can be derived by solving the associated derivative of the minimised cost function:

$$\frac{\partial C_{Total}(\beta^*)}{\partial \beta} = 0 \quad (\text{C.16})$$

The obtained optimum reliability index β^* is then compared with the acceptable lifetime target reliability index β_{acc} (see figure C.22). The acceptable reliability index is derived from stated acceptance criteria. These criteria encompass standardised acceptable annual values for e.g. the societal and economic risk.

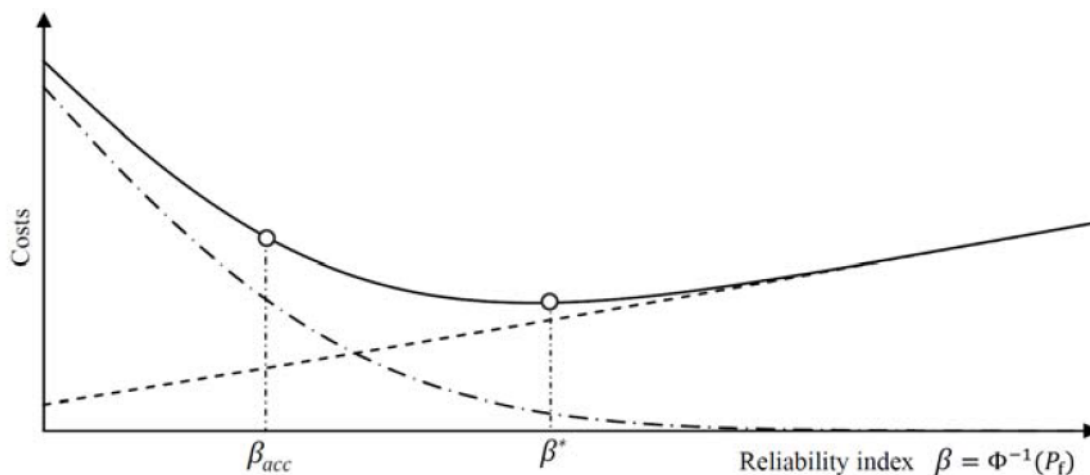


Figure C.22: Principles of cost estimation, reliability optimum and acceptable target reliability index [61].

So the target reliability optimum is then compared with the acceptable target reliability obtained by the risk criteria as is explained below.

Individual risk criterion:

$$P_{f|IR} = \frac{10^{-5}}{P_{d|f}} \quad (C.17)$$

Here oftentimes an acceptable individual risk value of $IR < 10^{-5}$ per year is taken. $P_{d|f}$ is the probability of casualties given a structural failure, specific values for different consequence classes were given in [85]. The annual acceptable target reliability index is then derived by: $\beta_{acc} = -\Phi^{-1}(P_{f|IR})$.

Societal risk criterion:

$$P_{f_{acc;t1}} = \Phi(-\beta_{acc;t1}) \leq AN_{F|f}^{-k} \quad (C.18)$$

The expected number of fatalities given a failure $N_{F|f}$, the annual acceptable risk A and the slope factor of the related F-N curve are all constants. A F-N curves gives the probability of exceedance of a casualty given the number of fatalities [42, p. 90]. For acceptable risks for structural failure the constant A would be around 10^{-6} and for marginally acceptable risks $A = 10^{-4}$. The slope factor k varies widely and depends as the annual acceptable risk A on the type of hazard and technical activity [55, p. 61]. In addition to that, the number of fatalities given a failure can be estimated by different formulae (see eq. C.19 [62]) or by given historical data.

$$N_{F|f} = N_{PAR}(1 - P_{Escape})P_{d|f} \quad (C.19)$$

N_{PAR} number of people at risk [-]

P_{Escape} probability of a successful escape [-]

$P_{d|f}$ conditional probability of a random human being present will die in the event of failure

Equation C.19 is especially applicable for quay walls. The **LQI-criterion** is estimated by the societal willingness to pay (SWTP), which gives a monetary value to a human life [2]. Accordingly, societal costs given a group failure is estimated:

$$C_{f:societal} = N_{F|f}SWTP \quad (C.20)$$

Hence, the monetary value for the societal costs of failure (see equation C.20) is used in equation C.14 to determine the new capitalised risk. For the discount rate, a societal discount rate γ_s is used. The positive minimised societal cost function is subsequently determined. As is shown in the earlier procedure, the annual acceptable target reliability index is determined by taking the derivative of the minimised societal cost function in terms of the decision parameter β (see eq. C.21).

$$\frac{\partial C_{f:societal}\beta^*}{\partial \beta} \geq 0 \quad (C.21)$$

Eventually, the target reliability index as is derived by cost optimisation, has to be determined on a yearly basis (β_{t1}^*) in order to check whether it is acceptable. To do so, the dependency of failure events in subsequent time periods has to be studied and an equivalent factor n_{eq} , which is the ratio between the reference period t_{ref} and the equivalence period t_{eq} , has to be derived. The equivalent period is the time period for which failure events are independent in subsequent years. [61] and [86] elaborate more on this.

C.4.4. Level III methods: Full probabilistic approach

A rather different approach than the risk-oriented approach as is explained in section C.4.3 is the level III approach, also called the full probabilistic approach. In this full probabilistic approach, a complete analysis of the problem is included. At the same time, the probability density functions of all stochastic variables are described and analysed. The probability density distribution(s) of the strength $f_R(r)$ and the loading $f_S(s)$ and the resulting limit state function are shown in figure C.23.

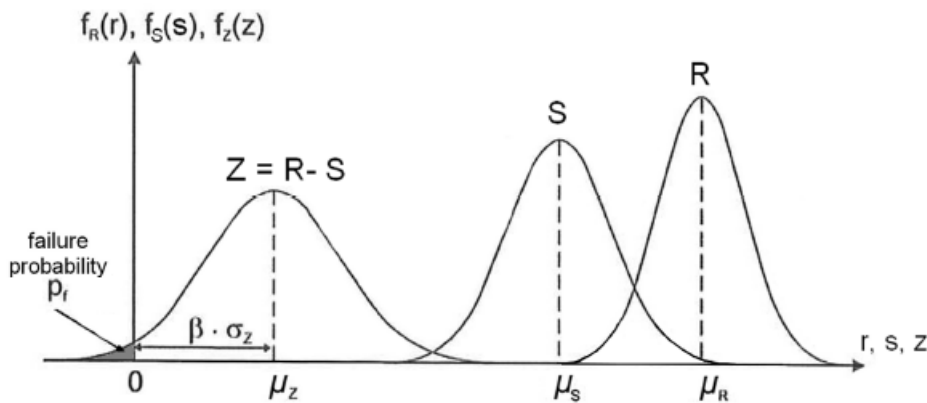


Figure C.23: Probability density distributions of the strength (R), the loading (S) and the limit state function (Z) [49, ch. 2.6]

Generally, this method includes the integration of the joint probability density over the failure domain [10]. The failure domain is indicated by the grey area where $Z < 0$ as indicated in figure C.23. Recall that the latter occurs when the load exceeds the strength in the limit state function (see equation C.7). Safety indicators that result from these methods are the reliability index β or failure probability P_f . β is the distance between $Z = 0$ and the mean value μ_Z of the limit state probability density distribution and is expressed in the number of standard deviations σ_Z .

$$\beta = \frac{\mu_Z}{\sigma_Z} \quad (\text{C.22})$$

Where:

μ_Z is the mean value of the limit state density function: $\mu_Z = \mu_R - \mu_S$

σ_Z is the standard deviation of the limit state density function: $\sigma_Z = \sqrt{\sigma_R^2 + \sigma_S^2}$

If the limit state function contains independent normally distributed random variables and the function is linear, then the probabilistic computations can easily be done by hand [42, ch. 5]. To accomplish that, a reliability computation according to the level III approach uses equation C.23.

$$P_f = \int_{g(x) < 0} f_X(x) dx = \iint_{R < S} f_R(r) f_S(s) dr ds \quad (\text{C.23})$$

This failure region might become more obvious if one uses a joint probability density distribution. The volume of the failure region is derived by using equations C.24 and C.25.

$$f_R r f_S(s) = f_{R,S}(r, s) \quad (\text{C.24})$$

$$P_f = \int_{-\infty}^{+\infty} \int_{-\infty}^{r=s} f_{R,S}(r,s) dr ds \quad (\text{C.25})$$

Figure C.24 shows the joint probability density distribution in combination with the limit state function.

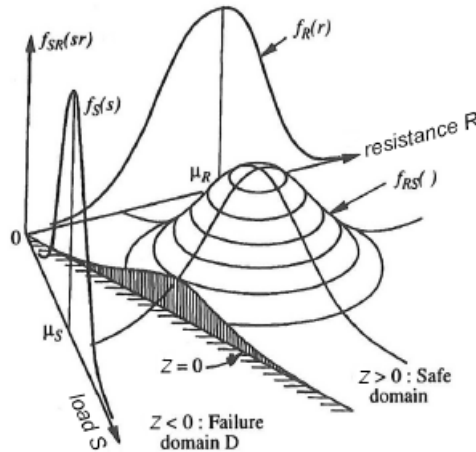


Figure C.24: Joint density function of the strength (R) and loading (S) [49, p. 17].

There is a several full probabilistic methods that can be used to solve this integration [42]:

- Numerical integration
- Monte Carlo Simulations
 - Importance Sampling (see appendix E.1)
 - Directional sampling (see appendix E.2)

Through numerical integration, the calculation of the failure probability P_f is rather difficult if the number of independent stochastic variables exceeds two. A more practical approach is therefore the use of Monte Carlo simulations. By using this method, random samples are generated. To realise the Monte Carlo simulations, the following procedure for limit state function $g(\underline{X})$ with vector \underline{X} can be used. For each function variable X_i (with $i = 1, 2, \dots, n$), N simulations are realised ($x_{i1}, x_{i2}, \dots, x_{iN}$). And for each set j ($j = 1, 2, \dots, N$), the outcomes of the limit state function $g(\underline{X})$ is calculated. After each calculation, it is verified whether $g(\underline{X}) < 0$ or not. If so, the number of failed samples N_f is increased by one. Eventually the number of failed samples determines the failure probability. Equation C.26 is used, the indicator function $I[g(\underline{x}) < 0]$ returns 1 if the statement between the squared brackets is true and 0 if the statement is false. The boundary line for the purpose of equation C.26 is in most cases given by $R = S$.

$$\hat{P}_f = \frac{1}{N} \sum_{j=1}^N I[g(\underline{x}) < 0] \quad (\text{C.26})$$

A higher accuracy can be obtained by increasing the number of samples N ($N \rightarrow \infty$). However, by increasing the number of samples this calculation becomes computationally rather intensive.

C.4.5. Level II methods: Approximation of the design point

The probabilistic approach as is outlined in section C.4.4, uses probability density functions including their uncertainties, for all stochastic variables that are involved in the limit state function. Level II methods are simplified methods for this full probabilistic analyses. By simplifying the full probabilistic approach of level III, one is saving in computational time and effort. Usually, the joint probability density function (see C.4.4) uses a linearised limit state function which is obtained by a Taylor approximation. The order of approximation is determined by the decision between [49, p. 17]:

- First Order Reliability Method (FORM)
- First Order Second Moment method (FOSM)
- Second Order Reliability Method (SORM)

This **First Order Second Moment methods (FOSM)** are based on the first order Taylor approximations of the mean and standard deviation of the limit state function linearised at the mean values of the random variables [10, p. 7]. This elementary method was first introduced by Cornell (1967). This method although has an important disadvantage and is therefore not elaborated in detail. It can only be used if the limit state function and the variables are linear in nature. It basically means that it is only useful if the variables are normally distributed.

Second Order Reliability Method SORM on the other hand, is based on a quadratic approximation of the limit state surface at the design point. In many cases, especially for non-linear limit state functions with a larger number of variables, this seems a rather complicated approach.

Based on experience, the results obtained from the most commonly applied **First Order Reliability Method FORM** are already sufficient for many civil engineering problems. FORM will therefore be elaborated in more detail. The FORM-method by Hasofer & Lind (1974), linearises the limit state function in the design point. The design point is basically the point on $Z = 0$ where failure is most probable, so where the joint probability density distribution has the highest probability density [42, p. 112]. When focusing on the joint probability density function in the standardised normal plane ($U_R, U_S - plane$), one perceives the computation of β to be a geometric problem. Hasofer & Lind generalised a property by stating: "The reliability index β is equal to the shortest distance from the origin to the surface which is bounded by $g(X) = 0$, so basically to the limit state surface $g(U) = 0$ ", see figure C.25 [42, p. 130]. FORM is based on this principle.

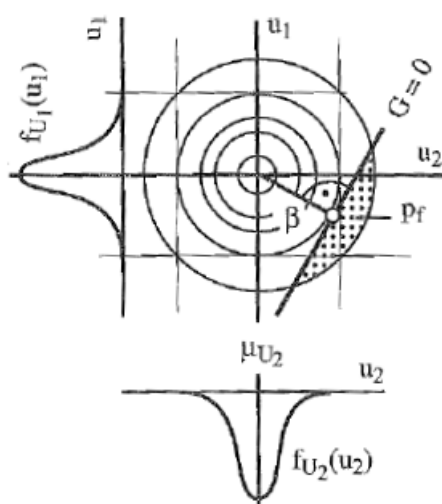


Figure C.25: In the standardised normal plane, β is the shortest distance between the origin and $Z = 0$.

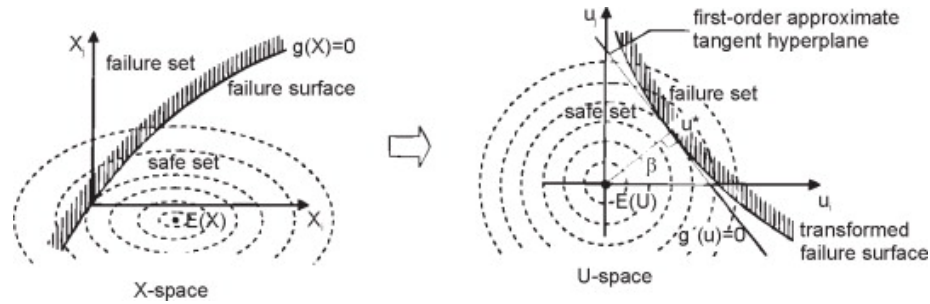


Figure C.26: Computation of the reliability according to Hasofer & Lind (1974) with the shortest distance to the design point β [14].

Hence when performing the FORM one usually starts with a limit state function. The First Order Reliability Method works as follows:

Given a limit state function with normalised and uncorrelated variables $g(\underline{X})$:

$$Z = g(X_1, X_2, \dots, X_i) \quad (\text{C.27})$$

The first step is to choose an estimate for the design point X_i^* . This can be done by using the mean values of all variables ($X_1^*, X_2^*, X_3^*, \dots, X_i^*$) in order to start the iterative procedure.

2. The mean value and standard deviation of the limit state function is derived with equations C.28 and C.29.

$$\begin{aligned} \mu_Z = g(X_1^*, X_2^*, \dots, X_n^*) &+ (\mu_{X_1} - X_1^*) \frac{\partial g}{\partial X_1}(X_1^*, X_2^*, \dots, X_n^*) \\ &+ (\mu_{X_2} - X_2^*) \frac{\partial g}{\partial X_2}(X_1^*, X_2^*, \dots, X_n^*) + \dots + (\mu_{X_n} - X_n^*) \frac{\partial g}{\partial X_n}(X_1^*, X_2^*, \dots, X_n^*) \end{aligned} \quad (\text{C.28})$$

$$\sigma_Z^2 = \left(\frac{\partial g}{\partial X_1}(X_1^*, X_2^*, \dots, X_n^*) \right)^2 \sigma_{X_1}^2 + \left(\frac{\partial g}{\partial X_2}(X_1^*, X_2^*, \dots, X_n^*) \right)^2 \sigma_{X_2}^2 + \dots + \left(\frac{\partial g}{\partial X_n}(X_1^*, X_2^*, \dots, X_n^*) \right)^2 \sigma_{X_n}^2 \quad (\text{C.29})$$

3. Consequently, the target reliability is calculated. Recall that for a linear reliability function with normally distributed variables the β is calculated with:

$$\beta = \frac{0 - \mu_Z}{\sigma_Z} = \frac{1}{V_Z} \quad (\text{C.30})$$

where V_Z is the coefficient of variation and the reciproke of β_Z , see equation C.22.

4. The following step is to determine the sensitivity factors α_i . These factors are a measure for the relative influence of the standard deviation of each variable to the reliability index of the system. So the larger the sensitivity factor α_i , the greater the influence of its accompanying basic variable X_i . Given the design point \underline{u}^* (with $u_1^*, u_2^*, \dots, u_n^*$) in the standardised normal plane, it follows from [42, p. 133] that:

$$\beta = - \sum_{i=1}^k \alpha_i u_i^* \quad (\text{C.31})$$

and

$$\sum_{i=1}^k \alpha_i^2 = 1 \quad (\text{C.32})$$

Hence, the sensitivity factors are derived in accordance with [42, p. 136]:

$$\alpha_i = \frac{\frac{\partial}{\partial X_i} g(\underline{X}^*) \sigma_{X_i}}{\sqrt{\sum_{i=1}^n \left(\frac{\partial}{\partial X_i} g(\underline{X}^*) \sigma_{X_i} \right)^2}} = \frac{\left\{ \frac{\partial}{\partial X_i} g(\underline{X}^*) \right\} \sigma_{X_i}}{\sigma_Z} \quad (\text{C.33})$$

5. Eventually the new design point can be determined according to equation C.34.

$$X_i^* = \mu_i - \alpha_i \beta_n \sigma_{X_i} \quad (\text{C.34})$$

This FORM analysis normally requires a number of iterations before the reliability index is sufficiently approximated. In order to achieve accuracy, steps 2 till 5 will be repeated until β , α and the design point \underline{X}^* are converged to certain values.

In the case of stochastic variables with different distributions, meaning not normally distributed such as lognormal or Gumbel distributions, one can determine the design value with equation C.35 [12, Annex C].

$$x_i^* = F_{x_i}^{-1}[\Phi(-\alpha_i \beta)] \quad (\text{C.35})$$

The FORM-method principle which is defined by Hasofer & Lind makes it a quite straightforward tool, reducing the computational effort [25, p. 14]. However, when a large number of variables and linearisations is used, the accuracy gets affected. In some cases a level III analysis would be inevitable for the verification of results.

C.4.6. Level I methods: Semi-probabilistic approach

In the level I approach one considers safety analysis from the perspective where load and strength variables are stochastic. Both the strength (R) and the load (S) have probability density distributions that illustrate their uncertainties. The different distributions are characterised by their variance and shape. Figure C.27 shows two typical distributions and the characteristic values.'

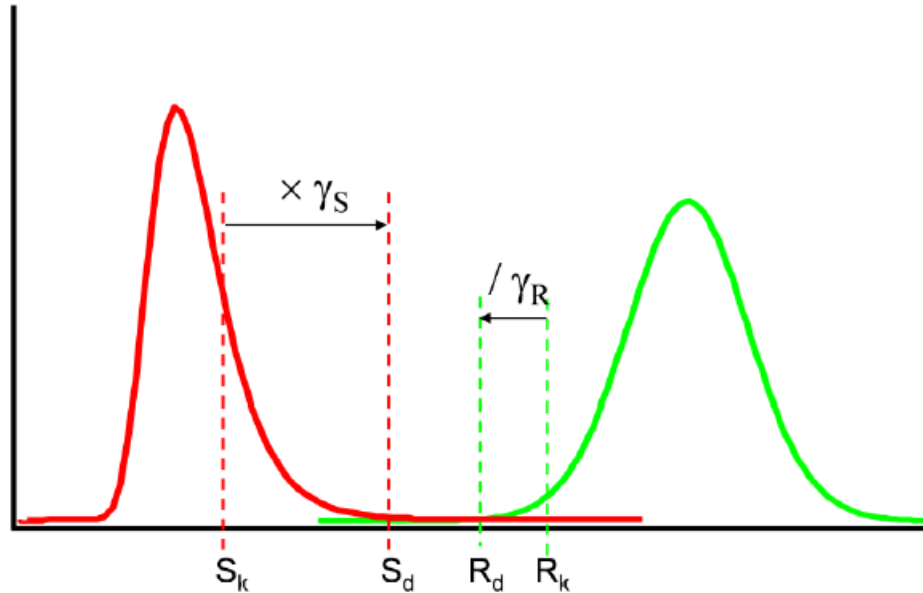


Figure C.27: Probability density functions of the load and strength with their design values chosen in such a way that the probability of failure is sufficiently low [42].

As is shown in figure C.27, the design value of the strength R_d is obtained by dividing the characteristic value R_k by a partial safety factor for the strength γ_R . The same procedure holds for the design value of the load S_d . Only difference is that the characteristic value is multiplied by a load factor. Hence, it follows from [42, p. 177] and [12] that:

$$R_d \geq S_d \quad (\text{C.36})$$

If the condition does not hold, then the probability of failure should be sufficiently low as is introduced by codes as standards such as EN 1990 [12]. Based on figure C.27 the following holds:

$$\frac{R_k}{\gamma_R} > \gamma_S S_k \quad (\text{C.37})$$

where:

R_k is the characteristic value of the strength

γ_R is the partial safety factor for the strength

S_k is the characteristic value of the load

γ_S is the partial safety factor for the load

The characteristic values, often called the representative values, of the strength and the load is derived by equation C.38. Here the multiplication constants k_R and k_S are used to obtain the characteristic values. For normally distributed variables the k-factors are equal to 1.64 [49, p. 7]. In the case of strength the k-factor is negative, whereas in the case for loads the k-factor can be positive or negative depending on whether the load is favourable or not.

$$\begin{aligned} R_k &= \mu_k + k_R \sigma_R \\ S_k &= \mu_S + k_S \sigma_S \end{aligned} \quad (\text{C.38})$$

The characteristic value of the strength R_k is the 5% non-exceedance value, while the characteristic value of the load S_k is the value that is exceeded by only 5% of the samples. Codes and standards (see section C.3) proposed partial safety factors regarding a safety class, to obtain the design values as such that the probability of exceedance is sufficiently limited. Sensitivity factors α_i are used with the design reliability index and the coefficient of variation V_x to determine the partial safety factors according to eqs. C.39. Using Level II and level III reliability methods is possible for calculating α -values. Level II methods although appear to be more appropriate since these influence values result directly from the calculation.

$$\begin{aligned} \gamma_S &= 1 + \alpha_s \beta_d V_r \\ \gamma_R &= 1 - \alpha_r \beta_d V_s \end{aligned} \quad (\text{C.39})$$

with:

$$V_x = \frac{\sigma_x}{\mu_x} \quad (\text{C.40})$$

α -values are standardised in European Engineering Codes and are determined by reliability calculations for several reference cases. These reference cases are comparable cases with the concerned engineering problem. On beforehand, alternatively mutually exclusive scenarios with diverging load situations or parameters are treated. Each calculation result in different outcomes with deviating sensitivity values. Eventually a weighted average can be extracted, for structures the following sensitivity values are established in the European Standards [42, p. 178]:

Variable	α
Dominant strength parameter	0.80
Remaining strength parameter	0.32
Dominant strength parameter	-0.70
Remaining load parameter	-0.28

Table C.8: Standardised α -values according to the European Standard.

Beside characteristic values that are obtained from statistical research of many samples, three other types of representative values [49, p. 7] exist. These representative values for quasi-permanent loads Q_k are multiplied with combination factors as explained below:

1. Combination values $\psi_0 Q_k$: These values are used for load combinations with time-dependent simultaneous loads of different independent actions. It is often too conservative to use for all different actions the representative values at the same time. In accordance with the Turkstra rule

[42, Ch. 10], for each load combination one load is assumed dominant while average values are assumed for the remaining loads. Eventually the normative load combination is used.

2. Frequent values $\psi_1 Q_k$: This type of value has an extremely small exceedance probability and it can only be exceeded during short periods of time. It is therefore mainly used in case of accidental actions in the ultimate limit state ULSC.3 and load actions for which exceeding of the limit value is accepted during certain time periods in the serviceability limit state SLS.
3. Quasi-permanent values $\psi_2 Q_k$: These values are chosen so that it is exceeded during significantly longer time periods. Mostly time-averaged values or the median fraction of the reference period is used.

Almost same procedures hold for material factors. Most of these factors are prescribed in the international standards. As it has appeared, the semi-probabilistic level I method seems an appropriate alternative for the deterministic approach as it accounts for uncertainty and variability in load actions.

C.5. Previous approaches and thereby used applications

This section addresses a comprehensive contemplation on previous studies performed on this subject. More importantly, the different used aspects are treated. Firstly, the treated concept is enlightened. In addition, a detailed description of uncertainties is provided. At last, a general consideration of the applicable tools is provided in section C.5.4.

C.5.1. Previous studies on reliability updating

Reliability methods are used in similar or comparable reference projects to determine target reliability indices for quay walls. Oftentimes, critical failure mechanisms are particularly considered in these reliability calculations. One of the first probabilistic analyses of geotechnical structures goes back to the development of the first CUR 166 in 1993. This guideline was mainly focusing on probabilistic level II and level I analyses of anchored sheet pile systems. Major failure mechanisms were given a large failure space "p" within the fault tree and minor mechanisms which are easily and inexpensively opposed: "0.2p." In addition, the system was considered to be serial with strongly mutual dependent components [71]. The adaptation of this approach in the derivation of partial factors, by means of the mentioned reliability methods, was performed for quay walls by Huijzer in 1996 [80]. An adaptation by the addition of extra components such as the relieving platform and foundation piles to the fault tree was performed in a research by Huijzer [80, p. 26].

For several existing constructed objects, different types of influencing phenomena on the reliability of the object have been investigated. Roubos (Port of Rotterdam) investigated the effect of corrosion-induced degradation on the reliability of service-proven quay walls [63]. It appears that the annual failure rates and the associated target reliability indices of existing quay walls are largely time-dependent. In view of that, the failure rate of non-deteriorating quay walls decreases over time as the confidence of the actual reliability increases since it is less likely that the strength properties of soil or steel, with high sensitivity factors, are unfavourable. For deteriorating quay walls, depending on the corrosion rate curve, the target reliability is critical in the first or last year of the service life.

Schweckendiek (TU Delft) studied the influence of corrosion on the reliability of sheet pile walls using an adapted fault tree [67]. Both studies were performed with Finite Element methods and probabilistic tools. Reliability updating or failure probability updating is applied in different knowledge areas. Moreover, other studies among which [11] [83] [77] [68] have set up a procedure in which historical observations or proof loads are used in the derivation of the adjusted reliability index given a dominant failure mechanism. These studies were concerned with levee sections in the Netherlands. On beforehand, the dominant failure mechanism (inward macro-stability or piping) was relevant for the determination of the limit state function. Eventually, the effect of past performance can be compared

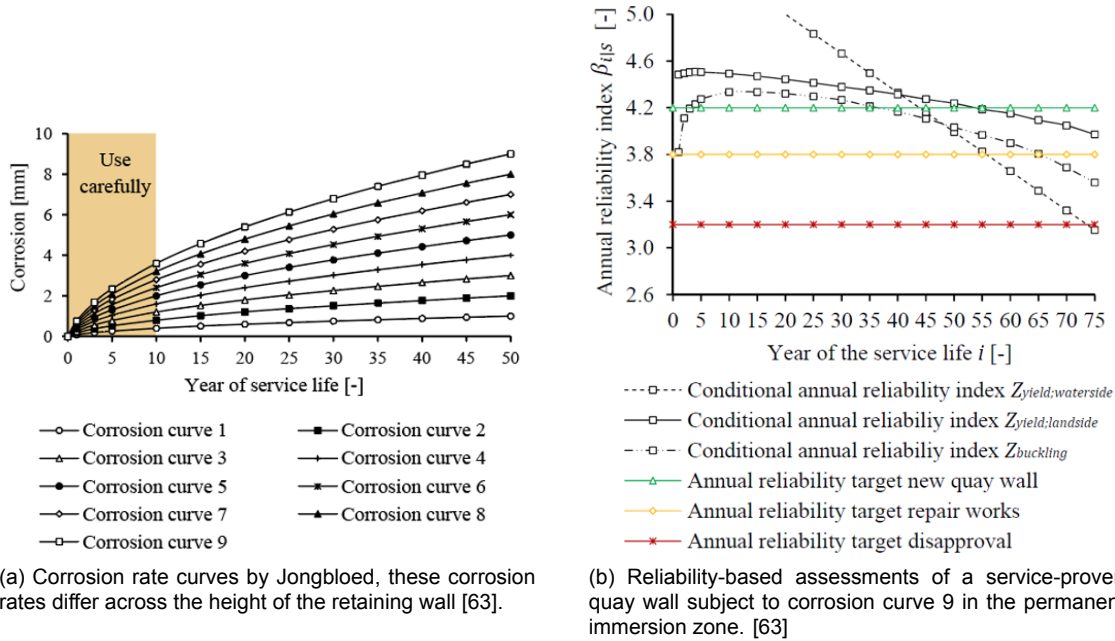


Figure C.28: Annual reliability index depends on the corrosion rate in a specific zone at the quay wall.

with the prior situation through probabilistic calculations (Crude Monte Carlo or FORM) and subsequently **fragility curves**. Fragility curves are functions describing the conditional failure probability for a dominant load variable (see figure C.29). By means of this figure, one is able to compare the initial stochastic assessment parameter "h" with the historical observation "h_{obs}" given the reliability indices [68].

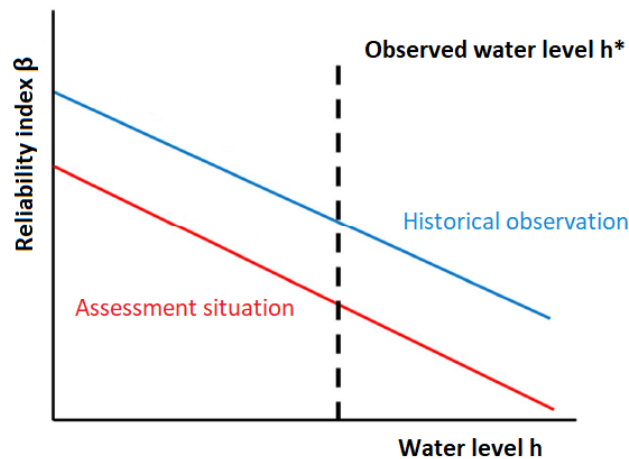


Figure C.29: Fragility curves for the observed situation and assessment situation [44, p. 30].

Important to notice is that there are always uncertainties (*aleatory* or *epistemic*) involved in such research cases. A dike ring consists of a number of sections in which stochastic variables might be auto-correlated. Meaning that the behaviour of one stochastic component (e.g. the elastic modulus of a clay layer within the dike) is in a way dependent on the behaviour of a stochastic parameter at another location. This (auto-)correlation can be expressed in the correlation length, which has some

resemblance with the equivalent length L_{eq} from section C.4.3. The correlation length is the distance within a section in which a stochastic variable is coherent [44, App. IV]. Past performance by the historical load often much acts as a proof test with additional randomness. In other words, the historical load variable for the observed situation E^* ³ is assumed to be randomly distributed, so uncertainty in the load magnitude is involved in this [36].

Beside the influence from historical observations of (load) actions, proof loads are used in the assessment of quay walls. Load testing can be evaluated through the application of Bayesian updating. This study has been done by den Adel (TU Delft/IV-Infra) in his Masters thesis [25]. This thesis included fictitious measurements as proof loads in the input for the deterministic and probabilistic calculations. As a result, a general trend is perceived in which the standard deviation of the load variable (uncertainty in the characteristic value) decreases. On the other side, the fictitious measurements support the prior prediction (model without proof loads) since the mean values are almost equal in both cases [25, p. 50].

Reliability indices appear to be of major importance in the assessment of existing structures. Favourably, a situation is aspired in which the actual reliability index of a system appears to be significantly higher. Reliability updating is the concept in which the actual reliability of a system is investigated and actualised, this subject and its implications are elaborately treated in sections C.5.2, C.5.3 and 2.3.

C.5.2. The concept of reliability updating

Basically all studies that were treated in the previous section dealt with Bayesian updating. Thomas Bayes was a British mathematician and Presbyterian clergyman who is known for formulating the Bayes Theorem. The Bayes' Theorem is derived from the law of conditional probability C.41 [21, p. 26] and the law of total probability, given two events A and B. This theorem makes it possible to rewrite equation C.41 to calculate the a-posteriori distribution on the basis of a prior distribution.

$$P(A|B) = \frac{P(A \cap B)}{P(B)} \quad (\text{C.41})$$

And hence, given a series of events B_i with $i = 1, 2, \dots, n$ and the law of total probability (see equation C.42), one is able to formulate the Bayes Theorem. Equation C.43 calculates the conditional probability of an event B_i given an arbitrary event A [21, p. 32].

$$P(A) = \sum_{i=1}^n P(A|B_i)P(B_i) = P(A|B_1)P(B_1) + P(A|B_2)P(B_2) + \dots + P(A|B_n)P(B_n) \quad (\text{C.42})$$

$$P(B_i|A) = \frac{P(A|B_i)P(B_i)}{P(A|B_1)P(B_1) + P(A|B_2)P(B_2) + \dots + P(A|B_n)P(B_n)} \quad (\text{C.43})$$

In practical sense, Bayesian updating uses equation C.43 in reliability updating of a system. Basically, two methods can be distinguished in reliability updating. The *indirect* method as is performed in [25], entails updating probability distributions of the stochastic variables and using the updated distributions in a new reliability analysis.

In the *direct* method however, preceding survived situations are taken into account by defining a new limit state for the cut set (intersection " \cap ") of failure and observations. In the direct method, the failure probability given the survival of historical observations or imposed loads are given by inequality information C.44. Although the direct and indirect method are equivalent, the direct method is easier for application [77].

³The letter E is, as is done in Eurocode NEN-EN 1990, frequently introduced as a symbol for the load effect [42, p. 178]

$$P(F|S) = \frac{P(\{g(X) < 0\} \cap \{h(X) \geq 0\})}{P(h(X) \geq 0)} \quad (\text{C.44})$$

Where "F" describes failure of the whole system and "S" the evidence of observed survivals. The limit state function of a considered failure mechanism $g(X)$ indicates failure when smaller than zero. The observation function can be written as $h(X)$. In equation C.44, an observed function can be greater than ">" or less than "<" zero depending on the random variables of interest.

For example, the observation function can be used to describe the survival of different load situations. In case of survival, R is greater than S. Hence, an observed load situation S_{obs} , which might be greater than the significant load \bar{s} (e.g. design load S_d), is survived by the object of interest. Equation C.45 describes the observation function in which a maximum random load or proof load is survived. The latter can be tested through imposing significant loads. These loads likely have a deterministic character, since the quantity can manually be determined. Swapping the time-variant random variable S_{obs} with a normative load \bar{s} , results in a similar formulation of equation C.45.

$$h(X) = R - S_{obs} \quad (\text{C.45})$$

The observed load quantity (from historical records e.g.) is usually a stochastic parameter. For multiple observations and given the limit state function defined by eq. C.45, the intersection of individual observations is used and this is reformulated from [77]:

$$S = \cap_i \{h_i(x) \geq 0\} \quad (\text{C.46})$$

Reliability updating is becoming more important due to rapid changes in the functional requirements regarding the design of quay walls. Quay walls are often reviewed on their functional use once in every few years. The subsequently increasing demand for renewal or replacement tasks are therefore mainly due to developments in global economy, changes in vessels and cargo handling equipment. Costs savings on safety measures or replacement activities can be obtained through precisely predicting the actual reliability index. If this actual reliability index is sufficiently high, measures are not required. To verify the latter, a target reliability criteria β_t in correspondence with currently used standards is used. Reliability updating is associated with uncertainties that are treated in section C.5.3.

C.5.3. Uncertainties

As for dikes, various types of uncertainties contribute in the total uncertainty within the assessment of the reliability of a quay wall. Thus, the understanding in which uncertainties are involved in the variables within the model is an essential aspect. The uncertainties related to a stochastic variable are quantified with the variance. Hence, each individual variable must be checked on whether it is an aleatory uncertainty or an epistemic uncertainty [44].

- **Epistemic uncertainty** or knowledge uncertainty means that the real value of an existing variable is not precisely known. An example is the mean value for the internal angle of friction ϕ' of a soil layer. Someone can perform many measurements and researches to obtain an exact value for this ϕ' with the knowledge that this variable is time-invariant. The probability distribution that is assigned to this variable has therefore nothing to do with randomness. Epistemic uncertainty has purely to deal with the lack of knowledge and information about the angle of friction through a limited amount of soil investigation. Effective soil variables are often time-independent and mostly describe epistemic uncertainties.
- **Aleatory uncertainty** or intrinsic variability in time is mostly described by load variables. Most load variables such as the basin side water level, ground water level, crane or terrain loads occur

arbitrarily. In other words, a measure of the maximum load within a certain year i tells almost nothing about the maximum load of the next year $i+1$. A large data series however contributes to reducing the uncertainty about the occurrence of a maximum load.

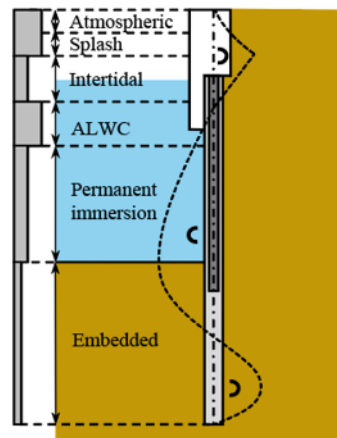


Figure C.30: The maximum water level at a quay wall is a load variable and is oftentimes an aleatory uncertainty [63].

The most important difference between epistemic uncertainty and aleatory uncertainty in this knowledge area is the possibility to reduce epistemic uncertainty. An epistemic uncertainty can be reduced by adding extra information, whereas the aleatory uncertainty can not be reduced. However, the statistical uncertainties of load variables can for a significant part be erased by performing additional measurements. In practical sense, it must be checked whether a variable significantly changes over time or if the probability distribution is purely represented by epistemic uncertainty [44]. The approach of dealing with the uncertainties is explained in the case study analyses. In advance, calculation models for tackling the research problem are treated in the next section.

C.5.4. Calculation models for quay wall design and assessment

In order to perform analyses to answer the main research question, a literature study together with an evaluation of the methodology is conducted. Reliability updating is achieved through the analysis with the in section C.4 discussed reliability methods. Together with these reliability methods, various calculation methods are applied in the design and reassessment of retaining walls. For quay walls, three commonly used methods are applied.

- Blum method
- Subgrade reaction method
- Finite Element Method

Blum Method

The Blum method invented in 1931, uses a strong simplification of the horizontal stress-strain behaviour. The soil pressure depends on the wall displacement and recognises immediate yielding of the soil at the passive or active side of the wall, as is indicated in red by figure C.31. Hence, by assuming plastic deformations the soil pressure is either fully active or fully passive, while in reality the soil pressure transition is rather gradually (see black line in figure C.31) [16]. In this method, the retaining wall

is modelled as a static determinate beam with a fixed earth support. Its fixity depends on the embedded depth of the retaining wall which is the distance between the bed level at the passive side and the below pile end.

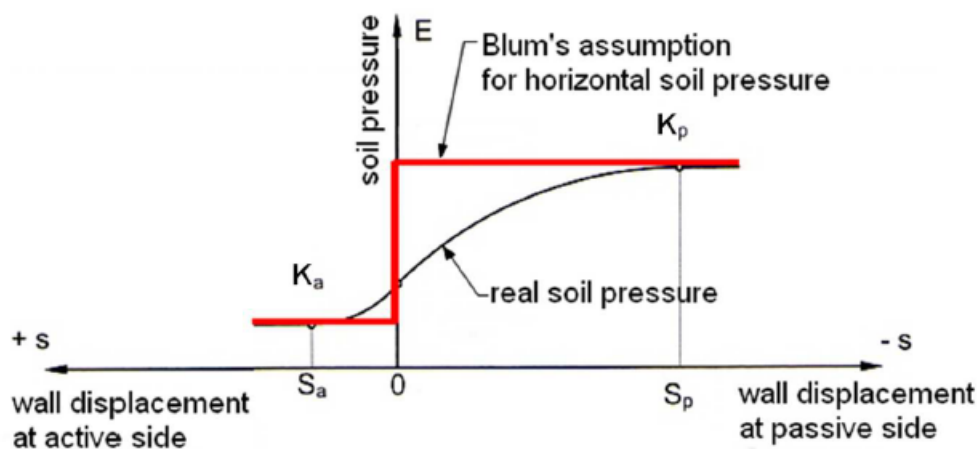


Figure C.31: Blum's assumption regarding horizontal soil pressures [49, p. 321].

The required embedded depth, length and type of sheet pile is determined by the balance of horizontal pressures and moment equilibrium. Hermann Blum's Method is an oversimplification of the deformation behaviour in the soil. In many cases, a hand-calculation with the Blum Method serve as a computation check for other methods. For design purposes, usually a spring- or finite element model is applied.

Subgrade reaction method

The subgrade reaction method models the retaining wall as an elasto-plastic beam which is continuously supported by uncoupled elasto-plastic springs. These elastic- and elasto-plastic springs represent the soil. Soil-structure interaction is only considered for the front wall, since this interaction is difficult to model. Uncoupled means that the springs do not influence each other and so are the different soil layers independent of each other. Arching effects are therefore not included in this calculation method [22] [25]. In this method, horizontal stress depends on the horizontal displacement of the front wall since the soil is connected by uncoupled springs. The struts and anchors are modelled as discrete springs with an elastic normal stiffness and a limited capacity, meaning a buckling force in case of struts and yielding resistance for anchors [17].

A significantly large assumption is the retaining wall to be acting like a Bernoulli beam. Meaning that the cross-sections of the retaining wall remain straight and perpendicular to the beam axis. Advantageously, the use of a spring model results in a simple, fast and user-friendly method. On the other hand, large simplifications in the non-linear stress-strain behaviour of the soil results in rough estimate of the soil deformations. The horizontal stress acts according figure C.32b.

This method was firstly introduced in 1970. By means of a personal computer the equations could be solved numerically [19, p. 131]. D-Sheet Piling is a modelling software package that makes use of this method. In its calculations, the retaining

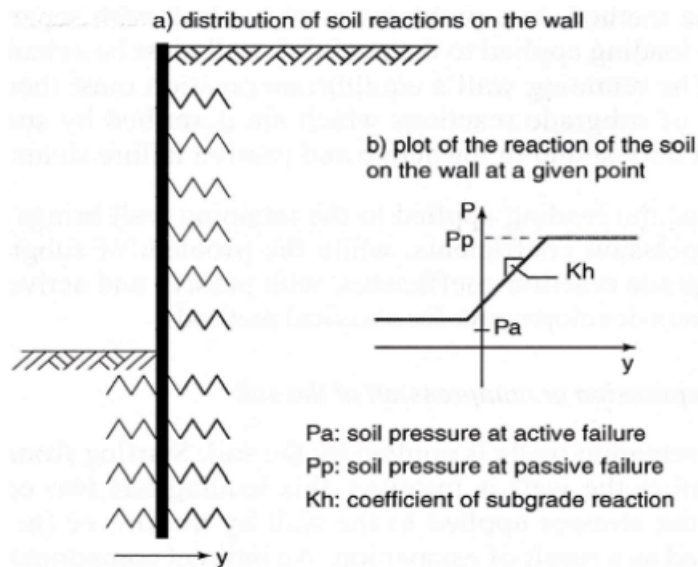


Figure C.32: Left: Subgrade reaction model used for the calculation of retaining walls, right: bi-linear horizontal stress displacement diagram [25].

wall is modelled as an elasto-plastic beam. Inclusion of relieving platforms, inclined walls or complex objects is difficult with this program whereas, the choice between straight or curved slip planes is possible. Another significant disadvantage is that accurate predictions of deformations right behind the quay wall is hardly achievable, because soil behaves as a non-linear elastic material. In Deltares Sheet Piling, a calculation may involve several construction stages: excavation, installation of sheet piling, anchors, struts and change in water table(s). It is strongly recommended to use the subgrade reaction method for simple quay wall structures of draft design(s) of more complex quay walls [17, p. 242].

Finite Element Method

For more accurate computations, finite element models are being used and therefore this method is preferred for most engineering computations. The soil properties are modelled by means of stress-deformation relations. With this method, calculation of sectional forces (including N-, V- and M-diagrams) of the structural elements, deformations and verification of global stability can be performed [17]. The finite element model can be used for two- or three-dimensional problems such as relieving platforms or the distribution of the soil pressures on both primary and secondary elements of the combined wall. The computation model is divided into a large finite number of elements and the model accounts for soil-structure interaction using non-linear stress-strain relations [16]. The displacement field and the strains are determined by interpolation between the nodes and taking the derivative of this interpolation respectively.

A finite element model requires many input parameters and is reasonably time-consuming. A commonly used software package for geotechnical structures is PLAXIS. This calculation toolkit makes use of a triangular or rectangular grid where adjacent elements are connected by common nodes. Within one node, a force equilibrium between the different elements is formulated. A constitutive soil model captures the soil's response to imposed loads and is used in the computation of soil stresses and deformations. The conventional constitutive soil models for quay wall design in FEM are summed up below [17]:

- Mohr-Coulomb (MC): suitable for a first analysis in draft designs
- Hardening Soil Model (HS): Most suitable for retaining structures
- Hardening Soil Small Strain Model (HSS): Used in case of demand for higher accuracy in calculation of deformations
- Soft Soil Creep Model (SSC): Dominant time-dependent behaviour due to the presence of soft soils.

An example of a finite element model in PLAXIS is shown in figure C.33.

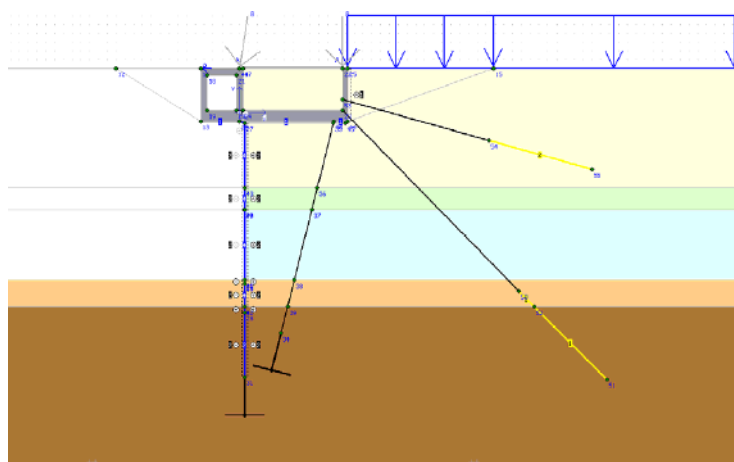
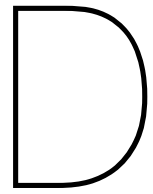


Figure C.33: A schematisation of a quay wall in a finite element model.



Fault tree of a quay wall

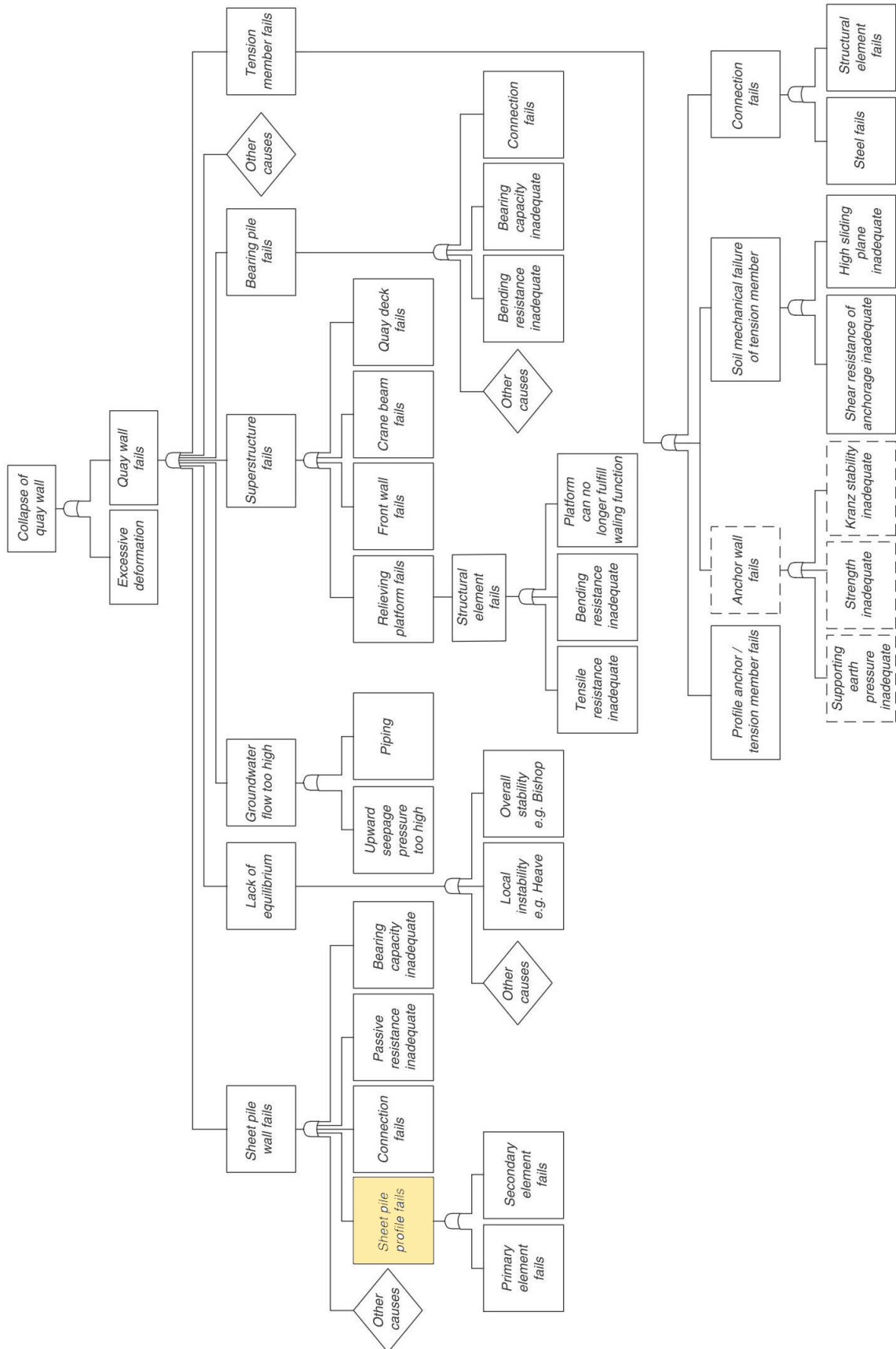
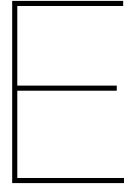


Figure D.1: Fault tree of a quay wall with a relieving platform [17].



Sampling methods

Level III calculations are in many cases computationally intensive. To reduce the required number of calculations, sampling methods are developed. These methods are developed to significantly increase the efficiency of the simulation. In fact, both techniques agree on the fact that taking samples from the original distribution is not efficient for low probabilities of failure. In other words, the chance that a failed number is taken from the sampling distribution is too low [25]. Two frequently used sampling methods are briefly explained in this section.

E.1. Importance sampling

To obtain a higher frequency of realisations in the unsafe domain D_f , more realisations of the random vector \underline{X} can be executed through importance sampling. This technique yields realisations in the domain of importance which is in this case: the unsafe domain D_f where $Z < 0$. An appropriate sampling function $f_s(\underline{x})$ is chosen as such that its maximum is located in the region that contributes the most to the failure probability P_f [42, Ch. 5.4.2]. Thus, the value with the highest value according to probability density function $f_X(\underline{x})$.

$$P_f = \int_{D_{\underline{x}}} I[g(\underline{x}) < 0] \frac{f_X(\underline{x})}{f_s(\underline{x})} f_s(\underline{x}) d\underline{x} \approx \frac{1}{N} \sum_{j=1}^N I[g(\underline{x}) < 0] \frac{f_X(\underline{x})}{f_s(\underline{x})} \quad (\text{E.1})$$

Importance sampling at the design point x^* : The design point is considered as the point on the limit state function ($Z = 0$) with a minimum distance to the origin and the highest failure probability density among all realisations in the failure domain. The sampling function can be approximated by a Gaussian distribution function. This approach may fail when the limit state function is highly nonlinear or gives inaccurate results since it significantly depends on the design point [40, Ch. 2.2.1].

However through **adaptive sampling**, the variable in which the sampling function $f_s(\underline{x})$ is distributed, can be estimated by statistics of the points in the failure domain

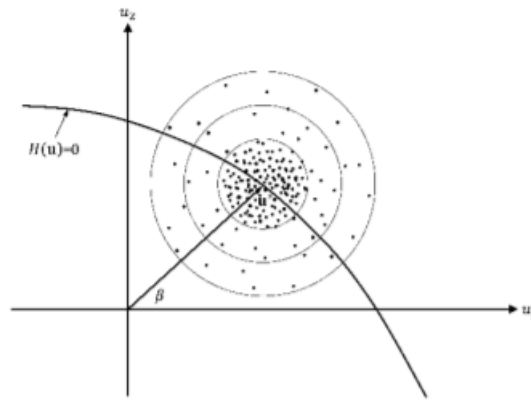


Figure E.1: Importance sampling at the design point [40, Ch. 2.2.1].

obtained by previous simulations. By subsequent sampling the new distribution, as is shown by equation E.2, the design point can be approximated.

$$f_s(\underline{x}) = f_s(s|s \in D_f) \quad (\text{E.2})$$

E.2. Directional simulation

Directional simulation is a sampling method that follows an iterative procedure such as FORM. It is although rather different from FORM, because FORM uses linear approximation. Directional simulation is carried out in the standardised normal space and basically reduces the dimension n of the probability integral by using a set of directions for integration. These directions are randomly determined and the probability is estimated as the weighed average of the direction integrals [40].

A point in the parameter space around $\underline{u} = 0$ is randomly generated and a n -dimensional direction vector $\underline{u} = \|\underline{u}\|\hat{u}$ with $\|\underline{u}\| \geq 0$ and random unit vector \hat{u} is determined. This directional vector intersects with the limit state $g(\underline{u}) = 0$. Assuming a factor $\lambda = \|\underline{u}\|$ (see figure E.2), of which $\sum_{i=1}^N \lambda_i^2$ is χ^2 -distributed. So practically, N random direction vectors are generated and the solutions k_i , given a random unit vector \hat{u}_i , for $g(k\lambda\hat{u}_i) = 0$ are derived. Equation E.3 derives the failure probability in a comparable way as for the Monte Carlo approach by equation C.26.

$$P_f = \frac{1}{N} \sum_{i=1}^N I[g(k\hat{u}_i) \leq 0] \quad (\text{E.3})$$

Basically, a line in each random direction is evaluated and checked whether a sign change occurs. If along the line a sign change occurs, failure occurs and the failure indicator denoted by $I[g(k\hat{u}_i) \leq 0]$ returns 1.

The accuracy of the solution is, as for other sampling methods, based on the number

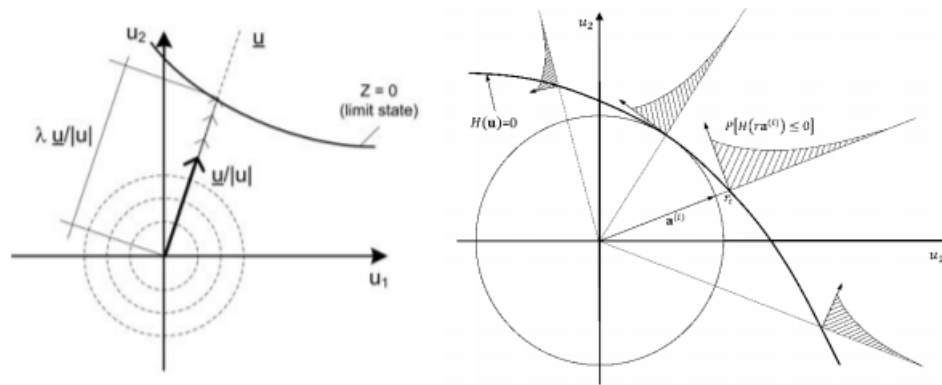


Figure E.2: Principle of directional simulation (l) [25, p. 17] and one-dimensional integration in each direction in the standardised normal space (r) [40, Ch. 2.4]

of directions or calculations [25]. Directional simulation gets rid of the limitations that are caused by non-linearity of the limit state function or the presence of multiple design points [40]. A combination which is called directional importance sampling combines importance and directional sampling, and can be used for reliability analysis as well. This sampling technique is concentrated in the importance region with the highest failure probability density (e.g. in the area around the design point). However, the latter will not be treated in this research.

F

Early analysis with Blum method

ACTIVE SOIL									
Soil layer nr.	Soil type	Depth rel. to ground surface		Layer thickness [m]	σ (total stress) [kN/m ²]	Cumulative stress [kN/m ²]	p (pore pressure) [kN/m ²]	σ' v (effective stress) [kN/m ²]	σ' h (effective stress) [kN/m ²]
		from [m]	to [m]						
1	Clay dry	0.00	-1.00	1.00	18.00	41.28	0.00	41.28	23.86
		-1.00	-1.17	0.17	3.06	44.34	0.00	44.34	25.63
2	Clay sat	-1.17	-1.50	0.33	5.94	50.28	3.30	46.98	27.16
		-1.50	-2.50	1.00	18.00	68.28	13.30	54.98	31.78
		-2.50	-3.50	1.00	18.00	86.28	23.30	62.98	36.40
		-3.50	-4.50	1.00	18.00	104.28	33.30	70.98	41.03
		-4.50	-5.50	1.00	18.00	122.28	43.30	78.98	45.65
		-5.50	-6.50	1.00	18.00	140.28	53.30	86.98	50.28
		-6.50	-7.50	1.00	18.00	158.28	63.30	94.98	54.90
		-7.50	-8.50	1.00	18.00	176.28	73.30	102.98	59.53
		-8.50	-9.50	1.00	18.00	194.28	83.30	110.98	64.15
		-9.50	-10.50	1.00	18.00	212.28	93.30	118.98	68.77
		-10.50	-11.50	1.00	18.00	230.28	103.30	126.98	73.40
-11.50	-12.33	0.83	16.60	246.88	111.60	135.28	78.20		
3	Sand sat	-12.33	-12.33-t	t	20t	246.88+20t	111.60+10t	246.88+20t-(111.6+10t)	0.447982949116254

PASSIVE SOIL									
Soil layer nr.	Soil type	Depth rel. to ground surface		Layer thickness [m]	σ (total stress) [kN/m ²]	Cumulative stress [kN/m ²]	p (pore pressure) [kN/m ²]	σ' v (effective stress) [kN/m ²]	σ' h (effective stress) [kN/m ²]
		from [m]	to [m]						
		-1.83	-2.00	0.17	1.7	1.7	0.00	0.00	0.00
		-2.00	-3.00	1.00	10	11.7	11.70	0.00	0.00
		-3.00	-4.00	1.00	10	21.7	21.70	0.00	0.00
		-4.00	-5.00	1.00	10	31.7	31.70	0.00	0.00
		-5.00	-6.00	1.00	10	41.7	41.70	0.00	0.00
		-6.00	-7.00	1.00	10	51.7	51.70	0.00	0.00
		-7.00	-8.51	1.51	15.1	66.8	66.80	0.00	0.00
2	Clay sat	-8.51	-9.00	0.49	8.82	75.62	71.70	3.92	6.78
		-9.00	-10.00	1.00	18.00	93.62	81.70	11.92	20.62
		-10.00	-11.00	1.00	18.00	111.62	91.70	19.92	34.46
		-11.00	-12.00	1.00	18.00	129.62	101.70	27.92	48.30
		-12.00	-12.33	1.33	23.94	153.56	115.00	38.56	66.71
3	Sand sat	-12.33	-12.33-t	t	20t	153.56+20t	115+10t	153.56+20t-(115+10t)	0.447982949116254

Embedded depth d₀: 7.84 m
Found with Maple

Depth in [m]	Net horizontal stress [kN/m ²]
0.00	0.00
-1.50	27.16
-2.50	31.78
-3.50	36.40
-4.50	41.03
-5.50	45.65
-6.50	50.28
-7.50	54.90
-8.50	59.53
-9.00	55.06
-10.00	45.84
-11.00	36.62
-12.00	27.99
-13.00	#VALUE!
-13.73	#VALUE!

CHARACTERISTICS			
Design values X _d *	Sand	Clay	Unit
Dry volumetric weight	20	18	kN/m ³
Wet volumetric weight	20	18	kN/m ³
Angle of internal friction	22.41	15.51	°
Angle of wall friction	0.53	0.36	
Cohesion	0	1.89	kN/m ²
Unit			
Surcharge	23.28		kN/m ²
Specific weight water	10		kN/m ³
Active earth coefficient	0.447982949	0.578025606	[-]
Passive earth coefficient	2.232227816	1.730027166	[-]
Neutral earth coefficient	0.618768266	0.732593443	[-]
Yield stress (fyd)	235		N/mm ²
Eff. second moment Weff,y		0	mm ³

Calculation sheet Blum

> **Input: design value of the excavation depth**

> $h := 8.51;$

$$h := 8.51$$

(1)

> **Sum of moments around anchor level: Ground Surface Level -1.5 m**

> $SumM := \left(\frac{1}{2}\right) \cdot 25.63 \cdot 1.17 \cdot \left(\left(\frac{1}{3}\right) \cdot 1.17 + 0.33\right) + 25.63 \cdot 0.33^2 \cdot \left(\frac{1}{2}\right) + (27.16 - 25.63)$

$$\begin{aligned} & \cdot \left(\frac{1}{2}\right) \cdot 0.33^2 \cdot \left(\frac{1}{3}\right) - (78.20 - 27.16) \cdot \left(\frac{1}{2}\right) \cdot \left(\frac{2}{3}\right) \cdot (12.33 - 1.5)^2 - 27.16 \cdot \frac{(12.33 - 1.5)^2}{2} \\ & - 78.20 \cdot \left((12.33 - 1.5) + \frac{(d0 - 3.82)}{2}\right) \cdot (d0 - 3.82) - 0.44798 \cdot (20 - 10) \cdot d0 \cdot \left(\frac{1}{2}\right) \\ & \cdot (d0 - 3.82) \cdot \left(\frac{2}{3}(d0 - 3.82) + 12.33 - 1.5\right) - \frac{1}{2} \cdot (73.3 + 10 \cdot d0) \cdot (8.51 - 1.17 + d0) \\ & \cdot \left(\frac{2}{3}\right) \cdot (8.51 - 1.5 + d0) + \left(\frac{1}{2}\right) \cdot 66.71 \cdot 3.82 \cdot \left(8.51 - 1.5 + \frac{2}{3} \cdot 3.82\right) + 66.71 \cdot (d0 \\ & - 3.82) \cdot \left(12.33 - 1.5 + \frac{1}{2} \cdot (d0 - 3.82)\right) + \left(\left(\frac{2}{3}\right) \cdot (d0 - 3.82) + 12.33 - 1.5\right) \cdot 10 \cdot d0 \\ & \cdot 2.23 \cdot \left(\frac{1}{2}\right) \cdot (d0 - 3.82) + \frac{1}{2} \cdot (66.8 + 10 \cdot d0) \cdot (8.51 - 1.83 + d0) \cdot \left(1.83 - 1.5 + \left(\frac{2}{3}\right) \right. \\ & \left. \cdot (8.51 - 1.83 + d0)\right) = 0 \end{aligned}$$

$SumM := -2358.366539 - (697.5440000 + 39.10000000 d0) (d0 - 3.82)$

(2)

$$+ 8.910100000 d0 (d0 - 3.82) \left(\frac{2 d0}{3} + 8.283333333\right)$$

$$- \frac{2 (36.65000000 + 5 d0) (7.34 + d0) (7.01 + d0)}{3} + (66.71 d0$$

$$- 254.8322) \left(8.920000000 + \frac{d0}{2}\right) + (33.40000000 + 5 d0) (6.68 + d0) \left(4.783333333$$

$$+ \frac{2 d0}{3}\right) = 0$$

> *simplify(SumM)*

$5.940066667 (d0 + 10.3778102728740) (d0 + 4.46082213163252) (d0$

(3)

$$- 7.84332253520062) = 0$$

>

> $sol = solve(SumM, d0)$

$$sol = (7.843322535, -4.460822133, -10.37781027)$$

(4)

> **Embedded depth d0**

> $d0 := 7.843322535$

$$d0 := 7.843322535$$

(5)

> $SumH := \left(\frac{1}{2}\right) \cdot 25.63 \cdot 1.17 - F + \frac{1}{2} \cdot (73.3 + 10 \cdot d0) \cdot (8.51 - 1.17 + d0) + 25.63 \cdot (12.33$

$$\begin{aligned}
& -1.17) + (78.20 - 25.63) \cdot \left(\frac{1}{2}\right) \cdot (12.33 - 1.17) + 78.20 \cdot (d0 - 3.82) + \frac{1}{2} \cdot 0.448 \cdot 10 \\
& \cdot d0 \cdot (d0 - 3.82) - \frac{1}{2} \cdot (66.8 + 10 \cdot d0) \cdot (8.51 - 1.83 + d0) - \frac{1}{2} \cdot 66.71 \cdot (12.33 - 8.51) \\
& - 10 \cdot d0 \cdot 2.23 \cdot \left(\frac{1}{2}\right) \cdot (d0 - 3.82) - 66.71 \cdot (d0 - 3.82) = 0
\end{aligned}$$

$$SumH := 329.2837019 - F = 0 \quad (6)$$

> **Sheet piling length L**

> $L := h + d0;$

$$L := 16.35332254 \quad (7)$$

> **Solution horizontal equilibrium: anchor force F**

> $F[A] := solve(SumH, F)$

$$F_A := 329.2837019 \quad (8)$$

ACTIVE SOIL									
Soil layer nr.	Soil type	Depth rel. to ground surface to [m]		Layer thickness [m]	σ (total stress) [kN/m ²]	Cumulative stress [kN/m ²]	p (pore pressure) [kN/m ²]	$\sigma'v$ (effective stress) [kN/m ²]	$\sigma'h$ (effective stress) [kN/m ²]
1	Clay dry	0.00	-1.00	1.00	18.00	41.28	0.00	41.28	23.86
		-1.00	-1.17	0.17	3.06	44.34	0.00	44.34	25.63
2	Clay sat	-1.17	-1.50	0.33	5.94	50.28	3.30	46.98	27.16
		-1.50	-2.50	1.00	18.00	68.28	13.30	54.98	31.78
		-2.50	-3.50	1.00	18.00	86.28	23.30	62.98	36.40
		-3.50	-4.50	1.00	18.00	104.28	33.30	70.98	41.03
		-4.50	-5.50	1.00	18.00	122.28	43.30	78.98	45.65
		-5.50	-6.50	1.00	18.00	140.28	53.30	86.98	50.28
		-6.50	-7.50	1.00	18.00	158.28	63.30	94.98	54.90
		-7.50	-8.50	1.00	18.00	176.28	73.30	102.98	59.53
		-8.50	-9.50	1.00	18.00	194.28	83.30	110.98	64.15
		-9.50	-10.50	1.00	18.00	212.28	93.30	118.98	68.77
		-10.50	-11.50	1.00	18.00	230.28	103.30	126.98	73.40
		-11.50	-12.33	0.83	16.60	246.88	111.60	135.28	78.20
3	Sand sat	-12.33	-13.00	0.67	13.40	260.28	118.30	141.98	83.60
		-13.00	-16.32	3.32	66.40	326.68	151.50	175.18	78.48

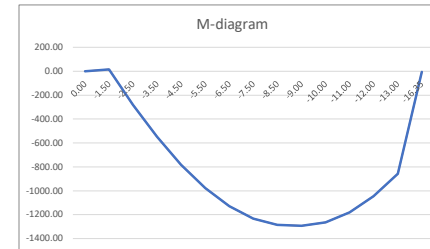
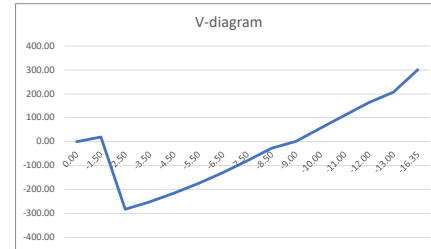
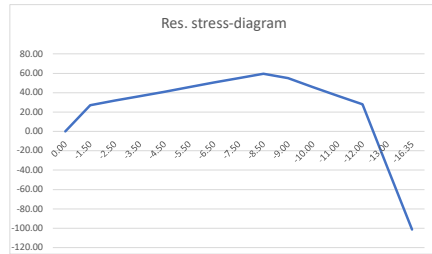
PASSIVE SOIL									
Soil layer nr.	Soil type	Depth rel. to ground surface to [m]		Layer thickness [m]	σ (total stress) [kN/m ²]	Cumulative stress [kN/m ²]	p (pore pressure) [kN/m ²]	$\sigma'v$ (effective stress) [kN/m ²]	$\sigma'h$ (effective stress) [kN/m ²]
1	Clay sat	-1.83	-2.00	0.17	1.7	1.7	1.70	0.00	0.00
		-2.00	-3.00	1.00	11.7	11.7	11.70	0.00	0.00
		-3.00	-4.00	1.00	10	21.7	21.70	0.00	0.00
		-4.00	-5.00	1.00	10	31.7	31.70	0.00	0.00
		-5.00	-6.00	1.00	10	41.7	41.70	0.00	0.00
		-6.00	-7.00	1.00	10	51.7	51.70	0.00	0.00
		-7.00	-8.51	1.51	15.1	66.8	66.80	0.00	0.00
		-8.51	-9.00	0.49	8.82	75.62	75.62	3.92	6.78
		-9.00	-10.00	1.00	18.00	93.62	93.62	11.92	20.62
		-10.00	-11.00	1.00	18.00	111.62	111.62	19.92	34.46
2	Sand sat	-11.00	-12.00	1.00	18.00	129.62	101.70	27.92	48.30
		-12.00	-12.33	0.33	23.94	153.56	115.00	38.56	66.71
		-12.33	-13.00	0.67	13.40	166.96	121.70	45.26	101.03
		-13.00	-16.35	3.35	67.07	234.03	155.23	78.79	175.88

CHARACTERISTICS			
Characteristic values X_k^*	Sand	Clay	Unit
Dry volumetric weight	20	18	kN/m ³
Wet volumetric weight	20	18	kN/m ³
Angle of internal friction	22.41	15.51	°
Angle of wall friction	11.8773	5.5836	°
Cohesion	0	1.89	kN/m ²
Unit			
Surcharge	23.28		kN/m ²
Specific weight water	10		kN/m ³
Anchor force F_a	329.28		
Active earth coefficient	0.447982949	0.578025606	[-]
Passive earth coefficient	2.232227816	1.730027166	[-]
Neutral earth coefficient	0.618768266	0.732593443	[-]

Yield stress (fyd)	235		N/mm ²
Eff. second moment $W_{eff,y}$		5169177.631	mm ³

Depth in [m]	Net horizontal stress [kN/m ²]	Shear force [kN/m]	Bending moment [kNm/m]
0.00	0.00	0.00	0.00
-1.50	27.16	20.36673221	15.27504916
-1.50	27.16	-308.9132678	15.27504916
-2.50	31.78	-279.4455224	-278.9043459
-3.50	36.40	-245.3535722	-541.3038933
-4.50	41.03	-206.6374171	-767.2993879
-5.50	45.65	-163.2970572	-952.2666251
-6.50	50.28	-115.3324925	-1091.5814
-7.50	54.90	-62.74372289	-1180.619508
-8.50	59.53	-5.530748451	-1214.756743
-9.00	55.06	23.11438896	-1210.360833
-10.00	45.84	73.56185552	-1162.022711
-11.00	36.62	114.7933096	-1067.845128
-12.00	27.99	147.097764	-936.8995916
-13.00	-37.43	142.3774886	-792.1619653
-16.35	-101.38	-90.11818155	74.23286877

Vmax: 308.9132678 kN/m
Mmax: 1214.756743 kNm/m





Early analysis with subgrade reaction method

Report for D-Sheet Piling 19.3

Design of Diaphragm and Sheet Pile Walls
Developed by Deltares



Company: ARCADIS
Infrastructure

Date of report: 8/4/2020
Time of report: 3:17:10 PM
Report with version: 19.3.1.27104

Date of calculation: 8/4/2020
Time of calculation: 3:12:52 PM
Calculated with version: 19.3.1.27104

File name: Deterministiccalc

Project identification: Probabilistic analysis

1 Table of Contents

1	Table of Contents	2
2	Summary	3
2.1	Maxima per Stage	3
2.2	Supports	3
3	Input Data for all Stages	4
3.1	General Input Data	4
3.2	Sheet Piling Properties	4
3.2.1	General Properties	4
3.2.2	Stiffness EI (elastic behaviour)	4
3.2.3	Maximum Allowable Moments	4
3.3	Calculation Options	4
4	Construction Stage 1: Final stage	5
4.1	Outline	5
4.2	General Input Data	5
4.2.1	Spring Supports	5
4.3	Input Data Left	5
4.3.1	Calculation Method	5
4.3.2	Water Level	5
4.3.3	Surface	5
4.3.4	Soil Material Properties in Profile: Excavated side	6
4.3.5	Modulus of Subgrade Reaction (Tangent D-Sheet Piling Classic)	6
4.4	Calculated Earth Pressure Coefficients Left	6
4.5	Calculated Force from a Layer - Left Side	7
4.6	Input Data Right	7
4.6.1	Calculation Method	7
4.6.2	Water Level	7
4.6.3	Surface	7
4.6.4	Soil Material Properties in Profile: Active soil structure	7
4.6.5	Modulus of Subgrade Reaction (Tangent D-Sheet Piling Classic)	8
4.6.6	Uniform Loads	8
4.7	Calculated Earth Pressure Coefficients Right	8
4.8	Calculated Force from a Layer - Right Side	10
4.9	Calculation Results	10
4.9.1	Charts of Moments, Forces and Displacements	11
4.9.2	Moments, Forces and Displacements	11
4.9.3	Charts of Stresses	14
4.9.4	Stresses	14
4.9.5	Percentage Mobilized Resistance	16
4.9.6	Rigid and Spring Supports	17

2 Summary

2.1 Maxima per Stage

Stage nr.	Stage name	Displacement [mm]	Moment [kNm]	Shear force [kN]	Mob. perc. moment [%]	Mob. perc. resistance [%]	Vertical balance
1	Final stage	-26.3	-697.79	-236.16	64.9	66.7	---

Max		-26.3	-697.79	-236.16	64.9	66.7	---
-----	--	--------------	----------------	----------------	-------------	-------------	-----

2.2 Supports

Stage name	Support Anker	
	Force [kN]	Moment [kNm]
Final stage	279.34	-

Max	279.34	-
-----	---------------	---

3 Input Data for all Stages

3.1 General Input Data

Model	Sheet piling
Check vertical balance	No
Number of construction stages	1
Unit weight of water	10.00 kN/m ³
Number of curves for spring characteristics	1
Unloading curve on spring characteristic	No
Elastic calculation	Yes

3.2 Sheet Piling Properties

Length	15.10 m
Level top side	0.00 m
Number of sections	1

3.2.1 General Properties

Section name	From [m]	To [m]	Material type	Acting width [m]
Sheet pile	-15.10	0.00	Steel	1.00

3.2.2 Stiffness EI (elastic behaviour)

Section name	Elastic stiffness EI [kNm ² /m']	Red. factor on EI [-]	Corrected elas. stiffness EI [kNm ²]	Note to reduction factor
Sheet pile	5.0000E+05	1.00	5.0000E+05	

3.2.3 Maximum Allowable Moments

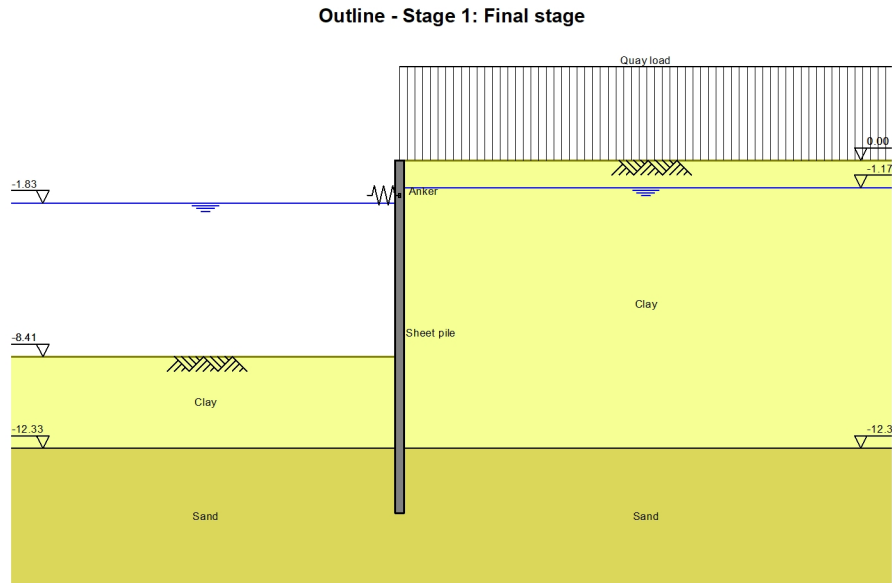
Section name	Mr;char;el [kNm/m']	Modification factor [-]	Material factor [-]	Red. factor allow. moment [-]	Mr;d;el [kNm]
Sheet pile	100000.00	1.00	1.00	1.00	100000.00

3.3 Calculation Options

First stage represents initial situation	No
Calculation refinement	Fine
Lambda recalculation	Automatic
Reduce delta(s) according to CUR	Yes

4 Construction Stage 1: Final stage

4.1 Outline



4.2 General Input Data

Passive side:

Left side

4.2.1 Spring Supports

Name	Level [m]	Rotation [kNm/rad/m']	Translation [kN/m/m']
Anker	-1.50	0.00000E+00	5.00000E+09

4.3 Input Data Left

4.3.1 Calculation Method

Calculation method: C, phi, delta

4.3.2 Water Level

Water level: -1.83 [m]

4.3.3 Surface

X [m]	Y [m]
0.00	-8.41

4.3.4 Soil Material Properties in Profile: Excavated side

Layer name	Level [m]	Unit weight	
		Unsat [kN/m ³]	Sat. [kN/m ³]
Clay	-8.41	18.00	18.00
Sand	-12.33	20.00	20.00

Layer name	Level [m]	Cohesion [kN/m ²]	Friction angle phi [°]	Delta friction angle*	
				Not reduced [°]	Reduced [°]
Clay	-8.41	2.02	18.81	6.77	6.77
Sand	-12.33	0.00	27.17	14.40	14.40

* The 'not reduced' Delta angle is used for the calculation of the active earth pressure coefficient of Culmann whereas the 'reduced' Delta angle is used for the passive earth pressure coefficient.

Layer name	Level [m]	Shell factor [-]	OCR [-]	Grain type
Clay	-8.41	1.00	1.00	Coarse
Sand	-12.33	1.00	1.00	Fine

Layer name	Level [m]	Earth pressure coefficients			Additional pore pressure	
		Active [-]	Neutral [-]	Passive [-]	Top [kN/m ²]	Bottom [kN/m ²]
Clay	-8.41	n.a.	n.a.	n.a.	0.00	0.00
Sand	-12.33	n.a.	n.a.	n.a.	0.00	0.00

4.3.5 Modulus of Subgrade Reaction (Tangent D-Sheet Piling Classic)

Layer name	Level [m]	Branch 1	
		Top [kN/m ³]	Bottom [kN/m ³]
Clay	-8.41	1000.00	1000.00
Sand	-12.33	10000.00	10000.00

4.4 Calculated Earth Pressure Coefficients Left

Segment number	Level [m]	Horizontal pressure		Fictive earth pressure coefficients		
		Active [kN/m ²]	Passive [kN/m ²]	Ka [-]	Ko [-]	Kp [-]
1	-8.54	0.0	9.1	0.00	0.68	8.69
2	-8.67	0.0	11.5	0.00	0.68	5.49
3	-8.80	0.0	13.9	0.00	0.68	4.43
4	-8.93	0.0	16.3	0.00	0.68	3.89
5	-9.06	0.0	18.1	0.00	0.68	3.64
6	-9.06	0.0	19.3	0.00	0.68	3.51
7	-9.19	0.0	21.1	0.00	0.68	3.36
8	-9.32	0.0	23.5	0.00	0.68	3.21
9	-9.46	0.0	25.9	0.00	0.68	3.09
10	-9.59	0.0	28.3	0.00	0.68	3.00
11	-9.72	0.0	30.1	0.00	0.68	2.95
12	-9.72	0.0	31.3	0.00	0.68	2.92
13	-9.85	2.0	33.0	0.17	0.68	2.87
14	-9.98	3.3	35.4	0.26	0.68	2.83
15	-10.11	3.8	37.8	0.28	0.68	2.78
16	-10.24	4.3	40.2	0.29	0.68	2.75
17	-10.37	4.6	42.0	0.30	0.68	2.73
18	-10.37	4.9	43.2	0.31	0.68	2.71
19	-10.50	5.2	45.0	0.31	0.68	2.69
20	-10.63	5.7	47.4	0.32	0.68	2.67
21	-10.76	6.2	49.8	0.33	0.68	2.65
22	-10.89	6.7	52.2	0.34	0.68	2.63
23	-11.02	7.1	54.0	0.34	0.68	2.62
24	-11.02	7.3	55.2	0.35	0.68	2.61
25	-11.15	7.7	57.0	0.35	0.68	2.60

Segment number	Level [m]	Horizontal pressure		Fictive earth pressure coefficients		
		Active [kN/m ²]	Passive [kN/m ²]	Ka [-]	Ko [-]	Kp [-]
26	-11.28	8.2	59.4	0.36	0.68	2.58
27	-11.42	8.7	61.8	0.36	0.68	2.57
28	-11.55	9.2	64.2	0.37	0.68	2.56
29	-11.68	9.6	66.0	0.37	0.68	2.55
30	-11.68	9.8	67.2	0.37	0.68	2.54
31	-11.81	10.2	69.0	0.38	0.68	2.54
32	-11.94	10.7	71.4	0.38	0.68	2.53
33	-12.07	11.2	73.7	0.38	0.68	2.52
34	-12.20	11.7	76.1	0.39	0.68	2.51
35	-12.33	12.1	77.9	0.39	0.68	2.49
36	-12.33	10.3	140.8	0.32	0.68	4.40
37	-12.47	10.6	142.1	0.32	0.54	4.31
38	-12.61	11.1	145.5	0.32	0.54	4.23
39	-12.75	11.5	149.7	0.32	0.54	4.18
40	-12.88	12.0	154.4	0.32	0.54	4.15
41	-13.02	12.3	158.0	0.32	0.54	4.14
42	-13.02	12.6	160.6	0.32	0.54	4.13
43	-13.16	12.9	164.4	0.32	0.54	4.12
44	-13.30	13.3	169.7	0.32	0.54	4.11
45	-13.44	13.8	175.0	0.32	0.54	4.10
46	-13.58	14.2	180.4	0.32	0.54	4.09
47	-13.71	14.6	184.4	0.32	0.54	4.09
48	-13.71	14.8	187.2	0.32	0.54	4.08
49	-13.85	15.2	191.3	0.32	0.54	4.08
50	-13.99	15.6	196.8	0.32	0.54	4.08
51	-14.13	16.1	202.3	0.32	0.54	4.08
52	-14.27	16.5	207.8	0.32	0.54	4.07
53	-14.41	16.8	212.0	0.32	0.54	4.07
54	-14.41	17.1	214.7	0.32	0.54	4.07
55	-14.55	17.4	218.9	0.32	0.54	4.07
56	-14.68	17.9	224.5	0.32	0.54	4.07
57	-14.82	18.3	230.1	0.32	0.54	4.07
58	-14.96	18.8	235.7	0.32	0.54	4.07
59	-15.10	19.1	239.9	0.32	0.54	4.07

4.5 Calculated Force from a Layer - Left Side

Name	Force
Clay	115.60
Sand	338.56

4.6 Input Data Right

4.6.1 Calculation Method

Calculation method: C, phi, delta

4.6.2 Water Level

Water level: -1.17 [m]

4.6.3 Surface

X [m]	Y [m]
0.00	0.00

4.6.4 Soil Material Properties in Profile: Active soil structure

Layer name	Level [m]	Unit weight	
		Unsat [kN/m ³]	Sat. [kN/m ³]
Clay	0.00	18.00	18.00
Sand	-12.33	20.00	20.00

Layer name	Level [m]	Cohesion [kN/m ²]	Friction angle phi [°]	Delta friction angle*	
				Not reduced [°]	Reduced [°]
Clay	0.00	2.02	18.81	6.77	6.77
Sand	-12.33	0.00	27.17	14.40	14.40

* The 'not reduced' Delta angle is used for the calculation of the active earth pressure coefficient of Culmann whereas the 'reduced' Delta angle is used for the passive earth pressure coefficient.

Layer name	Level [m]	Shell factor [-]	OCR [-]	Grain type
Clay	0.00	1.00	1.00	Coarse
Sand	-12.33	1.00	1.00	Fine

Layer name	Level [m]	Earth pressure coefficients			Additional pore pressure	
		Active [-]	Neutral [-]	Passive [-]	Top [kN/m ²]	Bottom [kN/m ²]
Clay	0.00	n.a.	n.a.	n.a.	0.00	0.00
Sand	-12.33	n.a.	n.a.	n.a.	0.00	0.00

4.6.5 Modulus of Subgrade Reaction (Tangent D-Sheet Piling Classic)

Layer name	Level [m]	Branch 1	
		Top [kN/m ³]	Bottom [kN/m ³]
Clay	0.00	1000.00	1000.00
Sand	-12.33	10000.00	10000.00

4.6.6 Uniform Loads

Name	Load [kN/m ²]
Quay load	23.28

4.7 Calculated Earth Pressure Coefficients Right

Segment number	Level [m]	Horizontal pressure		Fictive earth pressure coefficients		
		Active [kN/m ²]	Passive [kN/m ²]	Ka [-]	Ko [-]	Kp [-]
1	-0.12	9.3	64.8	0.37	0.68	2.55
2	-0.23	10.3	69.7	0.38	0.68	2.53
3	-0.35	11.3	74.5	0.38	0.68	2.52
4	-0.47	12.3	79.3	0.39	0.68	2.50
5	-0.58	13.1	82.9	0.39	0.68	2.49
6	-0.58	13.6	85.3	0.40	0.68	2.49
7	-0.70	14.3	89.0	0.40	0.68	2.48
8	-0.82	15.3	93.8	0.40	0.68	2.47
9	-0.94	16.3	98.6	0.41	0.68	2.46
10	-1.05	17.3	103.4	0.41	0.68	2.45
11	-1.17	18.1	107.0	0.41	0.68	2.44
12	-1.17	18.4	108.6	0.41	0.68	2.44
13	-1.24	18.6	109.5	0.41	0.68	2.44
14	-1.30	18.8	110.7	0.41	0.68	2.44
15	-1.37	19.1	111.9	0.42	0.68	2.44
16	-1.43	19.3	113.1	0.42	0.68	2.43
17	-1.50	19.5	114.0	0.42	0.68	2.43
18	-1.50	19.7	114.6	0.42	0.68	2.43
19	-1.57	19.8	115.5	0.42	0.68	2.43
20	-1.63	20.1	116.7	0.42	0.68	2.43
21	-1.70	20.3	117.9	0.42	0.68	2.43
22	-1.76	20.6	119.1	0.42	0.68	2.43
23	-1.83	20.8	120.0	0.42	0.68	2.43
24	-1.83	21.0	121.0	0.42	0.68	2.42
25	-1.98	21.4	123.0	0.42	0.68	2.42
26	-2.12	22.0	125.7	0.42	0.68	2.42
27	-2.27	22.5	128.4	0.42	0.68	2.42

Segment number	Level [m]	Horizontal pressure		Fictive earth pressure coefficients		
		Active [kN/m ²]	Passive [kN/m ²]	Ka [-]	Ko [-]	Kp [-]
28	-2.41	23.1	131.1	0.42	0.68	2.41
29	-2.56	23.5	133.1	0.43	0.68	2.41
30	-2.56	23.8	134.4	0.43	0.68	2.41
31	-2.71	24.2	136.4	0.43	0.68	2.41
32	-2.85	24.7	139.1	0.43	0.68	2.41
33	-3.00	25.3	141.8	0.43	0.68	2.40
34	-3.15	25.8	144.4	0.43	0.68	2.40
35	-3.29	26.2	146.5	0.43	0.68	2.40
36	-3.29	26.5	147.8	0.43	0.68	2.40
37	-3.44	26.9	149.8	0.43	0.68	2.40
38	-3.58	27.5	152.5	0.43	0.68	2.40
39	-3.73	28.1	155.2	0.43	0.68	2.39
40	-3.88	28.6	157.8	0.43	0.68	2.39
41	-4.02	29.0	159.8	0.43	0.68	2.39
42	-4.02	29.3	161.2	0.43	0.68	2.39
43	-4.17	29.7	163.2	0.43	0.68	2.39
44	-4.32	30.3	165.9	0.44	0.68	2.39
45	-4.46	30.8	168.6	0.44	0.68	2.38
46	-4.61	31.4	171.2	0.44	0.68	2.38
47	-4.75	31.8	173.2	0.44	0.68	2.38
48	-4.75	32.1	174.6	0.44	0.68	2.38
49	-4.90	32.5	176.6	0.44	0.68	2.38
50	-5.05	33.0	179.3	0.44	0.68	2.38
51	-5.19	33.6	181.9	0.44	0.68	2.38
52	-5.34	34.2	184.6	0.44	0.68	2.38
53	-5.49	34.6	186.6	0.44	0.68	2.38
54	-5.49	34.8	188.0	0.44	0.68	2.37
55	-5.63	35.3	190.0	0.44	0.68	2.37
56	-5.78	35.8	192.7	0.44	0.68	2.37
57	-5.92	36.4	195.3	0.44	0.68	2.37
58	-6.07	36.9	198.0	0.44	0.68	2.37
59	-6.22	37.3	200.0	0.44	0.68	2.37
60	-6.22	37.6	201.4	0.44	0.68	2.37
61	-6.36	38.0	203.4	0.44	0.68	2.37
62	-6.51	38.6	206.0	0.44	0.68	2.37
63	-6.66	39.1	208.7	0.44	0.68	2.37
64	-6.80	39.7	211.4	0.44	0.68	2.36
65	-6.95	40.1	213.4	0.44	0.68	2.36
66	-6.95	40.4	214.8	0.44	0.68	2.36
67	-7.09	40.8	216.8	0.44	0.68	2.36
68	-7.24	41.4	219.4	0.45	0.68	2.36
69	-7.39	41.9	222.1	0.45	0.68	2.36
70	-7.53	42.5	224.8	0.45	0.68	2.36
71	-7.68	42.9	226.8	0.45	0.68	2.36
72	-7.68	43.2	228.1	0.45	0.68	2.36
73	-7.83	43.6	230.2	0.45	0.68	2.36
74	-7.97	44.1	232.8	0.45	0.68	2.36
75	-8.12	44.7	235.5	0.45	0.68	2.36
76	-8.26	45.3	238.2	0.45	0.68	2.36
77	-8.41	45.7	240.2	0.45	0.68	2.36
78	-8.41	45.9	241.5	0.45	0.68	2.36
79	-8.54	46.3	243.3	0.45	0.68	2.35
80	-8.67	46.8	245.7	0.45	0.68	2.35
81	-8.80	47.3	248.0	0.45	0.68	2.35
82	-8.93	47.8	250.4	0.45	0.68	2.35
83	-9.06	48.2	252.2	0.45	0.68	2.35
84	-9.06	48.4	253.4	0.45	0.68	2.35
85	-9.19	48.8	255.2	0.45	0.68	2.35
86	-9.32	49.3	257.6	0.45	0.68	2.35
87	-9.46	49.8	260.0	0.45	0.68	2.35
88	-9.59	50.3	262.4	0.45	0.68	2.35
89	-9.72	50.6	264.2	0.45	0.68	2.35
90	-9.72	50.9	265.4	0.45	0.68	2.35
91	-9.85	51.3	267.2	0.45	0.68	2.35

Segment number	Level [m]	Horizontal pressure		Fictive earth pressure coefficients		
		Active [kN/m ²]	Passive [kN/m ²]	Ka [-]	Ko [-]	Kp [-]
92	-9.98	51.8	269.6	0.45	0.68	2.35
93	-10.11	52.3	272.0	0.45	0.68	2.35
94	-10.24	52.7	274.4	0.45	0.68	2.35
95	-10.37	53.1	276.2	0.45	0.68	2.35
96	-10.37	53.4	277.4	0.45	0.68	2.35
97	-10.50	53.7	279.2	0.45	0.68	2.35
98	-10.63	54.2	281.6	0.45	0.68	2.35
99	-10.76	54.7	283.9	0.45	0.68	2.35
100	-10.89	55.2	286.3	0.45	0.68	2.34
101	-11.02	55.6	288.1	0.45	0.68	2.34
102	-11.02	55.8	289.3	0.45	0.68	2.34
103	-11.15	56.2	291.1	0.45	0.68	2.34
104	-11.28	56.7	293.5	0.45	0.68	2.34
105	-11.42	57.2	295.9	0.45	0.68	2.34
106	-11.55	57.7	298.3	0.45	0.68	2.34
107	-11.68	58.1	300.1	0.45	0.68	2.34
108	-11.68	58.3	301.3	0.45	0.68	2.34
109	-11.81	58.7	303.1	0.45	0.68	2.34
110	-11.94	59.2	305.5	0.45	0.68	2.34
111	-12.07	59.7	307.9	0.45	0.68	2.34
112	-12.20	60.2	310.3	0.45	0.68	2.34
113	-12.33	60.6	312.1	0.45	0.68	2.34
114	-12.33	43.2	592.6	0.32	0.68	4.41
115	-12.47	43.6	592.1	0.32	0.54	4.38
116	-12.61	44.0	592.7	0.32	0.54	4.34
117	-12.75	44.5	594.3	0.32	0.54	4.31
118	-12.88	45.0	596.6	0.32	0.54	4.28
119	-13.02	45.3	598.7	0.32	0.54	4.26
120	-13.02	45.5	600.2	0.32	0.54	4.25
121	-13.16	45.9	602.8	0.32	0.54	4.24
122	-13.30	46.3	606.4	0.32	0.54	4.22
123	-13.44	46.8	610.3	0.32	0.54	4.21
124	-13.58	47.3	614.4	0.32	0.54	4.20
125	-13.71	47.6	617.6	0.32	0.54	4.19
126	-13.71	47.8	619.7	0.32	0.54	4.19
127	-13.85	48.2	623.1	0.32	0.54	4.18
128	-13.99	48.6	627.6	0.32	0.54	4.17
129	-14.13	49.1	632.3	0.32	0.54	4.16
130	-14.27	49.5	637.1	0.32	0.54	4.16
131	-14.41	49.9	640.7	0.32	0.54	4.15
132	-14.41	50.1	643.2	0.32	0.54	4.15
133	-14.55	50.5	646.8	0.32	0.54	4.15
134	-14.68	50.9	651.8	0.32	0.54	4.14
135	-14.82	51.4	656.9	0.32	0.54	4.14
136	-14.96	51.8	661.9	0.32	0.54	4.13
137	-15.10	52.2	665.8	0.32	0.54	4.13

4.8 Calculated Force from a Layer - Right Side

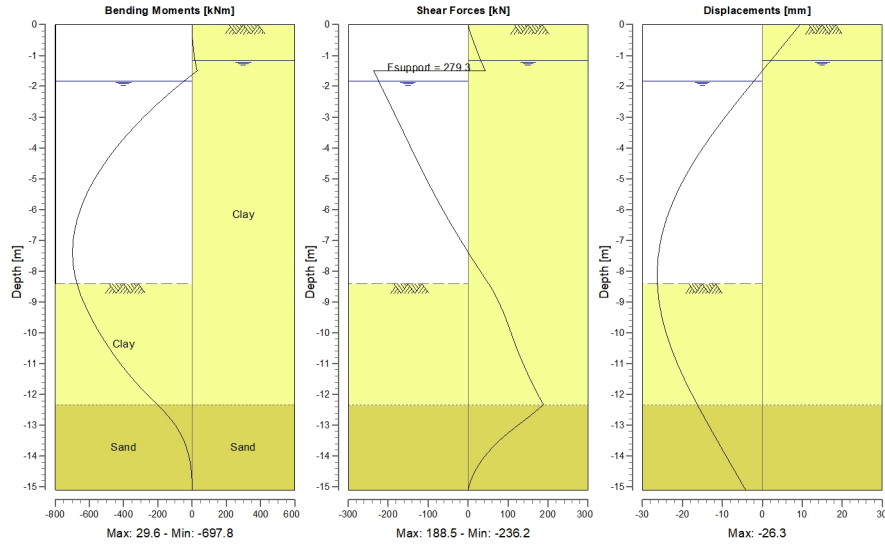
Name	Force
Clay	511.98
Sand	131.92

4.9 Calculation Results

Number of iterations: 4

4.9.1 Charts of Moments, Forces and Displacements

Moments/Forces/Displacements - Stage 1: Final stage



4.9.2 Moments, Forces and Displacements

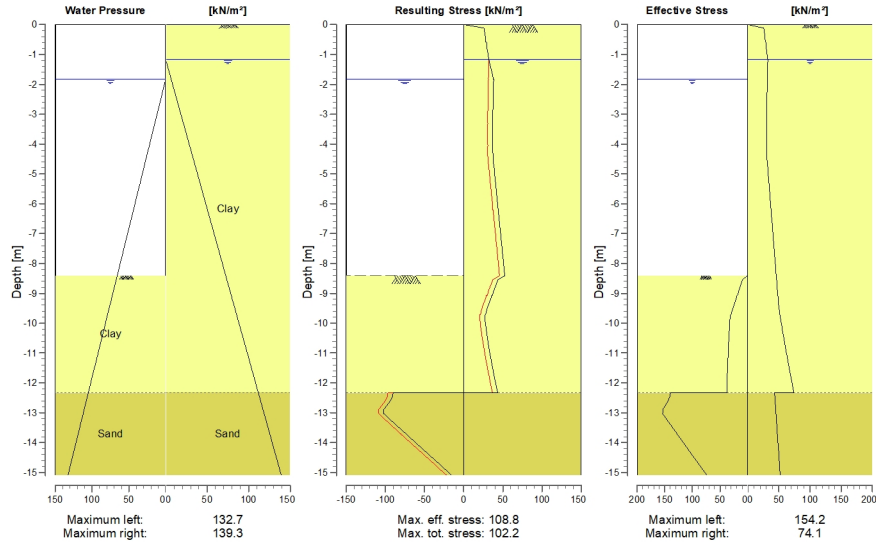
Segment number	Level [m]	Moment [kNm]	Shear force [kN]	Displacement [mm]
1	0.00	0.00	0.01	9.4
	-0.12	0.06	1.54	8.7
	-0.23	0.42	4.62	8.0
	-0.35	1.14	7.77	7.2
	-0.47	2.24	11.00	6.5
2	-0.58	3.72	14.30	5.8
2	-0.58	3.72	14.30	5.8
	-0.70	5.59	17.71	5.0
	-0.82	7.87	21.19	4.3
	-0.94	10.55	24.74	3.6
	-1.05	13.66	28.38	2.8
3	-1.17	17.20	32.08	2.1
3	-1.17	17.20	32.08	2.1
	-1.24	19.39	34.22	1.7
	-1.30	21.72	36.40	1.2
	-1.37	24.19	38.62	0.8
	-1.43	26.82	40.88	0.4
4	-1.50	29.59	43.18	0.0
4	-1.50	29.59	-236.16	0.0
	-1.57	14.08	-233.82	-0.4
	-1.63	-1.27	-231.44	-0.8
	-1.70	-16.47	-229.02	-1.3
	-1.76	-31.50	-226.56	-1.7
5	-1.83	-46.37	-224.07	-2.1
5	-1.83	-46.37	-224.07	-2.1
	-1.98	-78.73	-218.49	-3.0
	-2.12	-110.27	-212.94	-3.9
	-2.27	-141.00	-207.41	-4.8
	-2.41	-170.93	-201.90	-5.7
6	-2.56	-200.05	-196.42	-6.6
6	-2.56	-200.05	-196.42	-6.6

Segment number	Level [m]	Moment [kNm]	Shear force [kN]	Displacement [mm]
	-2.71	-228.37	-190.92	-7.5
	-2.85	-255.89	-185.45	-8.4
	-3.00	-282.60	-180.00	-9.3
	-3.15	-308.52	-174.55	-10.2
7	-3.29	-333.65	-169.13	-11.0
7	-3.29	-333.65	-169.13	-11.0
	-3.44	-357.98	-163.69	-11.8
	-3.58	-381.52	-158.26	-12.6
	-3.73	-404.27	-152.84	-13.4
	-3.88	-426.22	-147.42	-14.2
8	-4.02	-447.38	-142.01	-15.0
8	-4.02	-447.38	-142.02	-15.0
	-4.17	-467.75	-136.57	-15.7
	-4.32	-487.32	-131.13	-16.5
	-4.46	-506.09	-125.67	-17.2
	-4.61	-524.07	-120.16	-17.9
9	-4.75	-541.23	-114.58	-18.5
9	-4.75	-541.23	-114.59	-18.5
	-4.90	-557.57	-108.90	-19.1
	-5.05	-573.08	-103.14	-19.8
	-5.19	-587.73	-97.31	-20.4
	-5.34	-601.53	-91.39	-20.9
10	-5.49	-614.45	-85.40	-21.5
10	-5.49	-614.45	-85.40	-21.5
	-5.63	-626.50	-79.31	-22.0
	-5.78	-637.64	-73.14	-22.4
	-5.92	-647.88	-66.90	-22.9
	-6.07	-657.20	-60.58	-23.3
11	-6.22	-665.59	-54.18	-23.7
11	-6.22	-665.59	-54.18	-23.7
	-6.36	-673.04	-47.68	-24.1
	-6.51	-679.54	-41.12	-24.5
	-6.66	-685.06	-34.47	-24.8
	-6.80	-689.61	-27.74	-25.1
12	-6.95	-693.17	-20.93	-25.3
12	-6.95	-693.17	-20.93	-25.3
	-7.09	-695.73	-14.03	-25.5
	-7.24	-697.27	-7.06	-25.7
	-7.39	-697.79	0.00	-25.9
	-7.53	-697.27	7.13	-26.0
13	-7.68	-695.70	14.34	-26.2
13	-7.68	-695.70	14.34	-26.2
	-7.83	-693.07	21.65	-26.2
	-7.97	-689.36	29.03	-26.3
	-8.12	-684.58	36.49	-26.3
	-8.26	-678.69	44.03	-26.3
14	-8.41	-671.70	51.64	-26.3
14	-8.41	-671.70	51.64	-26.3
	-8.54	-664.53	57.93	-26.2
	-8.67	-656.59	63.54	-26.1
	-8.80	-647.93	68.89	-26.0
	-8.93	-638.60	73.99	-25.9
15	-9.06	-628.61	78.88	-25.7
15	-9.06	-628.61	78.88	-25.7
	-9.19	-618.00	83.45	-25.6
	-9.32	-606.81	87.81	-25.4
	-9.46	-595.06	91.92	-25.2
	-9.59	-582.79	95.82	-24.9
16	-9.72	-570.03	99.55	-24.7
16	-9.72	-570.03	99.54	-24.7
	-9.85	-556.79	103.09	-24.4
	-9.98	-543.08	106.67	-24.1
	-10.11	-528.91	110.32	-23.8
	-10.24	-514.25	114.06	-23.5
17	-10.37	-499.10	117.88	-23.1

Segment number	Level [m]	Moment [kNm]	Shear force [kN]	Displacement [mm]
17	-10.37	-499.10	117.88	-23.1
	-10.50	-483.44	121.80	-22.8
	-10.63	-467.26	125.81	-22.4
	-10.76	-450.56	129.93	-22.0
	-10.89	-433.31	134.15	-21.6
18	-11.02	-415.50	138.47	-21.2
18	-11.02	-415.50	138.47	-21.2
	-11.15	-397.11	142.91	-20.7
	-11.28	-378.14	147.47	-20.3
	-11.42	-358.57	152.15	-19.8
	-11.55	-338.38	156.95	-19.3
19	-11.68	-317.55	161.88	-18.8
19	-11.68	-317.55	161.88	-18.8
	-11.81	-296.07	166.93	-18.3
	-11.94	-273.92	172.12	-17.8
	-12.07	-251.08	177.44	-17.3
	-12.20	-227.54	182.90	-16.8
20	-12.33	-203.28	188.50	-16.3
20	-12.33	-203.28	188.49	-16.3
	-12.47	-178.03	175.97	-15.7
	-12.61	-154.54	163.18	-15.1
	-12.75	-132.85	149.93	-14.5
	-12.88	-113.04	136.12	-13.9
21	-13.02	-95.16	122.00	-13.3
21	-13.02	-95.17	121.87	-13.3
	-13.16	-79.25	108.12	-12.7
	-13.30	-65.19	95.16	-12.1
	-13.44	-52.86	83.01	-11.5
	-13.58	-42.16	71.65	-10.9
22	-13.71	-32.97	61.11	-10.3
22	-13.71	-32.97	61.10	-10.3
	-13.85	-25.19	51.35	-9.7
	-13.99	-18.71	42.41	-9.1
	-14.13	-13.41	34.28	-8.5
	-14.27	-9.18	26.95	-7.8
23	-14.41	-5.91	20.44	-7.2
23	-14.41	-5.91	20.44	-7.2
	-14.55	-3.48	14.73	-6.6
	-14.68	-1.79	9.83	-6.0
	-14.82	-0.72	5.74	-5.4
	-14.96	-0.16	2.46	-4.8
24	-15.10	0.00	0.00	-4.2
Max		-697.79	-236.16	-26.3

4.9.3 Charts of Stresses

Stress States - Stage 1: Final stage



4.9.4 Stresses

Node number	Level [m]	Left				Right			
		Effective Stress [kN/m²]	Water stress [kN/m²]	Stat*	Mob** [%]	Effective Stress [kN/m²]	Water stress [kN/m²]	Stat*	Mob** [%]
1	0.00	0.00	0.00	-	0.24	0.00	P	-	
	-0.12	0.00	0.00	-	25.91	0.00	-	40	
	-0.23	0.00	0.00	-	26.60	0.00	-	38	
	-0.35	0.00	0.00	-	27.29	0.00	-	37	
	-0.47	0.00	0.00	-	27.98	0.00	-	35	
2	-0.58	0.00	0.00	-	28.32	0.00	-	34	
	-0.58	0.00	0.00	-	29.03	0.00	-	34	
	-0.70	0.00	0.00	-	29.36	0.00	-	33	
	-0.82	0.00	0.00	-	30.06	0.00	-	32	
	-0.94	0.00	0.00	-	30.75	0.00	-	31	
3	-1.05	0.00	0.00	-	31.44	0.00	-	30	
	-1.17	0.00	0.00	-	31.77	0.00	-	30	
	-1.17	0.00	0.00	-	32.22	0.00	-	30	
	-1.24	0.00	0.00	-	32.07	0.66	-	29	
	-1.30	0.00	0.00	-	32.01	1.32	-	29	
4	-1.37	0.00	0.00	-	31.95	1.98	-	29	
	-1.43	0.00	0.00	-	31.89	2.64	-	28	
	-1.50	0.00	0.00	-	31.74	3.30	-	-	
	-1.50	0.00	0.00	-	31.92	3.30	-	-	
	-1.57	0.00	0.00	-	31.77	3.96	-	-	
5	-1.63	0.00	0.00	-	31.71	4.62	-	-	
	-1.70	0.00	0.00	-	31.65	5.28	-	-	
	-1.76	0.00	0.00	-	31.59	5.94	-	-	
	-1.83	0.00	0.00	-	31.45	6.60	-	-	
	-1.83	0.00	0.00	-	31.73	6.60	-	-	
6	-1.98	0.00	1.46	-	31.41	8.06	-	-	
	-2.12	0.00	2.92	-	31.28	9.52	-	-	
	-2.27	0.00	4.39	-	31.16	10.99	-	-	
	-2.41	0.00	5.85	-	31.04	12.45	-	-	
6	-2.56	0.00	7.31	-	30.74	13.91	-	-	

Node number	Level [m]	Left				Right			
		Effective Stress [kN/m ²]	Water stress [kN/m ²]	Stat*	Mob** [%]	Effective Stress [kN/m ²]	Water stress [kN/m ²]	Stat*	Mob** [%]
6	-2.56	0.00	7.31	-		31.13	13.91	-	
	-2.71	0.00	8.77	-		30.84	15.37	-	
	-2.85	0.00	10.24	-		30.75	16.84	-	
	-3.00	0.00	11.70	-		30.67	18.30	-	
	-3.15	0.00	13.16	-		30.60	19.76	-	
7	-3.29	0.00	14.62	-		30.35	21.22	-	
7	-3.29	0.00	14.62	-		30.75	21.22	-	
	-3.44	0.00	16.08	-		30.51	22.68	-	
	-3.58	0.00	17.55	-		30.49	24.15	-	
	-3.73	0.00	19.01	-		30.48	25.61	-	
	-3.88	0.00	20.47	-		30.49	27.07	-	
8	-4.02	0.00	21.93	-		30.32	28.53	-	
8	-4.02	0.00	21.93	-		30.72	28.53	-	
	-4.17	0.00	23.40	-		30.57	30.00	-	
	-4.32	0.00	24.86	-		30.63	31.46	-	
	-4.46	0.00	26.32	-		30.83	32.92	A	
	-4.61	0.00	27.78	-		31.38	34.38	A	
9	-4.75	0.00	29.24	-		31.80	35.84	A	
9	-4.75	0.00	29.24	-		32.08	35.84	A	
	-4.90	0.00	30.71	-		32.49	37.31	A	
	-5.05	0.00	32.17	-		33.05	38.77	A	
	-5.19	0.00	33.63	-		33.60	40.23	A	
	-5.34	0.00	35.09	-		34.16	41.69	A	
10	-5.49	0.00	36.56	-		34.57	43.16	A	
10	-5.49	0.00	36.56	-		34.85	43.16	A	
	-5.63	0.00	38.02	-		35.27	44.62	A	
	-5.78	0.00	39.48	-		35.82	46.08	A	
	-5.92	0.00	40.94	-		36.38	47.54	A	
	-6.07	0.00	42.40	-		36.93	49.00	A	
11	-6.22	0.00	43.87	-		37.35	50.47	A	
11	-6.22	0.00	43.87	-		37.62	50.47	A	
	-6.36	0.00	45.33	-		38.04	51.93	A	
	-6.51	0.00	46.79	-		38.59	53.39	A	
	-6.66	0.00	48.25	-		39.15	54.85	A	
	-6.80	0.00	49.72	-		39.70	56.32	A	
12	-6.95	0.00	51.18	-		40.12	57.78	A	
12	-6.95	0.00	51.18	-		40.40	57.78	A	
	-7.09	0.00	52.64	-		40.81	59.24	A	
	-7.24	0.00	54.10	-		41.37	60.70	A	
	-7.39	0.00	55.56	-		41.92	62.16	A	
	-7.53	0.00	57.03	-		42.48	63.63	A	
13	-7.68	0.00	58.49	-		42.89	65.09	A	
13	-7.68	0.00	58.49	-		43.17	65.09	A	
	-7.83	0.00	59.95	-		43.59	66.55	A	
	-7.97	0.00	61.41	-		44.14	68.01	A	
	-8.12	0.00	62.88	-		44.70	69.48	A	
	-8.26	0.00	64.34	-		45.25	70.94	A	
14	-8.41	0.00	65.80	-		45.67	72.40	A	
14	-8.41	0.00	65.80	P		45.93	72.40	A	
	-8.54	9.08	67.11	P		46.30	73.71	A	
	-8.67	11.48	68.41	P		46.80	75.01	A	
	-8.80	13.88	69.72	P		47.29	76.32	A	
	-8.93	16.28	71.03	P		47.79	77.63	A	
15	-9.06	18.08	72.33	P		48.16	78.93	A	
15	-9.06	19.28	72.33	P		48.41	78.93	A	
	-9.19	21.07	73.64	P		48.78	80.24	A	
	-9.32	23.47	74.95	P		49.28	81.55	A	
	-9.46	25.86	76.25	P		49.79	82.85	-	
	-9.59	28.26	77.56	P		50.73	84.16	-	
16	-9.72	30.05	78.87	P		51.52	85.47	-	
16	-9.72	31.25	78.87	P		51.87	85.47	-	
	-9.85	32.20	80.17	-	97	52.67	86.77	-	
	-9.98	32.61	81.48	-	92	53.67	88.08	-	
	-10.11	33.01	82.79	-	87	54.69	89.39	-	

Node number	Level [m]	Left				Right			
		Effective Stress [kN/m ²]	Water stress [kN/m ²]	Stat*	Mob** [%]	Effective Stress [kN/m ²]	Water stress [kN/m ²]	Stat*	Mob** [%]
	-10.24	33.40	84.09	-	83	55.72	90.69	-	
17	-10.37	33.58	85.40	-	80	56.60	92.00	-	
17	-10.37	33.94	85.40	-	79	56.95	92.00	-	
	-10.50	34.11	86.71	-	76	57.85	93.31	-	
	-10.63	34.44	88.01	-	73	58.93	94.61	-	
	-10.76	34.75	89.32	-	70	60.04	95.92	-	
	-10.89	35.05	90.63	-	67	61.15	97.23	-	
18	-11.02	35.16	91.93	-	65	62.11	98.53	-	
18	-11.02	35.51	91.93	-	64	62.46	98.53	-	
	-11.15	35.60	93.24	-	62	63.43	99.84	-	
	-11.28	35.86	94.55	-	60	64.59	101.15	-	
	-11.42	36.10	95.85	-	58	65.77	102.45	-	
	-11.55	36.34	97.16	-	57	66.95	103.76	-	
19	-11.68	36.38	98.47	-	55	67.97	105.07	-	
19	-11.68	36.73	98.47	-	55	68.32	105.07	-	
	-11.81	36.76	99.77	-	53	69.36	106.37	-	
	-11.94	36.96	101.08	-	52	70.57	107.68	-	
	-12.07	37.15	102.39	-	50	71.80	108.99	-	
	-12.20	37.33	103.69	-	49	73.04	110.29	-	
20	-12.33	37.33	105.00	-	48	74.10	111.60	-	
20	-12.33	139.63	105.00	P		43.14	111.60	A	
	-12.47	141.00	106.39	P		43.49	112.98	A	
	-12.61	144.36	107.77	P		43.95	114.37	A	
	-12.75	148.59	109.16	P		44.41	115.75	A	
	-12.88	153.27	110.54	P		44.87	117.14	A	
21	-13.02	153.85	111.92	-	98	45.22	118.53	A	
21	-13.02	154.23	111.92	-	97	45.45	118.53	A	
	-13.16	148.79	113.31	-	91	45.79	119.91	A	
	-13.30	143.51	114.69	-	85	46.25	121.30	A	
	-13.44	138.20	116.08	-	79	46.71	122.68	A	
	-13.58	132.86	117.47	-	74	47.17	124.06	A	
22	-13.71	127.33	118.85	-	69	47.52	125.45	A	
22	-13.71	127.71	118.85	-	69	47.74	125.45	A	
	-13.85	122.16	120.23	-	64	48.09	126.83	A	
	-13.99	116.79	121.62	-	60	48.55	128.22	A	
	-14.13	111.41	123.00	-	55	49.00	129.60	A	
	-14.27	106.03	124.39	-	51	49.46	130.99	A	
23	-14.41	100.46	125.78	-	48	49.81	132.38	A	
23	-14.41	100.84	125.78	-	47	50.03	132.38	A	
	-14.55	95.26	127.16	-	44	50.38	133.76	A	
	-14.68	89.87	128.54	-	40	50.83	135.15	A	
	-14.82	84.48	129.93	-	37	51.29	136.53	A	
	-14.96	79.09	131.31	-	34	51.75	137.91	A	
24	-15.10	73.52	132.70	-	31	52.09	139.30	A	

Stat* Status (A=active, P=passive, Number is branche, 0 is unloading)
 Mob** Percentage passive mobilized

4.9.5 Percentage Mobilized Resistance

Horizontal soil pressure	Left [kN]	Right [kN]
Effective	454.2	643.9
Water	880.5	970.2
Total	1334.6	1614.1

Considered as passive side
 Left side is assigned as passive side by user
 Maximum passive effective resistance 681.17 kN
 Mobilized passive effective resistance 454.16 kN
 Percentage mobilized resistance 66.7 %
 Position single support -1.50 m
 Maximum passive moment 7923.01 kNm
 Mobilized passive moment 5144.67 kNm

Percentage mobilized moment 64.9 %

4.9.6 Rigid and Spring Supports

Node number	Level [m]	Force [kN]	Moment [kNm]
4	-1.50	279.34	0.00

End of Report

Design Sheet Piling Length

D-Sheet Piling version 19.3

Date: 7/20/2020

Time: 1:56:12 PM

Problem identification

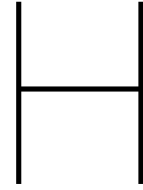
Probabilistic analysis

Stage 1: Final stage

Sheet piling length [m]	Mobilized resistance [%]	Anchor force [kN]	Maximum moment		Maximum displacement [mm]
			Negative [kNm]	Positive [kNm]	
25.00	41.5		-729.7	327.0	-28.8
24.90	41.6		-729.7	327.0	-28.8
24.80	41.8		-729.7	327.0	-28.8
24.70	42.0		-729.7	326.9	-28.8
24.60	42.2		-729.8	326.7	-28.8
24.50	42.4		-729.8	326.6	-28.8
24.40	42.6		-729.8	326.5	-28.8
24.30	42.7		-729.8	326.3	-28.8
24.20	42.9		-729.8	326.1	-28.8
24.10	43.2		-729.8	325.8	-28.8
24.00	43.3		-729.6	325.6	-28.8
23.90	43.6		-729.8	325.3	-28.8
23.80	43.8		-729.8	325.1	-28.8
23.70	44.0		-729.8	324.9	-28.8
23.60	44.2		-729.9	324.5	-28.8
23.50	44.5		-730.2	323.9	-28.8
23.40	44.7		-730.0	323.6	-28.8
23.30	44.9		-729.2	322.6	-28.8
23.20	45.1		-729.2	321.9	-28.8
23.10	45.4		-729.3	321.3	-28.8
23.00	45.6		-729.4	320.7	-28.8
22.90	45.9		-729.5	320.0	-28.9
22.80	46.1		-729.6	319.2	-28.9
22.70	46.4		-729.8	318.3	-28.9
22.60	46.7		-729.9	317.3	-28.9
22.50	46.9		-730.1	316.1	-28.9
22.40	47.2		-730.2	314.9	-29.0
22.30	47.5		-730.5	313.6	-29.0
22.20	47.8		-730.6	312.2	-29.0
22.10	48.1		-730.8	310.7	-29.0
22.00	48.4		-731.1	309.0	-29.1
21.90	48.7		-731.5	307.2	-29.1
21.80	49.0		-731.8	305.2	-29.1
21.70	49.3		-732.2	303.1	-29.2
21.60	49.7		-732.6	301.0	-29.2
21.50	50.0		-733.1	298.8	-29.3
21.40	50.4		-733.6	296.4	-29.3
21.30	50.7		-734.2	293.8	-29.4
21.20	51.1		-734.7	291.0	-29.4
21.10	51.4		-735.4	287.9	-29.5
21.00	51.8		-736.2	284.6	-29.5
20.90	52.1		-736.8	281.5	-29.6
20.80	52.5		-737.8	277.7	-29.7
20.70	52.9		-738.7	274.1	-29.7
20.60	53.3		-739.7	270.2	-29.8
20.50	53.7		-740.7	266.1	-29.9
20.40	54.1		-741.9	261.7	-30.0
20.30	54.6		-743.3	256.9	-30.1
20.20	55.0		-744.6	252.0	-30.2
20.10	55.4		-746.0	246.8	-30.3
20.00	55.9		-748.1	241.0	-30.4
19.90	56.3		-749.1	236.4	-30.5

19.80	56.8	-750.9	230.6	-30.6
19.70	57.2	-752.8	224.6	-30.7
19.60	57.7	-754.7	218.4	-30.9
19.50	58.2	-756.7	212.0	-31.0
19.40	58.6	-758.8	205.3	-31.1
19.30	59.1	-761.1	198.5	-31.2
19.20	59.6	-763.4	191.6	-31.4
19.10	60.1	-765.3	184.5	-31.5
19.00	60.6	-767.6	177.4	-31.6
18.90	61.1	-770.5	169.5	-31.8
18.80	61.6	-773.1	161.7	-31.9
18.70	62.1	-775.8	153.9	-32.1
18.60	62.7	-778.6	146.1	-32.2
18.50	63.2	-781.5	138.1	-32.3
18.40	63.8	-784.5	129.9	-32.5
18.30	64.3	-787.5	121.7	-32.6
18.20	65.0	-791.1	113.0	-32.8
18.10	65.5	-793.7	105.7	-32.9
18.00	66.1	-796.9	97.5	-33.0
17.90	66.7	-800.1	89.5	-33.1
17.80	67.3	-803.2	81.8	-33.3
17.70	68.0	-807.0	73.3	-33.4
17.60	68.6	-809.5	66.7	-33.5
17.50	69.2	-812.6	59.3	-33.6
17.40	69.9	-815.7	52.1	-33.7
17.30	70.6	-818.6	45.5	-33.7
17.20	71.3	-821.5	39.1	-33.8
17.10	72.0	-824.2	33.2	-33.9
17.00	72.8	-826.8	33.0	-33.9
16.90	73.5	-829.0	33.0	-34.0
16.80	74.3	-831.7	33.0	-34.0
16.70	75.2	-834.0	33.0	-34.0
16.60	76.0	-836.0	33.0	-34.1
16.50	76.9	-837.9	33.0	-34.1
16.40	77.9	-839.5	33.0	-34.1
16.30	78.9	-840.9	33.0	-34.1
16.20	79.9	-842.1	33.0	-34.1
16.10	81.1	-842.9	33.0	-34.1
16.00	82.3	-843.4	33.0	-34.0
15.90	83.6	-843.5	33.0	-34.0
15.80	85.1	-843.2	33.0	-34.1
15.70	86.6	-842.6	33.0	-34.1
15.60	88.2	-841.8	33.0	-34.1
15.50	89.8	-840.7	33.1	-34.2
15.40	91.7	-839.4	33.1	-34.3
15.30	93.3	-837.4	33.1	-34.4
15.20	95.1	-834.8	33.1	-34.7
15.10	97.0	-831.5	33.2	-35.2
15.00	99.3	-818.2	33.8	-40.4
14.90	Sheet piling unstable ...			

End of Design Calculation



Prior analyses

Initially, three failure mechanisms are considered. The calculated reliability is verified according to the results by GeoDelft [71] [72]. These failure mechanisms are used in the derivation of the prior assumptions among which:

- Geometrical properties: e.g. sheet piling length.
- Overall safety factor: bending moment capacity.

Hence, the following failure mechanisms are subsequently treated. The outcome of one failure mechanism should be contributory to the study of the subsequent limit state.

1. Excessive deformation(s) of the front wall
2. Exceedance of the passive soil resistance (mobilised moment resistance)
3. Yielding of the front sheet pile wall

H.1. Deformations and passive soil resistance

In this section, two different failure mechanisms are considered: soil yielding and excessive deformations. Both issues were mentioned in the report by CUR Commission in 1993 [71]. Whereas the latter depends on for instance the ship dimensions or clients' demands in the serviceability limit state, is the first mechanism confronted with the ultimate limit state. An oftentimes selected rule of thumb is presented by equation H.1 and is depicted for failure mechanism: excessive deformations. The maximum allowable displacement is described in terms of retaining height h .

$$u_{max} = \frac{h}{100} \quad (\text{H.1})$$

With h being normally distributed $h \sim N(-8, 0.25)$. Equation H.1 asserts a displacement up to 1% of h is acceptable. Accordingly, a limit state function can be formulated:

$$Z = u_{max} - |u| \quad (\text{H.2})$$

First Order Reliability Methods are used for the computation of the prior 50 year reliability index β_{50} . These computations are performed with the Deltares Probabilistic Toolkit. Since there is no necessity for a detailed output level III methods such as: numerical integration, crude Monte Carlo simulations, directional sampling, importance sampling are computationally intensive methods and not specifically needed. FORM is very efficient and suffices for achieving the required information. A level III method may be used to validate the results. Table H.1 presents information about the convergence criterion and the realisation loops. These input values are default settings for FORM in the Probabilistic Toolkit and are maintained for the first calculations. If the calculations become unstable, modification of these values can be considered.

Method	FORM
Relaxation factor	0.75
Relaxation loops	1
Maximum number of iterations	50
Gradient step size	0.3
Precision reliability criterion	0.01

Table H.1: Definition of the criteria regarding the method, realisations and convergence.

The FORM-analyses use the failure definition "Z" to define the boundary between failure and non-failure. The computations start at a predefined starting point in the standardised normal space. In this case, the mean values of all parameters are used as start values. FORM uses an iterative calculation procedure where in each step the current point is moved closer to the design point. In view of the latter, a "predicted" next point u_{pred} is determined. At the start of this case study a gradient step size of 0.3 is used. Furthermore, a relaxation factor is determined to indicate which percentage of the gradient step size is used between the subsequent iterations. This latter is to overcome instabilities in the numerical procedure. A relaxation factor f_{relax} equal to 1 means that the full gradient step size is used. Hence, a relaxation factor larger than 1 reduces the computation time whereas a higher accuracy is obtained with a relaxation factor smaller than 1. Initially, a relaxation factor of 0.75 is used in this computation.

The number of relaxation loops prevents the simulation from undergoing a large number of auxiliary iterations. The convergence criterion as given by the last row of table H.1 provides a band width within which the required accuracy is achieved. Both the relaxation factor and gradient step size can be modified to endure numerical difficulties which are detected in the convergence chart [24].

For the limit state regarding excessive deformations, the effect of each normally distributed parameter is studied. The effects are studied through changing the coefficient of variation CoV for each individual variable. Other input parameters are kept on their initial values and the effect on the cross-sectional reliability is investigated for various mean values. The stochastic parameters $x = \{\delta, \phi, q, c, w_a, w_p\}$ are selected

for this approach. Deterministic parameters such as $\gamma_i, K0_i$ for $i = 1, 2$ and EI are ignored in this approach. In addition, the calculations are realised for one limit value u_{max} . The limit value for the displacement u is determined by means of a rule of thumb considering excavation depth. The limiting value u_{max} is chosen as 0.5% of the retaining height h . This value is selected to avoid convergence problems. Here the design value $h_d = 8.51$ m is used, Figure H.1 presents the diagrams illustrating the reliability index as a function of CoV for the considered input variable. Each diagram shows 4 graphs, each illustrating the case with a different mean value μ_x of the considered parameter. Notice that a fixed value for u_{max} is used. In figure H.1, $\beta_{50} = 0$ indicates that no reliability value is found for the combination μ and σ . For other values of μ and σ , it appears that several reliability indices are found

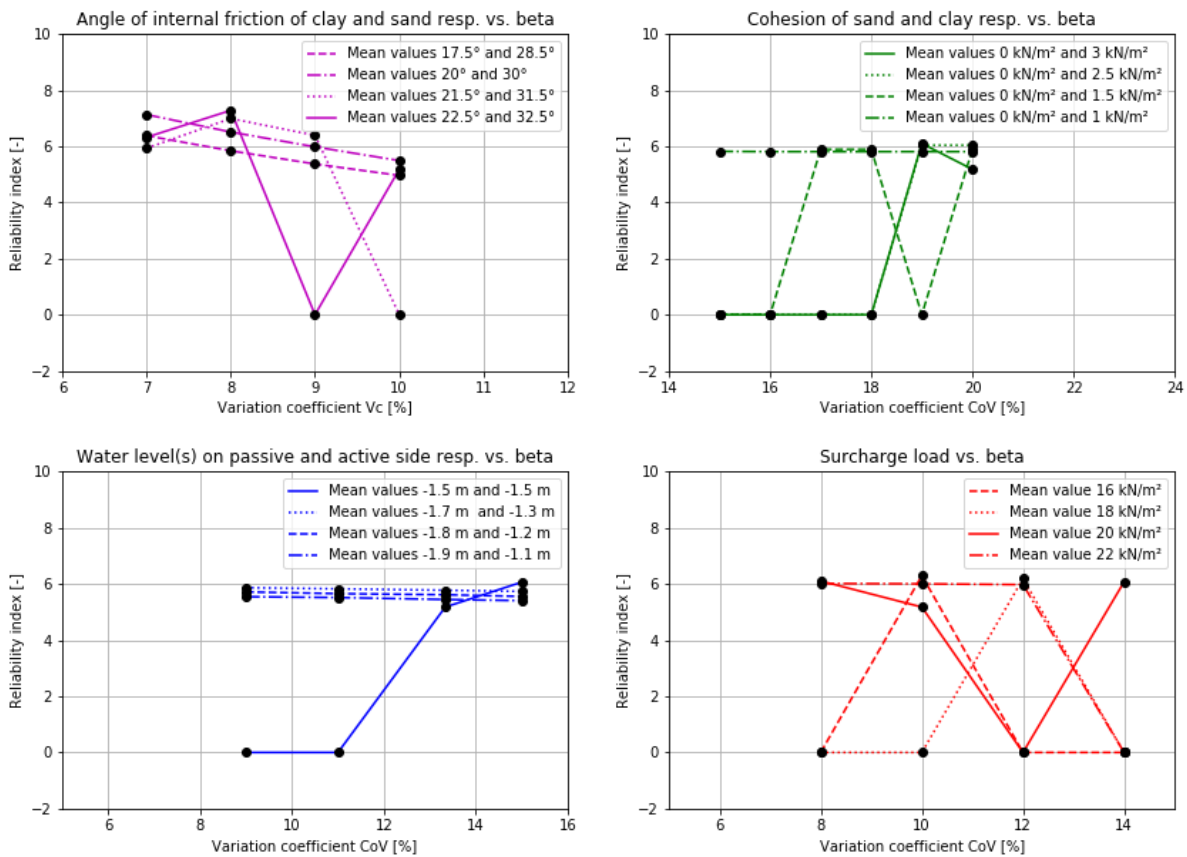


Figure H.1: Reliability index as a function of the coefficient of variation CoV, regarding the limit state regarding excessive deformations. The chosen limit value is 0.5% of $h_d = 8.51$ m ($u_{max} = 0.04255$).

Some combinations result in numerical difficulties and no output for the 50 year reliability index β_{50} . Parameters such as the retaining height $h \sim N(-8, 0.25)$ (relative to the ground surface level), layer separation level $s \sim N(-12, 0.20)$ are not treated. These parameters cause instabilities within the FORM-iterations. As a result, unrealistically extreme values are computed for the reliability indices. Thus, s and h are ignored in the analyses. Hence variables exist where unrealistic reliability indices are yielded for different mean values and given the varying coefficients of variation. These variables are therefore partly excluded from the a-priori reliability computations. The deterministic variables γ , EI and K_0 proved to work effectively in these computations

since realistic output is generated. Reliability indices equal to 0 indicate that no reliability is calculated with the selected mean value and coefficient of variation.

It is found that for several parameters among which the internal friction angle: ϕ_1 and ϕ_2 , significant effects are observed on the reliability. For other parameters, among which the cohesion of clay c_1 and water levels w_a and w_p , unrealistically extreme values are yielded. Hence, the FORM iterations for this case study appears to be vulnerable for numerical instabilities due to involvement of certain input parameters.

Afterwards, the input parameters that are studied with equation H.2, are included in the a-priori reliability calculations. Prior to the realisation of the analyses, the distribution characteristics of the input parameters EI , q , K_{oi} (with $i = 1, 2$) and ϕ are set according to table 1.3 and assumed to be uncorrelated. Initially, the model is run for two limit states:

- Passive resistance: $Z = F_{p,max} - F_{p,mob}$
 - Where $F_{p,max}$ is the limit value for mobilised resistance and $F_{p,mob}$ the mobilised resistance.
- Excessive deformation: $Z = u_{max} - |u|$ (see eq. H.2)

The limit value for passive resistance is for the first limit state at 90% of the maximum passive resistance. Normally, up to 100% is accepted [22, p. 432] for the degree of mobilisation (yielding of the soil). Since this will lead to significantly larger deformations and numerical problems, a lower upper value (e.g. 90%) is used. Hence, $F_{p,max} = 90\%$. Leaving aside the geometrical properties (h , s) all input variables mentioned in table 1.3 are used in the computations. Table H.1 presents the initially used default input for the FORM method in view of the realisations and convergence. Numerical and convergence problems are treated through reduction of the relaxation factor f_{rel} or by modification of the gradient step size. A convergence limit of $\epsilon \leq 0.01$, f_{rel} of 0.3 and a gradient step size of 0.3 are used in combination with 50 iterations. The a-priori results among which sensitivity coefficients and design points are provided in table H.2. Figure H.2 presents the circle histogram of the influence distribution ("α-values").

Considering passive resistance, an a-priori 50 year reliability index of $\beta_{50} = 5.25$ is for obtained $t_{ref} = 50$ years. This is significantly larger than the prescribed target reliability $\beta_t = 4.5$ in the CUR [72]. This is largely due to the modelling disproportions between the model used by CUR C69 in [71] and the model used in this research. Different geometrical and strength properties are used for the sheet piling element and horizontal anchor. These differences are reducible as will appear in chapter H.2.

Variable	α -value [-]	Design point [X]	Unit
Clay cohesion	0.150	2.5266	kN/m ²
Clay ϕ	0.727	20.092	°
Sand ϕ	0.606	15.332	°
Clay δ	0.088	10.732	°
Sand δ	0.252	18.794	°
Uniform load q	-0.100	21.047	kN/m ²

Table H.2: Prior FORM output for passive resistance

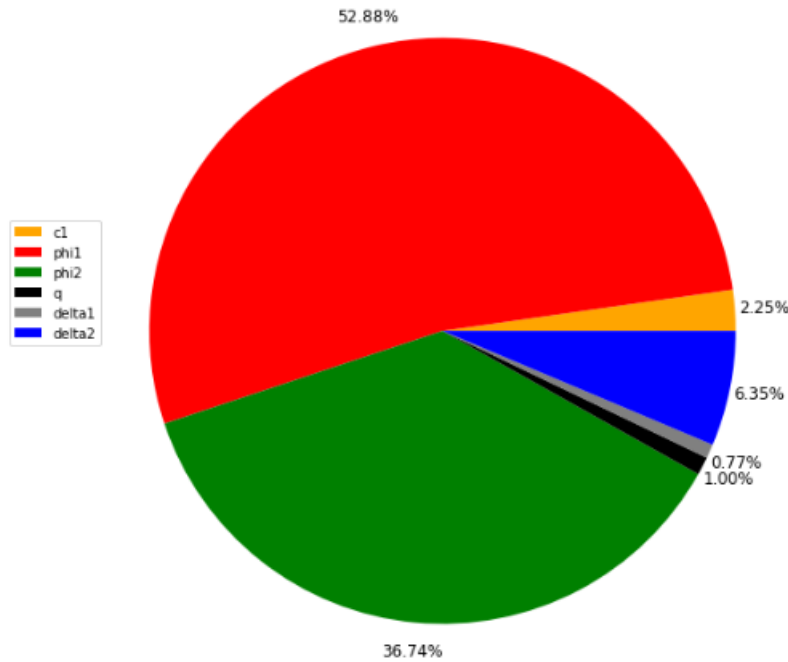


Figure H.2: Circle histogram of the relative influence considering passive resistance.

The second limit state is considered for a maximum value $u_{max} = 0.01|h_d|$ with $|h_d| = 8.51$ m. FORM-computations resulted a large reliability index: $\beta_{50} = 42.4$. Hence, the probability of the stochastic load value $|u|$ exceeding the deterministic resistance value u_{max} is negligibly small based on these level II analysis. This result is not realistic when regarding the prescribed target values. Using a reliability level III method predominantly yields limit state values unequal to zero. The approach with the second limit state (excessive deformations) does not result in suitable starting points.

H.2. Yielding of the front wall

Differences between the prior β_{50} and the target value β_t appeared to be significantly large considering the first two limit states. The third limit state is concerned with the yielding capacity of the front wall. In this approach, all variables from table 4.1 except the layer separation level s and surface height h are taken into account. The latter two parameters cause convergence problems as became clear in the earlier calculations with the previous limit states. In this limit state, the front wall yields if equation H.3 is smaller than zero.

$$Z = fy - \left(\frac{M_{max}}{W_{el,y}} + \frac{N}{A} \right) \quad (\text{H.3})$$

Minor elongations or shortenings of the horizontal anchor are expected since the axial stiffness KA approaches major values. Therefore, the anchor predominantly deforms in vertical directions as the rotational stiffness KR is minimal. As a consequence, mainly vertical sheet pile displacements are expected. For this reason, the normal force in the front wall is neglected ($N \rightarrow 0$), so the steel stress is mainly depending on the bending moment. Appendix H.2.1 determines the elastic section modulus $W_{el,y}$ is determined following the characteristics of the equivalent combined sheet pile profile. No variance is included. The uncertainty regarding the yield stress fy is characterised by a normal distribution with a mean:

$$\mu_{fy} = fy_{nom} \cdot e^{1.64V_{fy}} - 20 \quad (\text{H.4})$$

where:

- fy_{nom} is the value based on the steel quality [N/mm²]
- V_{fy} is the coefficient of variation [-]

A coefficient of variation V_{fy} of 7% is applied on the yield stress of steel [56]. The steel stress S235 is commonly applied in fabricated steel for quay walls and is less vulnerable to pitting corrosion. Given the default method parameters from table H.1 one obtains results from FORM computations. Given the determined section modulus $W_{el,y} = 4696 \cdot 10^3 \text{ mm}^3$ from appendix H.2.1 and without a model uncertainty factor ξ , a reliability value of $\beta_{50} = 6.46$ is computed. Again a large difference with the target value $\beta_t = 4.5$ is observed. Hence, the resistance parameters should be adjusted. The latter is in order to obtain analogous starting points for the reliability computations.

H.2.1. Determination of sheet pile profile

No specific sheet pile profile is defined in the description of example 3 in [72, p.58]. However, a bending stiffness EI is provided and an embedded depth D is determined with the initial ratio of passive resistances $F_{p,max}$ and $F_{p,mob}$. After calculation with the elastic spring model, a penetration level of -15.1 m is found. Hence a comparable profile is sought at common manufacturers.

The manual and calculation web tool of [9] is used. An important aspect is the flexural rigidity. It appears after trial and error that only combined profile reach this flexural rigidity. A combined profile which consists of a tubular pile $\varnothing 1016 - 14$ and a double AU18-profile has a bending stiffness EI of approximately $5 \cdot 10^5 \text{ kNm}^2$.

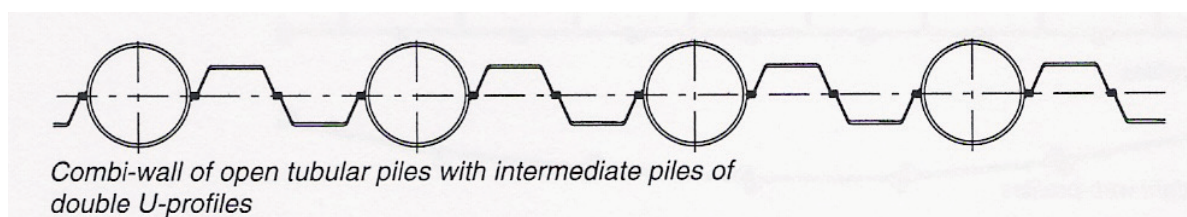


Figure H.3: General cross-section of a combined profile with tubular sections and double U-sections [19].

In addition, characteristics of the selected combined wall are given in table H.3.

Parameter	Value	Unit
Tubular pile wall thickness	14	mm
System width	2,566	mm
Moment of inertia	238,559	mm ⁴
Section modulus	4,696·mm ³	mm ³
System weight	204	kg/m ²
Bending stiffness	500,974	kNm ² /m
Bending moment capacity	1,104	kNm/m

Table H.3: Combined wall consisting of tubular pile and 2x AU18.

Reliability index and sensitivity values found with a normally distributed yield stress f_y

The sheet pile characteristics $W_{el,y}$ and L are found in chapter 4.1.1. The sheet pile characteristics are used in combination with a normally distributed yield stress f_y . The mean value μ_{f_y} and coefficient of variation CoV are determined in accordance with section H.2: $f_y \sim N(243.59, 17.05)$. All other input variables, except for s and h are involved with the same values. After substitution of the resistance parameters $W_{el,y} = 3266 \cdot 10^3 \text{ mm}^3$ and f_y , a prior reliability index $\beta_{50} = 3.52$ for $t_{ref} = 50$ years is obtained. The applied section modulus $W_{el,y}$ is almost similar to that of an AZ32-750-section [8]. Including an uncertainty in the yield stress f_y results in a prior reliability index with a significant difference relative to the target value $\beta_t = 4.3$ conform CUR safety class III [17] or $\beta_t = 4.5$ according to [71]. Moreover, the yield stress f_y appears to have a large influence, especially at the expense of the cohesion c_1 and the wall friction angle of clay δ_1 (see table I.1).

According to:	β_{50} [-]	
GeoDelft report	4.5	
CUR class III	4.3	
FORM given $\gamma_m = 1.1$	3.52	
	Calculated	Geodelft
Variable	α [-]	α [-]
Cohesion of clay: c_1	0.0333	0.41
Internal friction angle: ϕ_1	0.518	0.69
Wall friction angle: δ_1	0.0124	0.17
Uniform load: q	-0.193	-0.24
Yield stress: f_y	0.779	0

Table I.1: Comparison between the β - and α -values calculated with FORM, and the values found in the research report "Veiligheid van damwandconstructies" [71]. This calculation includes parameter uncertainty of the yield stress f_y .

The case which results in values from table 4.2 (including $\beta_{50} = 4.53$) in chapter 4.1.1 has proven to be an acceptable starting point for the research on the effects of past performance. These values are calculated by assuming $f_y \sim D(235)$. For comparative reasons, results including the effect of $f_y \sim N(243.59, 17.05)$ are added in table I.2. The distribution and the convergence of this analysis are shown in figures I.1 - I.2.

Reliability index [-]	Probability of failure [%]	Probability of non failure [%]	Return period [years]
3.52	0.0217	100	$4.6 \cdot 10^3$
Variable	Alpha [-]	Influence factor [%]	Physical value [X]
c_{clay}	0.0333	0.111	2.9297
ϕ_{clay}	0.518	26.790	18.403
ϕ_{sand}	-0.0236	0.0556	32.77
w_a	-0.0822	0.675	-1.4422
w_a	0.282	7.967	-1.6986
q	-0.193	3.715	21.356
δ_{clay}	0.0124	0.0154	11.171
δ_{sand}	$-3.77 \cdot 10^{-3}$	$1.42 \cdot 10^{-3}$	21.703
f_y	0.779	60.669	196.87

Table I.2: Stochastic output for $t_{ref} = 50$ year including a normally distributed yield stress f_y .

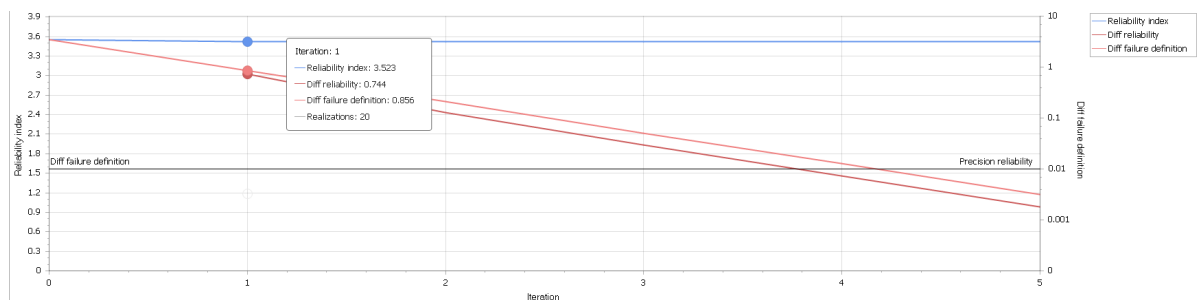


Figure I.1: Convergence diagram of the FORM-analysis considering example 3 from [71] and including a normally distributed yield stress f_y .

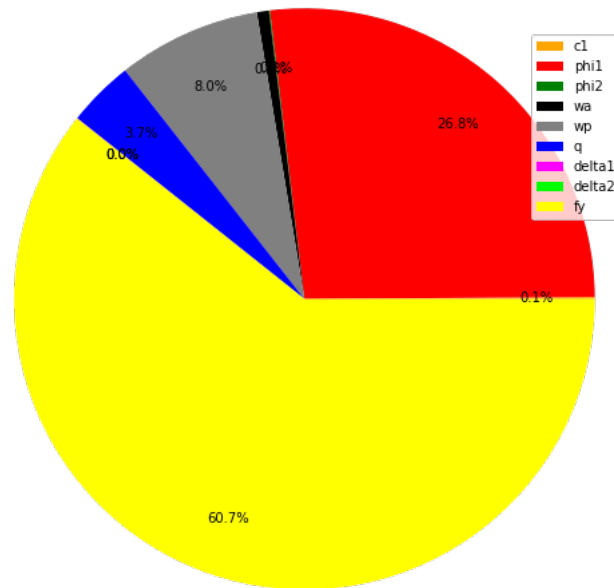


Figure I.2: Relative influence of stochastic parameters for the case with a normally distributed yield stress f_y .

I.1. Approach CUR 166 by GeoDelft and C69

The same methodology can be applied on a different example: example 2 from the GeoDelft research report [72, p. 57]. This example describes a building pit that mainly consists of firm sand layers (might be representative for a Maasvlakte I cross-section). A water sealing layer is present at 8 m below ground surface level. The cross-section is shown on figure I.3, other used input variables beside f_y are presented in table I.3. The horizontal anchor is as in the previous case assumed to have an infinitely large translation stiffness $K_A = 5 \cdot 10^9$ kN/m/m. Limit state H.3 is examined and the case is initially investigated without cross-correlations and model uncertainty.

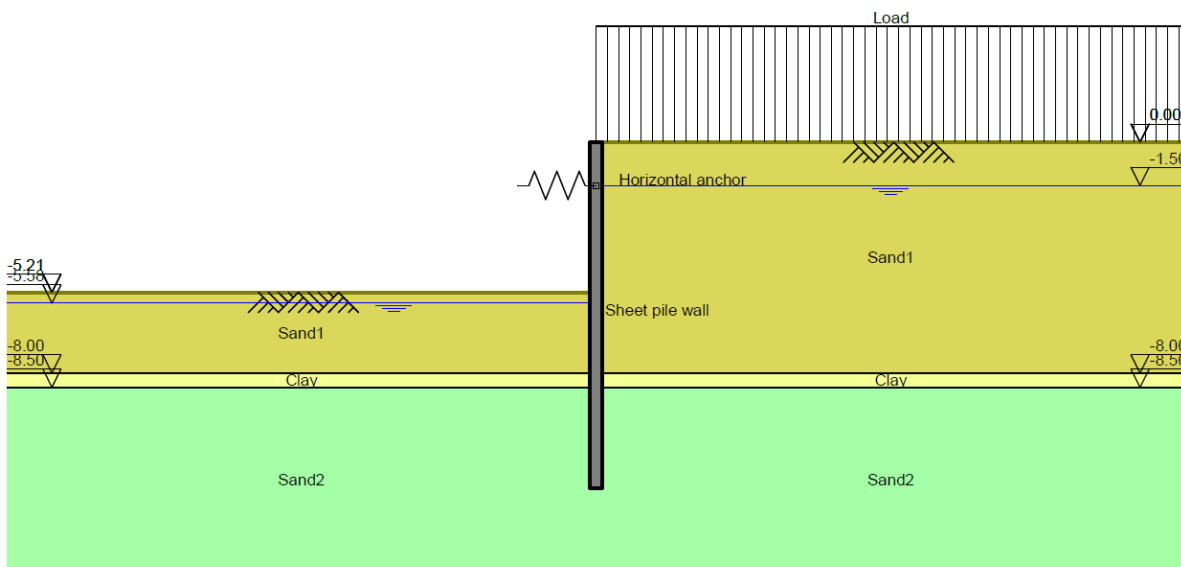


Figure I.3: Cross-section of example 2 from [72].

Parameter	Symbol	$\mu(i)$	$\sigma(i)$	$X_{kar}(i)$	$X_d(i)$	$X_{d^*}(i)$	Unit
Cohesion	c_1	3.0	0.60	2.02	2.08	2.02	kN/m ²
Angle of internal friction	ϕ_1	30	3.00	25.08	22.24	22.24	°
	ϕ_2	22.5	2.25	18.81	16.68	16.68	°
	ϕ_3	30	3.00	25.08	22.24	22.24	°
Angle of wall friction	δ_1	$\frac{2}{3}\phi_1$	0.125μ	0.53	0.61	0.53	-
	δ_2	$0.50\phi_2$	0.16μ	0.36	0.45	0.36	-
	δ_3	$\frac{2}{3}\phi_3$	0.125μ	0.53	0.61	0.53	-
Surcharge load	q	4.0	0.4	4.66	4.36	4.66	kN/m ²
Retaining height rel. to ground surface level	h	-5.00	0.125	-5.21	-5.32	-5.32	m
Water level active side	w_a	-1.50	0.00	-1.50	-1.50	-1.50	m
Water level passive side	w_p	-5.50	0.05	-5.58	-5.55	-5.58	m
Layer separation	s	-12.00	0.20	-12.33	-12.33	-12.33	m
Specific weight	γ_1	20.0		20.0	20.0	20.0	kN/m ³
	γ_2	18.0		18.0	18.0	18.0	kN/m ³
	γ_3	20.0		20.0	20.0	20.0	kN/m ³
Additional active pore pressure	20.0		20.0	20.0	20.0	kN/m ²	
Additional passive pore pressure	20.0		20.0	20.0	20.0	kN/m ²	
Bending stiffness	EI	$1.1 \cdot 10^5$					kNm ²
Modulus of subgrade reaction	k_1	$1.0 \cdot 10^4$					kN/m ³
	k_2	$1.0 \cdot 10^3$					kN/m ³
	k_3	$1.0 \cdot 10^4$					kN/m ³

Table I.3: Input parameters of example 2 [72, p. 53].

By calibrating the sheet pile length in the model, The ratio of equation 4.1 $\gamma_{gr} = 1.5$ is obtained. Afterwards, the resisting moment M_{yield} is found through calculation with eq. 4.2. The value of $\gamma_m = 1.5$ is used in the determination of the resisting moment. As a consequence, a strongly deviating reliability index $\beta_{50} = 6.98$ is obtained. The overall safety value γ_m is afterwards substituted with a value equal to 1.1. Eventually a length of 12 m and a section modulus $W_{el,y} = 1600 \cdot 10^3 \text{ mm}^3$ is obtained for $\gamma_m = 1.1$ and a deterministic yield stress $f_y = 235 \text{ N/mm}^2$.

Consequently, a reliability index $\beta_{50} = 4.14$ is obtained so a marginal difference with the target reliability for CUR class II ($\beta_t = 3.8$) is observed. After comparison of the partial safety factors, one observes minor differences. Table J.7 in appendix J includes the reliability indices and sensitivity factors of example assuming a deterministic yield stress f_y . In addition, table J.8 presents results including correlated variables and model uncertainty. The influence of the random variables is visualised by figures J.5 and J.6.

J

A-priori reliability results: yielding of the front wall

J.1. Example 3: Quay wall CUR class III

Reliability index [-]	Probability of failure [%]	Probability of non failure [%]	Return period [years]
4.53	$2.93 \cdot 10^{-4}$	100	$3.42 \cdot 10^5$
Variable	Alpha [-]	Influence factor [%]	Physical value [x]
c_{clay}	0.188	3.537	2.4886
ϕ_{clay}	0.826	68.176	14.081
ϕ_{sand}	-0.0117	0.0136	32.672
w_a	-0.155	2.392	-1.3598
w_p	0.417	17.363	-1.8777
q	-0.253	6.383	22.29
δ_{clay}	0.146	2.135	10.058
δ_{sand}	$-2.02 \cdot 10^{-3}$	$4.09 \cdot 10^{-4}$	21.691

Table J.1: Output FORM-computations for $t_{ref} = 50$ years.

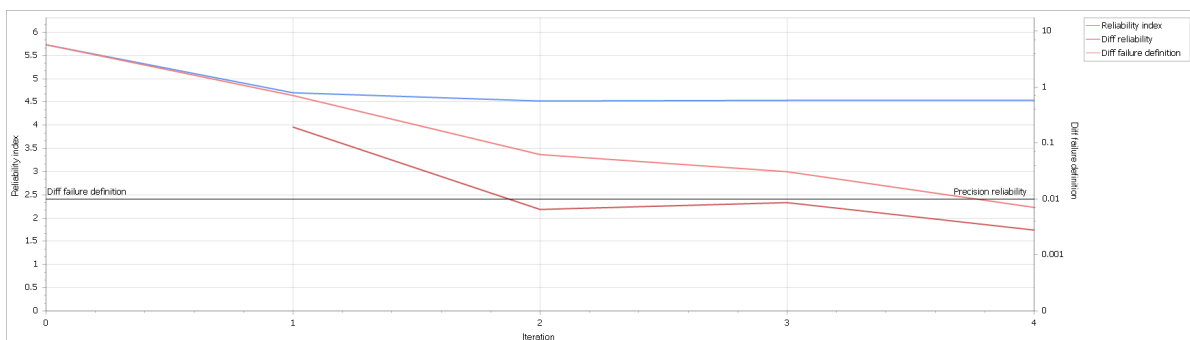


Figure J.1: Convergence diagram for limit state function H.3, given $f_{rel} = 0.75$ and gradient step size = 0.3.

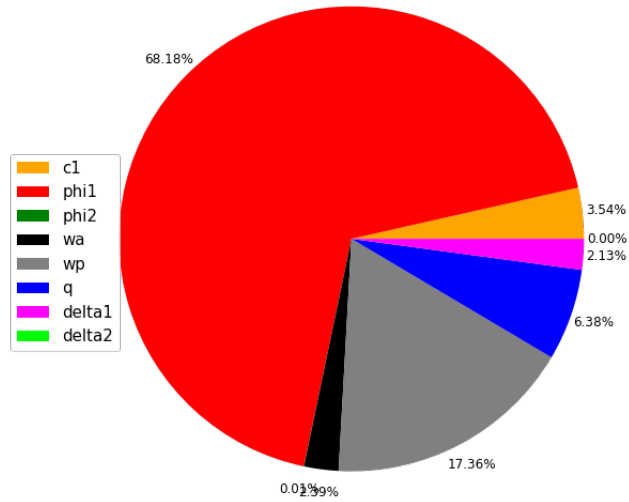


Figure J.2: Influence circle histogram for limit state function H.3

Reliability index [-]	Probability of failure [%]	Probability of non failure [%]	Return period [years]	
4.97	$3.43 \cdot 10^{-5}$	100	$2.92 \cdot 10^6$	
Variable	Alpha [-]	Influence factor [%]	Correlated alpha [-]	Physical value [X]
c_{clay}	-0.478	22.883	-0.486	4.4472
ϕ_{clay}	0.744	55.350	0.876	11.536
ϕ_{sand}	-0.0185	0.0343	-0.0217	32.851
w_a	0.190	3.591	0.195	-1.6934
w_p	0.285	8.138	0.336	-1.8657
q	-0.287	8.256	-0.294	22.92
δ_{clay}	0.132	1.747	0.538	2.6968
δ_{sand}	$-1.96 \cdot 10^{-3}$	$3.86 \cdot 10^{-4}$	-0.0162	22.024

Table J.2: Output FORM-computations given correlated variables and $t_{ref} = 50$ years.

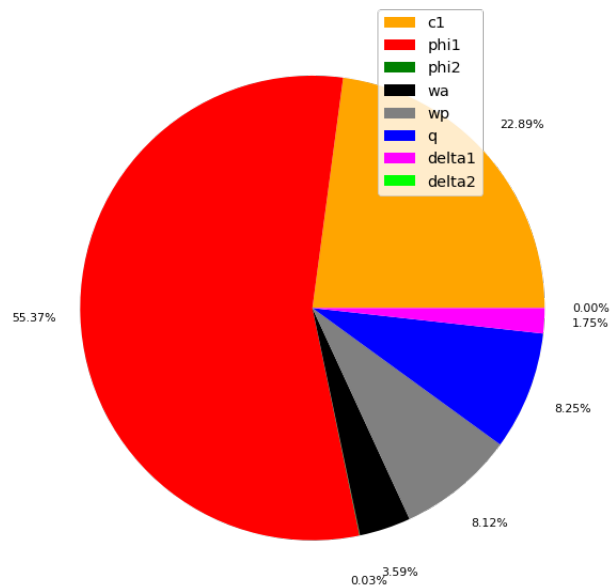


Figure J.3: Circle diagram illustrating the influence of the stochastic parameters for $t_{ref} = 50$ years and given correlated variables.

Reliability index [-]	Probability of failure [%]	Probability of non failure [%]	Return period [years]	
2.83	0.235	99.8	425	
Variable	Alpha [-]	Influence factor [%]	Correlated alpha [-]	Physical value [X]
c_{clay}	-0.299	8.949	-0.300	3.5079
ϕ_{clay}	0.376	14.102	0.480	18.94
ϕ_{sand}	-0.0257	0.0663	-0.0258	32.737
w_a	0.117	1.363	0.109	-1.5617
w_p	0.177	3.141	0.194	-1.6188
q	-0.180	3.230	-0.180	21.02
δ_{clay}	$7.32 \cdot 10^{-3}$	$5.37 \cdot 10^{-3}$	0.247	8.7397
δ_{sand}	$-2.93 \cdot 10^{-3}$	$8.56 \cdot 10^{-4}$	-0.0194	21.909
ξ	-0.832	69.142	-0.831	1.2579

Table J.3: Output FORM-computations given correlated variables, $t_{ref} = 50$ years and taking into account model uncertainty.

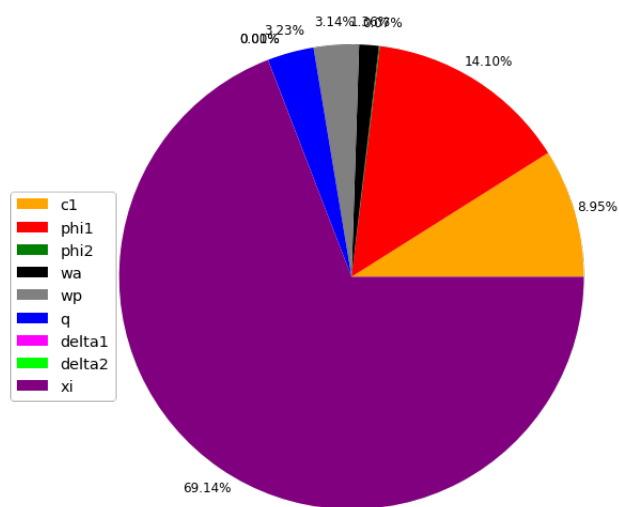


Figure J.4: Circle diagram illustrating the influence of the stochastic parameters for $t_{ref} = 50$ years, given correlated variables and model uncertainty.

J.1.1. With equivalent sheet pile profile

Reliability index [-]	Probability of failure [%]	Probability of non failure [%]	Return period [years]
8.37	$2.92 \cdot 10^{-15}$	100	$7.92 \cdot 10^{28}$
Variable	Alpha [-]	Influence factor [%]	Physical value [X]
c_{clay}	0.231	5.333	1.8403
ϕ_{clay}	0.850	72.177	6.5009
ϕ_{sand}	0.189	3.577	27.355
w_a	-0.0840	0.705	-1.3594
w_p	0.294	8.633	-1.9919
q	-0.204	4.179	23.422
δ_{clay}	0.217	4.688	7.9881
δ_{sand}	0.0841	0.707	19.76

Table J.4: Output FORM-computations with a combined sheet pile profile for $t_{ref} = 50$ years.

Reliability index [-]	Probability of failure [%]	Probability of non failure [%]	Return period [T]	
8.62	$3.33 \cdot 10^{-16}$	100	$7.92 \cdot 10^{28}$	
Variable	Alpha [-]	Influence factor [%]	Correlated alpha [-]	Physical value [X]
c_{clay}	-0.442	19.540	-0.448	5.3173
ϕ_{clay}	0.743	55.248	0.863	4.1222
ϕ_{sand}	0.307	9.422	0.274	24.82
w_a	0.141	2.002	0.144	-1.7489
w_p	0.176	3.106	0.224	-1.9424
q	-0.204	4.147	-0.205	23.54
δ_{clay}	0.243	5.891	0.646	-4.7877
δ_{sand}	0.0802	0.643	0.238	13.253

Table J.5: Output FORM-computations with a selected combined sheet pile profile, given correlated variables and $t_{ref} = 50$ years.

Reliability index [-]	Probability of failure [%]	Probability of non failure [%]	Return period [years]	
6	$1.02 \cdot 10^{-7}$	100	$9.81 \cdot 10^8$	
Variable	Alpha [-]	Influence factor [%]	Correlated alpha [-]	Physical value [X]
c_{clay}	-0.287	8.227	-0.287	4.0325
ϕ_{clay}	0.366	13.411	0.466	15.209
ϕ_{sand}	-0.0234	0.0547	-0.0234	32.956
w_a	0.123	1.508	0.123	-1.6473
w_p	0.165	2.720	0.201	-1.7702
q	-0.180	3.228	-0.180	22.156
δ_{clay}	0.0113	0.0129	0.243	6.0664
δ_{sand}	$-2.41 \cdot 10^{-3}$	$5.81 \cdot 10^{-4}$	-0.0174	22.131
ξ	-0.842	70.837	-0.843	1.6469

Table J.6: Output FORM-computations with a combined sheet pile profile, given correlated variables and taking model uncertainty into account for $t_{ref} = 50$ years.

J.2. Example 2: building pit CUR class II

J.2.1. With calibrated elastic section modulus

Reliability index [-]	Probability of failure [%]	Probability of non failure [%]	Return period [years]
4.14	$1.76 \cdot 10^{-3}$	100	$5.69 \cdot 10^4$
Variable	Alpha [-]	Influence factor [%]	Physical value [X]
c_{clay}	$8.77 \cdot 10^{-4}$	$-7.69 \cdot 10^{-5}$	2.9978
ϕ_{clay}	0.0220	0.0483	22.295
ϕ_{sand1}	0.920	84.637	18.581
ϕ_{sand2}	0.270	7.287	26.649
w_p	0.0301	0.0906	-5.5062
q	-0.0431	0.186	4.0714
δ_{clay}	$-4.28 \cdot 10^{-3}$	$1.83 \cdot 10^{-3}$	11.282
δ_{sand1}	0.242	5.880	17.492
δ_{sand2}	0.137	1.870	18.585

Table J.7: Output FORM-computations with example 2 from [72] after calibration of $W_{el,y}$ and given input from table I.3.

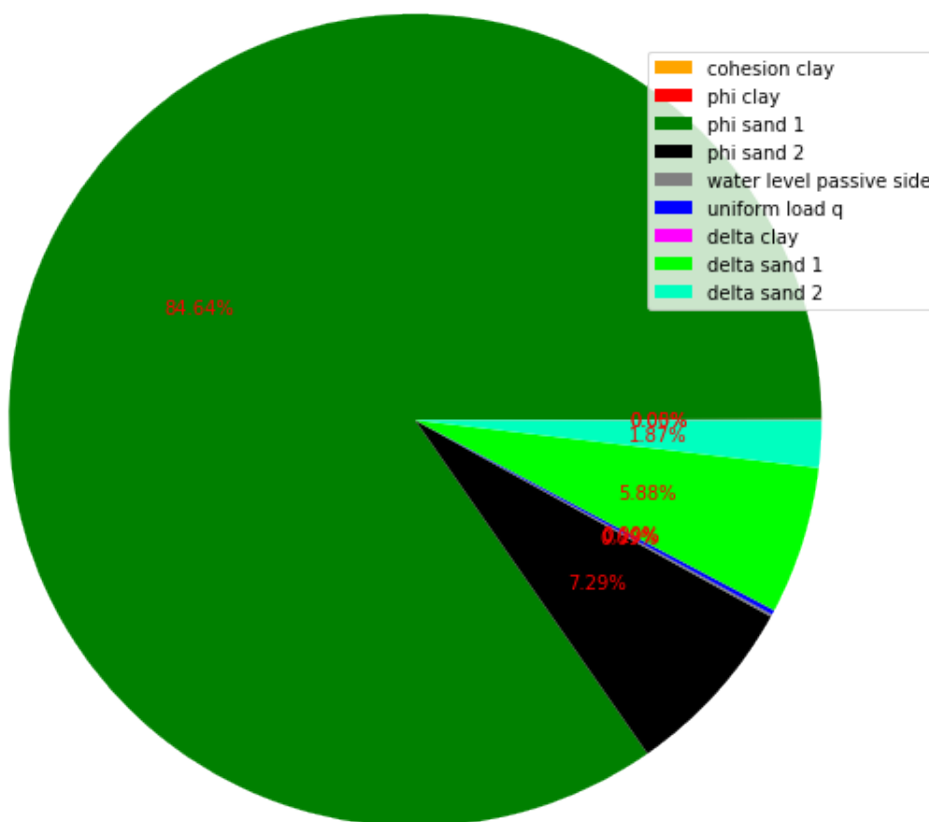


Figure J.5: Circle diagram showing the relative influence of the correlated variables for $t_{ref} = 50$ years.

Reliability index [-]	Probability of failure [%]	Probability of non failure [%]	Return period [years]	
2.38	0.863	99.1	115	
Variable	Alpha [-]	Influence factor [%]	Physical value [X]	Correlated alpha [-]
c_{clay}	$8.06 \cdot 10^{-3}$	$6.49 \cdot 10^{-3}$	$-8.04 \cdot 10^{-3}$	3.0115
ϕ_{clay}	$9.38 \cdot 10^{-3}$	$8.7 \cdot 10^{-3}$	0.0124	22.422
ϕ_{sand1}	0.656	43.034	0.656	25.317
ϕ_{sand2}	$8.43 \cdot 10^{-3}$	$7.11 \cdot 10^{-3}$	$8.4 \cdot 10^{-3}$	29.94
w_p	-0.0132	0.0174	-0.0145	-5.4983
q	-0.0222	0.0493	-0.0221	4.021
δ_{clay}	0.000	0.000	$6.23 \cdot 10^{-3}$	11.196
δ_{sand1}	0.122	1.484	0.527	15.059
δ_{sand2}	$2.64 \cdot 10^{-3}$	$6.96 \cdot 10^{-4}$	$7.60 \cdot 10^{-3}$	19.933
ξ	-0.744	55.393	-0.742	1.1867

Table J.8: Output from FORM-computations of example 2 given correlated variables, $t_{ref} = 50$ years and taking into account model uncertainty.

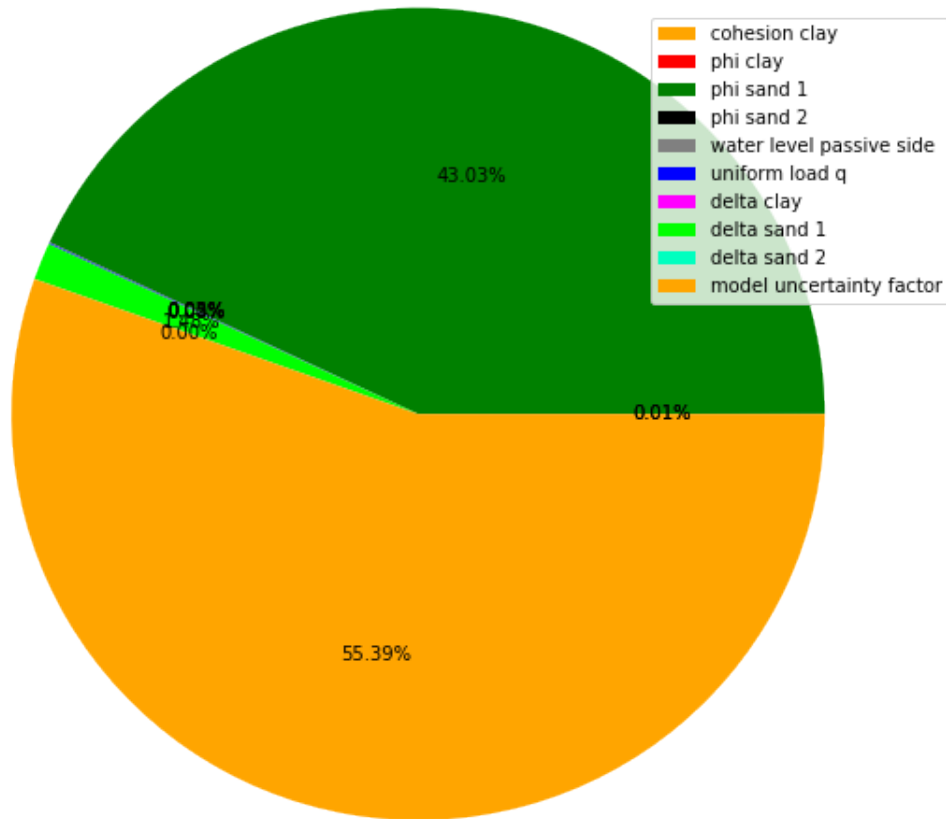
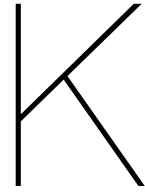


Figure J.6: Circle diagram showing the relative influence of the correlated variables for $t_{ref} = 50$ years.

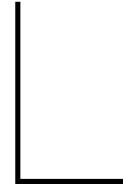


Verification of the level II analyses

K.1. Verification of the results with Importance Sampling

Number of realisations	321,000		
Convergence constant	0.0984 (<0.10)		
Reliability index [-]	Probability of failure [%]	Probability of non failure [%]	Return period [years]
4.86	$5.94 \cdot 10^{-5}$	100	$1.68E \cdot 10^6$
Variable	Alpha [-]	Influence factor [%]	Physical value [x]
c_{clay}	0.285	8.143	2.1683
ϕ_{clay}	0.622	38.641	15.706
ϕ_{sand}	0.115	1.333	30.677
w_a	-0.145	2.091	-1.3595
w_p	0.181	3.288	-1.6762
q	-0.669	44.720	26.497
δ_{clay}	0.133	1.780	10.083
δ_{sand}	$-5.54 \cdot 10^{-3}$	$3.07 \cdot 10^{-3}$	21.74

Table K.1: Verification of the level II analysis with importance sampling considering $t_{ref} = 50$ years, no correlations and no model uncertainty.



Derivation of stochastic parameters for variable q

The extreme value distribution of the dominant load parameter q changes as the reference period extends. As a result, the probability that extreme values occur is getting bigger. The mean value increases as the reference period extends. The standard deviation remains however constant. Hence the coefficient of variation V_q decreases. Table 4.11 presents the parameters of the simulated Type I distributions. These distributions are in accordance with the reference period and the number of distributed intervals. Assumed is that the dominant load parameter is independent in the different time intervals. Figure L.1 presents the Python algorithm in which the extreme value distributions are simulated with the normally distributed uniform load q . In addition, for each reference period different distribution parameters are determined.

```

In [5]: 1 import numpy as np
        2 import matplotlib.pyplot as plt
        3 import scipy.stats as sc
        4
        5 %matplotlib inline

In [8]: 1 #nr of samples:
        2 n = 10000
        3
        4 #50y mean and standard deviation
        5 mean50 = 20
        6 std50 = 2
        7
        8 norm50 = mean50 + np.random.randn(n, n)*std50
        9 max50 = []
       10 for i in range(len(norm50)):
       11     max50.append(max(norm50[i]))
       12
       13
       14 print(" ")
       15 print('tref = 50y')
       16 mu_m50 = np.mean(max50)
       17 sigma_m50 = np.std(max50)
       18 print("Standard deviation", sigma_m50); print("Mean value", mu_m50);
       19 alpha50 = np.pi/(np.sqrt(6)*sigma_m50)
       20 u_50 = mu_m50 - 0.5772/alpha50
       21 print("location parameter", u_50);
       22
       23
       24 u_1 = u_50 - np.log(50)/alpha50
       25 alpha1 = alpha50
       26 sigma_m1 = np.pi/(np.sqrt(6)*alpha1)
       27 mu_m1 = u_1 + 0.5772/alpha1
       28 print(" ")
       29 print('tref = 1y')
       30 print("Standard deviation", sigma_m1); print("Mean value", mu_m1);print("location parameter", u_1);
       31
       32
       33 u_5 = u_1 +np.log(5)/alpha1
       34 alpha5 = alpha1
       35 mu_m5 = u_5 + 0.5772/alpha5
       36 sigma_m5 = np.pi/(np.sqrt(6)*alpha5)
       37 print(" ")
       38 print('tref = 5y')
       39 print("Standard deviation", sigma_m5); print("Mean value", mu_m5); print("location parameter", u_5);
       40
       41
       42 u_10 = u_1 +np.log(10)/alpha1
       43 alpha10 = alpha1
       44 mu_m10 = u_10 + 0.5772/alpha10
       45 sigma_m10 = np.pi/(np.sqrt(6)*alpha10)
       46 print(" ")
       47 print('tref = 10y')
       48 print("Standard deviation", sigma_m10); print("Mean value", mu_m10); print("location parameter", u_10);
       49
       50
       51 u_25 = u_1 +np.log(25)/alpha1
       52 alpha25 = alpha1
       53 mu_m25 = u_25 + 0.5772/alpha25
       54 sigma_m25 = np.pi/(np.sqrt(6)*alpha25)
       55 print(" ")
       56 print('tref = 25y')
       57 print("Standard deviation", sigma_m25); print("Mean value", mu_m25); print("location parameter", u_25);
       58
       59
       60
       61 u_100 = u_1 +np.log(100)/alpha1
       62 alpha100 = alpha1
       63 print(" ")
       64 print('tref = 100y')
       65 mu_m100 = u_100 + 0.5772/alpha100
       66 sigma_m100 = np.pi/(np.sqrt(6)*alpha100)
       67 print("Standard deviation", sigma_m100); print("Mean value", mu_m100); print("location parameter", u_100);
       68
       69
       70 kwargs = dict(bins = 50, cumulative = False, alpha = 0.5, histtype = 'stepfilled' );

```

Figure L.1: Determination of the distribution parameter per each considered reference period.



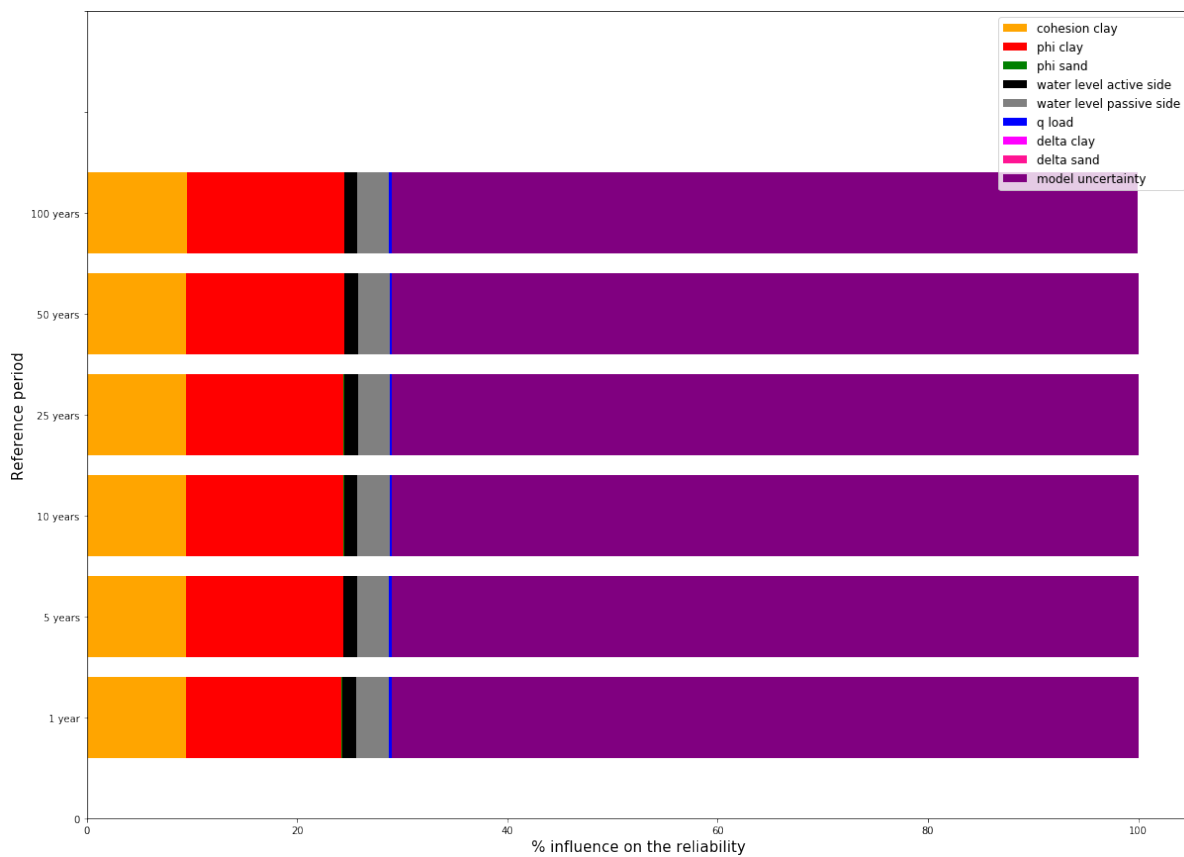


Figure L.3: Relative influence of the stochastic parameters per reference period in the case of correlated variables including model uncertainty. These cases are calculated with FORM.



Hohenbichler-Rackwitz algorithm for reliability updating

The algorithm which is provided in section M.1, originates from OpenEarthTools library of Deltares. This algorithm is a preview and is slightly adjusted for the reference case study. This algorithm considers a similar cross-section in two or more years as different components. The algorithm derives the failure probability of cross-section in year i given survival of the preceding years: $P(F_i | S_1 \cap S_2 \cap \dots \cap S_{i-1})$.

M.1. Two-component system

```

function [betaOR, betaAND] = HohenBichler(beta, pf, rho, method)

% the Hohenbichler method for computing P(Z1>0 OR Z2<0) and P(Z1>0 AND
% Z2<0). Z1 is described by its failure probability pf.
% Z2 is described by reliability index beta. The
% mutual correlation is described by random variable rho

% Input
% - beta: reliability index of Z2
% - pf: failure probability of Z1
% - rho: correlation between Z1 and Z2
% - method: 'Numerical'(default) or 'FORM'
%
% Output
% - betaOR:    beta for P[Z1>0 OR Z2<0]
% - betaAND:   beta for P[Z1>0 AND Z2<0]

% If components fully uncorrelated:
if abs(rho-1)<1e-5
    beta1 = -norminv(pf);
    betaOR = min(beta, beta1);
    betaAND = max(beta, beta1);

% otherwise: start HohenBichler procedure
else
    stochast = struct('Name', {...
        'Pu1st',...
        'Pu2st',...
    });

%}

%% option default: compute P(Z'<0) with Numerical integration
if strcmp(method, 'Numerical')

    beta1 = -norminv(pf);    % beta-value of element 1
    ngrid = 1001;           % number of grids for numerical integration

```



```
%format long
beta2 = beta;

PfOR = pf + (1-pf) - PfAND;
betaOR = -norminv(PfOR);

%{
% compute P(Z1<0 AND Z2<0)

% compute P(Z1<0 OR Z2<0)
PfOR = normcdf(-beta)+pf - PfAND;
betaOR = norminv(1-PfOR);
%}
end
```

Figure M.1: Preview of the applied Hohenbichler-Rackwitz algorithm [58].

M.2. Verification of a two-component system

Chapter 6.2 covers the theory behind the algorithm which is provided in the previous section. The application on the case study is shown in chapter 6.2.2. This chapter validates the results by means of two approaches: verification of the intermediate result(s) and Bayesian updating with the Deltares PTK.

M.2.1. Verification of the intermediate output

The Hohenbichler-Rackwitz method uses FORM or Numerical Integration in the derivation of the conditional failure probability $P(Z_2 < 0 | Z_1 < 0)$ or $P_{F_2|F_1}$. In the script this is denoted as "PZcond" and is used in the derivation of the combined reliability by means of the law of total probability or/and Bayes' Theorem. With Numerical Integration the computed conditional probability "PZcond" equals 0.6778. FORM yields a totally different value for the conditional failure probability: $P_{F_2|F_1} = 2.238 \cdot 10^{-4}$. The latter value is practically 0. One should be critical on whether this value is justified since Numerical Integration is very accurate for a limit state with $n = 2$ unknown variables [43, p. 55]. Besides, it is more believable that a cross-section fails if another component (in this case the same cross-section a year earlier) fails. In view of that, the value which obtained with Numerical Integration is checked through a different calculation engine.

$$Z_2 = \beta_2 - \rho \cdot u_2 - \sqrt{1 - \rho^2} \cdot u_3 \quad (\text{M.1})$$

in which:

ρ is the correlation between two components

u_1 is the standard normally distributed variable comprising the right hand side of equation 5.6 [43, p. 55]

u_2 is the introduced standard normally distributed variable capturing the upper tail ($u_1 > \beta_2$) of u_1

Numerical Integration solves the marginal distribution represented by equation M.1. This is realised by using a step size $Deltau = \frac{10}{1001} \approx 0.01$. Lines x - xx contain the algorithm for Numerical Integration. The outcome of $P_{F_2|F_1} = 0.6778$ is validated with the Deltares Probabilistic Toolkit. A uniform distribution $U(0,1)$ is selected for the Variables u_2 and u_3 . This is done in order to simulate the variables in the standard normal u -space. Figure M.2 shows the settings in the Deltares toolkit. The verification's are in first instance performed with Importance Sampling (level III) and afterwards complemented with FORM. Table M.1 summarises the results from the computations.

EPM algorithm	Deltares PTK: Importance sampling	Deltares PTK: FORM
0.6778	0.67	0.6270

Table M.1: Verification of $P_{F_2|F_1}$ (PZcond) with FORM and importance sampling in a different calculation engine.

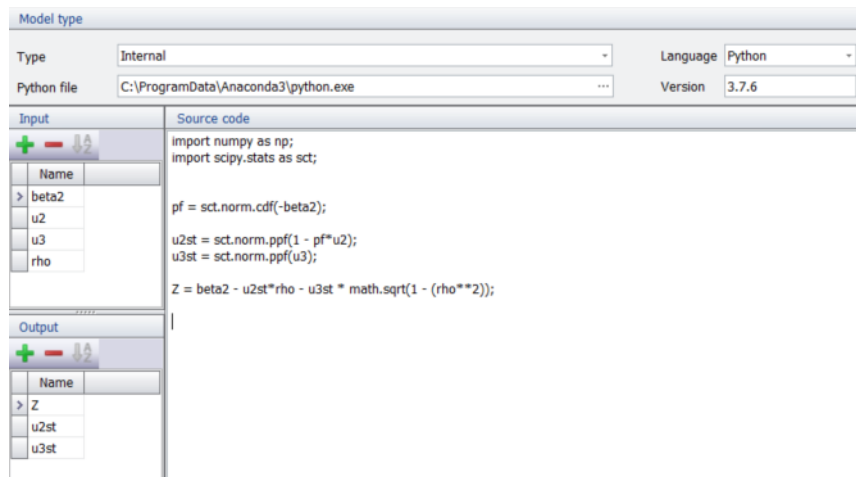


Figure M.2: Internal Deltares PTK calculation of the conditional failure probability $P_{F2|F1}$.

Marginal differences are observed between the outcomes. Further results such as the updated reliability $\beta_{F2|S1}$ by means of Numerical Integration seem justifiable. So the choice with Numerical Integration as the default method is very accurate.

M.2.2. Verification trough Bayesian updating with Deltares PTK

Computations in the Deltares Probabilistic Toolkit are executed with FORM in view of time-related effort and efficiency. The case study cross-section with a reference period t_{ref} of 1 year is treated as one component. In accordance with chapter 4.4, a Gumbel-distributed dominant load with $\mu_q = 25.8 \text{ kN/m}^2$ and $\sigma_q = 0.61 \text{ kN/m}^2$ is chosen. Cross-correlations as described in chapter 4.2 are assumed. The lognormally distributed model uncertainty factor ($\xi \sim \text{LN}(1, 0.1)$) is applied as well. Table M.2 shows the input for this verification. Statement M.2 presents the row vector consisting of the sensitivity values per each variable.

$$\begin{aligned} \underline{\alpha}_i &= [\alpha_{i\gamma_1} \alpha_{i\gamma_2} \alpha_{ic_1} \alpha_{ic_2} \alpha_{i\phi_1} \alpha_{i\phi_2} \alpha_{iL} \alpha_{iw_a} \\ &\quad \alpha_{iw_p} \alpha_{iEI} \alpha_{iq} \alpha_{i\delta_1} \alpha_{i\delta_2} \alpha_{ik_{01,clay}} \alpha_{ik_{01,sand}} \alpha_{iW_{el}} \alpha_{if_y} \alpha_{i\xi}] \\ &= [0, 0, -0.307, 0, 0.385, -0.026, 0, 0.114, 0.176, 0, -0.051, 0.008, -0.003, 0, 0, 0, 0, -0.843] \end{aligned} \quad (\text{M.2})$$

Reliability index [-]	Probability of failure [%]	Probability of non failure [%]	Return period [years]	
2.36	0.922	99.1	108	
Variable	Alpha [-]	Influence factor [%]	Correlated alpha [-]	Physical value [x]
c_{clay}	-0.307	9.407	-0.306	3.4332
ϕ_{clay}	0.385	14.841	0.491	19.464
ϕ_{sand}	-0.0259	0.0671	-0.0259	32.698
w_a	0.114	1.306	0.114	-1.5537
w_p	0.176	3.094	0.202	-1.6032
q	-0.0513	0.263	-0.0511	25.767
δ_{clay}	$8.19 \cdot 10^{-3}$	$6.72 \cdot 10^{-3}$	0.253	9.1075
δ_{sand}	$-2.91 \cdot 10^{-3}$	$8.48 \cdot 10^{-4}$	-0.0194	21.869
ξ	-0.843	71.014	-0.841	1.2124

Table M.2: Input values for the equivalent planes method for the purpose of computing the combined failure probability.

Reliability updating with the Equivalent Planes method is validated through application of the Deltares Probabilistic Toolkit. Within this toolkit it is possible to calculate the conditional failure probability of a system, meaning the probability of failure given a condition statement to be true. In this case study, failure occurs when the stress resulting from the maximum bending moment exceeds the front wall yield stress.

$$P(A) = P\left(fy < \frac{M_{max}}{W_{el,y}} | t = t_i\right) \quad (M.3)$$

$$P(B) = P\left(fy > \frac{M_{max}}{W_{el,y}} | t \in [t_0, t_{i-1}]\right) \quad (M.4)$$

Accordingly, the conditional failure statement by equation M.5 is calculated. $P(B)$ is the event in which equation M.4 occurs. Hence, the latter is the condition. In addition, $P(A)$ indicates the occurrence of equation M.3. The computation of the second year conditional failure probability is performed with statements M.3 and M.4. This can be performed with several probabilistic techniques including FORM and importance sampling. For simple reasons, this is performed with FORM.

$$P(A|B) = \frac{P(A \cap B)}{P(B)} \quad (M.5)$$

Results

Table M.3 presents the results (β and α 's) which were found with the Hohenbichler method in MATLAB and the Deltares Probabilistic Toolkit. Beside what computation tool is used, it is indicated which reliability method is used. Some differences between the results are observed but these are marginal. The reliability indices and sensitivity factors of the two-component system are broadly the same.

Differences can although be explained by the irregularities in the numerical computations with the MATLAB FORM algorithm relative to the Deltares Probabilistic Toolkit,

Hohenbichler method		Deltares Probabilistic Toolkit	
Reliability index [-]	Probability of failure [%]	Reliability index [-]	Probability of failure [%]
2.3566	$9.2 \cdot 10^{-3}$	2.18	0.0145
Variable	Alpha [-]	Variable	Alpha [-]
c_{clay}	-0.3006	c_{clay}	-0.470
ϕ_{clay}	0.3775	ϕ_{clay}	-0.0135
ϕ_{sand}	-0.0254	ϕ_{sand}	-0.0327
w_a	0.1585	w_a	-0.111
w_p	0.2439	w_p	0.415
q	0.000429	q	0.00641
δ_{clay}	0.008	δ_{clay}	0.0910
δ_{sand}	-0.0028	δ_{sand}	-0.107
ξ	-0.8258	ξ	-0.757

Table M.3: Verification of the Hohenbichler reliability updating in MATLAB method and Bayesian updating with the Deltares PTK. The same starting points are used.

or the other way around. The FORM algorithm uses the predetermined yearly reliability index β_1 and sensitivity factors for derivation of the second year output. Deltares Probabilistic Toolkit on the other hand, takes all input variables into account. Hence, the procedures of how the reliability indices and sensitivity values are determined differs. Hohenbichler mainly follows a numerical approach in which the determined β 's are used, whereas the toolkit uses explicit information among which the variable uncertainties, parameter distributions.

N

Results Hohenbichler-Rackwitz method combined with FORM

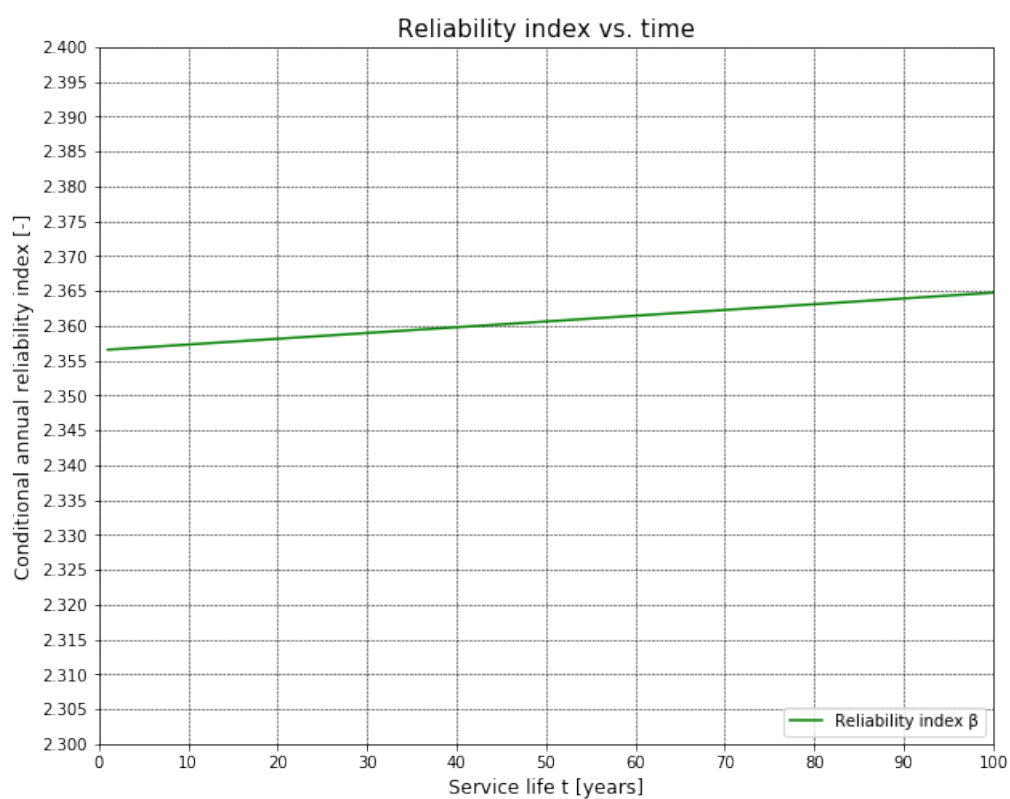


Figure N.1: Time-dependent reliability curve of example 3 from [72] derived with FORM, given correlated variables and model uncertainty.

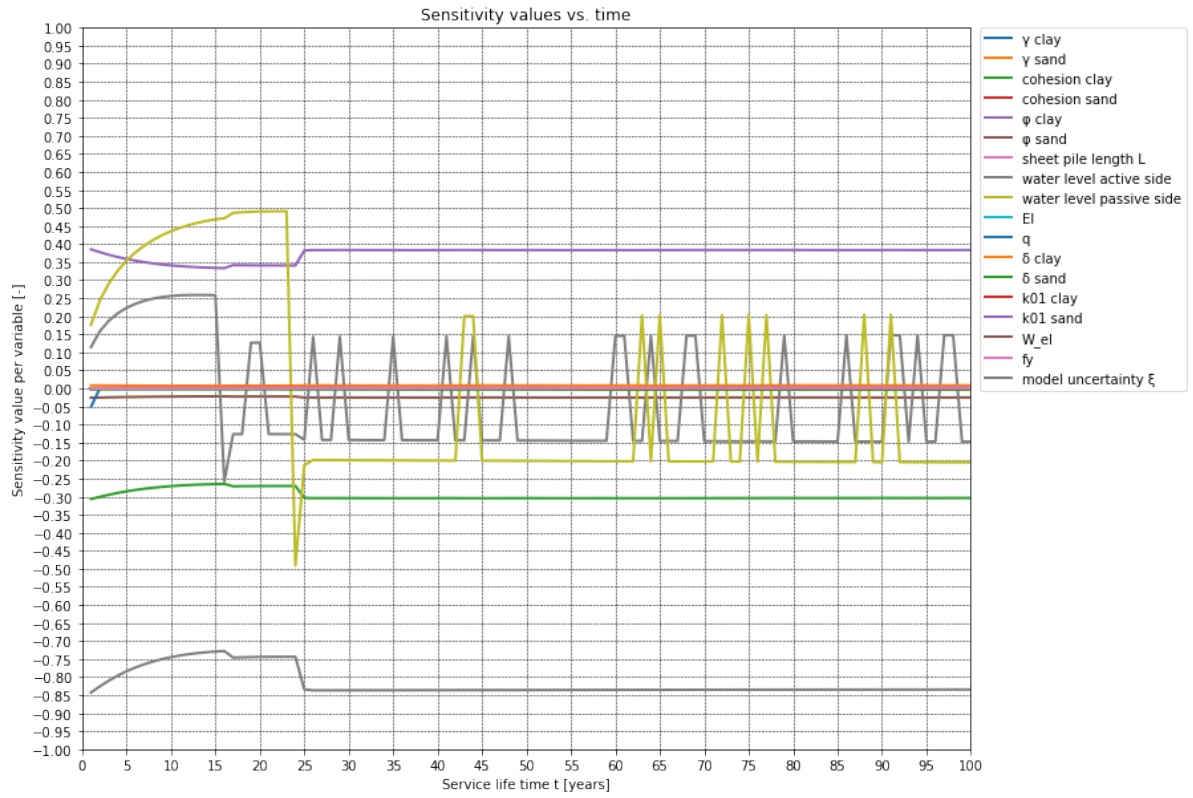
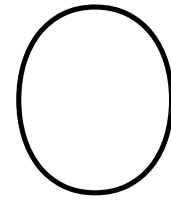


Figure N.2: Numerical instabilities emerge when a numerical FORM routine is applied in the computation of time-dependent sensitivity values given information about survived years.

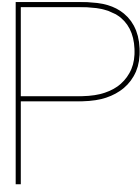


Effects of extreme loads

```
1 #nr of samples:
2 n = 10000
3
4 #50y mean and standard deviation
5 mean50 = -1.5
6 std50 = 0.20
7
8 norm50 = mean50 + np.random.randn(n, n)*std50
9 min50 = []
10 for i in range(len(norm50)):
11     min50.append(min(norm50[i]))
12
13
14 mu_m50 = np.mean(min50)
15 sigma_m50 = np.std(min50)
16 alpha = np.pi/(np.sqrt(6)*sigma_m50)
17 u_50 = mu_m50 + 0.5772/alpha
18
19 u_1 = u_50 + np.log(50)/alpha
20 mu_m1 = u_1 - 0.5772/alpha
21 sigma_m1 = np.pi/(alpha*np.sqrt(6))
22
23
24 tref = [10, 20, 30, 40, 50, 60, 70, 80, 90, 100]
25
26
27 u = np.ones(len(tref))
28 mu = np.ones(len(tref))
29 std = np.ones(len(tref))
30
31
32 for i in range(0, len(tref)):
33     u[i] = u[i]*(u_1-np.log(tref[i])/alpha)
34     mu[i] = u[i] - 0.5772/alpha
35     std[i] = np.pi/(alpha*np.sqrt(6))
36
37 print("u given type I minima:",u); print("mu given type I minima:", mu); print("std given type I minima:", std);
38
39 plt.plot(tref, u, mu);
40 plt.grid()
41 plt.legend(['u', 'mu'], loc='best');
```

u given type I minima: [-2.16748631 -2.19989291 -2.21884956 -2.23229952 -2.24273211 -2.25125616
-2.25846315 -2.26470612 -2.27021281 -2.27513872]
mu given type I minima: [-2.19447205 -2.22687866 -2.2458353 -2.25928526 -2.26971786 -2.27824191
-2.28544889 -2.29169186 -2.29719856 -2.30212446]
std given type I minima: [0.05996286 0.05996286 0.05996286 0.05996286 0.05996286 0.05996286
0.05996286 0.05996286 0.05996286 0.05996286]

Figure O.1: Determination of the type I minima distribution parameters given the normal distributions of w_p (similar procedure is performed for the maxima of w_q and q).



Derivation of the reduced W and EI

The initial section modulus W_0 and inertia I_0 that were used in chapter 6 are the start values. The new values are determined with the ratio between a reduced primary element and its initial profile characteristics.

Dimension	Value	Unit
D	1,016	mm
e_0	14	mm

Table P.1: Characteristics of a $\varnothing 1016-14$ tubular pile.

Firstly, geometric characteristics of the primary tubular elements are determined:

$$A_{tube;0} = \frac{\pi \left(D^2 - (D - 2e_0)^2 \right)}{4} \quad (P.1)$$

Since corrosion is solely considered at the water side. Distinction is made between corroded area on the water- and land side.

$$A_{corr;land} = \frac{\pi \left(D^2 - (D - 2e_0)^2 \right)}{8} \quad (P.2)$$

$$A_{corr;water} = \frac{\pi \left((D - 2\Delta e)^2 - (D - 2e_0)^2 \right)}{8} \quad (P.3)$$

The corroded area of the primary element is the sum of equations P.2 and P.3.

$$A_{corr} = \frac{\pi \left(\frac{1}{2}D^2 + \frac{1}{2}(D - 2\Delta e)^2 - (D - 2e_0)^2 \right)}{4} \quad (P.4)$$

Similar calculation procedure is performed for the inertia on both sides of the tubular element.

$$I_{corr;land} = \frac{\pi \left(D^4 - (D - 2e_0)^4 \right)}{128} \quad (P.5)$$

$$I_{corr;water} = \frac{\pi \left((D - 2\Delta e)^4 - (D - 2e_0)^4 \right)}{128} \quad (P.6)$$

The total inertia of the primary element is determined with equation P.7

$$I_{corr;tube} = \frac{\pi}{64} \left(\frac{1}{2} D^4 + \frac{1}{2} (D_{tube} - 2\Delta e)^4 - (D_{tube} - 2e_0)^4 \right) \quad (P.7)$$

For the derivation of the reduced section modulus, the distance between the central axis and the outer fibre Z_y is calculated. Prior to that, the shifting of the central axis on both sides is determined by equations P.8 and P.9.

$$Z_{tube;land} = \frac{2}{3\pi} \cdot \frac{(D - 2\Delta e)^3 - (D - 2e_0)^3}{(D - 2\Delta e)^2 - (D - 2e_0)^2} \quad (P.8)$$

$$Z_{tube;water;corr} = \frac{2}{3\pi} \cdot \frac{(D)^3 - (D - 2e_0)^3}{(D)^2 - (D - 2e_0)^2} \quad (P.9)$$

$$Z_y = \frac{Z_{tube;land} A_{corr;land} - Z_{tube;water;corr} A_{corr;water}}{A_{corr}} \quad (P.10)$$

As a result, the reduced inertia of the tubular primary element is derived according to equating P.11.

$$I_{corr} = I_{corr;tube} - A_{corr} Z_y^2 \quad (P.11)$$

Accordingly, the modified section modulus can be determined. This is performed with equations P.12 and P.13.

$$W_{corr;land} = \frac{I_{corr;land}}{0.5D - Z_y} \quad (P.12)$$

$$W_{corr;water} = \frac{I_{corr;water}}{0.5D - \Delta e + Z_y} \quad (P.13)$$

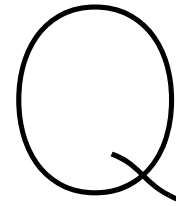
The sum of the outcomes of equations P.12 and P.13 is of course the corroded section modulus $W_{corr;tube}$ of the tubular pile.

Sufficient information is available for deriving the reduced cross-section characteristics given W_0 and I_0 .

$$I_{el,y}(t) = I_0 \cdot \frac{I_{corr}(t)}{I_{0;tube}} \quad (\text{P.14})$$

$$W_{el,y}(t) = W_0 \cdot \frac{W_{corr;water}(t)}{W_{0;tube}} \quad (\text{P.15})$$

The values determined equations P.14 and P.15 are iteratively applied in the limit state calculation for each year.



Time-dependent effects on the quay wall

This chapter firstly includes the time-dependent conditional annual reliability curve which is found with the refined approach. This approach derives the section modulus $W_{el,y}(t)$ and second moment of inertia $I_{el,y}(t)$ based on corrosion curve 3. In the first 60 years, the effect(s) of survived years S_1, S_2, \dots, S_i seem(s) greater than the effect(s) of corrosion as the reliability increases over time. Afterwards, the time-dependent reliability flattens and marginally decreases (see figure Q.1). The corresponding fluttering sensitivity values are shown in figure Q.2. Figure Q.2 is described in chapter 7.

In addition, the reliability indices as a function of the reference period are presented by figures Q.3-Q.4. These curves include the effects of corrosion considering Jongbloed curve number 3.

Q.1. Refined or "second order" approach for including corrosion

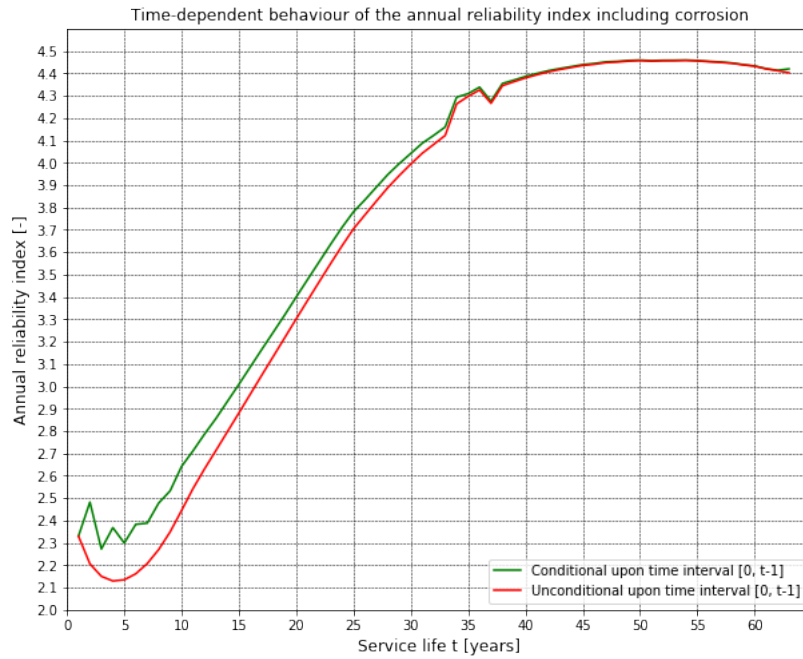


Figure Q.1: The time-independent development of the annual reliability index including corrosion and unconditional upon time interval [0, t-1] (red line), including corrosion and conditional upon time interval [0, t-1] (green line). The time-dependent annual reliability index is calculated for 100 years with the "second order" approach.

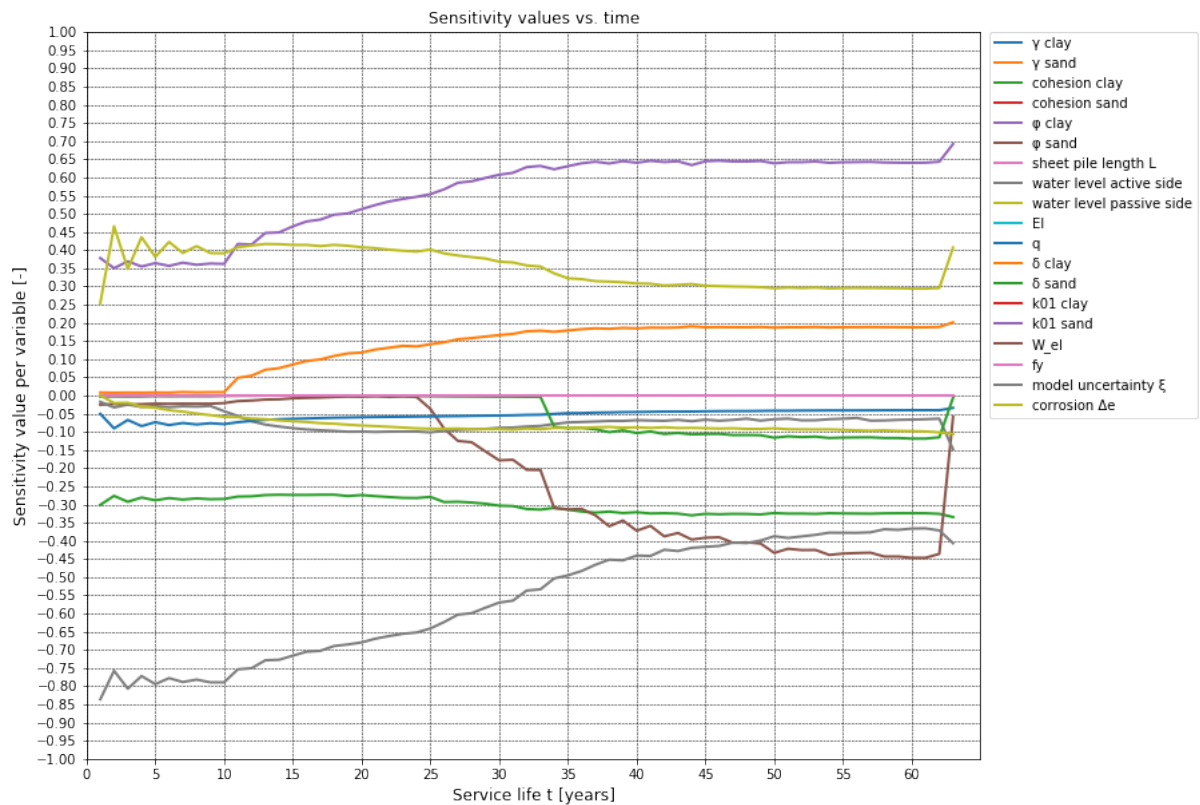


Figure Q.2: Time-dependent sensitivity values given corrosion, derived with the "second order" approach.

Q.2. Reliability index as a function of the reference period

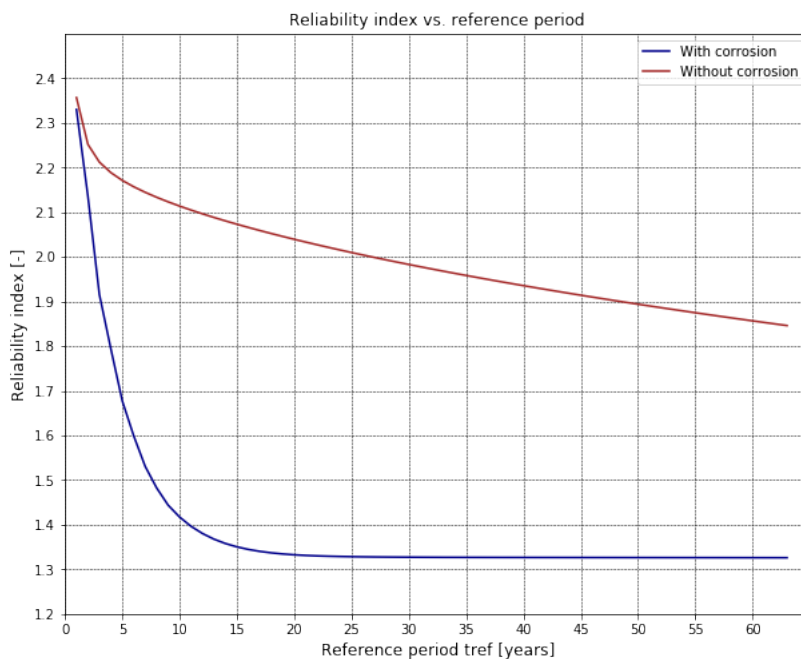


Figure Q.3: The reliability index as a function of the reference period in years, in the case with corrosion (blue line) and without corrosion (brown line).

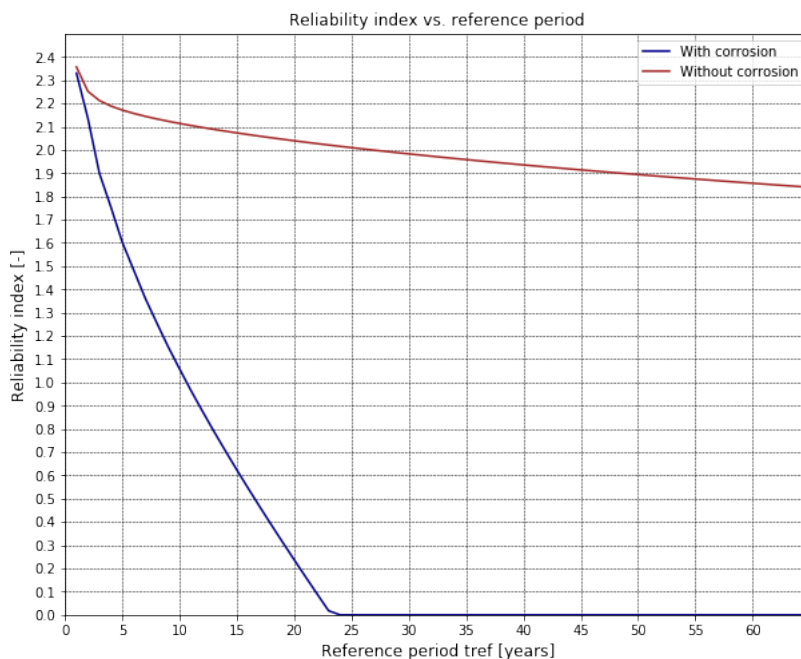


Figure Q.4: The reliability index as a function of the reference period in years, in the case with corrosion (blue line) and without corrosion (brown line). These curves are derived with the engineering approach.

R

Approach follow-up case study

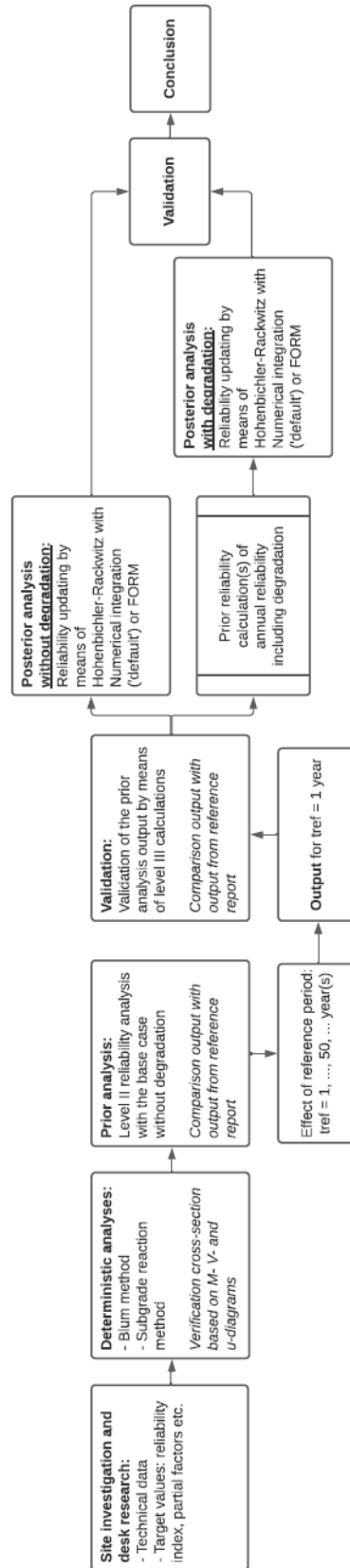


Figure R.1: Process scheme of reliability updating by means of the subgrade reaction method (D-sheet Piling and Deltares PTK).

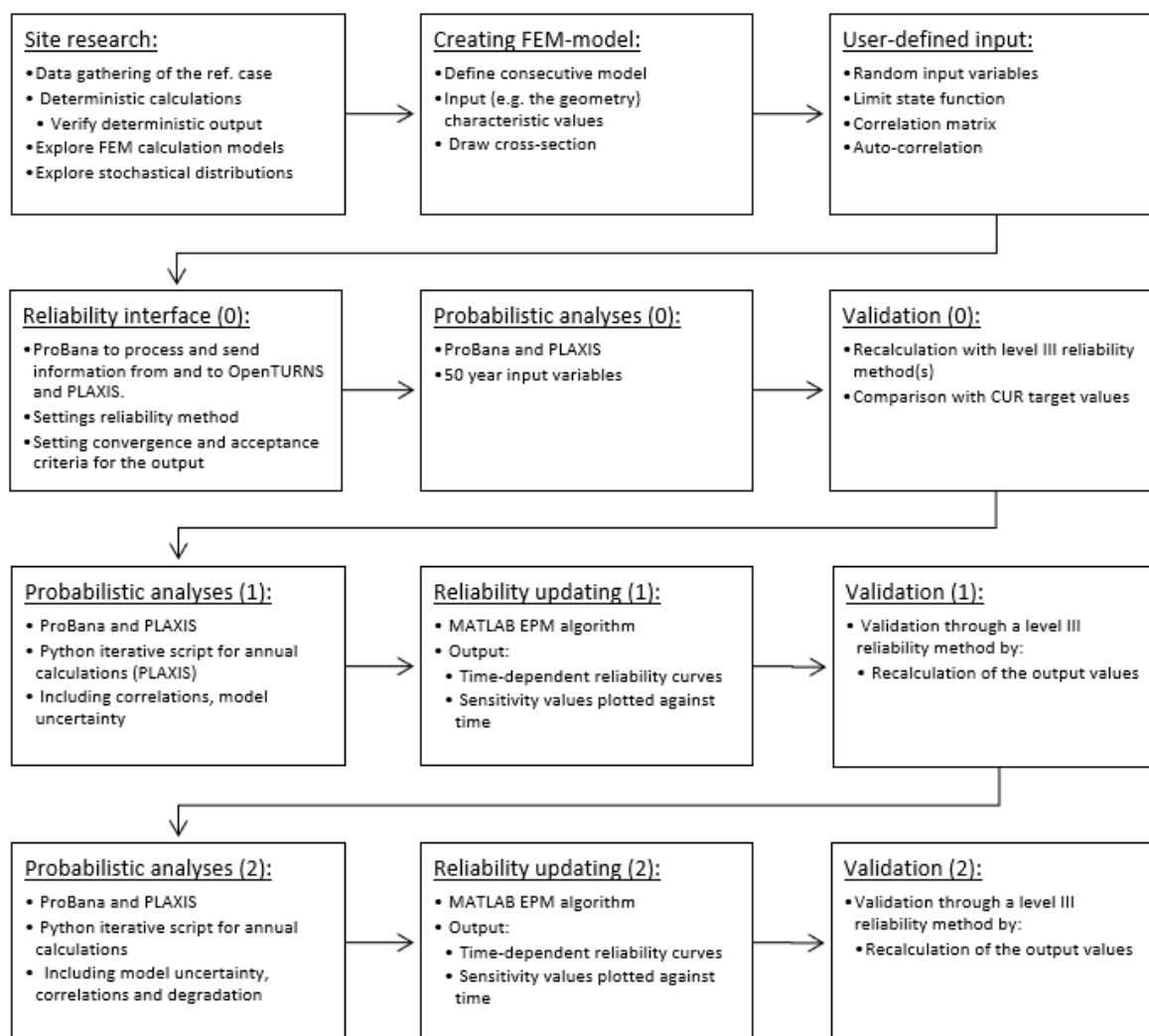


Figure R.2: Process scheme of reliability updating using FEM-model coupled with a reliability interface named ProBana.